

UNCLASSIFIED

AD NUMBER
AD254472
NEW LIMITATION CHANGE
TO Approved for public release, distribution unlimited
FROM Distribution authorized to U.S. Gov't. agencies and their contractors; Administrative/Operational Use; Feb 1961. Other requests shall be referred to Office of Naval Research, 800 North Quincy Street, Arlington, VA 22217-5660.
AUTHORITY
ONR ltr, 15 Jun 1977

THIS PAGE IS UNCLASSIFIED

CLASSIFIED

AD 254 472

*Reproduced
by the*

SERVICES TECHNICAL INFORMATION AGENCY
ARLINGTON HALL STATION
ARLINGTON 12, VIRGINIA



20050204081

UNCLASSIFIED

Best Available Copy

AD 524 115

NOTICE: The Government or other drawings, specification or other data are used for any purpose other than in connection with a definitely related government procurement operation. The U. S. Government hereby incurs no responsibility, nor any obligation whatsoever; and the fact that the Government may have formulated, furnished, or in any way supplied the said drawings, specifications, or other data is not to be regarded by implication or otherwise as in any manner licensing the holder or any other person or corporation, or conveying any rights or permission to manufacture, use or sell any patented invention that may in any way be related thereto.

18040632002

Best Available

CATALOGED BY ASTIA 254472
AS AD NO.



Interim Report

I-A2049-12

AN ANALYTICAL AND EXPERIMENTAL
STUDY OF THE STABILITY OF EXTERNALLY-
PRESSURIZED, GAS-LUBRICATED
THRUST BEARINGS

by

L. Licht and H. G. Elrod, Jr.

February 1961

Prepared under

Contract Nonr-2342(00)
Task NR 061 - 113

Jointly Supported by

DEPARTMENT OF DEFENSE
ATOMIC ENERGY COMMISSION
MARITIME ADMINISTRATION
NATIONAL AERONAUTICS AND SPACE ADMINISTRATION

Administered by

OFFICE OF NAVAL RESEARCH
Department of the Navy

COPY NO.

THE FRANKLIN INSTITUTE
LABORATORIES FOR RESEARCH AND DEVELOPMENT
PHILADELPHIA PENNSYLVANIA

THE FRANKLIN INSTITUTE • *Laboratories for Research and Development*

Interim Report

I-A2049-12

AN ANALYTICAL AND EXPERIMENTAL
STUDY OF THE STABILITY OF EXTERNALLY-
PRESSURIZED, GAS-LUBRICATED
THRUST BEARINGS

by

I. Licht and H. G. Elrod, Jr.

Prepared under

Contract Nonr 2342(00)
Task NR 061-113

Jointly Supported by

DEPARTMENT OF DEFENSE
ATOMIC ENERGY COMMISSION
MARITIME ADMINISTRATION
NATIONAL AERONAUTICS AND SPACE ADMINISTRATION

Administered by

OFFICE OF NAVAL RESEARCH
Department of the Navy

Reproduction in Whole or in Part is Permitted
for any Purpose of The U S Government

FOREWORD

This report deals with both the theoretical and experimental phases of an investigation of the stability of externally-pressurized, gas-lubricated bearings.

The analysis, presented in Interim Report No. I-A2049-4, has been extended and complemented by additional material in Appendices 2 through 7 and is included in this report for the sake of completeness. Detailed descriptions of apparatus, instruments and experiments are given and are supplemented by 65 figures, containing graphs, drawings and photographic records.

The theoretical predictions of the present and of earlier analyses are compared with experimental results, areas of further research are suggested and recommendations are made for utilizing the results of the present investigation for design purposes.

ACKNOWLEDGEMENT

This research was performed under contract administered by the Office of Naval Research and supported jointly by the Department of Defense, Atomic Energy Commission and Maritime Administration. The authors are indebted to Captain W. T. Sawyer and Mr. S. W. Doroff, Office of Naval Research, for their assistance and the cooperation received in all phases of this investigation.

Professor D. D. Butler, whose counsel greatly contributed to the success of this undertaking, initiated and coordinated the research in gas lubrication at The Franklin Institute. — The Franklin Institute Laboratories, under the direction of Mr. F. L. Jackson, provided ideal conditions and atmosphere in which to carry out this project and the Friction and Lubrication Branch, headed by Mr. W. A. Shugarts, cooperated wholeheartedly in all phases of this investigation. The authors wish to thank Miss S. Goff, Mr. S. Mulanoski and Mr. C. Stevenson, who shared in the laborious numerical calculations, and Mr. L. McGinn and Mr. W. Ruegner, who were responsible for the programming of the computer. The meticulously detailed set of engineering drawings of the experimental apparatus is due to Mr. J. Kuehn. Mr. C. Bognar installed the apparatus and assisted in the course of the experiments.

The apparatus was manufactured by the Peter J. Salmon Company, Glenside, Pa., and the bearing surfaces were lapped by Dr. H. C. Stein of the Stein Seal Company, Philadelphia. Dr. B. Sternlicht, General Electric Laboratories, Schenectady, New York and Dr. W. Gross, International Business Machines Laboratories, San Jose, California and Dr. S. Ausman, Autonetics, Downey, California, provided useful technical information and offered constructive criticism.

To these people and many others not mentioned specifically, who contributed to the success of this work, the authors owe their gratitude.

TABLE OF CONTENTS

	Page
I. ABSTRACT	1
II. INTRODUCTION	2
1. Instabilities of Gas-Lubricated Bearings and Related Problems — Review of Pertinent Literature	2
2. Purpose and Outline of the Present Investigation	3
III. ANALYSIS	5
1. Derivation of Characteristic Equations	5
2. Stability Boundary — Evaluation of Critical (Limiting) Parameters	17
a. Rectangular Geometry	17
b. Circular Geometry	18
3. Discussion of Theoretical Results	21
4. Conclusions and Summary of Theoretical Results	23
IV. EXPERIMENTAL APPARATUS	24
1. Design of Experimental Apparatus	24
2. Instruments — Performance and Calibration	27
a. Air Gauges	27
b. Vibrometers — Primary and Auxiliary Probe Systems	29
c. Pressure Gauges, Flow Meters and Regulators	31
V. EXPERIMENTS	33
1. Static Tests	33
2. Preliminary Stability Experiments	35
3. Concluding Stability Experiments	39

THE FRANKLIN INSTITUTE - *Laboratories for Research and Development*

I-A2049-12

TABLE OF CONTENTS (Continued)

	Page
VI. DISCUSSION	44
1. Comparison of Analytical and Experimental Results	44
2. Remarks on the Relative Validity of Theoretical Assumptions and their Applicability to the Experimental Model	44
VII. CONCLUDING REMARKS AND RECOMMENDATIONS	49
VIII. BIBLIOGRAPHY	51
IX. NOMENCLATURE	56

LIST OF APPENDICES

Appendix 1. The Pressure Integral, \bar{p}	61
Appendix 2. Simplified Stability Analyses	64
Appendix 3. Rectangular Geometry - Tabulation of Calculated Results	71
Appendix 4. Circular Geometry - Determination of Critical Recess Depths, Tabulation of Calculated and Experimental Results	72
Appendix 5. The Periodic Charging and Discharging of a Variable - Volume Recess	81
Appendix 6. Derivation of the Dynamic Lubrication Equation	95
Appendix 7. Tabulation of Computer Solutions	103

LIST OF FIGURES

Figure No.	TITLE	Page
1.	Schematic Diagram of Bearing Geometries	151
2.	Approximations to Rectangular Geometry	152
3.	Critical Recess Depth vs. Pressure Parameter (Calculated) — Rectangular Geometry	153
4.	Determination of Critical Recess Depth — Circular Geometry (Equation 43b)	154
5.	Critical Recess Depth vs. Pressure Parameter (Calculated) — Circular Geometry	155
6.	Schematic Diagram of Dynamic Pressure Profiles with Reference to Present and Simplified Analyses	156
7.	Test Bearing Assembly	157
8.	Upper Thrust Plate	158
9.	Piston No. 1	159
10.	Piston No. 2	160
11.	Piston No. 3	161
12.	Nozzle Plate	162
13.	Shaft and Thrust Plate	163
14.	Journal (Guide) Bearing	164
15.	Journal Bearing Orifice	165
16.	Load-Deflection Characteristic of Guide Bearings	166
17.	Schematic Diagram of Air Supply System	167
18.	View of Test Apparatus, Instruments and Air Supply System	168
19.	View of Bearing Thrust Plates (1)	169
20.	View of Bearing Thrust Plates (2)	170
21.	Close View of Test Bearing Assembly	171
22.	Modified Piston No. 2 — Secondary Recess	172
23.	Nozzle Plates for Piston No. 3	173
24.	Primary Capacitance Probes and Probe Holders	174
25.	Calibration Fixtures and Auxiliary Probe	175
26.	Calculated (Approximate) Air Gauge Characteristics	176
27.	Calibration Curve — Air Gauge No. 1	177

LIST OF FIGURES (Continued)

Figure No.	TITLE	Page
28.	Calibration Curve — Air Gauge No. 2	178
29.	Calibration Curve — Air Gauge No. 1	179
30.	Schematic Diagram of Instruments for Vibration Detection and Measurement	180
31.	Frequency Response of Vibration Instruments	181
32.	Calibration Curve 1 — Primary Capacitance Probe	182
33.	Calibration Curve 2 — Primary Capacitance Probe	183
34.	Calibration Curve 3 — Primary Capacitance Probe	134
35.	Calibration Curve — Auxiliary Capacitance Probe	185
36.	Results of Thrust Plate Alignment Test	186
37.	Effect of Decrease in Recess Depth on Bearing Gap Width	187
38.	Variation of Load Capacity and/or Recess Pressure with Supply Pressure	188
39.	Bearing Mass Flow Rate vs. Supply Pressure (Constant Load = 472 lb)	189
40.	Bearing Gap Width vs. Supply Pressure (Constant Load = 472 lb)	190
41.	Bearing Reynolds Number vs. Supply Pressure (Constant Load = 472 lb)	191
42.	Bearing Mass Flow Rate and Reynolds Number vs. Supply Pressure (Constant Load = 222 lb)	192
43.	Bearing Gap Width vs. Supply Pressure (Constant Load = 222 lb)	193
44.	Critical Recess Depth vs. Supply Pressure — Effect of Decrease in Recess Depth for Single Nozzle Supply	194
45.	Mean Critical Recess Depth vs. Supply Pressure — Results of Constant Load and Constant Recess Pressure Tests (Modified Piston No. 2 and Single Nozzle Supply)	195
46.	Mean Critical Recess Depth vs. Supply Pressure — Hysteresis Effect (Modified Piston No. 2, Single Nozzle Supply and Open Pressure Tap)	196
47.	Critical Recess Depth vs. Supply Pressure — Effect of Resonance with Non-Isolated Test Stand (Twelve Nozzle Supply and Piston No. 3)	197
48.	Critical Frequency vs. Supply Pressure — Effect of Resonance with Non-Isolated Test Stand (Twelve Nozzle Supply and Piston No. 3)	198
49.	Critical Recess Depth vs. Supply Pressure — Effect of Resonance with Non-Isolated Test Stand (Reduced, 222 lb Load, Twelve Nozzle Supply and Piston No. 3)	199
50.	Determination of Natural Frequencies of Test Stand and Upper Thrust Plate	200

LIST OF FIGURES (Continued)

Figure No.	TITLE	Page
51.	Amplitude Growth of Auto-Oscillations in Approaching Stability Boundary ($P_s = 90.50$ psia).....	201
52.	Amplitude Growth of Auto-Oscillations in Approaching Stability Boundary ($P_s = 87.50$ psia).....	202
53.	Amplitude Growth of Auto-Oscillations in Approaching Stability Boundary ($P_s = 87.50$ psia).....	203
54.	Amplitude Growth of Auto-Oscillations in Approaching Stability Boundary ($P_s = 95.45$ psia).....	204
55.	Critical Recess Depth vs. Supply Pressure - Concluding Results (Twelve Nozzle Supply and Piston No. 3).....	205
56.	Critical Frequency vs. Supply Pressure - Concluding Results (Twelve Nozzle Supply and Piston No. 3).....	206
57.	Determination of Critical Frequencies (Bearing Mass = 6.477×10^{-2} lb-sec ² /in).....	207
58.	Determination of Critical Frequencies (Bearing Mass = 11.68×10^{-2} lb-sec ² /in).....	208
59.	Comparison of Amplitudes of Axial and Pitching Modes of Vibration	209

APPENDIX FIGURES

A1-1.	Pressure Profile and Comparison with Straight Line Approximation	63
A2-1.	Schematic Diagram of Bearing and Flexible Support	70
A4-1.	Determination of the Critical Recess Depth for $\alpha = 0.050$	78
A5-1.	Schematic Diagram of the Variable-Volume Bearing Recess	93
A5-2.	Amplitudes and Phase Relations of Pressure and Density in Variable-Volume Recess.....	94
A7-1.	Plot of Computer Solutions of Equations 40b for $\alpha = 0.093$	101

I. ABSTRACT

The subject of this investigation is the stability of externally-pressurized, gas-lubricated bearings. An analysis is made which treats the flow within the gas film on a distributed, rather than on a lumped parameter basis. Rectangular and circular bearing configurations are considered and the effect of several parameters on stability is investigated. Results of the present analysis are compared and contrasted with those obtained from earlier, simplified theories. The experimental program pursued here is guided by the analysis. An apparatus is designed, constructed and instrumented to provide for the variation of governing parameters and for the accurate determination of their critical values. Comparison of theory and experiment is made and the validity of theoretical assumptions, relative to the experimental model, is discussed.

II. INTRODUCTION

1. Instabilities of Gas-Lubricated Bearings and Related Problems — Review of Pertinent Literature

Recent advances in space, computer and nuclear technology have precipitated a renewed interest in gas lubrication. Gas bearings are being successfully incorporated in systems precluding the use of conventional lubricants and rolling elements. To quote contrasting examples of application — gas bearings have been used for small turbine rotors, driven and supported by hot exhaust gases, and also at very low temperatures in gas liquefaction machines. They have been employed as a method of gyroscope support in inertial guidance devices, as sensing elements in computers and as low-friction guides in accelerometers, dynamometers, vibration tables and torque measuring instruments. In nuclear reactors, gas bearings have provided a solution for sealed and isolated systems, in which radioactive gases furnish the only available lubrication medium.

Gas bearings may be broadly classified into two types:

- a. Self-acting bearings, in which the load capacity is induced through the relative motion of surfaces.
- b. Externally-pressurized bearings, which rely for their load capacity on an external pressure source.

One major difficulty encountered in applications of gas bearings is their susceptibility to self-excited vibrations. In unstable, self-acting bearings, the center of the rotating journal may either describe a closed path within the clearance circle, or follow a spiral path until surface contact and destruction take place. This type of instability, generally referred to in literature as "whirl", occurs also with incompressible lubricants, but appears to be particularly troublesome with gases. It has been the subject of numerous theoretical and experimental investigations [36, 37, 38, 39, 40, 41, 42, 43][†], but its mechanism is not yet fully understood.

The subject of the present investigation is an instability, associated with externally-pressurized bearings and sometimes referred to as "air" or "pneumatic hammer". It is frequently encountered in valves, regulators and other elements of pneumatic and hydraulic control systems [8, 9, 12, 13, 14, 15, 16], and is closely allied to such seemingly unrelated phenomena as self-excited vibrations of fuel injectors [17, 57] and pressure reducers [52], axial auto-oscillations of steam-cushioned turbine rotors [57] and violent pressure fluctuations in fan-ventilated chambers [18, 57]. The "pneumatic hammer" in externally-pressurized bearings is not associated with the steady, relative motion of surfaces, nor greatly influenced by it at moderate rotational speeds. If, however, the amplitude of vibration becomes excessively large in relation to the clearance, surfaces may contact and scoring, or complete destruction ensue. Moreover, even relatively minute auto-oscillations cannot be tolerated in applications involving sensitive instruments, or inertial guidance devices. On the other hand, unless the selection of geometrical and

[†] Numbers in brackets refer to bibliography.

fluid parameters is governed by, at least, a qualitative understanding of the physical mechanism of instability, it is probable that the bearing will be unstable in all, or part of the contemplated region of operation.

The phenomenon was observed in externally-pressurized thrust and journal bearings by Mueller [24], Wilfong [23], Comollet [19], Pigott and Macks [25], Fischer, Cherubini and Fuller [37], Robinson and Sterry [29], Graneck and Kerr [30], Allen, Stokes and Whitley [32] and many others. Raithe [28] established empirical criteria for specific bearing configurations used in inertial guidance. A number of investigators have speculated on likely causes of instability and have suggested remedial measures, based on observation, or on intuition [26, 30, 32, 33]. The first, rational explanations of the phenomenon in gas lubrication were given independently by Licht, Fuller and Sternlicht [5], who considered the instability of a simple, air-lubricated thrust bearing, and by Richardson [2, 3], who concentrated on the dynamics of externally-pressurized, air-lubricated journal bearings, assuming the initial eccentricity to be small and motion to be limited to a single degree of freedom. More recently, Licht [7] extended the analysis to multiple-rod journal bearings, assuming plane motion of the journal, initially in an eccentric equilibrium position. Roudelush [6] considered the stability of a circular thrust bearing and obtained digital computer solutions for the nonlinear, lumped, fluid-dynamic equations. His conclusions were in agreement with those based on linearized analyses, although computer solutions were necessarily limited to a number of specific cases.

The analyses referred to in the preceding paragraphs were of the lumped-parameter type and relied on arbitrary, a priori assumptions with regard to variation of pressure profile and flow in the bearing clearance. The objective in making these assumptions was to permit a simple formulation of the problem and to avoid the use of partial differential equations in the mathematical description of the fluid-dynamic phenomena occurring in the bearing clearance.

2. Purpose and Outline of the Present Investigation

Because of the large number of parameters which influence the stability of externally-pressurized bearings, and because of the complexity introduced through nonlinearity, the present investigation is restricted to a perturbation analysis. The limitation that perturbation analyses give necessary conditions of instability, not sufficient conditions of stability, is recognized, but linearization has frequently provided a good first approximation in the solution of fundamental problems of fluid dynamics. More specifically, analog and digital computer studies of pneumatic controls indicate that results obtained from linearized equations often compare very favorably with exact solutions [10, 52]. Some encouragement may also be derived from the fact that analog solutions of non-linear equations for a bearing using an incompressible lubricant, but geometrically identical with the model proposed in this investigation, were in good agreement with results obtained from their linearized equivalents [11].

Results of previous experiments, reported in reference [4], agreed only qualitatively with theoretical predictions of simplified analyses [4, 5]. It was felt that, although the simplified analyses explained the basic aspects of the physical mechanism of "pneumatic hammer" in gas bearings, the degree of simplification in formulating the problem was excessive. Richardson [2, 3] recognized that dynamic changes in pressure-profile depended on time rates of boundary

motion. In fact, a priori assumptions with regard to pressure-profile variation and mass continuity appear to have little justification, particularly for configurations in which the surface corresponding to the slot constitutes a large fraction of the total bearing area. Equally questionable are the results of simplified analyses, according to which stability is not influenced by the bearing mass [3, 5].†

In the theoretical part of the present investigation, while retaining the method of small perturbations and a number of simplifying assumptions, the nonsteady flow in the bearing clearance is treated on a continuous, rather than on a lumped basis. The fluid-dynamic phenomenon in the slot is described by a partial differential equation. The latter is required to satisfy the boundary condition at the outer bearing perimeter and to be compatible with the continuity equation for a centrally located, variable-volume recess, and also with the equation of motion of the bearing mass. Stability analyses are made for axial motion of parallel-surface thrust bearings. Rectangular and circular configurations†† are considered and stability boundaries are obtained to show the effect of several, important bearing parameters and to show how the results compare with those obtained from lumped-parameter theories.

In the experimental part of the present investigation, the bearing is circular and identical in geometry to the theoretical model. The surface bounded by the perimeter of a centrally-located, adjustable-volume recess, constitutes a small fraction of the total bearing area, in order to hinder the escape of fluid and magnify the trapping and squeezing effect in the slot. Provision is also made to vary the bearing mass without altering the load, in order to observe the influence of mass on stability.

† See also Appendix 2.

†† Schematics, drawings and photographs of actual thrust plates are shown in Figures 1, 7, 8, 13, 19 and 20.

III. ANALYSIS[†]

1. Derivation of Characteristic Equations

In what follows, equations are simultaneously developed for the rectangular and circular configurations shown in Figures 1a and 1b. Equations applicable to both geometries are denoted with *italic* numbers. Those denoted by the letter "a" refer to the rectangular geometry, while those denoted by the letter "b" refer to the circular geometry.

Equations (1) through (4) are those developed by G. I. Taylor and P. G. Saffman [1], who investigated compressibility effects at low Reynolds number. One case they considered consisted of two parallel discs, separated by a narrow air gap, when rotation was accompanied by small amplitude, forced vibration in the axial direction. In contrast, the present investigation concerns itself with the onset of self-excited oscillations. It differs also because, in the absence of rotation, fluid flow is induced by means of an external pressure source connected to an internal, variable-volume reservoir.

It is assumed that forces due to inertia are small compared with those due to viscous stresses, and that the pressure gradient in the transverse direction of the slot is negligible. The amplitude of oscillations in the anticipated frequency band width can be considered arbitrarily small in comparison with the magnitude of the gap width. The mean flow velocity in the annulus can then be obtained from the reduced Navier-Stokes equation and written as:

$$\bar{u} = - \frac{H^2}{12\mu} \frac{\partial P}{\partial x} \quad (1a)$$

$$\bar{u} = - \frac{H^2}{12\mu} \frac{\partial P}{\partial r} \quad (1b)$$

Since the dimension of the annulus separating the metallic surfaces is small in comparison with the linear dimension of the slot, it is reasonable to assume that conductivity prevents any appreciable variation in temperature and that the relation

$$\frac{P}{\rho} = \text{constant} \quad (2)$$

represents the thermodynamic process to a sufficient degree of approximation.

[†] Material contained in this section was presented at the 23rd National Conference of the Applied Mechanics Division, ASME, June 1960, and was published under the title "A Study of the Stability of Externally Pressurized Gas Bearings", L. Licht and H. Lohm, Jr., *Journal of Applied Mechanics*, Vol. 27, No. 2, June 1960, pp. 250-258.

The continuity equation then becomes:

$$\frac{\partial}{\partial t} (\rho H) + \frac{\partial}{\partial x} (\rho H \bar{u}) = 0 \quad (3a)$$

$$\frac{\partial}{\partial t} (\rho H) + \frac{1}{r} \frac{\partial}{\partial r} (r \rho H \bar{u}) = 0 \quad (3b)$$

Substitution of equations (1) and (2) in the continuity equation (3) yields a dynamic lubrication equation:

$$\left\{ \begin{aligned} \frac{\partial}{\partial x} P \left(\frac{\partial P}{\partial x} \right) &= \frac{12\mu}{H^3} \frac{\partial}{\partial t} (PH) \\ \frac{1}{r} \frac{\partial}{\partial r} \left(r P \frac{\partial P}{\partial r} \right) &= \frac{12\mu}{H^3} \frac{\partial}{\partial t} (PH) \end{aligned} \right. \quad (4a)$$

$$(4b)$$

The basic assumptions and the derivation of these equations are given in Appendix 6.

Equation (4) must satisfy the boundary condition

$$P(R, t) = P_{at} \quad (5b)$$

$$P(X, t) = P_{at} \quad (5b)$$

and be compatible with the equation of motion†:

$$\left\{ \begin{aligned} m \frac{d^2 H}{dt^2} &= 2X_r (P_r - P_{ro}) + 2 \int_{X_r}^X (P - P_o) dx + F(t) \\ m \frac{d^2 H}{dt^2} &= \pi R_r^2 (P_r - P_{ro}) + 2 \pi \int_{R_r}^R (P - P_o) r dr + F(t) \end{aligned} \right. \quad (6a)$$

$$(6b)$$

in which $F(t)$ is the excitation function.

† The effect of external damping is negligibly small

In addition, the continuity equation of the variable-volume recess is as follows:

$$\frac{dM_r}{dt} = \dot{w}_1 - \dot{w}_2 \quad (7)$$

In expressing the quantities on the right hand side of equation (7), it is assumed that the flow can be treated as quasi-steady. Theoretical and experimental investigations of pulsating flow through orifices were conducted by Schlicht-Grunow [46], who discussed the conditions under which instantaneous flow rates could be evaluated from steady-flow equations and gave criteria for their applicability. To express the left hand side of equation (7), it is necessary to describe an extremely complex process, associated with simultaneous charging and discharging of a variable-volume container. In the present analysis it will be assumed that fluid properties throughout the recess volume are uniform at any instant of time and that the process may be adequately described by the pressure-density relation $P/\rho^{\gamma} = \text{constant}$. The quasi-static charging and discharging of an adiabatic container, for example, may be considered as isentropic to the first degree of approximation, perfect mixing of entering gas being assumed. Experiments conducted by Shearer [9] and Skinner and Wagner [56] also indicate that, for relatively rapid rates of charging and discharging, the assumption $P/\rho^{\gamma} = \text{constant}$ is reasonable. The effect of wave propagation, heat transfer and irreversibilities, associated with the processes of charging and discharging of fixed and variable volume containers, cannot always be neglected [51, 53, 54, 55]. However, assumptions identical with those made in implementing equation (7) have been frequently and successfully employed in related problems, in the field of pneumatic controls and regulators [9, 14, 52]. Consequently, the quantities appearing in equation (7) are expressed as follows:

$$\dot{w}_1 = 2 \left(\frac{\pi d_N^2}{4} \right) \left[\frac{\gamma}{RT_0} \left(\frac{2}{\gamma+1} \right)^{\frac{\gamma+1}{\gamma-1}} (P_s P_r - P_r^2) \right]^{1/2} \quad (8)^{\dagger}$$

$$\left\{ \begin{array}{l} \dot{w}_2 = - \frac{11^3}{6\mu} \left(\rho \frac{\partial P}{\partial x} \right)_{x_r} \\ \dot{w}_2 = - \frac{\pi H^3}{6\mu} \left(r \rho \frac{\partial P}{\partial r} \right)_{r_r} \end{array} \right. \quad (9a) \quad (9b)$$

[†] The flow through the supply nozzle can be approximated closely by a quadrant of an ellipse whenever P_r/P_s is considerably above the critical-pressure ratio. This is Fliegner's approximation, and is convenient for computational purposes.

$$\left\{ \begin{array}{l} M_r = 2X_r(\delta + 11)\rho_r \\ M_r = \pi R_r^2(\delta + 11)\rho_r \end{array} \right. \quad \begin{array}{l} (10a) \\ (10b) \end{array}$$

while the pressure-density relation for the recess volume is taken as:

$$\left(\frac{\rho_r}{\rho_{ro}}\right)^{\gamma} = \frac{P_r}{P_{ro}} \quad (11)$$

In the next step the perturbation quantities

$$P - P_o = p$$

$$P_r - P_{ro} = p_r \quad (12)$$

$$H - H_o = h$$

and their derivatives are introduced. Neglecting their squares and cross products as quantities of higher order, we obtain instead of equations (4), (6) and (7) a set of corresponding expressions.

The nonlinear, partial differential equation (4) is replaced by one which is linear, but contains variable coefficients.

Thus in terms of perturbation quantities we have:

$$\left\{ \begin{array}{l} \frac{\partial^2 p}{\partial x^2} + \left(\frac{2P_o'}{P_o}\right) \frac{\partial p}{\partial x} + \left(\frac{P_o''}{P_o}\right) p = \frac{12\mu}{H_o^2} \left(\frac{1}{P_o} \frac{\partial p}{\partial t} + \frac{1}{H_o} \frac{dh}{dt}\right) \\ \frac{\partial^2 p}{\partial r^2} + \left(\frac{2P_o'}{P_o} + \frac{1}{r}\right) \frac{\partial p}{\partial r} + \left(\frac{P_o''}{P_o} + \frac{1}{r} \frac{P_o'}{P_o}\right) p = \frac{12\mu}{H_o^2} \left(\frac{1}{P_o} \frac{\partial p}{\partial t} + \frac{1}{H_o} \frac{dh}{dt}\right) \end{array} \right. \quad \begin{array}{l} (13a) \\ (13b) \end{array}$$

From equation (6) we obtain,

$$\left\{ \begin{aligned} m \frac{d^2 h}{dt^2} &= 2X_r p_r + 2 \int_{X_r}^X p dx + f(t) \end{aligned} \right. \quad (14a)$$

$$\left\{ \begin{aligned} m \frac{d^2 h}{dt^2} &= \pi n_r^2 p_r + 2\pi \int_{R_r}^R p r dr + f(t) \end{aligned} \right. \quad (14b)$$

in which $f(t)$ is the disturbance,

equation (7) reduces to

$$\left\{ \begin{aligned} K_1 \frac{dh}{dt} - K_4 h &= (K_3 + K_5) p_r + K_6 \frac{\partial p_r}{\partial r} - K_2 \frac{\partial p_r}{\partial t} \end{aligned} \right. \quad (15a)$$

$$\left\{ \begin{aligned} C_1 \frac{dh}{dt} - C_4 h &= (C_3 + C_5) p_r + C_6 \frac{\partial p_r}{\partial r} - C_2 \frac{\partial p_r}{\partial t} \end{aligned} \right. \quad (15b)$$

in which the coefficients K_i and C_i represent the quantities listed in the following:

$$\left. \begin{aligned} K_1 &= \left(\frac{\partial M_r}{\partial h} \right)_0 = \frac{2X_r P_{ro}}{8T_o} \\ K_2 &= \left(\frac{\partial M_r}{\partial P_r} \right)_0 = \frac{2X_r H_o}{\gamma K T_o} \left(\frac{\partial}{\partial H_o} + 1 \right) \\ K_3 &= \left(\frac{\partial W_1}{\partial P_r} \right)_0 = \frac{W_o}{2P_{ro}} \left(\frac{\frac{P_s}{P_{ro}} - 2}{\frac{P_s}{P_{ro}} - 1} \right) \\ K_4 &= \left(\frac{\partial W_2}{\partial H} \right)_0 = -\frac{3W_o}{H_o} \\ K_5 &= - \left(\frac{\partial W_2}{\partial P} \right)_0 = -\frac{W_o}{P_{ro}} \\ K_6 &= - \left(\frac{\partial W_2}{\partial \left(\frac{\partial P}{\partial x} \right)} \right)_0 = -\frac{2P_{ro} W_o}{A_o} \end{aligned} \right\} \quad (16a)$$

in which

$$P_o(x) = [P_o^2 + A_o(x - X_r)]^{1/2}$$

$$A_o = -\frac{P_{ro}^2 - P_{st}^2}{X - X_r}$$

$$\left. \begin{aligned}
 C_1 &= \left(\frac{\partial M_r}{\partial H} \right)_0 = \frac{\pi R_r^2 P_{ro}}{RT_0} \\
 C_2 &= \left(\frac{\partial M_r}{\partial P_r} \right)_0 = \frac{\pi R_r^2 H_0}{\gamma k T_0} \left(\frac{\delta}{H_0} + 1 \right) \\
 C_3 &= \left(\frac{\partial W_1}{\partial P_r} \right)_0 = \frac{W_0}{2 P_{ro}} \left(\frac{\frac{P_s}{P_{ro}} - 2}{\frac{P_s}{P_{ro}} - 1} \right) \\
 C_4 &= - \left(\frac{\partial W_2}{\partial H} \right)_0 = - \frac{3 W_0}{H_0} \\
 C_5 &= - \left(\frac{\partial W_2}{\partial P} \right)_{r=R_r} = - \frac{W_0}{P_{ro}} \\
 C_6 &= - \left(\frac{\partial W_2}{\partial \left(\frac{\partial P}{\partial r} \right)} \right)_{r=R_r} = - \frac{2 R_r P_{ro} W_0}{B_0}
 \end{aligned} \right\} (16b)$$

in which

$$P_0(r) = \left(P_{ro}^2 + B_0 \log_e \frac{r}{R_r} \right)^{1/2}$$

$$B_0 = - \frac{P_{ro}^2 - P_{at}^2}{\log_e \frac{R}{R_r}}$$

Solutions of equation (13) must satisfy equations (14) and (15) as well as the boundary condition

$$\begin{cases} p(X, t) = 0 & (17a) \\ p(R, t) = 0 & (17b) \end{cases}$$

The first space derivative in equation (13) can be eliminated by means of the following substitution:

$$\begin{cases} p = \frac{v}{P_0} = \frac{v}{z^{1/2}} & (13a) \\ p = \frac{v}{r^{1/2} P_0} & (18b) \end{cases}$$

Introducing the new variable v into equations (13), (14) and (15) we take the Laplace transform under the assumption of initial rest conditions.

Then with

$$\bar{v}_1(s) = \bar{V} = \int_0^\infty v e^{-st} dt$$

$$\bar{h}_1(h) = \bar{h} = \int_0^\infty h e^{-st} dt$$

$$\bar{v}_1(f) = \bar{f} = \int_0^\infty f e^{-st} dt$$

equation (13) transforms to:

$$\bar{V}'' - \frac{\epsilon s}{z^3} \bar{V} = \epsilon s z^{1/2} \frac{\bar{h}}{H_0} \quad (19a)$$

$$\bar{V}'' + \left(\frac{1}{4r^2} - \frac{\eta s}{P_0} \right) \bar{V} = \eta s r^{1/2} P_0 \frac{\bar{h}}{H_0} \quad (19b)$$

in which

$$\epsilon = \frac{12\mu}{H_0^2 A_0^2} = \frac{12\mu}{H_0^2} \left(\frac{X - X_r}{P_{ro}^2 - P_{at}^2} \right)^2 \quad (20a)$$

$$\eta = \frac{12\mu}{H_0^2} \quad (20b)$$

Equation (14) transforms to:

$$\left\{ \begin{aligned} ms^2 \frac{\bar{h}}{H_0} - \frac{2X_r}{H_0 P_{ro}} (\bar{V})_{r_{ro}} + \frac{2(X - X_r)}{H_0 (P_{ro}^2 - P_{at}^2)} \int_{r_{ro}^2}^{P_{at}^2} \frac{\bar{V}}{z^{3/2}} dz = \bar{f}(s) \end{aligned} \right. \quad (21a)$$

$$\left\{ \begin{aligned} ms^2 \frac{\bar{h}}{H_0} - \frac{\pi P_r^{3/2} (\bar{V})_{R_r}}{H_0 P_{ro}} - \frac{2\pi}{H_0} \int_{R_r}^{R} \frac{\bar{V}_r^{1/2}}{r'} dr = \bar{f}(s) \end{aligned} \right. \quad (21b)$$

Equation (15) transforms to:

$$\left\{ \begin{aligned} (sK_1 - K_4) \frac{\bar{h}}{H_0} + (sK_2 - K_3) \frac{(\bar{V})_{P_{ro}^2}}{H_0 P_{ro}^2} - \frac{2P_{ro}}{H_0} K_5 \left(\frac{\partial \bar{V}}{\partial z} \right)_{P_{ro}^2} &= 0 \end{aligned} \right. \quad (22a)$$

$$\left\{ \begin{aligned} (sC_1 - C_4) \frac{\bar{h}}{H_0} + \left(sC_2 - C_3 + C_5 \frac{P_{ro}^2}{B_0} \right) \frac{(\bar{V})_{R_r}}{H_0 R_r^2 P_{ro}} - \frac{2R_r^2 P_{ro}}{B_0 H_0} C_5 \left(\frac{\partial \bar{V}}{\partial r} \right)_{R_r} &= 0 \end{aligned} \right. \quad (22b)$$

in which the terms K_5 and C_5 have been replaced by means of the identity

$$\left\{ \begin{aligned} K_6 &= \frac{2P_{ro}^2}{A_0} K_5 \end{aligned} \right. \quad (23a)$$

$$\left\{ \begin{aligned} C_6 &= \frac{2R_r P_{ro}^2}{B_0} C_5 \end{aligned} \right. \quad (23b)$$

Finally, the boundary condition (17) transforms to

$$\left\{ \begin{aligned} \bar{V}(P_{at}^2, s) &= 0 \end{aligned} \right. \quad (24a)$$

$$\left\{ \begin{aligned} \bar{V}(R, s) &= 0 \end{aligned} \right. \quad (24b)$$

Furthermore, by integrating equation (15) between the appropriate limits, we can replace the integral in equation (21). For this purpose we have:

$$\left\{ \begin{aligned} \int_{P_{ro}^2}^{P_{at}^2} \frac{\bar{V}}{z^2} dz &= \frac{2}{3} (P_{ro}^3 - P_{at}^3) \frac{\bar{h}}{H_0} - \frac{1}{\epsilon s} \left[\left(\frac{\partial \bar{V}}{\partial z} \right)_{P_{ro}^2} - \left(\frac{\partial \bar{V}}{\partial z} \right)_{P_{at}^2} \right] \end{aligned} \right. \quad (25a)$$

$$\left\{ \begin{aligned} \int_{R_r}^R \frac{\bar{V}}{r^2} dr &= -\frac{\bar{h}}{H_0} - \frac{1}{7s} \left[R_r^2 \left(\frac{\partial \bar{V}}{\partial r} \right)_{R_r} - R^2 \left(\frac{\partial \bar{V}}{\partial r} \right)_R - \frac{(\bar{V})_{R_r}}{2R_r} \right] \end{aligned} \right. \quad (25b)$$

in which

$$c = \int_{R_0}^R P_0(r) dr \quad (26b)$$

The for z -ing integral is expressed explicitly in Appendix 1.

A particular solution of equation (19) is:

$$\begin{cases} \bar{V}_p = -\frac{\bar{h}}{H_0} z & (27a) \end{cases}$$

$$\begin{cases} \bar{V}_n = -\frac{\bar{h}}{H_0} r^{-1} I_0^2(r) & (27b) \end{cases}$$

If v_I and v_{II} are independent solutions which satisfy the homogeneous part of the differential equation (19), then

$$\begin{cases} Q(z, z) = \frac{v_I(z)v_{II}(z) - v_I(z)v_{II}(z)}{v_I(p_{to}^2)v_{II}(p_{at}^2) - v_I(p_{at}^2)v_{II}(p_{to}^2)} & (28a) \end{cases}$$

$$\begin{cases} Q(r, r) = \frac{v_I(r)v_{II}(r) - v_I(r)v_{II}(r)}{v_I(R)v_{II}(R) - v_I(R)v_{II}(R)} & (28b) \end{cases}$$

are also solutions having the following properties:

$$\left. \begin{aligned} Q(z, z) &= 0 \\ Q(p_{to}^2, p_{at}^2) &= -Q(p_{at}^2, p_{to}^2) = 1 \\ \frac{\partial Q}{\partial z}(z, z) &= \text{constant}^\dagger \end{aligned} \right\} \quad (29)$$

[†] The Wronskian of second-order differential equations having the form $y'' + f(x)y = 0$ is a constant.

$$\left. \begin{aligned} Q(r, r) &= 0 \\ Q(P_r, P) &= -Q(P, R_r) = 1 \\ \frac{\partial Q}{\partial r}(r, r) &= \text{constant}^{\dagger} \end{aligned} \right\} \quad (29b)$$

The solution of (19) which satisfies the boundary condition (24) can then be written as:

$$\bar{V} = \bar{A}Q(P_{at}^2, z) + \frac{\bar{h}}{H_0} \left[P_{at}^2 Q(P_{to}^2, z) - z \right] \quad (30a)$$

$$\bar{V} = \bar{A}Q(R, r) + \frac{\bar{h}}{H_0} \left[R^{1/2} P_{at}^2 Q(R_r, r) - r^{1/2} P_0^2(r) \right] \quad (30b)$$

in which $\bar{A}(s)$ and $\bar{h}(s)$ are determined from equations (21) and (22).

Using equation (25) and substituting into equation (22) the boundary values of \bar{V} and its derivatives obtained by differentiation of equation (30), we have at our disposal two simultaneous equations for the determination of $\bar{A}(s)$ and $\bar{h}(s)$. The "two by two" determinant formed from the coefficients of the homogeneous parts of these equations is then set equal to zero. The location in the complex plane of roots of this characteristic equation determines the stability of the bearing. The characteristic determinant referred to in the foregoing is as follows:

[†] The Wronskian of second-order differential equations having the form $y'' + f(x)y = 0$ is a constant.

0 (31a)

$\frac{m H_0}{2 N_5} \left(\frac{P_{ro}^2 - P_{at}^2}{V_r - 1} \right) s^3 + \frac{2}{3} (P_{ro}^2 - P_{at}^2) s$ $- \left[P_{ro}^2 \frac{\partial}{\partial \zeta} (P_{at}^2, P_{ro}^2) + P_{at}^2 \frac{\partial}{\partial \zeta} (P_{ro}^2, P_{at}^2) \right]$ $- (P_{ro}^2 + P_{at}^2) \frac{\partial}{\partial \zeta} (z, z)$	$- P_{ro} \left(\frac{P_{ro}^2 - P_{at}^2}{V_r - 1} \right) s$ $+ \left[P_{ro}^2 \frac{\partial}{\partial \zeta} (P_{at}^2, P_{ro}^2) + P_{at}^2 \frac{\partial}{\partial \zeta} (P_{ro}^2, P_{at}^2) \right]$	$\frac{K}{2 N_5} \frac{V_0}{P_{ro}} s - \frac{V_0}{2 K_3} \frac{H_0}{P_{ro}}$ $+ \left[P_{ro}^2 \frac{\partial}{\partial \zeta} (P_{at}^2, P_{ro}^2) - P_{at}^2 \frac{\partial}{\partial \zeta} (z, z) + 1 \right]$	$\frac{K_2}{2 K_3} s - \frac{K_2}{2 K_3} + \left[P_{ro}^2 \frac{\partial}{\partial \zeta} (P_{at}^2, P_{ro}^2) \right]$
--	--	--	--

0 (31b)

$\frac{n H_0 \eta}{2 \pi P_{at}^2} s^3 + \frac{\eta \delta s}{P_{at}^2} - \left\{ R \frac{\partial Q}{\partial \rho} (R, R) \right.$ $+ \left(\frac{P_{ro}}{P_{at}} \right)^2 R_r \frac{\partial Q}{\partial \rho} (R, R_r) - \left[\left(\frac{P_{ro}}{P_{at}} \right)^2 + 1 \right] \times$ $\times R_r^{\frac{1}{2}} R^{\frac{1}{2}} \frac{\partial Q}{\partial \rho} (r, r) + \frac{1}{2} \left[\left(\frac{P_{ro}}{P_{at}} \right)^2 - 1 \right] \left. \right\}$	$\frac{P_{ro} R_r^2 \eta}{2 P_{at}^2} s + \left\{ \left(\frac{P_{ro}}{P_{at}} \right)^2 R_r \frac{\partial Q}{\partial \rho} (r, R_r) \right.$ $- \left(\frac{P_{ro}}{P_{at}} \right)^2 R_r^{\frac{1}{2}} R^{\frac{1}{2}} \frac{\partial Q}{\partial \rho} (r, r) + \frac{1}{2} \left(\frac{P_{ro}}{P_{at}} \right)^2 \left. \right\}$
$- \frac{C_1}{2 C_5} \left(\frac{H_0}{P_{ro}} \right) \frac{\left(\frac{P_{ro}}{P_{at}} \right)^2 - 1}{\log_e \frac{R}{R_r}} s + \frac{C_4}{2 C_5} \left(\frac{H_0}{P_{ro}} \right) \frac{\left(\frac{P_{ro}}{P_{at}} \right)^2 - 1}{\log_e \frac{R}{R_r}} \frac{R}{R_r}$ $+ \left(\frac{P_{ro}}{P_{at}} \right)^2 R_r \frac{\partial Q}{\partial \rho} (R, R_r) - R_r^{\frac{1}{2}} R^{\frac{1}{2}} \frac{\partial Q}{\partial \rho} (r, r)$ $+ \frac{1}{2} \left(\frac{P_{ro}}{P_{at}} \right)^2 \frac{\left(\frac{P_{ro}}{P_{at}} \right)^2 - 1}{\log_e \frac{R}{R_r}} \left. \right\}$	$\frac{C_2}{2 C_5} \frac{\left(\frac{P_{ro}}{P_{at}} \right)^2 - 1}{\log_e \frac{R}{R_r}} s - \frac{C_3}{2 C_5} \frac{\left(\frac{P_{ro}}{P_{at}} \right)^2 - 1}{\log_e \frac{R}{R_r}} \frac{R}{R_r}$ $- \left\{ \left(\frac{P_{ro}}{P_{at}} \right)^2 R_r \frac{\partial Q}{\partial \rho} (R, R_r) + \frac{1}{2} \left(\frac{P_{ro}}{P_{at}} \right)^2 \right\}$

2. Stability Boundary — Evaluation of Critical (Limiting) Parameters

Further progress in the analysis depends on a knowledge of the solutions y_I and y_{II} of the homogeneous part of equation (19). Even with such knowledge the location of roots in the complex plane of the characteristic equation (31) might be very involved. Our interest lies in assessing the limiting values of certain bearing parameters which influence stability. Within limits of applicability of our equations, we are guided in the expected range of their magnitudes by results obtained by means of a simplified analysis summarized in Appendix 2. Different approaches were employed for the rectangular and circular geometries and these are described in what follows:

a. Rectangular Geometry

The homogeneous part of equation (19a) is

$$y'' - \epsilon s z^{-1/2} y = 0 \quad (32a)$$

Two independent solutions, which involve Bessel functions of order $\pm 2/3$, can be written as [60]:

$$y_{I,II} = z^{1/2} J_{\pm 2/3} \left(\frac{4}{3} z^{3/4} i \sqrt{\epsilon s} \right) \quad (33a)$$

in which $+2/3$ corresponds to I and $-2/3$ to II.

The series representing the Bessel function $J_\nu(2i\lambda^{1/2})$ can be written as [61]:

$$J_\nu(2i\lambda^{1/2}) = (i\lambda^{1/2})^\nu \left[\frac{1}{\Gamma(\nu+1)} + \frac{\lambda}{1!\Gamma(\nu+2)} + \frac{\lambda^2}{2!\Gamma(\nu+3)} + \dots \right] \quad (34a)$$

With

$$\nu = \pm \frac{2}{3} \quad \text{and} \quad 2i\lambda^{1/2} = \frac{4}{3} z^{3/4} i \epsilon s$$

the first four terms of the expansion of y_I and y_{II} become

$$y_I = \frac{\left(\frac{2}{3} i \sqrt{\epsilon s} \right)^{2/3}}{\Gamma\left(\frac{2}{3}\right)} \left[\frac{3}{2} z + \frac{2}{5} z^{5/2} (\epsilon s) + \frac{1}{30} z^{8/2} (\epsilon s)^2 + \frac{2}{1485} z^{11/2} (\epsilon s)^3 \right] \quad (35a)$$

$$y_{II} = - \frac{\left(\frac{2}{3} i \sqrt{\epsilon s}\right)^{-2/3}}{\Gamma\left(\frac{1}{3}\right)} \left[1 + \frac{4}{3} z^{3/2} (\epsilon s) + \frac{2}{9} z^{6/2} (\epsilon s)^2 + \frac{8}{567} z^{9/2} (\epsilon s)^3 \right] \quad (36a)$$

These truncated series are then substituted into the expression $Q(z, \zeta)$ in (25a) and the derivative $(\partial Q / \partial \zeta)(z, \zeta)$ evaluated with z and ζ assuming the boundary values of P_{ro}^2 and P_{at}^2 in the order indicated in the components of the characteristic determinant (31a). In forming the expressions for the afore-mentioned derivatives of Q , we retain in all subsequent multiplications, divisions, and so on, terms of order s^3 and lower. The assumption that higher powers in s may be neglected, because of the relative smallness of their coefficients, is justified post factum by noting the magnitude of the complex-conjugate roots $s = \pm i\omega$ of the characteristic cubic to which the determinant (31a) is thus reduced. The coefficients of this cubic and those obtained by means of the simplified analysis in Appendix 2 are not the same. The effect of this difference in results is best illustrated by reference to Figure 3 and the table of results in Appendix 3.

b. Circular Geometry

In this case computer solutions for a set of discrete values of $s = i\omega$ on the axis of the imaginaries were obtained. The probable range of values for ω was dictated by predictions based on the simplified analysis and by taking into account the difference in the results of the two analyses for the rectangular case. Stability was assessed from physical conditions rather than proved. If we write

$$\xi = \frac{r}{R_r}; \quad \sigma = \frac{12\mu\omega R_r^2}{P_{ro} H_o^2}; \quad s = i\omega; \quad \beta = \frac{1 - \left(\frac{P_{at}}{P_{ro}}\right)^2}{\log_e \frac{R}{R_r}}$$

then the homogeneous part of equation (19b) becomes

$$y'' + \left[\frac{1}{4\xi^2} - \frac{i\sigma}{(1 - \beta \log_e \xi)^{1/2}} \right] y = 0 \quad (37b)$$

the solutions of which

$$y_{II} = \phi_{II}(\xi) + i\psi_{II}(\xi) \quad (38b)$$

satisfy the conveniently chosen boundary conditions

$$\begin{aligned} y_I(1) &= 1; \quad y_I'(1) = 0 \\ y_{II}(1) &= 0; \quad y_{II}'(1) = 1 \end{aligned} \quad (39b)$$

The set of equations corresponding to (34b) is

$$\begin{aligned} \phi'' + \frac{c}{4\xi^2} &= -\frac{\alpha\psi}{(1-\beta \log_e \xi)^{1/2}} \\ \psi'' + \frac{\psi}{4\xi^2} &= \frac{\alpha\phi}{(1-\beta \log_e \xi)^{1/2}} \end{aligned} \quad (40b)$$

and the boundary conditions (36b) become

$$\begin{aligned} \phi_I(1) &= 1; \quad \phi_I'(1) = 0 \\ \phi_{II}(1) &= 0; \quad \phi_{II}'(1) = 1 \\ \psi_I(1) &= \psi_I'(1) = \psi_{II}(1) = \psi_{II}'(1) = 0 \end{aligned} \quad (41b)$$

Solutions of equations (40b), satisfying the conditions (41b) were obtained for a fixed value of β and a set of values of the parameter

$$\alpha = \frac{12\mu\omega R_r^2}{P_{ro} H_o^2}$$

by means of a digital computer. Those shown in Figure A7-1, Appendix 7, correspond to the value of $\alpha = 0.093$.

We are now in a position to express numerically the derivatives

$$\begin{aligned}\frac{\partial Q}{\partial P}(P, R) &= \frac{\phi_I'(R) + i \psi_I'(R)}{\phi_{II}(R) + i \psi_{II}(R)} \\ \frac{\partial Q}{\partial P}(P_r, R) &= \frac{\phi_{II}'(R) + i \psi_{II}'(R)}{\phi_{II}(R) + i \psi_{II}(R)} \\ \frac{\partial Q}{\partial P}(r, r) &= \frac{1}{\phi_{II}(R) + i \psi_{II}(R)}\end{aligned}\quad (42b)$$

for discrete values of α .

Let the bearing geometry and the parameters P_{at} , P_{ro} , T_o , γ and μ be specified. One may then express the gap width, H_o , as a function of the supply pressure, P_s , by simply equating the outflow through the slot and the inflow through the nozzle. When explicit expressions are substituted for quantities which constitute the elements of the determinant (31b) and α is also specified, the only undetermined parameters are the recess depth, δ , and the supply pressure, P_s . In fact, the characteristic equation assumes the form:

$$a [\delta - g_1(\alpha, P_s)] - ib [\delta - g_2(\alpha, P_s)] = 0 \quad (43b)$$

in which a and b are numerical constants. Therefore, given α , the problem reduces to finding specific values of P_s and δ , for which the real and imaginary parts of equation (43b) vanish simultaneously, e.g.,

$$\delta - g_1 = g_2 = \delta_c \quad (44b)$$

The experimental counterpart of this procedure is to maintain the ambient and recess pressures constant and to set the gap width by varying the supply pressure. The recess depth is then increased and its value on the threshold of instability is noted.

Critical recess depths and supply pressures were determined by trial and error. The method is illustrated by a numerical example in Appendix 4, and in the corresponding Figure A4-1 for $\alpha = 0.050$. A plot of g_1 and g_2 against P_s , showing the points of intersection of loci corresponding to $\alpha = 0.093$, is contained in Figure 4. Results of the present analysis are shown and compared with those based on the lumped-parameter theory in Figure 5.

A. Discussion of Theoretical Results

The effect of varying several important parameters on the stability of the rectangular bearing is shown in Figure 3. Here one finds reasonably good agreement between results based on the distributed and lumped-parameter theories, although the latter theory tends to predict values of allowable recess depth which are either conservative, when the pressure drop across the supply nozzle is relatively small, or slightly optimistic, when the pressure difference is increased. The agreement is particularly good for values of the pressure parameter between 0.10 and 0.14, that is for pressure differences in the order of 10 psi.

It is seen that when the recess width is decreased by a factor of two, the allowable recess depth is nearly doubled, so that the critical recess volume remains essentially unaffected by a 12.5 percent increase in slot length. (Compare curves I and II in Figure 3.) Values of allowable recess depth, approximately twice as large again, may be obtained if the supply nozzle diameter is increased by a factor of 3. (Compare curves II and III in Figure 3.)

It is appropriate to remark at this point that decreasing the recess area and increasing the supply nozzle diameter have the adverse effect of lowering the load capacity and static stiffness of the bearing, so that stabilization is often a compromise in the selection of important design parameters.

A number of calculations were also carried out in order to investigate the effect of bearing mass on stability. An increase in mass by a factor of ten showed that the effect was generally negligible for those rectangular geometries which were considered. The effect was greatest for the configuration corresponding to curve II, Figure 3, characterized by a relatively long slot and a relatively small supply nozzle. At a value of the pressure parameter of approximately 0.04, for example, the tenfold increase in mass had the effect of reducing the allowable recess depth by 7.5 percent.

On the other hand, as shown in Figure 5, the mass had a significant effect in the case of the circular bearing geometry, particularly at low values of the pressure parameter. At $P_s - P_{ro}/P_o = 0.14$, for example, an increase in mass by a factor of 3.25 resulted in a 50 percent decrease in the allowable recess depth. The deviation of results based on lumped-parameter theories was also significantly greater than for the rectangular configurations, particularly in the case of the smallest mass. (Curve III, Figure 5.)

The smaller the mass of a bearing, the greater the rate of response of the bearing tends to become. When the response rate is large, the gas in each volume element becomes partly trapped, rather than squeezed out. This, in turn, causes the film "stiffness" in the annulus to increase and permit greater "compliance" of a deeper recess without compromising stability. When the mass is large, the changes in pressure and density approach the quasi-static condition, and the foregoing effects are reversed. These two cases are illustrated diagrammatically and in an exaggerated manner in Figure 6 for the conditions of a heavily (a) and lightly (b) loaded bearing. In the circular bearing the surface corresponding to the annulus constitutes 96 percent of the total area and the slot converges toward the recess periphery where the gas density is highest. If the boundary motion is relatively rapid, the gas cannot readily escape from the slot.

Because of this, the influence of mass on stability is more pronounced in the case of the circular bearing, as may be observed by comparing curves I, II and III in Figure 5. It can also be seen, that, as the mass increases, the agreement between results of the present and simplified analyses improves, because changes occur nearly quasi-statically.

The simplified, lumped-parameter analysis is based on assumptions of quasi-static changes in pressure and gas content and does not properly account for the effect of mass on the rate of response. In fact, when the inequality (A2-7), Appendix 2, is written explicitly:

$$\left(\frac{\lambda_1 + \lambda_5}{\lambda_2} \right) \left(\frac{\lambda_6}{m} \frac{\lambda_1}{\lambda_2} \right) > \left(\frac{\lambda_6}{m} \frac{\lambda_4}{\lambda_2} \right) \quad (45)$$

the quantity m cancels in the denominators on both sides, so that the stability condition is independent of mass. Though perhaps deficient from the quantitative point of view, the simplified, lumped-parameter analysis, Appendix 2, does give explicit relationships between other parameters which affect the stability of the bearing. The inequality (A2-8), for example, can be written as follows:

$$\frac{\left(\frac{\partial M}{\partial H} \right)_0}{\left(\frac{\partial M}{\partial P_r} \right)_0} > \frac{\frac{\partial}{\partial H} (W_2 - W_1)_0}{\frac{\partial}{\partial P_r} (W_2 - W_1)_0} \quad (46)$$

in which, for a given bearing geometry,

$$M = f(T_o, P_{at}, P_{ro}, P_r, H)$$

$$(W_2 - W_1) = F(T_o, P_{at}, P_r, H)$$

It follows that the stability condition also can be written as:

$$-\left[\frac{dP_r}{dH} \right]_{M=M_0} > -\left[\frac{dP_r}{dH} \right]_{W_1+W_2=W_0} \quad (47)$$

The physical interpretation of the above inequality is as follows. The left side of inequality (47) represents a change in recess pressure caused by a rapid change in gap width, each volume element acting as a closed cylinder in which the gas becomes trapped. The right side of inequality (47) represents a change in pressure caused by slow, quasi-static displacement, the annulus having a flow-regulating, rather than gas-trapping effect.

4. Conclusions and Summary of Theoretical Results

An analysis was made which treats the flow within the gas film in a thrust bearing on a continuous, rather than "lumped," basis. It shows that within the limitation imposed upon the design of the bearing by other considerations, the following parameters or combinations of parameters should be minimized or maximized in order to insure stability:

Minimized

1. Depth of pockets
2. Difference between supply and recess pressures
3. Effective mass of bearing

Maximized

1. Supply nozzle diameter
2. Length of annulus
3. Area ratio of annular and pocket regions

One may also conclude from results of earlier, simplified analyses [2,3,6] which show good qualitative agreement with the present one, that high gas temperatures and adiabatic conditions favor stability.

The most important factor influencing the stability of externally pressurized bearings is the interaction of the total gas-storage capacitance with the flow-regulating characteristics of a fixed supply restrictor and a variable annulus. The ratio L/mg , where L is the load and m the mass of the bearing, also influences stability. Deeper pockets can generally only be tolerated for very moderate pressure drops across the supply nozzle. The limiting depth increases with the nozzle diameter and decreases with the length of the annulus, as well as with the mass of the bearing. These trends are illustrated in Figures 3 and 5.

The advantage of recessed pockets, channels, or grooves is that they increase the load capacity and static stiffness. The recess perimeter also provides a larger area of admission into the annulus, thereby reducing entrance velocities and preventing shocks [19,20,21]. These advantages, however, must be weighed very carefully in the light of requirements dictated by stability conditions.

IV. EXPERIMENTAL APPARATUS

1. Design of Experimental Apparatus

The main objectives in designing the test apparatus were the following:

- a) To insure maximum flatness and rigidity, as well as hardness and material stability, of the thrust plates.
- b) To provide means of precise alignment, and of accurate methods for checking the parallelism and separation of the bearing surfaces.
- c) To restrain the mode of oscillation to an axial direction with minimum friction.
- d) To place a variable-volume, leak-proof cavity in the center of one thrust plate and to provide for precise adjustment and accurate measurement of its depth.
- e) To furnish means of applying a constant, non-massive, axial load which would not be affected by the motion of the bearing.
- f) To design for maximum rigidity of the entire structure for the purpose of minimizing deflections and preventing a condition of system resonance within the anticipated frequency band width of oscillations.
- g) To provide sensitive vibration pick-ups and associated electronic and photographic apparatus in order to detect, measure and record amplitudes of oscillations which are small in comparison with the magnitude of the equilibrium gap width.
- h) To furnish a well regulated, relatively clean and moisture-free air supply. To select reliable pressure gauges, manometers and flow meters for the purpose of determining the static characteristics of the test bearing.

The test bearing assembly drawing is shown in Figure 7. The sturdy construction of individual parts and of the entire structure, particularly the plates and columns, is self-evident. All members were machined to extremely close tolerances, subjected to proper heat treatment and inspected prior to, during, and after manufacture and assembly. The upper thrust plate (1)† could be aligned by means of three 2 inch diameter, 48 threads per inch, adjusting screws (2) and securely bolted to the supporting columns (27). The lower thrust plate was integral with the shaft (21). Both thrust faces were chrome plated and lapped flat to the order of 1-1/2 interference bands of monochromatic sodium light (approx. 20×10^{-6} inches). Final inspection, using 6 inch diameter optical flats, showed that the convexity of a symmetric and almost circular central region of both plates did not exceed one interference band up to approximately four-fifths of the 5 inch diameters. Three sensing probes (4) of an air gauging system, incorporated in the upper plate, were equally spaced along the perimeter of the thrust face and lapped together with it.

An exact determination of deflections and modes of vibrations of the thrust plates was not attempted because of the complexity of the problem involving thick plates, supported in a manner described in the foregoing. A conservative estimate, based on approximate plate theory, the

†Circled numbers correspond to those in Figure 7 and refer to assembly components.

assumption of simple support along the column pitch circle diameter and a concentrated 500 lb. load, showed that the deflection of the center of the upper thrust plate with reference to its edge was of the order of 20×10^{-6} inches. The deflection of the lower thrust plate, in which the cantilever-like, overhanging ring was subjected to pressures which in that region approached the ambient value, would be negligible in comparison. It was concluded, therefore, that load deflections would have a compensating effect on the slight, initial convexity of the surfaces.

The theory of vibrations of plates, even in approximate form, is very complex. On the assumption that the frequency, p_1 , of the lowest mode of vibration could be estimated from the equation (58):

$$p_1 = a \left(\frac{Et^2}{12r^4\rho(1-\nu^2)} \right)^{1/2}$$

in which a is a constant depending on the method of support, E is Young's modulus, ν the Poisson's ratio, ρ the mass density of the metal, r and t the radius and thickness of the plate, the lowest frequency was estimated to be of the order of 10^4 radians per second and, consequently, considerably higher than the anticipated frequency band width of auto-oscillations.

The upper thrust plate, Figure 8, contained a centrally located recess, the depth of which could be varied by means of a sliding piston (19) and a micrometer adjusting screw (15). Three tightly fitted "O" rings served as sliding seals. The piston could be locked in any desired position and the recess depth varied from zero to 3/4 inches. Air was supplied through a 7/16 inch diameter, drilled duct in the upper plate. It flowed into a chamber, the volume of which comprised the sealed space between the "O" rings and the bore of the piston, Figure 9. The flow restriction between this chamber and the recess was effected by means of a short, bell-mouthed, 0.055 inch diameter nozzle (8).† The drawing of an auxiliary piston (Figure 10), shows a 0.0135 inch diameter pressure tap, located at 11/32 inches from the piston center. The tap was connected through an internal duct to a gauge which indicated the static, equilibrium recess pressure at that point. In the modified version of the piston, the pressure tap was centrally located and plugged when dynamic tests were conducted.

The drawing of the shaft and lower thrust plate is shown in Figure 13. The shaft was hollow so that the movable mass corresponded to 25 lbs. The weight could be increased to 45 lbs. by attaching a 20 lb. bronze disc to the shaft, midway between the 3 inch journals. (It will be recalled that theoretical stability loci were constructed for masses corresponding to weights of approximately 13.9, 25 and 45 lbs.) Rigidity requirements, however, precluded a less massive shaft and thrust plate construction and no provision could be made to obtain experimental data for the smallest mass. The 3 inch diameter, circular area of the plugged end of the shaft provided a surface exposed to the pressure of the loading cylinder (20) by means of which the thrust load was applied to the bearing. Impulse turbine buckets were milled in the shaft to provide a high speed drive for experimental work involving rotation which could be conducted upon the completion of

† In a modified, later version of the piston, provision was made for replacement of a single restrictor by 4, 8 or 12 nozzles. In each case the total cross-sectional throat area was adjusted to give approximately calculated rates of mass flow (see Figures 11 and 12).

this phase of the investigation.† The size, concentricity, roundness and taper of the shaft journals were found to fall within tolerances specified on drawings. The total indicated runout of the thrust face with respect to the journals, measured on a 5-3/4 inch diameter, was less than 0.0002 inches. The shaft was balanced to within 0.00025 inch-pounds.

The problem of restraining the motion of the shaft and the lower thrust plate to a purely axial direction by means of low-friction guides was solved by mounting the shaft in externally-pressurized, air-lubricated journal bearings (24). There were two main reasons for this type of lateral support. First, the analysis was predicted on the assumption that external damping was negligible, since primary interest was only in those stability parameters associated with the bearing itself. Secondly, from the practical point of view, it was desirable to simulate as far as possible a method of gas bearing support which could be eventually applied to small turbines, compressors or centrifuges. A drawing of one bearing is shown in Figure 14. The main feature of the design was a set of six, grooved, centrally located and equally spaced pressure pads. Air was supplied to the pads through 0.016 inch diameter, brass orifices (25), shown in Figure 15. The purpose of the grooves was to minimize the storage volume of each pad, while extending a relatively uniform, high-pressure area to the outer perimeter of the grooves. The net effect of this arrangement contributed to the stability of the bearing and produced a steep load-deflection characteristic, Figure 16. Needle valves (26) were placed in drilled air ducts leading to alternate pads. The function of the needle valves was to allow for controlled misalignment of the shaft within the limits of the bearing clearance. By varying the pressure in individual pads, an excellent method of making final adjustments in the alignment of the thrust surfaces was provided, furnishing improvement on the high degree of parallelism already achieved by means of the levelling screws.

The bearings were dowel-pinned and bolted to the supporting members prior to final machining, during which both bearings and the sleeve of the loading cylinder were ground to size in one operation. The grinding operation was performed with a degree of precision which made it possible to span all three bores with a single plug gage, barely 0.0003 inches smaller than the minimum, measured bearing diameter. All grooves were indicated on the grinding machine and their depth varied from 0.006 to 0.007 inches. The orifice inserts, needle valves and the annular supply chamber of the bearing were sealed by means of "O" rings.

It was estimated that a bearing stiffness†† of 3×10^5 to 5×10^5 pounds per inch could be realized when the journal was in the concentric position. With the bearings and the shaft assumed as a spring-mass system having two degrees of freedom, approximate values of frequencies of natural modes of vibrations were calculated by considering a pivoting motion of the shaft about one bearing, the other journal being acted upon by a spring. The "constrained" frequencies, p , are given by (58):

$$p = \ell \left(\frac{k}{I_c + m \ell_c} \right)^{1/2}$$

† The grooves at the end of the shaft were intended to suppress instability (whirl) due to hydrodynamic forces in the clearance of the loading cylinder sleeve.

†† The slope of the load-deflection curve is sometimes referred to as the "stiffness" or more correctly, as the "static stiffness". (See Figure 16.)

in which l is the span length between the bearings, l_c the distance from the chosen pivot to the center of gravity of the shaft, k the stiffness, m and I_g the mass and moment of inertia of the shaft about its center of gravity. The estimated natural frequencies for the 25 lb. shaft were in the order of 3×10^3 and 5×10^3 radians per second and could be substantially reduced, or raised, by varying the supply pressure. It was concluded, therefore, that in the absence of appreciable unbalance and moments in planes passing through the shaft axis, the pitching motion of the shaft within the clearance of the journal bearings would be relatively small in comparison with the amplitude of axial oscillations.

The loading cylinder (20) consisted of a 7-1/2 x 3-1/2 inches pressure vessel attached to the lower end of the supporting structure. A constant pressure maintained in the cylinder and acting on the end of the shaft protruding through the cylinder sleeve, balanced the load applied to the lower thrust plate. For small amplitudes of oscillation, volume changes would be negligible in comparison with 155 cubic inches of cylinder displacement. The cylinder pressure would remain essentially constant, unless the frequency of oscillation produced a condition of acoustic resonance in the chamber, in which case the shape and volume of the cylinder could be altered accordingly. The cylinder provided a simple method of applying a constant, non-massive load to the test bearing.

The lower ends of the 3 inch diameter columns of the test rig were press-fitted into a 2 inch thick plate (19) in which one of the journal bearings was mounted. The upper ends of the columns were located and bolted to a similar plate (18) containing the second journal bearing. The column locating holes in both plates were jig bored in tandem. The concentricity and squareness of the columns and locating bosses were indicated from the head of the precision grinder after the bearings and the bore of the loading cylinder sleeve were finished to size. The assembly was bolted to a massive and very rigid tripod. The weight of the entire structure was approximately 750 lbs. In the course of experimentation it was found necessary to interpose relatively soft isolators between the tripod and the foundation floor. The reason for doing so is discussed later in the text. A schematic of the air supply system is shown in Figure 17. Photographs of test apparatus, its components and of auxiliary equipment are shown in Figures 18 through 25.

2. Instruments -- Performance and Calibration

a. Air Gauges

The threefold function of the air gauging system, briefly referred to in the foregoing section, was (a) to facilitate the alignment of thrust surfaces to a high degree of parallelism, (b) to measure the equilibrium gap width, H_0 , and (c) to provide a quick and direct method of calibrating the primary capacitance probe without disturbing its initial position and offset.

The well-known method of measuring small displacements in terms of pressure utilizes two flow restrictors, placed in series, a constant, well regulated pressure source and suitable pressure indicators. Air enters an intermediate chamber from a constant pressure reservoir through a small, fixed (or adjustable) orifice. The variation of pressure in the intermediate chamber is recorded and depends on the supply pressure level, as well as the relative size and flow characteristics of

the restrictors. The cross-sectional flow area of the second restrictor is made to vary with displacement, so that resistance to flow is furnished by a slot, or a circumferential orifice formed between the surfaces of the sensing probe and the displaced member.

For a fixed orifice size, the slope and curvature of the pressure-displacement characteristics depend mainly on the size and geometry of the probe restriction, and on the magnitude of the supply pressure. The characteristics are nonlinear and exhibit an inflection point, in the neighborhood of which the amplification is highest. The probe can be made in the shape of a short, thin-walled or a thick-walled cylinder. In the latter case, the restriction between the probe and the displaced member has the form of a narrow, radial slot rather than that of a circumferential orifice. All other factors being equal, a slot-like, variable restrictor produces a higher sensitivity, though at some expense of linearity in the pressure-displacement characteristic. This effect is due to a more pronounced influence of viscous forces in a narrow slot than in a circumferential orifice.

It was considered that a low supply-pressure gauging system, integral with the upper thrust plate, would have an advantage over commercially available units, which generally operate at supply-pressure levels of thirty to sixty pounds per square inch. The system was to be conveniently incorporated into the test rig assembly, with probes rigidly mounted in the upper thrust plate and lapped in the plane of the thrust surface. A well regulated supply head of two to three feet of water could be obtained by means of a standpipe, with the excess air in the supply reservoir being allowed to escape at the end of an immersed tube. It was also desirable to avoid the impingement of relatively high velocity probe jets associated with high pressure systems, since this impingement might have involved difficulties in calibration, and possibly minor effects of heat transfer on the accuracy of measurement.

An estimate of orifice and probe dimensions for a low pressure system was made by assuming the flow to be incompressible. Dimensionless pressure-displacement characteristics were obtained by equating the inflow through the orifice to the outflow through the probe restriction, considered either as (a) a narrow, radial slot or (b) a circumferential orifice. Results of these preliminary calculations used in establishing approximate values of design parameters are shown in Figure 26, which also contains a schematic of the supply head regulator.

The effect of changes in barometric pressure on gap width measurement could be estimated from equations (8) and (9), the flow through the orifice and probe restrictions being essentially analogous to that through the bearing supply nozzle and gap. The gap width is then given by:

$$H_o^3 = K \frac{(P_s P_{to} - P_{to}^2)^{1/2}}{P_{to}^2 - P_{at}^2}$$

† The principles involved in determining the pressure-displacement characteristic of an air gauge are essentially similar to those which apply to load-displacement characteristics of externally pressurized, gas bearings.

in which P_s , P_{ro} and P_{at} now refer to the absolute values of the supply, intermediate and ambient pressures of the air gauge system, and K is a constant. Taking the logarithm of both sides of this expression and differentiating, the approximate error in gap width measurement, associated with a change of $\pm \Delta P$ in barometric pressure, is:

$$\frac{\Delta H_0}{H_0} \approx \mp \frac{\Delta P}{6P}$$

where in the last step it was assumed that the pressure differences are sensibly small, e.g., $P_s - P_{ro} - P_{at} = P$. A change of ± 0.5 psi, relative to the barometer reading during calibration, would cause an error of ∓ 0.5 percent in the measured gap width, less than 10 micro-inches.

Initial difficulties were encountered because of supply pressure fluctuations caused by the surface tension of bubbles, forming and breaking away from drillings at the immersed end of the tube. This was circumvented by inserting a damper in the form of a series of perforated discs in the reservoir end of the tube and reduced the ripple to an almost imperceptible magnitude, relative to the smallest manometer scale reading or 1/10 of an inch. The supply pressure was adjusted to a steady, constant value of 39.2 inches of water by varying the setting of a fine, long taper needle valve.

The calibration was performed in steps of 0.0001 inches over a gap width range from 0.001 to 0.002 inches. Square, 1 x 1 inch precision gauge blocks, having a dimensional and parallelism tolerance of 1 microinches, were used for this purpose. Two blocks, differing in thickness by a multiple of 0.0001 inches, and a third block were wrung together. The step gauge created in this fashion was then wrung together with the lapped thrust surface, the step extending from the edge of and overlapping the entire probe diameter. (See schematic in Figure 27.) The probes were spaced 120 degrees apart and located 1/4 of an inch from the edge of the upper thrust surface. The blocks were taken apart and reassembled after each round of manometer readings for all three probes. This was repeated 21 times for each probe and every one of the 11 calibration points, a total of 691 manometer readings. The gauge blocks were assembled at random and it was reasonable to assume the arithmetic average of 21 manometer readings as the most probable value corresponding to the nominal dimension of the step gauge offset. The curvature of the pressure-displacement characteristic in the experimental range of gap width was very slight. The maximum difference in any set of 21 manometer readings was less than 0.4 inches of water. At a representative sensitivity of 0.15 inches of water per 10^{-5} inches displacement, this was equivalent to 2.7×10^{-5} inches, or less than 3 percent of minimum gap width in the experimental range. Least-square-fitted calibration curves, Figures 27, 28 and 29, were considered adequate for gap width measurement to an accuracy of 1 to 2 percent.

b. Vibrometers — Primary and Auxiliary Probe Systems

The validity of assumptions made in the analysis increases if the amplitude of motion is small in comparison with the equilibrium gap width. For reasons arising from practical considerations, such as the impossibility of insuring perfect isolation, ideal rigidity of structural members, absolute steadiness of air flow etc., the feasibility of detection and, above all, meaningful interpretation of amplitudes in the order of 10^{-6} inches was doubtful. It was arbitrarily decided, therefore, to regard amplitudes of oscillation in the order of one percent of the gap width, or to 10^{-5} inches, as small.

The function of each probe system was to interpret dynamic capacitance changes in terms of relative displacement of the probe and the vibrating member. The primary probe system, shown on the left side of Figure 30, was used in measuring the axial oscillations with which the experiments were mainly concerned. The auxiliary probe system, shown on the right side of Figure 30 employed inductive capacitive pick-up, which could be mounted in several positions along and around the shaft. The function of the auxiliary probe was to detect transverse modes of vibrations which might be coupled with the axial motion of the shaft. It was, of course, desirable to reduce this motion to a bare minimum and the air-lubricated guide bearings were designed with this objective in mind. The auxiliary system thus played a monitoring role in the course of experimentation. The operation of these vibrometers was based on different principles. Their operation, performance and calibration are described in the next paragraphs.

In the schematic diagram of the primary instrument, a Fielden Proximity Meter, model TM-951-1, the variable probe capacitance, C_p , is shown shunted across one of the two balancing capacitors of an impedance bridge. The source of bridge excitation was a 450 K.C. oscillator (modulated by 2.4 kc when using the meter for static measurements). The out-of-balance voltage of the bridge was applied in succession to the tube grids of a two-stage, radio frequency amplifier. The gain of the amplifier could be controlled by a variable, tapped resistor in the cathode circuit of the amplifier tubes by means of a six-position switch, providing an attenuation up to 50 decibels in steps of 10 decibels. The bridge could be balanced by means of capacitors, C_1 and C_2 , and the potentiometer R, which balanced the probe lead resistance. The frequency response of the instrument, Figure 31, was flat from D.C. to approximately 1200 cps and, therefore, more than adequate for measurements in the anticipated 100-400 cps band width. The output of the instrument was applied to one pair of terminals of a dual trace preamplifier of the cathode ray oscilloscope. The preamplifier had nine sensitivity settings in the range of 0.05v/cm to 20v/cm and a variable vernier adjustment. The frequency response of the oscilloscope-preamplifier unit (Tektronix, type 532, and dual-trace preamplifier, type 53-540) was 3 decibels down at 5 megacycles, considerably higher than that of the Fielden instrument.

The primary probe, Figure 24, consisted of a 1.4 inch diameter, brass disc, mounted in an insulating sleeve. The disc and sleeve assembly were pressed into the opening of a 4.5 inch long probe holder and lapped square with its axis. The body of the holder, which also served as part of the outer shield, was rigidly clamped to the upper thrust plate by means of a split collet and a gripping clamp. With the radio frequency amplifier control adjusted to approximately one third of maximum gain and a preamplifier vertical deflection setting of 1 volt per centimeter, the sensitivity corresponded to 1 centimeter vertical deflection per 10^{-5} inches displacement when viewed on the display of the cathode ray oscilloscope. The observed noise level and drift at this setting, after an initial, one hour warm up period, was of the order of 0.05 to 0.1 volts. The maximum room temperature variation during any test run was between 74 and 77 degrees Fahrenheit. The probe lead was double-shielded to prevent stray voltage pick-up and relatively short, in order to minimize capacitance in parallel with that of the probe. For this reason also, the thickness of the insulating sleeve (dielectric constant of 2) was 0.1 inches and, therefore, large in comparison with the initial, 0.003 inch offset between the 1.4 inch probe disc and the lower thrust plate.

Following the parallel alignment of thrust surfaces, the probe was calibrated in three positions, corresponding to approximately the end and midpoints of the experimental range of gap widths. The calibration was performed, using the air gauges as a standard. The calibration

curves are shown in Figures 32, 33 and 34. From their appearance it could be concluded that for amplitudes of displacement in the order of 1×10^{-5} inches to 2×10^{-5} inches, no large error would be incurred by assuming linearity in the neighborhood of null points and a sensitivity value of 1 volt per 10^{-5} inches displacement.

The schematic diagram of the auxiliary instrument (Decker, Delta Unit 902-1 and Monitor Unit 902-2) shows the capacitance probe, C_y , mounted in one of the positions along the shaft. The main component of the system was a tube, containing gas[†] under reduced pressure. The tube was placed between two external electrodes connected to a 250 KC oscillator. The excitation caused a luminous discharge, so that the two internal electrodes of the tube were in contact with the plasma of the ionized gas. Any asymmetry in the spacing of the electrodes would give rise to a potential difference between the internal electrodes, caused by the migration of electrons. The effect of asymmetry could also be produced by changing the magnitude of the sensing capacitor, C_y , relative to the balancing capacitor, C_o , both shown in the schematic diagram of Figure 30. The operation of the auxiliary probe, C_y , was based on this principle [62]. A cathode follower provided a low impedance output at the preamplifier terminals and a filtering network eliminated the fraction of oscillator excitation passed through the transducer.

The transducer, probe, mounting bracket and calibration fixture are shown in Figure 25. The probe and the balancing capacitor were mounted very close to the internal tube electrodes and all leads were relatively short in order to minimize the adverse effect of stray capacitances on the output and frequency response of the instrument.

The frequency response of the auxiliary instrument, Figure 31, was flat to approximately 300 cps, 0.5 decibels down at 400 cps and, therefore, quite adequate in the anticipated, experimental frequency band width. The calibration curve of the auxiliary probe, Figure 35, displayed a greater degree of nonlinearity than that of the primary probe. The sensitivity in the neighborhood of the null point was approximately 0.02 volts per 10^{-5} inches displacement, representing 0.4 centimeters vertical deflection per 10^{-5} inches displacement on the cathode ray oscilloscope display at the highest preamplifier sensitivity setting of 0.05 volts per centimeter. The observed noise level was of the order of 0.005 volts. Since the maximum sensitivity of the auxiliary probe was considerably less than that of the primary, the monitoring test of lateral shaft vibrations was conducted under conditions of axial oscillations approximately twenty times as large as the amplitudes of self-excited vibrations observed in the course of stability experiments.

c. Pressure Gauges, Flowmeters and Regulators

The supply, recess and loading piston pressures were measured by means of two, dual bourdon tube construction, eight and one half inch dial diameter, absolute pressure gauges. The gauges were graduated in steps of 0.1 and 0.2 psi over their respective ranges of 0-100 and 0-150 psia. The ranges were covered in approximately two revolutions of the pointer. The scale had a mirrored surface reflecting the fine blade of the pointer to eliminate parallax errors and the size of the smallest subdivisions permitted reliable estimates of readings to the nearest 0.05 psi. The pressure gauges were calibrated by the manufacturer by means of a precision mercury barometer, a duplicate of a Bureau of Standards reference barometer. The accuracy of the pressure

[†] Argon or Neon

gauges was guaranteed to be within 0.02 percent of full scale deflection, representing 0.027 percent for the 0-100 psia gauge and 0.041 percent for the 0-150 psia gauge at 73.5 psia, the lowest test reading. The scales were hand drawn to match over one hundred calibration points. The hysteresis, backlash and "dead zone" of the pressure gauges were entirely negligible. As an additional check, the gauges were connected to the same pressure source and their readings compared. No perceptible difference was observed in the range from 50 to 100 psia.

Flow measurements were performed, using a variable area flow meter (rotameter) in conjunction with a calibrated, bellows type gas meter. The position of the rotameter float was registered along the scale of the 600 millimeter long tube for any particular setting of the bearing supply pressure. With this setting maintained and the position of the rotameter float unchanged, the flow was diverted to the gas meter. The rotameter thus merely served as a secondary, indicating instrument, while the actual flow rates were determined from the gas meter readings. The calibration of the gas meter was performed by means of an inverted-tank-type gasometer of 20 cubic feet capacity, used as a standard by a local utility company. Five calibration runs were made after the final adjustment of the counter mechanism, at a representative bearing flow rate of 5 cubic feet per minute, referred to standard atmospheric conditions. (Approximately four revolutions of the five cubic foot counter.) The differences in the final positions of the gasometer displacement indicator were negligible in comparison with the total displacement. The speed of the counter, approximately one revolution per minute, was slow enough to enable the observer to estimate the position of the pointer, relative to a predetermined mark, at least within 6 degrees, or better. This, in terms of displacement, corresponded to approximately 0.5 percent of the gasometer volume.

The rotameter float was operated in the upper half of the tube. Slight oscillations of the float were observed in the uppermost tube region, but their peak-to-peak amplitudes were of the order of 2 to 3 millimeters, as compared with the 600 millimeter length of the tube. An estimate of 2 to 3 percent accuracy in flow measurements obtained in the course of experimentation appears to be reasonable.

The pressure regulators used in the test-bearing air-supply system, Figure 17, were capable of maintaining a downstream pressure setting within 0.1 psi over their entire flow range and a 25 psi variation in delivery pressure. One regulator was installed ahead of a 7.5 cubic foot air storage tank and individual regulators were placed in the supply lines leading from the tank to the loading cylinder, test and guide bearings. The performance of the regulators was most satisfactory and pressure settings could be accurately maintained, with drift not exceeding 0.05 psi over periods of two to three hours.

V. EXPERIMENTS

1. Static Tests

The calibrated air gauges furnished the means of bearing surface alignment. The 25 lb. shaft was inserted in the pressurized guide bearings and the upper thrust plate placed on the column locating bosses. The concentricity of the bearing members was checked and adjusted to within 0.001 inches. The thrust surfaces were then brought into parallel alignment by means of leveling screws and air gauges and secured to the columns. As an additional check of parallelism, the following test was performed. A spacer, approximately 1.53×10^{-3} inches thick, was lightly clamped between the thrust surfaces at twelve, thirty degree, angular intervals along their perimeter. Manometer readings of one air gauge only were registered for each position. This was repeated nine times and the arithmetic average of readings for each position was taken. An identical test was carried out with a spacer 1.53×10^{-3} inches thick. In the process of sampling, the spacer was clamped by a constant, 0.5 lb. force, at an average distance of two inches from the bearing center. The guide bearings, spaced nine inches apart, were pressurized and their stiffness in the concentric position, Figure 16, was in the order of 4×10^{-5} pounds per inch per bearing. Any misalignment, therefore, caused by the moment of the small clamping force, would be negligible. The results of this alignment test are shown in Figure 36, in which the circularly spaced numbers refer to average manometer readings of gauge No. 1 obtained with both spacers. By reference to the calibration curve in Figure 27, it can be seen that the thrust surfaces were parallel within one percent of the equilibrium gap widths, that is inclined under an angle in the order of 4×10^{-5} degrees.† The shaft thrust face had a total indicated runout of 0.0002" relative to the journals and the alignment would have been destroyed, had the shaft been allowed to drift in its guide bearings. An additional constraint, therefore, was furnished by means of two opposed and narrowly spaced air jets, impinging on a light, thin fin, attached to the shaft collar. (See Figure 18, for example.) The alignment was thus performed with the shaft maintained in the same position relative to the guide bearings.

The analysis was based on the existence of an essentially uniform pressure plateau, extending over the entire, one inch diameter recess area. It was postulated that, as long as the recess depth remained relatively large, the effects of the air jet issuing from the 0.055 inch diameter nozzle and the acceleration of the fluid as it entered the slot would be local and detract little from the recess volume conceived as a constant pressure reservoir. Since the stability boundary for critical recess depths in the order of 10^{-2} inches was of particular interest, the question which presented itself was the degree to which the foregoing suppositions were valid for recess depths smaller than the nozzle throat diameter and comparable in magnitude with the bearing gap width. The following possibilities deserved careful consideration. (a) For $\delta \sim 1$ to $4 d_n$, the cylindrical area bounded by the nozzle diameter and its projection on the lower thrust surface would replace the nozzle throat as the controlling restriction. (b) The recess, its depth sufficiently reduced, could act as an inward extension of the bearing gap and virtually cease to function as an intermediate reservoir. (c) The accelerating flow in the diverging region adjoining the nozzle exit could attain supersonic velocities, followed by shock and a transition to the predominantly viscous flow

† Interference fringes observed under optical flats indicated that each 1.5×10^{-5} to 2.0×10^{-5} plate convexity was quite concentric and approaching in shape that of a surface of revolution. Parallelism, or inclination, therefore could be thought of in reference to the circular bases of those elevations.

region in the slot [19, 20, 21], a situation analogous to that which might exist in a duct fed by a converging-diverging nozzle.

A test was conducted, in which the load and a representative value of the supply pressure, 87.5 psia, were held constant, while the recess was being reduced in depth from a relatively large value. The objective of the test was to determine the "cut-off" point, at which any further reduction in depth would cause a change in the steady-state flow pattern and pressure distribution. This would then be accompanied by an easily detectable and measurable departure from the initial gap setting. Results of this test, presented in Figure 37, indicate that, for a centrally located, 0.055 inch diameter nozzle, the "cut-off" point corresponded to a recess depth of 0.030 inches.

Since the critical stability parameter was the volume, rather than the depth of the recess, the first, successful attempt at a remedy was to surround the nozzle exit by a 0.375 inch diameter, 0.026 inches deep cavity (see Figure 22). This, however, did not provide an entirely satisfactory solution, since for small critical volumes the delineation between slot and recess became rather vague. For this reason, and because the linear dimensions of the restrictor influence the degree of unsteadiness in pulsating flow, the pistons were replaced by modified version, Figure 11, which incorporated interchangeable, multiple-nozzle plates. The plates, Figures 12 and 23, contained either four, nine, or twelve short, bell-mouthed nozzles, equally spaced on a 0.5 inch diameter circle. Their total, cross-sectional throat area was later adjusted to give a flow characteristic approximating the calculated one within the experimental range of pressure ratios. The twelve nozzle plate was used in the concluding experiments. At a supply pressure of 87.5 psia, a reduction in recess depth from 0.008 inches, the "cut-off" point, to 0.006 inches, was accompanied by a decrease in gap width in the order of two percent only. The effects of decrease in recess depth on gap width for single and multiple nozzle feeders are compared in Figure 37.

The calculated load capacity of the test bearing, based on the assumptions of laminar flow in the clearance, negligible entrance effects and uniformity of pressure in the recess, varies almost linearly with the recess pressure and is independent of the supply pressure.

In order to ascertain the extent to which the actual conditions conformed to this idealization, a test was conducted in which (a) the load was adjusted to maintain a constant recess pressure† of 73.5 psia, or (b) the load was held constant at the calculated value of 472 lb, and the recess pressure† was allowed to seek its own level. The result of this test is presented in Figure 38 and indicates that in case (a) an increase of the supply pressure to 95 psia was accompanied by a 5 percent reduction in load capacity, whereas in case (b) a 4 percent increase in recess pressure was observed. Throughout this test the recess depth was larger than the "cut-off" value, referred to in the preceding paragraphs.

The desirability of minimizing differences between the actual and theoretical, steady-state bearing characteristics was of considerable importance with reference to the mass flow rate, since its partial derivatives with respect to gap width and pressure, equation (16b), played an important role in establishing the limiting values of stability parameters. Preliminary flow measurements indicated, that in the experimental range of pressure ratios the overall discharge coefficient, using a

† Pressure tap centrally located. Recess depth $\delta > 0.010$ inches.

twelve nozzle supply restrictor, varied approximately from 0.78 to 87. The total throat area was then increased by approximately 10 percent, in order to narrow down the gap between actual and calculated flow rates.[†]

Mass flow rates were determined in the range of supply pressures from 75 to 95 psia, with a constant load of 172 lb., the calculated value corresponding to a recess pressure of 73.5 psia and ambient pressure of 14.7 psia., applied to the test bearing. (A condition analogous to that under which stability tests were conducted.) The recess depth was always maintained at a value greater than the "cut-off" point referred to in the preceding paragraphs. The mass flow rates in the experimental range of supply pressures, obtained with slightly increased nozzle diameters, were 94 to 97 percent of the calculated values, while deviations of measured gap widths were in the order of one percent. Results of mass flow and gap width measurements are presented in Figures 39 and 40. The corresponding bearing Reynolds number, $N_R = \left(\frac{\rho_r \Gamma_r h}{\mu} \right)_0 = \frac{W_o}{2\pi\mu\{h}_r$ is

given in Figure 41. Mass flow rates and the Reynolds number obtained in a supply pressure range for a bearing load of 222 lb. and corresponding to a stability test conducted under reduced load conditions are given in Figures 42 and 43.

It seemed highly unlikely that absolute, one-to-one correspondence between calculated and actual, steady-state values of pressure, gap widths, and flow rates could be simultaneously achieved throughout the experimental range. It was considered that, in the presence of slight deviations in several static bearing characteristics from those of the idealized model, a fair compromise was reached, and that the deviations were of a reasonable order of magnitude.

2. Preliminary Stability Tests

Initial differences in calculated and actual, static bearing characteristics and subsequent modifications incorporated in the apparatus, were described in the preceding section. These modifications, and a number of additional changes, were also dictated by evidence gathered from results of simultaneously conducted, preliminary, dynamic tests. The preliminary tests furnished considerable information, of interest in itself, and useful from a practical point of view. In this section an account of preliminary experiments is presented in a logical sequence, not necessarily in the order in which they were conducted.

The dynamic experiments, with the exception of one comparison test, in which the recess pressure^{††} was held constant, were conducted under constant load conditions. Results of static tests indicated that, in the latter case, deviations from predicted, static bearing characteristics appeared to be less pronounced. Moreover, since the recess pressure could be measured at one point only, there remained the uncertainty of its distribution in the entire recess region, whereas, on the other hand, the load could easily be set and held constant at a predetermined value.

[†] Flow rates were calculated for a 0.055 inch diameter nozzle. The single nozzle was replaced by twelve nozzles and their diameters were enlarged from 0.0159 inches to approximately 0.0164 inches.

^{††} As measured by a tap located at a radial distance of 0.344 inches from the center.

The tests were conducted in the following manner. The load was applied to the bearing and the supply pressure adjusted to a predetermined value. The recess depth was then increased (or decreased) quasi-statically, until the bearing became unstable. In certain cases the procedure was reversed, e.g., the recess depth was set and the supply pressure increased (or decreased) very gradually, up to the threshold of instability. The axial oscillations were detected by the primary capacitance probe and viewed on the display of the cathode ray oscilloscope. Photographic records of amplitudes and frequencies of oscillations were made for a number of runs. A simultaneous check on previously determined, steady-state flow rates and gap widths was made for points in the immediate vicinity of the stability boundary. The boundary was always approached by proceeding from the stable region to the unstable region.

The first, preliminary stability test was performed, using a plane-faced piston and a centrally located, 0.055 inch diameter supply nozzle. Results of this test are shown in Figure 44. The abrupt transition in the lower branch of the curve, associated with the reduction in recess depth below the "cut-off" point (see Figure 37), provided yet another, valid reason for modifying the piston and, finally, replacing the single nozzle feed by a multiple-nozzle supply system. The upper branch of the stability boundary constituted a marked departure from the predicted, single-valued locus. This trend persisted in all subsequent experiments.

Figure 45 contains results obtained with a modified piston, having a secondary, fixed volume recess, but retaining a single, centrally-located supply nozzle. It can be seen that the unstable region enclosed by the curve corresponding to a constant load test was smaller than the unstable region bounded by the locus obtained when the load was adjusted in order to maintain a constant pressure at a tap, located 0.334 inches from the recess center. Both curves were marked by the absence of the sharp transition observed in the case of the plane-faced piston†, but continued to display two characteristic branches, separated by the point at which their slopes became infinite.

A secondary stability experiment was conducted in parallel with previously described, static tests, the objective of the latter being to assess the reliability of the assumption that the recess pressure at constant load was not appreciably affected by changes in the supply pressure. It was observed that when the 0.0135 inch diameter, 0.125 inch long pressure tap (see Figure 10) connected the recess to a relatively large, closed volume††, an effect, which could justly be described as hysteresis, was present. With the bearing stable at a particular setting of supply pressure and recess depth, the supply pressure was increased very slowly and gradually, particular care being exercised to avoid disturbances which might be large in comparison with those randomly produced and always present in the fluid, foundation and the surrounding atmosphere. Under those conditions it was possible to increase the supply pressure considerably above the value at which the bearing became unstable if jarred, displaced or subjected to a sharp impact in the axial direction. The supply pressure was then reduced to a level at which the bearing became stable again. At this level, instability could no longer be induced, regardless of rate and magnitude of the disturbance. Identical effects could be observed with the supply pressure held constant and the recess depth being varied quasi-statically. With an isolated recess volume (e.g., closed pressure tap), no hysteresis effects were present, at least no measurable difference in limiting values

† It is to be noted that in Figure 45 the ordinate is the mean recess depth, that is the recess volume divided by the recess area.

†† Consisting of drilled passages, holes and the volume of the bourdon tube.

of stability parameters was noted. Results of observations of this rather remarkable phenomenon are shown in Figure 16. It is realized, of course, that the region "unstable if disturbed" is quite arbitrary, since, ideally, the system could remain in the state of unstable equilibrium if all disturbances, no matter how small, were absent.

In the conduct of stability experiments described up to this point, the emphasis was rather on qualitative than on quantitative aspects of bearing performance. Subsequent tests, although their description and results are presented in this section under the heading of "preliminary", were carried out with considerably greater accuracy and precision of measurements. Closer spacing of intervals at which data was recorded and the determination of frequencies of auto-oscillations on the threshold of instability contributed to the detection and elimination of certain troublesome characteristics inherent in the test rig, and subsequent improvements in correlation between predicted and experimental results.

Stability boundaries, obtained with a twelve supply nozzle, plane-faced piston, under constant load (472 lb) conditions, for 0.477×10^{-2} and 11.68×10^{-2} lb-sec² in effective bearing masses[†], are presented and compared with predicted results in Figure 17. Measured and predicted critical frequencies, e.g., frequencies, ω_c , associated with limiting values of parameters on the observed threshold of instability and their calculated equivalents, for which the roots of the characteristic equation (31b) on the axis of imaginaries were $s = \pm i\omega_c$, are presented and compared in Figure 18. Results of a test conducted under reduced load (222 lb) conditions are shown in Figure 19. The stability boundaries referred to in the foregoing, although similar in shape to those shown in Figures 14, 15 and 16, exhibited yet another, unusual property in regions denoted by "resonance" on all pertinent figures. This peculiar trend in all loci, characterized by inflection points and abrupt changes in curvature, occurred invariably at frequencies between 220 and 225 cps, indicating the existence of resonance in the system.

The phenomenon described in the foregoing, a major source of discrepancy between theory and experiment, might well have gone unnoticed if critical values of supply pressure and recess depth had been recorded at more widely spaced intervals. Fortunately also, frequencies were recorded in parallel with other measurements, so that the local, abrupt transitions in several stability loci could be identified with the same value of approximately 220-225 cps. The preliminary dynamic tests indicated a considerable area of qualitative and quantitative disagreement between predicted and experimental results, far in excess of what might have been anticipated on the basis of comparison between calculated and actual, static bearing characteristics. There remained the problem of detecting possible sources of trouble inherent in the experimental apparatus and the application of corrective measures before final experiments could be conducted. Specifically, it was essential to (a) identify parts and components of the test rig assembly responsible for the existence of resonance at particular frequencies of auto-oscillation and (b) to investigate possible interactions between the motion of the bearing and fluid flow in regulators, supply lines, guide bearings, the loading cylinder, etc.

[†] The effective bearing mass consisted of the shaft and lower thrust plate assembly (Approximately 25 lb and 45 lb weights respectively).

3. Concluding Stability Experiments

This section begins with the description of preparatory test and adjustments of the experimental apparatus which preceded and were of considerable importance in the final, experimental phase of the investigation. It contains a detailed report of concluding experiments and ends with an account of tests, performed as a check of repeatability of results.

It was suspected that the singular trends associated with frequencies of auto-oscillations in the neighborhood of 220-225 cps, were caused by resonance of the entire test stand, considered as one large mass (Approximately 750 lb weight), supported on an elastic foundation. The possibility of exciting one of the graver modes of vibrations in the massive, upper thrust plate was highly unlikely, but could not be entirely excluded, because of the rather indefinite manner of support on three columns and levelling screws.

The test bearing assembly was bolted to a very sturdy and rigid tripod (see Figure 18 for example), mounted directly on an asphalt tile covered, concrete floor. Crude deflection measurements, using a dial indicator and the experimenter's weight for the applied load, yielded a natural frequency for the test rig mass and the elastic foundation of approximately 230 cps, a value extremely close to the narrow band in which the inflection points and rapid changes in curvature of stability loci were observed. In order to measure the natural frequency of this mass-spring system, as well as the response of the upper thrust plate, it was decided to utilize the floated shaft as the seismic mass and the primary capacitance probe as the sensing element of a vibrometer, providently, though inadvertently incorporated in the test rig design. A very minute, axial load was applied to the shaft thrust plate and balanced by the pressure in the loading cylinder. This furnished the desired "soft" suspension for the floated mass and a correspondingly low, damped natural frequency of less than 1 cps. The base of the tripod was then pressed down and released, while the response was recorded by means of the oscilloscope camera. As anticipated, the recorded frequency was approximately 220-225 cps.

The cause of the observed singularities thus firmly established, the entire test rig structure was mounted on isolators. A record, obtained in a manner similar to that described in the foregoing, showed that the natural frequency of the isolated structure was 15 cps. A further, effective reduction of isolator stiffness, such as could be obtained with a Julius suspension, for example, or a sizeable increase in mass, was not feasible because of physical limitations. The response of the upper thrust plate was also of interest. The plate was struck a light blow near the center with a small hammer, and the resulting trace of the cathode ray oscilloscope was recorded. The frequency observed in this case was approximately 730 cps, twice as large as the maximum frequency of auto-oscillations encountered in all experiments, but considerably lower than the magnitude estimated in the design phase of the apparatus.

Photographic records of frequency measurements described in the preceding paragraphs are presented in Figure 50, in which I represents the trace obtained with the structure resting on the floor, II is the response of the upper thrust plate and III refers to the structure when mounted on isolators. The uneven appearance of traces is due to the fact that, with relatively low pressures applied at the extremities, the shaft drifted continuously in the axial direction, producing corresponding changes in the electrostatic field between the probe and the "seismic mass". The oscillations of the upper thrust plate, II, are superimposed on the trace produced by vibrations of the test rig structure on isolators, both induced by the light hammer blow.

The concluding stability experiments were conducted with an isolated structure, so that the ratios of lowest, observed frequencies of auto-oscillations and the natural frequency of the assembly-isolator system were in the order of 14:1. Bearing alignment, leakproofness, zero settings of instruments, etc., were thoroughly checked. A low frequency generator, the triangular wave output of which was used as a marker on photographic records, was checked against an electronic, digital counter and found to be stable and accurate within 1 percent in the 500-1200 cps band width. Particularly great care was taken in recording readings of the recess depth dial indicator and of pressure gauges. Pressure readings were corrected to the nearest 0.05 psi for head loss between the measuring station and the point of admission to the reservoir, upstream of the supply nozzles. In approaching the critical recess depth on the threshold of instability, the piston was locked, so that final setting was made by very gradually overcoming a substantial amount of frictional resistance, in addition to that offered by four sliding "O"-ring seals. Whenever the stability boundary was approached by varying the supply pressure, the regulator control was adjusted in a manner, for which, perhaps, the most apt description would be "creeping".

It will be recalled that the stability analysis was based on linearized equations of motion, implying among other things that, in the course of the experimental part of this investigation, sensibly small amplitudes of oscillation, possibly one percent of the equilibrium gap width, would have to be observed. Now, since sources of small, random disturbances were always present in the fluid, the foundation and the surrounding atmosphere, more or less well defined wave forms of bearing response, with amplitudes of the order of microinches, were always observed on the display of the cathode ray oscilloscope. On the other hand, no significant growth of oscillation was noted for very large changes of supply pressure and recess depth, until their values approached a region in which relatively minute changes in either parameter were accompanied by an abrupt increase in the amplitude of vibration. In this narrow transition region the amplitude of vibration was modulated by irregular "beats". Their incidence, relative to the frequency of oscillation, occurred at more frequent intervals for large values of the critical recess depth.

Perfect discontinuities and ideally defined boundaries seldom occur in physical problems. Nevertheless, the transition in amplitudes from the microinch noise level to magnitudes approaching the gap width itself was invariably accomplished by changes smaller than one percent of the stability parameters designated as "critical". Thus the stability boundary is sharply defined. Otherwise stated, the amplitude of oscillation remained very small and its rate of change (slope) with recess depth, at constant supply pressure†, remained essentially zero, until both changed almost discontinuously in a narrow region, the amplitude becoming very large and its rate of change (slope) almost infinite.

The concepts and ideas contained in the preceding paragraphs can be summarized by stating (a) that amplitudes of the order of 10^{-5} inches were small compared with the bearing gap width, (b) that the available instruments were capable of detecting and measuring amplitudes of the order of 10^{-5} inches and, moreover, (c) that the order of magnitude of 10^{-5} inches was not very critical as a criterion of limiting values of recess depth and supply pressure at the inception of instability.

† Alternatively, with supply pressure at constant recess depth.

The foregoing statement may be substantiated by referring to Figures 51, 52, 53 and 54, which illustrate the abrupt transition in amplitude growth when approaching the boundary from the stable side, by increasing (or decreasing) the recess depth at several settings of the supply pressure. The lower photographs in each row were obtained with long exposure times and slow sweep rates. They show quite clearly the irregular "beats" referred to previously. The upper photographs display wave forms of auto-oscillations in random time intervals and were obtained with sweep rates one thousand times faster than corresponding photographs in the lower rows.

Stability boundaries and frequency determinations, obtained in the course of concluding experiments, are presented and compared with predicted results in Figures 55 and 56. A corresponding tabulation of experimental data is included in Appendix 4, following the table of calculated results. Photographic records of frequency measurements are shown in Figures 57 and 58. In the presence of irregular beats, described in the foregoing paragraphs, particularly at large values of the recess depth, the determination of critical parameters was unavoidably subject to judgment of the observer. The procedure followed by the experimenter was to observe the trace on the cathode ray oscilloscope while adjusting the recess depth, without noting the reading of the recess depth dial indicator. The objective was to avoid bias in selecting the point at which auto-oscillations were estimated to have reached amplitudes between approximately 1×10^{-5} to 2×10^{-5} inches. An alternative method was used for a number of points in which the stability boundary was approached by varying the supply pressure instead of the recess depth, thus providing a check on the reliability of measurement. In the latter case, the attention of the experimenter was focused on the oscilloscope display without observing the pressure gauge reading until the critical point was determined. No significant differences were noted, regardless of the manner in which the stability boundary was approached, indicating that results were reproducible according to the selected criterion, as well as rather insensitive to inexactitudes involved in its selection. Several measurements were repeated on days when the barometric pressure and the ambient (room) temperature were slightly higher, or lower, but the observed differences were negligibly small. It is estimated that the repeatability of limiting stability parameter measurements is at least within 1 to 2 percent of readings obtained in the course of concluding experimental runs.

The very substantial and, in this case, rather encouraging qualitative and quantitative differences in results of preliminary and concluding experiments were attributed entirely to the isolation of the test rig structure, since no other changes were effected in the system. On the other hand, all static and dynamic experiments seemed to indicate that, under certain conditions, even minute changes in system characteristics had an enormous effect on the stability of the bearing. In the final phase of this investigation, therefore, the experiments were accompanied by numerous and important secondary tests, with the objective of (a) discovering possible causes of remaining divergencies between theory and experiment, particularly such as might have accounted for the double-valuedness of stability loci, or, failing this, (b) adding weight to the reliability of the concluding experiments. Those secondary tests will now be described.

All experimentally determined stability boundaries were double-valued and exhibited an "upper" branch, not predicted by the present analysis. Although no calculated data were available for recess pressures other than 73.5 psia (corresponding to a 472 lb load), a stability test under reduced load conditions (222 lb), cursorily mentioned in a preceding section, was carried out. The reduced load test was dictated by the desirability of ascertaining whether the double-valuedness would also persist in the case of a locus corresponding to lower Reynolds number,

$$N_R = \frac{p_{to} \Gamma_{ro} H_o}{\mu} = \frac{W_o}{2\pi \mu R_r} \quad \text{A qualitative comparison of results in Figures 55 and 49, or Figures 47 and 49, in conjunction with reference to Figures 41 and 42, clearly indicates the presence of "upper branches" in loci corresponding to different ranges of the Reynolds number.}$$

Next, effects of misalignment were investigated. This investigation was accomplished by two methods. First, the constraint of the shaft† was removed and the relative positions of the upper and lower thrust plates were altered. These changes produced a very substantial misalignment due to the run-out of the lower thrust surface with respect to the shaft journals. Although very minor differences in limiting values of supply pressure and recess depth were noted, no significant change in the trend of the stability boundary was observed. Similar conditions prevailed when the rotor was brought up to a speed of approximately 2500 rpm, by means of an air jet directed onto the turbine wheel buckets. In the second misalignment test, the supply pressures of the upper and lower guide bearings was varied in such a manner as to tilt the shaft within the limits of bearing clearance. In addition to misalignment, the accompanying effect, in this case, was to change the "stiffness" of the guide bearings. No substantial changes in stability characteristics were observed, except when the supply pressure to one, or both bearings, was reduced to the extent which precluded their functioning as effective guides and constraints, or when metal to metal contact between the bearings and journals was established.

Experiments conducted with the isolated and non-isolated test rig assembly not only demonstrated local effects in the vicinity of the resonance point, but also the presence of large differences in limiting values of stability parameters for frequencies of incipient auto-oscillation considerably removed from the critical. The existence of other critical frequencies in the experimental band width and the effect of small vibrations of the upper thrust plate could not be entirely dismissed. It was, therefore, decided to stiffen the upper thrust plate. This was accomplished by placing three 3/4 inch diameter jacking screws between the column-bracing, upper plate and the upper thrust plate (see assembly drawing Figure 7) in positions straddling the columns and as close to the bearing center as was feasible. The jacking resulted in a slight amount of controlled, symmetrical deflection. It was known, however, at that time that no significant changes in stability characteristics were associated with a moderate degree of misalignment. The rigidity of the upper thrust plate thus considerably increased, measurements for a series of previously established, experimental points were repeated, without, however, any appreciable departures having been noted.

In the analysis, as well as in the course of experimental investigation, it was postulated that the load, and consequently the pressure in the loading cylinder, remained constant at all times. Accordingly, the design of the loading cell was such that fractional pressure changes, associated with motion of the shaft, were to be of the order of smallness of the displaced to total cylinder volume ratio. (Approximately 10^{-6} .) There existed the possibility, however, that the lower end of the shaft, acting as a piston type source, gave rise to a complex, stationary wave system. If wave reinforcement occurred, the effect could be appreciable and divergence between the theoretical and the physical models significant. The possible presence and influence of resonance in the chamber could be confirmed or disproved by altering the shape and volume of the

† Two jets impinging on each side a guide fin, mounted on the shaft collar. See Figure 18

loading cylinder. A simple method was employed, in which the cylinder was fitted with a small standpipe and then filled with water in increments up to three quarters of the total volume. No significant departures, however, from previously established results were observed.

The validity of the concept of a "constant pressure supply reservoir" depends on the absence of pulsations transmitted through the supply restrictors. The likelihood of propagation and, possibly, of reflection of pressure disturbances upstream of the supply nozzles could not be dismissed. Unfortunately, installation of suitably small and sensitive pressure pick-ups, or hot wire anemometers, in the immediate vicinity of the nozzle entrance and exit would have involved substantial changes in design and elaborate, additional instrumentation. Subsequent investigations, therefore, were limited to a series of simple checks, intended to locate possible sources of trouble in the air supply system. It is, perhaps, both useful and instructive to render a brief account of some of the steps taken in this "trouble-shooting" procedure:

- a. A two cubic foot plenum chamber was installed at a point where the supply line was joined to the upper thrust plate (see assembly drawing in Figure 7), in order to increase the capacity of the supply reservoir and provide a zone in which small fluid disturbances could be dissipated.
- b. The compressor was shut off so that no unsteadiness of flow originated at the source of the supply while readings were recorded. The capacity of the main supply reservoir was sufficiently large to maintain a constant supply pressure in a time interval required to perform one or several measurements.
- c. Since instabilities of pressure regulators and pneumatic valves are similar in nature to those occurring in externally pressurized bearings, the regulators and valves, placed in series in lines supplying the bearings and loading cylinder (see Figure 17), were adjusted for varying degrees of pressure drop across the metering elements. Various settings were made and a number of measurements were repeated.

None of the foregoing measures had any effect on the stability characteristics of the test bearing.

Valid comparisons between theoretical and experimental results could only be made if the pitching (cocking) motion of the shaft remained small in comparison with the amplitudes of axial oscillation. In the course of several preliminary and final runs, the auxiliary capacitance probe was mounted in different positions around and along the shaft, but no measurable amplitudes were detected. Preliminary calculations carried out in the design phase of the apparatus, in which the shaft and the guide bearings were considered as a simple, two-degree-of-freedom system, indicated that the slower mode of vibration could possibly be excited by frequencies of auto-oscillation in the upper range of the experimental band width. Figure 59 shows results of a vibration test, in which the auxiliary capacitance probe was located in a position† where large amplitudes at frequencies close to that of the first mode could most readily be observed. Since the sensitivity of the auxiliary probe was considerably less than that of the primary probe, the gain of the primary instrument was decreased and the amplitude of auto-oscillations increased to 4×10^{-4} inches, approximately twenty times the value observed on the threshold of instability. This permitted a better comparison to be drawn between amplitudes of axial and pitching motions. The frequency of

† Along the six inch outer diameter of the shaft thrust plate.

auto-oscillations was then varied from 375 to 200 cps. The second photograph in Figure 59 shows the largest amplitude of pitching which was observed, occurring at 2091 rad/sec (333 cps). It is realized, of course, that more than two modes could be excited, that the shaft could perform small, conical gyrations within the limits of bearing clearance, or momentarily rotate and translate, but not necessarily in the plane of the capacitance probe. Nevertheless, Figure 59 shows the largest amplitude ratio (approximately 100:1) ever observed in any of the monitoring positions and there is little doubt, therefore, that the overall effect of pitching was a very minor one.

VI. DISCUSSION

1. Comparison of Analytical and Experimental Results

Comparison of theoretical and experimental loci in Figure 53 indicates reasonably good agreement in the region in which pressure differences between the supply reservoir and the recess are highest. In this region, values of δ obtained from the present analysis represent a considerable improvement when compared with those predicted from the simplified, lumped-parameter theory. (See Figure 5.) As the pressure drop across the supply nozzle decreases, the deviation of empirical curves from their calculated equivalents becomes more pronounced. Beyond the points of vertical tangency neither quantitative nor qualitative agreement exists.

With regard to slope, empirical curves and those predicted from the present analysis agree fairly well over a considerable part of the experimental range. The same situation does not hold true for the single locus obtained from the simplified theory. The present analysis predicts conservative (safe) limits, whereas the simplified analysis gives values which are either too high or too low. A most significant improvement, introduced through the refinements incorporated in the distributed-parameter approach, is that the present analysis gives a correct interpretation with regard to influence of the effective bearing mass on stability, a fact to which experimental results lend unequivocal support. As emphasized previously, one of the major shortcomings of lumped-parameter analyses is that they predict the same locus, regardless of magnitude of the bearing mass.[†]

It is interesting to note that for the larger mass, agreement between predicted and experimental loci in Figure 53 is better and extends over a larger portion of the curves. It is more than probable that, as the bearing mass increases, agreement between predicted and actual results progressively improves. This inference may be particularly important, because in actual applications one might expect considerably higher than 0.05 or 0.10 weight to thrust ratios. Since from a practical point of view one is usually interested in "safe depths" of the order of 5×10^{-3} to 20×10^{-3} inches, it is encouraging to note that it is precisely in this region where predictions based on the present analysis constitute a considerable improvement in comparison with those based on simplified analyses.

2. Remarks on the Relative Validity of Theoretical Assumptions and Their Applicability To the Experimental Model

The present investigation included both, analysis and experiment. To the investigators, who have engaged in this dual undertaking, falls the difficult task of accounting for disagreement in areas where it exists. In what follows, an attempt is made to inquire into likely causes of divergence between analytical predictions and empirical results, particularly the single and double valuedness of the respective stability loci.

It will be recalled that the dynamic lubrication equation (4) was required to satisfy a boundary condition at the outer bearing perimeter and to be compatible with the continuity equation

[†] The bearing mass becomes a significant stability parameter in presence of appreciable, external damping only. (See Appendix 2.)

(7) of the variable-volume recess. Now, in implementing the continuity equation, it was assumed that the inflow through the supply nozzle, W_1 , and the outflow along the perimeter of the recess, W_2 , could be considered as quasi-steady. The quasi-steady approach has been successfully employed in problems of charging and discharging of fixed and variable-volume cylinders, in research related to the dynamics of pneumatic controls. A typical example is the work of Shearer [9]. The flow through orifices, under pulsating downstream conditions, has been investigated, both theoretically and experimentally, by Schultz-Grunow [16]. He suggested that limits of applicability of steady-flow equations could be assessed from the reciprocal of the Strouhal number:

$$\phi = \frac{\bar{U} t_0}{d}$$

\bar{U} = Average velocity

t_0 = Period of pulsation

d = Orifice diameter

which is directly related in unidimensional, inviscid flow to the ratio of local and convective acceleration components, $1 + \frac{\partial U}{\partial x} \frac{\partial t}{\partial t}$. He concluded, that for values of $\phi > 510$, the steady-

flow equations yielded accurate values of instantaneous flow rates and the effect of local acceleration was negligible. Although maximum values of ϕ obtained in the course of present experiments were larger than 10^3 , magnitudes of ϕ were generally comparable with 510, and thus not sufficiently far removed from a transition zone, in which the effect of pulsation may have been significant. Other investigators discovered that pulsations propagated upstream of the restrictor and gave rise to complex wave patterns and phase relations on either side of the orifice [47, 48, 49, 50].

The adequacy of considering inflow as quasi-steady is questionable, at least in certain ranges of pressure, frequency and geometrical parameters of the system. In the limiting case, when P_r/P_s approaches the critical ratio, no pressure pulses propagate upstream of the nozzle throat. If one assumes, however, that acoustic equations hold when P_r/P_s approaches unity, the theory of horns, to which the supply nozzles bear a geometrical resemblance, predicts definite phase relations between pressure and flow at the throat [64]. The existence, therefore, of appreciable time lags cannot be entirely dismissed, in which case the assumed, "in phase" perturbation relation, $w_1 = C_3 p_r$, may be deficient.

If we now direct our attention to the outflow from the recess, the entrance effects, associated with fluid acceleration and flow separation at the sharp edge of the perimeter, are further complicated by the variation of the area of admission to the slot under dynamic conditions. Here,

the use of equation (9), e.g., $W_2 = -(\text{constant}) H^3 P_r \frac{\partial P_r}{\partial t}$, implied not only that the outflow could be considered as quasi-steady, but also that there was no transition and that a viscous, laminar flow regime became at once established as the fluid entered the slot. Consider also the case of small-amplitude vibration when the recess volume is large and the pressure deviation, p_r , tends to become very small in comparison with p , the perturbation pressure in the slot. In fact, due to

the trapping and squeezing of the fluid in the slot, maxima of p are likely to occur close to the recess perimeter, where the gas is relatively dense. This may cause large variations of the perturbation pressure gradient in the immediate vicinity of the recess and, in turn, induce appreciable fluid acceleration and deceleration in the region of admission to the slot.[†] Moreover, the

linearized expression, $w_2 = C_4 h - C_5 p_r - C_6 \frac{\partial p_r}{\partial r}$, corresponding to equation (9), does not take into account the complex phenomena occurring in the neighborhood of the recess boundary. Divergence of results may be due partly to the cumulative discrepancy involved in expressing the difference, $w_1 - w_2$, corresponding to the righthand side of the continuity equation (7).

Next, we consider possible shortcomings of assumptions involved in the mass accumulation term on the left-hand side of the continuity equation (7). If we now focus our attention on the internal processes occurring within the variable-volume recess, such as the impingement, deflection or disintegration of jets and the interaction between decelerating and accelerating fluid streams, the physical picture defies mathematical description. Unavoidably, therefore, it becomes necessary to resort to simplifying assumptions, or postulates, such as uniformity of "average" properties at any instant of time. The latter assumption was made in the qualitative analysis of periodic charging and discharging of the variable-volume recess in Appendix 5.

Granted the high degree of oversimplification in formulating the problem, the analysis of Appendix 5 nevertheless suggests that the pressure and density in the recess are not in phase. Numerical examples, indicate, however, that no appreciable time lag is involved, so that the process may be reasonably well described by $P/\rho^n = \text{constant}$. Although the exponent, n , is then not a function of time, it does depend on a dimensionless "charge" parameter, $Q = W_0/\rho_{r0} V_{r0} \omega$, in which W_0 , ρ_{r0} , V_{r0} refer to the equilibrium flow rate, the recess gas density and the recess volume, and ω is the circular frequency of oscillation.

Considerable numerical discrepancies between theoretical and experimental results could be accounted for by selecting more "representative" values of the exponent n , but it is by no means implied here that an explanation for the double valuedness of experimental loci could be supplied by assigning to n values other than $n = 1$ in the recess, or other than $n = 1$ in the slot.^{††}

It is considered that the inertia forces in the slot were small in comparison with viscous forces. Although no definite, analytical proof has been furnished to support this contention, the derivation in Appendix 6 suggests that the neglect of inertia contributions in the bearing clearance may not be very serious, and that the dynamic lubrication equation (4) is a good first approximation. Moreover, in the presence of significant inertia effects, one would expect the disagreement between predicted and empirical results to be greatest at relatively high frequencies of oscillation, whereas exactly the opposite is indicated by the experimental evidence.

In the foregoing discussion, an attempt was made to probe into the more questionable aspects of the present analysis. A critical inquiry would be incomplete and one-sided, if one omitted to

[†] An analogous condition is illustrated diagrammatically in Figure 6a., showing a grossly exaggerated, instantaneous pressure profile and positive gradient at the edge of the recess.

^{††} In the slot, $P/\rho = \text{constant}$ was the assumed relation. See also Appendix 6.

examine both the experimental model and the procedure for possible deficiencies and inherent sources of error. Here, however, the numerous, secondary tests, described in the section "Concluding Stability Experiments," have narrowed down considerably the area of search for a feasible explanation.

The turning point in the experimental phase of this investigation was the discovery of resonance in the system. Isolation of the test structure not only altered the shape of stability loci near resonance points, but also displaced the curves in a direction effecting considerably better agreement between theory and experiment. The extent to which actual motion departs from the idealization of an undamped, single-degree-of-freedom system, for which perfect isolation, absolute rigidity and absence of external damping are assumed, is most difficult to assess. One need only to consider that 10^{-6} inches represented 10 percent of what could be meaningfully interpreted in the presence of mechanical and electronic noise. Since the capacitance gauge measured the relative, instantaneous displacement of bearing surfaces at a point, it provided no information with regard to the absolute motion of boundaries. Nor was it feasible to furnish a perfectly isolated and immobile reference frame for external mounting of capacitance probes.

The extension of the simplified analysis of Appendix 2 to a damped, two-degrees-of-freedom system suggested the possibility of a double valued stability locus. An approximate value of the critical damping ratio was estimated from Figure 30.[†] Calculations then indicated limiting values of critical recess depth on the upper branch of the locus to be of the order 10^{-3} inches, as compared with 10^{-1} inches in the case of experimental results. The simplified analysis, of course, lends only qualitative support to the existence of double valued loci and may predict grossly exaggerated results in this region. It is not unlikely that the extension of the present analysis, to include the effects of elastic and damping properties of the entire system, would result in more realistic predictions of critical values of stability parameters. At any rate, one cannot rule out that the divergence between theory and experiment was due to appreciable motion and accompanying dissipative effects in the supporting structure, whereas perfect rigidity and motion of one boundary only were hypothesized for the idealized model. The importance of considering the motion of the supporting structure was stressed in a recent paper by Tsai [52], who investigated the stability of a simple, pneumatic pressure reducer. The author states in the introduction: "Also, the vibrations of the mounting structure may induce undesirable oscillations in the reducer. To obtain a complete picture of performance, one must therefore investigate the dynamic characteristics of the reducer and analyze the problems of its natural frequency and stability."

Of equal importance is the extent to which the actual, steady-flow pattern conforms to that which has been postulated for the idealized model. The flow of compressible fluids in narrow channels and in externally-pressurized bearings, in various Reynolds and Mach number regimes, has been the subject of numerous, theoretical and experimental investigations.^{††} The Reynolds and Mach numbers corresponding to the flow range of the present investigation were sensibly small, and deviations from calculated, steady-flow bearing characteristics were of the order 2-5 percent. Nevertheless, once oscillation is started, the influence of entrance phenomena on stability may become of far greater significance than their effect under static conditions would seem to indicate.

[†] Trace of decaying vibration of structure when mounted on isolators.

^{††} Representative examples may be found in references [19, 20, 21, 22, 23, 24, 27, 31]. A rather complete list is contained in a bibliography by E.B. Sciulli, reference [44].

The flow pattern in the entrance region does not conform to the idealization of the experimental model. In the flow around the sharp edge of the recess, separation takes place and the fluid stream converges, a toroidal vortex forming beneath the contraction. McGinn [35] obtained streamline patterns for water flow in a sharp-edged, radial diffuser by means of dye filaments, and recorded photographically the vortices formed downstream of the separation point. Shires [22], using air, demonstrated the existence of pressure depressions in the entrance zones of several parallel-surface slot configurations, for various pressure ratios and slot width. The Reynolds number in the experiments of McGinn and Shires was of the same order as that in the present investigation.

Consider a vibration, induced by a random disturbance and accompanied by changes of pressure gradient in the entrance region. The vibration will cause alternate elongation and contraction of the transverse dimension of the vortex ring. The outflow from the recess depends on the width of the effective flow area, rather than on the width of the slot. The amplitude and phase relation between the slot width and the width of the contraction may not be a simple one, and the representation of the instantaneous flow rate by the expression $Q_2 = -(\text{constant}) \left(l^3 p_r \frac{\partial^2 r}{\partial r} \right)$ may lead to considerable error. Conceivably also, an appreciable amount of energy, which would otherwise be dissipated in the process of a self-sustained oscillation, may instead be absorbed through entrance losses. The entrance zone may thus provide an internal damping mechanism and have a stabilizing effect on the bearing. Since entrance phenomena were not considered in the analysis, theory may predict instability in regions which experiments show to be stable.

On the other hand, as one follows the lower branch of a locus and departure from predicted results increases, the Reynolds and Mach numbers decrease, so that entrance effects become less pronounced, up to the point of vertical tangency of the locus. Thereafter, the opposite holds true. It would be inconsistent, therefore, to attribute the main cause of divergence of results solely to entrance effects, except to say that their disregard may have been a contributing factor.

In this section, a number of likely, but by no means proven sources of divergence between theoretical and empirical results, have been discussed. Although the observed discrepancies may have been a cumulative result of several deficiencies involved in the theoretical assumptions, as well as those inherent in the experimental apparatus, the most probable sources of error which suggest themselves are:

- a. The possible insufficiency of the quasi-steady flow representation and of the postulation of uniform properties in expressing the continuity equation of the variable-volume recess.
- b. An appreciable effect of the relative motion of the bearing surfaces, associated with imperfect isolation and/or the distributed, elastic and damping properties of the supporting structure.
- c. The presence of entrance effects in the experimental model, contrasted with their neglect in the present analysis.

VII. CONCLUDING REMARKS AND RECOMMENDATIONS

It has been demonstrated that the dynamic lubrication equation (4) gives a more faithful representation of the effects of partial trapping and squeezing of a compressible fluid film in a long and narrow slot than could hitherto be obtained with the aid of arbitrary assumptions with regard to the flow and the pressure profile. Moreover, the present results have been obtained without resort to any correction factors. It has also been shown, both theoretically and experimentally, that the bearing mass has a significant effect on stability and that stability is enhanced by decreasing the bearing mass. As a consequence of results of the analytical and the experimental phases of this investigation, it has been possible to assess more critically the earlier, lumped-parameter theories.

Experience gained in the course of experiments has shown that the response of the bearing can be greatly influenced by the method of mounting, indicating that in actual applications the mass and the elastic and damping properties of the supporting structure may have to be considered in formulating the stability problem. Stability has been shown to be extremely sensitive to minute changes of certain bearing parameters and system characteristics and quite insensitive to others. The experimental results have also substantiated the validity of the linearized approach in the analysis, since, in regions designated as "stable," no self-sustaining oscillation could be induced, regardless of the magnitude of disturbance.

There are several areas in which the present research could be further extended and supplemented. The stability of bearings cannot be treated as a separate problem and must be dealt with in conjunction with other aspects of an entire system. It is not always possible, however, to formulate the equations of motion of a complex system in terms of distributed parameters. Even after such formulation, it may be impossible to obtain solutions. Moreover, system considerations aside, the distributed parameter approach may also become too involved for more complex bearing configurations. Clearly, therefore, a more rational method of lumped-parameter representation would be desirable.

The present analysis suggests an approach in this direction which merits further consideration. It will be recalled in the case of the rectangular geometry, that in the series representation of the functions y_I and y_{II} we capitalized on the smallness of the parameter ϵ and neglected higher order terms of the expansion. When the first four terms of the expansion are retained, the characteristic equation reduces to a polynomial of the third degree in s . On the other hand, it has been shown in Appendix 2 that the characteristic equation obtained from the simple analysis is also a polynomial of the third degree in s . Since both equations are of the same form and differ only in their coefficients, the results of the present analysis may be helpful in devising a rational method of correlation of the distributed and the lumped-parameter representations. In the case of the circular bearing, it may also be feasible to obtain solutions y_I and y_{II} in the form of series expansions in terms of the small parameter, $12\mu R^2/P_o h_o^2$, which characterizes the equation (19b). It may then be possible to represent the characteristic equation (31b) by a polynomial in s , following a procedure analogous to that which was employed in the case of the rectangular bearing configuration. A correlation of coefficients in the characteristic polynomials of the present and simplified analyses would give the advantage of formulating the problem in terms of ordinary, rather than partial differential equations.

It would be desirable to retain the quasi-steady flow representation in future stability analyses, because of the inherent simplicity of such an approach. Nevertheless, in certain flow regimes, it may become necessary to modify the mathematical description of the charging - discharging process of variable volumes in bearings. Perhaps, as a first step in this direction, it would be useful to determine the throat impedances of simple nozzles and of orifices, in a manner analogous to derivations in the acoustic theory. A better understanding of the phenomena occurring in the entrance region of a slot is also needed, before an attempt is made at an improved mathematical description of fluid flow in the entrance zone. A study of streamline patterns and of vortex formations should be made, when the boundary oscillates in the transverse direction of the slot. A complete time record of flow patterns could be obtained with the aid of a high speed camera, using otherwise methods similar to those employed by McGinn [35] for the case of steady flow of water in the entrance zone of a sharp-edged, radial slot.

Advance consideration has been given to future experiments which would involve rotation of the shaft. For this purpose, an air-driven turbine has been incorporated in the design of the shaft, details of which are shown in Figure 13. The effect on stability and other rotor characteristics due to pressure gradients, induced through centrifugal forces and surface misalignment, is of considerable interest and should be studied. Also, additional stability loci could be obtained for various pressure ratios and types of supply restrictor, under rotating, or non-rotating conditions. The experimental apparatus is capable of providing a great deal of valuable information and can also be modified for the purpose of experimentation with other bearing configurations. It is recommended, therefore, that full use be made in the future of the existing facility.

Finally, since the simple geometries considered in this investigation are frequently encountered in practical applications, and since good agreement exists in regions which are of interest, the programming of a digital computer, to provide design data for a representative range of parameters, is warranted and recommended.

VIII. BIBLIOGRAPHY

1. "Effect of Compressibility at Low Reynolds Number," G. I. Taylor and P. G. Saffman, *Journal of the Aeronautical Sciences*, Vol. 21, No. 8, 1957, pp. 553-562.
2. "A Dynamic Analysis of Externally Pressurized Air Bearings," H. H. Richardson, MIT, Department of Mechanical Engineering, MS thesis, Cambridge, Mass., January 1955.
3. "Static and Dynamic Characteristics of Compensated Gas Bearings," H. H. Richardson, *Trans. ASME*, Vol. 80, No. 7, 1958, pp. 1503-1509.
4. "Instability of an Externally Pressurized Non-Rotating Air Thrust Bearing," L. Licht, General Electric Laboratories, Technical Information Series Report No. R55GL341, September 1955.
5. "Self-Excited Vibrations of an Air-Lubricated Thrust Bearing," L. Licht, D. D. Fuller and B. Sternlicht, *Trans. ASME*, Vol. 80, No. 2, 1958, pp. 411-414.
6. "An Analysis of the Effect of Several Parameters on the Stability of an Air-Lubricated Hydrostatic Thrust Bearing," W. H. Roudebush, NACA TN4095, September 1957.
7. "Air-Hammer Instability in Pressurized Journal Gas Bearings," L. Licht, Paper No. 60-WA-10, presented at the ASME Winter Annual Meeting, New York, December 1960. (To be published *Trans. ASME*.)
8. "Transient Flow Forces and Valve Instability," S. Y. Lee and J. F. Blackburn, *Trans. ASME*, Vol. 74, 1952, pp. 1005-1011.
9. "Study of Pneumatic Processes in Continuous Control of Motion with Compressed Air," J. L. Shearer, *Trans. ASME*, Vol. 78, No. 2, 1956, pp. 233-249.
10. "Nonlinear Analog Study of a High-Pressure Pneumatic Servomechanism," J. L. Shearer, *Trans. ASME*, Vol. 79, No. 3, 1957, pp. 465-472.
11. "Axial Relative Motion of a Circular Step Bearing," L. Licht, *Trans. ASME, Journal of Basic Engineering*, Vol. 81, No. 2, 1959, pp. 109-117.
12. "The Effect of Conduit Dynamics on Control-Valve Stability," F. D. Ezekiel, *Trans. ASME*, Vol. 80, No. 4, 1958, pp. 901-908.
13. "The Design and Analysis of a Servovalve with Flow Feedback," E. Bahniuk and S. Y. Lee, *Trans. ASME, Journal of Basic Engineering*, Vol. 82, No. 1, 1960, pp. 73-80.
14. "Analysis and Design of a Servomotor Operating on High-Pressure Compressed Air," G. Reethof, *Trans. ASME*, Vol. 79, No. 4, 1957, pp. 875-885.

15. "The Effect of Oil-Column Acoustic Resonance on Hydraulic Valve 'Squeal'," F. W. Ainsworth, *Trans. ASME*, Vol. 78, No. 4, 1956, pp. 773-778.
16. "Static and Dynamic Control Characteristics of Flapper-Nozzle Valves," Tsun-Ying Feng, *Trans. ASME, Journal of Basic Engineering*, Vol. 81, No. 3, 1959, pp. 275-284.
17. "Die Vorgänge in Federbelasteten Einspritzdüsen von Kompressorlosen Ölmaschinen," O. Lutz, *Ing. Archiven*, 1953, p. 155.
18. "Dynamical Instability in Flow Systems," T. Baron, *Proceedings of the First Midwestern Conference on Fluid Dynamics*, Ann Arbor, Mich., 1951, pp. 216-225.
19. "Ecoulement d'un Fluide entre Deux Plans Paralleles. Contribution a l'Etude des Butees d'Air," R. Comolet, *Publications Scientifiques et Techniques de l'Air*, No. 334, September 1957.
20. "Ecoulement Radial d'un Palier à Air," E. A. Deuker and A. Wojtech, *Revue Générale l'Hydraulique*, Vol. 17, 1951, pp. 228-234, 285-294.
21. "A Theoretical Investigation of Pressure Depression in Externally Pressurized Gas-Lubricated Circular Thrust Bearings," H. Mori, MIT Lubrication Laboratory, Contract NOrd 17366 (53-138), Cambridge, Mass., 1959.
22. "The Viscid Flow of Air in a Narrow Slot," G. L. Shires, *National Gas Turbine Establishment*, Memo No. 46, December 1948, Farnborough, England.
23. "Flow of a Compressible Fluid in a Thin Passage," S. K. Grinnell, *Trans. ASME*, Vol. 78, No. 4, 1956, pp. 765-771.
24. "Heat Transfer Effects in Hydrostatic Thrust Bearing Lubrication," W. F. Hughes and J. F. Osterle, *Trans. ASME*, Vol. 79, No. 6, 1957, pp. 1225-1228.
25. "Air Bearing Studies at Normal and Elevated Temperatures," J. D. Pigott and E. F. Macks, NACA paper presented at the ASLE Meeting, Boston, Mass., April 1953.
26. U. S. Patent No. 2,683,635, Air Bearing, R. M. Wilcox, 1954.
27. "A Preliminary Investigation of an Air-Lubricated Hydrostatic Thrust Bearing," L. Licht and D. D. Fuller, ASME paper No. 54-Lub-18, presented at the First, Joint ASME/ASLE Conference, October 1954.
28. "Air Bearings for Guidance Components of Ballistic Missiles and their Production Aspects," H. C. Rothe, Paper presented at the First International Symposium on Gas-Lubricated Bearings, Washington, D. C., October 1959.
29. "The Static Strength of Pressure Fed Gas Journal Bearings," C. H. Robinson and F. Sterry, Atomic Energy Research Establishment, Report No. AERE-ED/R 1672, 1958, Harwell, England.

30. "Air Bearings - Research and Applications at the National Engineering Laboratory, Scotland," M. Graneck and J. Kerr, paper presented at the First International Symposium on Gas-Lubricated Bearings, Washington, D. C., October 1959.
31. "The Analysis and Design of Hydrodynamic Gas Bearings," R. R. Weber, North American Aviation Co., Aerophysics Laboratory Report, No. AL-699, September 1949.
32. "The Performance of Externally Pressurized Bearings Using Simple Orifice Restrictors," D. S. Allen, P. J. Stokes and S. Whitley, ASLE paper No. 60L.C-17, presented at the Joint ASME-ASLE Lubrication Conference, Boston, Mass., October 1960.
33. "Air Driven Spinners," L. W. Wightman, *Machine Design*, Vol. 20, No. 5, 1948, pp. 121-125.
34. "Air-Lubricated Bearings," P. M. Mueller, *Product Engineering*, Vol. 22, No. 8, 1951, pp. 112-115.
35. "Observations of Radial Flow of Water Between Fixed Parallel Plates," J. R. McGinn, *Applied Scientific Research, Sec. A*, Vol. 5, 1955, pp. 255-264.
36. "Varieties of Shaft Disturbances Due to Fluid Films in Journal Bearings," B. L. Newkirk, *Trans. ASME*, Vol. 78, 1956, pp. 985-989.
37. "Whirling of a Journal in a Sleeve Bearing," D. Robertson, *Philosophical Magazine, Series 7*, Vol. 15, January 1933, pp. 113-120.
38. "Contribution to the Theory of Oil Whip," H. Poritsky, *Trans. ASME*, Vol. 75, 1953, pp. 1153-1161.
39. "Investigation of Translatory Fluid Whirl in Vertical Machines," G. F. Boeker and B. Sternlicht, *Trans. ASME*, Vol. 78, 1956, pp. 13-19.
40. "Experimental Investigation of Oil Whip," O. Pinkus, *Trans. ASME*, Vol. 78, 1956, pp. 975-983.
41. "Gleitlager mit Luftschmierung," H. Drescher, *Zeit. V.D.I.*, Vol. 95, No. 35, 1953, pp. 1182-1190.
42. "A Theory of Oil Whip," Y. Hori, *Trans. ASME, Journal of Applied Mechanics*, Vol. 26, No. 2, 1959, pp. 189-198.
43. "Some Instabilities and Operating Characteristics of High Speed Gas-Lubricated Journal Bearings," G. K. Fischer, J. L. Cherubim and D. D. Fuller, ASME paper No. 58-A-231.
44. "Bibliography of Gas-Lubricated Bearings," E. B. Scullli, The Franklin Institute Laboratories, Philadelphia, Pa., Interim Report No. I-A2049-6, Contract Nonr 2342 (00), Task NR 697-147, September 1959.[†]

[†] A comprehensive bibliography, containing 290 references directly related to gas lubrication.

45. "Refinement of the Theory of the Infinitely-Long, Self-Acting, Gas-Lubricated Journal Bearing," H. C. Elrod, Jr. and A. Burgdorfer, presented at the First International Symposium on Gas-Lubricated Bearings, Washington, D. C., (October 1959)
46. "Durchflussmessverfahren für Pulsierende Strömungen," F. Schultz-Grunow, *Forschung auf dem Gebiete des Ingenieurwesens*, Vol. 12, 1941, pp. 117-126.
47. "Basic Difficulties in Pulsating Flow Metering," A. R. Deschere, *Trans. ASME*, Vol. 74, 1952, pp. 919-924.
48. "Pulsation and its Effects in Flowmeters," E. J. Lindahl, *Trans. ASME*, Vol. 68, 1946, pp. 883-894.
49. "The Dynamics of Pulsative Flow Through Sharp-Edged Restrictions," R. C. Baird and I. C. Bechtold, *Trans. ASME*, Vol. 74, 1952, pp. 1381-1388.
50. "Pulsating-Flow Measurement - A Literature Survey," A. K. Oppenheim and E. G. Chilton, *Trans. ASME*, Vol. 77, No. 2, 1955, pp. 231-248.
51. "Nonsteady Discharge of Subcritical Flow," G. Rudinger, ASME paper No. 60-WA-152, presented at the ASME Winter Annual Meeting, New York, December 1960. (To be published *Trans. ASME*.)
52. "Dynamic Behavior of a Simple Pneumatic Pressure Reducer," D. H. Tsai and E. C. Cassidy, ASME paper No. 60-WA-186, presented at the ASME Winter Annual Meeting, New York, December 1960. (To be published *Trans. ASME*.)
53. "Rapid Discharge of Gas from a Vessel into the Atmosphere," E. Giffen, *Engineering*, Vol. 150, 1940, p. 134.
54. "Discharge of Exhaust Gases in Two-stroke Engines," J. H. Weaving, *Proc. Inst. Mech. Eng.*, Vol. 161, 1949, pp. 98-120. (See also discussion by J. Kestin.)
55. "The Rapid Discharge of Gases from Vessels," J. Kestin and J. S. Glass, *Aircraft Engineering*, Vol. 23, 1951, pp. 300-304.
56. "A Study of the Processes of Charging and Discharging Constant Volume Tanks with Air," C. K. Skinner and F. D. Wagner, MIT, Department of Mechanical Engineering, SB thesis, Cambridge, Mass., 1954.
57. "Mechanical Vibrations," J. P. Den Hartog, McGraw-Hill Book Co., 3rd. ed., New York, 1941, pp. 356-358, 363-366, 382-386, 386-392.
58. "Vibration Problems in Engineering," S. Timoshenko, Van Nostrand Co., 3rd. ed., New York, 1955, pp. 199-204, 450-452.

59. "Mathematics of Engineering Systems," D. F. Lawden, Wiley and Sons, 1st ed., New York, 1954, pp. 119-128.
60. "Differentialgleichungen Lösungsmethoden und Lösungen," E. Kamke, Chelsea Publishing Co., 3d ed., New York 1948, p. 440, equation 2.162(10).
61. "Tables of Functions," E. Jahnke and F. Emde., Dover Publications, 4th ed., New York, 1945, p. 128.
62. "Mechanic-Electric Transducer," K. S. Lion, Review of Scientific Instruments, Vol. 27, No. 4, 1956, pp. 222-225.
63. "Laplace Transformation - Theory and Engineering Applications," W. T. Thomson, Prentice-Hall Inc., 1st. ed., New York, 1950.
64. "Elements of Acoustical Engineering," H. F. Olson, Van Nostrand Co., 1st. ed., New York, 1940, pp. 86-94.
65. "Viscous Flow Theory," Vol. I, S. I. Pai, Van Nostrand Co., 1st. ed., New York, 1956, p. 134.

IX. NOMENCLATURE

SYMBOL	MEANING	FIRST APPEARANCE	UNITS
A_e	"Equivalent" area, defined in Appendix 2	A2-1	in^2
A_r	Recess area	A2-1, A5-6	in^2
A_c	Coefficient, $-(P_{ro}^2 - P_{at}^2)/X - X_r$	16a	lb^2/in^5
$\bar{A}(s)$	Complex function, defined in text	30	
B_o	Coefficient, $-(P_{ro}^2 - P_{at}^2)/\log_e \frac{R}{R_r}$	16b	lb^2/in^4
$C_{1...6}$	Coefficients, defined in text	15b	
c	Damping constant associated with mass M, Appendix 2	A2-10	lb-sec/in
c_p	Specific heat at constant pressure	A6-4	$\text{in}^2/\text{sec}^2\text{-}^\circ\text{F}$
c_v	Specific heat at constant volume		$\text{in}^2/\text{sec}^2\text{-}^\circ\text{F}$
d_N	Nozzle throat diameter	8	in
e	Base of natural logarithms, 2.718...	16b	No dim.
$F(t)$	Forcing function	6	lb
$f(t)$	Perturbation forcing function in text, $(H(t)/H^*$ in Appendix 6)	14, (A6-7)	lb , (No dim.)
$g_{1,2}$	Functions of a and P_a , defined in text	43b	in
H	Bearing gap width	1	in
H_e	Bearing gap width, equilibrium	12	in
h	Bearing gap width perturbation, $H - H_o$	12	in
h_o	Bearing gap width perturbation amplitude	A5-6	in
\mathcal{Q}	Pressure integral, defined in text and expressed in Appendix I	26b, A1-3	lb
i	$\sqrt{-1}$	33a	No dim.
J	Bessel function	33a	No dim.
K	Spring constant associated with mass M, Appendix 2	A2-10	lb/in
$K_{1...6}$	Coefficients, defined in text	15a	
k	Thermal conductivity	A6-4	$\text{lb/sec-}^\circ\text{F}$

THE FRANKLIN INSTITUTE • Laboratories for Research and Development

I-A2049-12

SYMBOL	MEANING	FIRST APPEARANCE	UNITS
L	Bearing load in text and in Appendix 1 ($R - R_r$ in Appendix 6)	A1-9, (A6-7)	lb, (in)
M	Mass of bearing support	A2-10	lb-sec ² /in
M	Total gas mass-content of bearing	A2-4	lb-sec ² /in
M_r	Gas mass-content of recess volume	7	lb-sec ² /in
m	Bearing mass (Movable, or effective bearing mass)	6	lb-sec ² /in
P	Pressure in bearing gap, abs.	1	lb/in ²
P_{at}	Atmospheric (ambient) pressure, abs.	5	lb/in ²
P_e	Pressure in bearing gap, abs., equilibrium	6	lb/in ²
P_r	Pressure in bearing recess, abs.	6	lb/in ²
P_{ro}	Pressure in bearing recess, abs., equilibrium	6	lb/in ²
P_s	Supply pressure, abs.	8	lb/in ²
p	Perturbation pressure in bearing gap†, $P - P_o$	12	lb/in ²
P_r	Perturbation pressure in bearing recess, $P_r - P_{ro}$	12	lb/in ²
Q	Complex function, defined in text	28	No dim.
Q	"Charge" parameter, defined in Appendix 5	A5-11	No dim.
R	Radius of bearing	5b	in
R_r	Radius of recess	6b	in
c_p	Gas constant, $c_p - c_v$	8	in ² /sec ² -°F
r	Radial coordinate	1b	in
s	Complex variable	19	1/sec
T	Temperature, abs.	A6-4	°F
T_o	Temperature in bearing gap, abs., equilibrium ($T_o = T_{at} = T_{ro} = T_s$)	8	°F
t	Time	3	sec
\bar{V}_i	Velocity functions, defined in Appendix 6	A6-15	No dim.
u	Component of velocity in the x and/or r-direction	A6-1	in/sec
\bar{u}	Mean velocity in the x and/or r-direction	1	in/sec

† Except in Appendix 5, in which $p = P_r - P_{ro}$ is the perturbation pressure in the recess and the subscript "r" is omitted.

SYMBOL	MEANING	FIRST APPEARANCE	UNITS
\bar{V}_1	Velocity functions, defined in Appendix 6	A6-15	No dim.
V_r	Recess volume	A5-6	in ³
V_{ro}	Recess volume, equilibrium	A5-6	in ³
p	Pressure variable, defined in text	18	
\dot{W}_o	Bearing gas mass flow rate, equilibrium	16	lb-sec/in
\dot{W}_1	Rate of gas inflow through supply nozzle	7	lb-sec/in
\dot{W}_2	Rate of gas outflow from recess (or outflow from bearing)	7, A5-1, (A2-4)	lb-sec/in
\bar{W}_1	Velocity functions, defined in Appendix 6	A6-15	No. dim.
w	Velocity component in the z-direction	A6-1	in/sec
w_1	Perturbation inflow, $\dot{W}_1 - \dot{W}_o$	A5-6	lb-sec/in
w_2	Perturbation outflow, $\dot{W}_2 - \dot{W}_o$	A5-6	lb-sec/in
X	Half width of rectangular bearing	5a	in
X_r	Half width of rectangular recess	6a	in
x	Coordinate	1a	in
$x_{I,II}$	Solutions of homogeneous part of equation 19	28, 32a, 37b	
z	Substitution variable, $z = P_o^2$	18	lb ² /in ⁴
z	Coordinate	A6-1	in
α	Compressibility parameter, $12\mu\omega R_f^2 / P_{ro}H_o^2$	37b	No dim.
β	Parameter, $1 - \left(\frac{P_{at}}{P_{ro}} \right)^2 / \log_e \frac{R}{R_r}$	37b, A1-3	No dim.
β	Parameter, $H_o / \delta + H_o$	A5-6	No dim.
γ	Ratio of specific heats, c_p / c_v	8	No dim.
δ	Recess depth	10	in
δ_c	Critical recess depth	44b	in
ϵ	Coefficient, $\frac{12\mu}{H_o^2} \left(\frac{X - X_r}{P_{ro}^2 - P_{at}^2} \right)^2$, text	20a	in ⁶ -sec/lb ³
ϵ	Dimensionless amplitude, h_o / H_o , Appendix 5	A5-6	No dim.

SYMBOL	MEANING	FIRST APPEARANCE	UNITS
z	Parameter, $H^*/R - R_r$, Appendix 6	A6-7	No dim.
ξ	Dummy variable, corresponding to $z = P_o^2$	28a	lb ² /in ⁴
η	Coefficient, $12\mu/H_o^2$	20b	lb-sec/in ⁴
$\bar{\theta}_i$	Temperature functions, defined in Appendix 6	A6-15	No dim.
$\lambda_{1...5}$	Coefficients, defined in Appendix 2	A2-4	
$\Lambda_{0...5}$	Coefficients, defined in Appendix 2	A2-17	
μ	Dynamic viscosity	1	lb-sec/in ²
ν	Kinematic viscosity	A6-7	in ² /sec
ξ	Dimensionless radius, r/R_r	37b	No dim.
π	Constant, 3.141...	8	No dim.
$\bar{\pi}_i$	Pressure functions, defined in Appendix 6	A6-15	No dim.
ρ	Dummy variable, corresponding to r	28b	in
ρ	Gas density in bearing gap	2	lb-sec ² /in ⁴
ρ_r	Gas density in bearing recess	10	lb-sec ² /in ⁴
ρ_{ro}	Gas density in bearing recess, equilibrium	11	lb-sec ² /in ⁴
σ	Perturbation density, $\rho_r - \rho_{ro}$	A5-6	lb-sec ² /in ⁴
$\phi_{I,II}$	Real component of $y_{I,II}$	38b	
$\psi_{I,II}$	Imaginary component of $y_{I,II}$	38b	
ϕ	Phase angle, defined in Appendix 5	A5-36	No dim.
ψ	Phase angle, defined in Appendix 5	A5-37	No dim.
ω	Circular frequency of forced vibration	A5-6	1/sec
ω	Imaginary part of s , $\omega = \alpha P_{ro} H_o^2 / 12\mu R_r^2$	37b	1/sec
ω_c	Critical frequency, corresponding to $s = \pm i\omega_c$ and $\delta = \delta_c$	37b	1/sec

SUBSCRIPTS AND OPERATORS

SYMBOL	REFERS TO	FIRST APPEARANCE
at	Atmospheric, or ambient	5
c	Critical	44b
e	Equivalent	A2-1
i	Ordering subscript (also isentropic, Appendix 5)	16, (A5-20)
m	Amplitude of perturbation, Appendix 5	A5-36
r	Recess and recess boundary	6
s	Supply	8
o	Equilibrium condition	6
D	Differentiation with respect to $\bar{t} = \omega t$, Appendix 5	A5-12
(\cdot)	Differentiation with respect to $\bar{t} = \frac{\nu^*}{L^2} t$, Appendix 6	A6-8
(\cdot)	Differentiation with respect to t , Appendix 2	A2-1
($'$)	Differentiation with respect to $z = P_o^2$, text	19a, 32a
($'$)	Differentiation with respect to x and r (or $\xi = r/R_p$), text	13, (37b)
($-$)	Laplace transform of variable	19
($-$)	Dimensionless quantity	A5-6, A6-7
($-$)	Mean value of quantity	1
($*$)	Reference quantity	A6-7

APPENDIX 1
THE PRESSURE INTEGRAL, β .†

In the integral

$$\beta = \int_{R_r}^R P_o(r) r dr \quad (A1-1)$$

in which

$$P_o(r) = P_{ro} \left(1 - \epsilon \log_e \frac{r}{R_r} \right)^{\frac{1}{2}} \quad (A1-2)$$

and

$$\epsilon = \frac{1 - \left(\frac{P_{at}}{P_{ro}} \right)^2}{\log \frac{R}{R_r}} \quad (A1-3)$$

let

$$2P_o^2 = P_{ro}^2 \epsilon \theta^2 \quad (A1-4)$$

The quantities under the integral sign then become:

$$\left. \begin{aligned} P_o &= P_{ro} \left(\frac{\epsilon}{2} \right)^{\frac{1}{2}} \theta \\ r &= R_r \left(\frac{R}{R_r} \right)^{\frac{P_{ro}^2}{P_{ro}^2 - P_{at}^2} - \frac{\theta^2}{2}} \\ dr &= R_r \left(\frac{R}{R_r} \right)^{\frac{P_{ro}^2}{P_{ro}^2 - P_{at}^2} - \frac{\theta^2}{2}} \frac{\theta}{2} d\theta \end{aligned} \right\} \quad (A1-5)$$

†The method employed here in deriving an expression for β is identical with that contained in reference [27]

so that:

$$\Delta = -P_{ro} P_r^2 \left(\frac{R}{R_r} \right)^{\frac{2 P_{ro}^2}{P_{ro}^2 - P_{at}^2}} \left(\frac{\beta}{2} \right)^{\frac{1}{2}} \int_{\theta(R_r)}^{\theta(R)} \theta^2 e^{-\theta^2} d\theta \quad (A1-6)$$

Integration by parts and introduction of the factor $\frac{2}{\sqrt{\pi}}$ then yields:

$$\Delta = P_{ro} R_r^2 \left(\frac{\pi}{32} \right)^{\frac{1}{2}} \left(\frac{R}{R_r} \right)^{\frac{2 P_{ro}^2}{P_{ro}^2 - P_{at}^2}} \left[\frac{2}{\sqrt{\pi}} \theta e^{-\theta^2} - \frac{2}{\sqrt{\pi}} \int e^{-\theta^2} d\theta \right]_{\theta(R_r)}^{\theta(R)} \quad (A1-7)$$

in which

$$\left. \begin{aligned} \theta(R_r) &= \left(\frac{2}{\beta} \right)^{\frac{1}{2}} \\ \theta(R) &= \frac{P_{at}}{P_{ro}} \left(\frac{2}{\beta} \right)^{\frac{1}{2}} \end{aligned} \right\} \quad (A1-8)$$

Values of the probability integral

$$\frac{2}{\sqrt{\pi}} \int_0^{\theta} e^{-x^2} dx$$

are listed in standard mathematical tables. The integral can be used in determining the load capacity, I , of the bearing:

$$I = \pi R_r^2 P_{ro} \left(\frac{2\Delta}{P_{ro} P_r^2} - \frac{P_{at}}{P_{ro}} \frac{R^2}{R_r^2} + 1 \right) \quad (A1-9)$$

A good approximation of the load capacity, I , may also be obtained in assuming a linear pressure profile. (See Figure A1-1.)

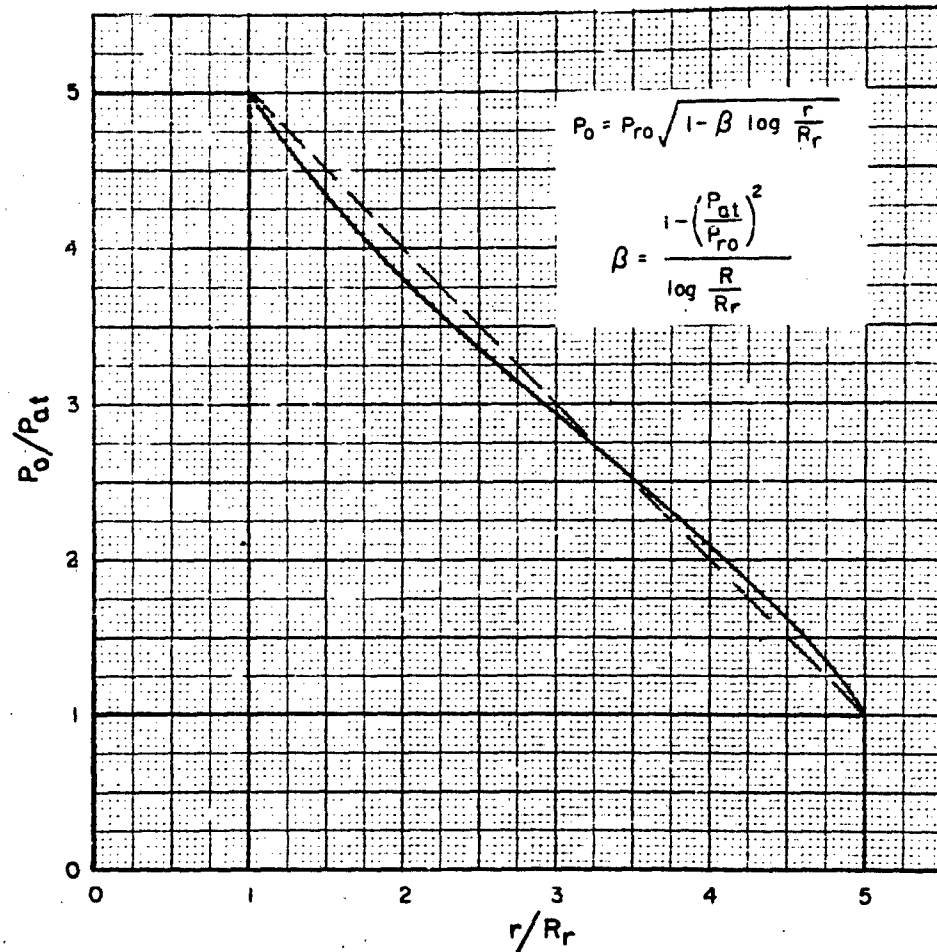


FIG. A1-1. PRESSURE PROFILE AND COMPARISON WITH STRAIGHT LINE APPROXIMATION

APPENDIX 2

SIMPLIFIED STABILITY ANALYSES

In the simplified approach to the stability problem [2,5], the flow in the slot is treated in terms of lumped parameters, and the dynamic pressure profile at any instant of time is assumed to be similar to that which would result if the bearing load were applied statically. In the case of the circular bearing, a further simplification is made by assuming a linear profile along the annulus. (See Figure A1-1, Appendix 1.)

The perturbation equations, which correspond to equations (13), (14) and (15) of the more exact analysis, can then be expressed in terms of the variation of gap width, h , and of the recess pressure, p_r , as follows.

$$m\ddot{h} = A_r p_r + \iint_{A_a} p dA + f(t) = A_e p_r + f(t) \quad (\text{A2-1})$$

$$\lambda_1 \dot{h} + \lambda_2 \dot{p}_r = -\lambda_4 h - (\lambda_3 + \lambda_5) p_r \quad (\text{A2-2})$$

in which

A_r = area over recess

A_a = area over annulus

A_e = "equivalent" area

the explicit expression for A_e being:

$$A_e = 2Y_r \left[1 + \frac{2}{3} \left(\frac{X}{X_r} - 1 \right) \frac{\left(\frac{P_{ro}}{P_{at}} \right)^2 + 2 \left(\frac{P_{at}}{P_{ro}} \right) - 3}{\left(\frac{P_{ro}}{P_{at}} - \frac{P_{at}}{P_{ro}} \right)^2} \right] \quad (\text{A2-3a})$$

$$A_e = \frac{1}{3} \pi R_r^2 \left[\left(\frac{R}{R_r} \right)^2 + \left(\frac{R}{R_r} \right) + 1 \right] \quad (\text{A2-3b})$$

while the coefficients λ_i are as follows:

$$\left. \begin{aligned} \lambda_1 &= \left(\frac{\partial M}{\partial H} \right)_o = \frac{2X_r P_{ro}}{RT_o} \left\{ 1 + \frac{2}{3} \left(\frac{X}{X_r} - 1 \right) \left(\frac{P_{ro}}{P_{at}} \right) \frac{1 - \left(\frac{P_{at}}{P_{ro}} \right)^3}{\left(\frac{P_{ro}}{P_{at}} - \frac{P_{at}}{P_{ro}} \right)} \right\} \\ \lambda_2 &= \left(\frac{\partial M}{\partial P_r} \right)_o = \frac{2X_r H_o}{\gamma RT_o} \left\{ \left(\frac{\delta}{H_o} + 1 \right) + \frac{2}{3} \gamma \left(\frac{X}{X_r} - 1 \right) \frac{\left(\frac{P_{ro}}{P_{at}} \right)^2 + 2 \left(\frac{P_{at}}{P_{ro}} \right) - 3}{\left(\frac{P_{ro}}{P_{at}} - \frac{P_{at}}{P_{ro}} \right)^2} \right\} \\ \lambda_3 &= - \left(\frac{\partial W_1}{\partial P_r} \right)_o = \frac{W_o}{2P_{ro}} \left(\frac{2 - \frac{P_a}{P_{ro}}}{\frac{P_a}{P_{ro}} - 1} \right) \\ \lambda_4 &= \left(\frac{\partial W_2}{\partial H} \right)_o = \frac{3W_o}{H_o} \\ \lambda_5 &= \left(\frac{\partial W_2}{\partial P_r} \right)_o = \frac{2\Gamma_{ro} W_o}{P_{ro}^2 - P_{at}^2} \end{aligned} \right\} \quad (A2-4a)$$

$$\left. \begin{aligned}
 \lambda_1 &= \left(\frac{\partial M}{\partial H} \right)_0 = \frac{\pi R_r^2 P_{ro}}{k T_o} \left\{ 1 + \left(\frac{P_{at}}{P_{ro}} \right) \left[\left(\frac{R}{R_r} \right)^2 - 1 \right] + \left(1 - \frac{P_{at}}{P_{ro}} \right) \frac{\left(\frac{R}{R_r} \right)^3 - 3 \left(\frac{R}{R_r} \right) + 2}{3 \left(\frac{R}{R_r} - 1 \right)} \right\} \\
 \lambda_2 &= \left(\frac{\partial W}{\partial P_r} \right)_0 = \frac{\pi R_r^2 H_o}{2 k T_o} \left\{ \left(\frac{\delta}{H_o} + 1 \right) + \gamma \frac{\left(\frac{R}{R_r} \right)^2 - 3 \left(\frac{R}{R_r} \right) + 2}{3 \left(\frac{R}{R_r} - 1 \right)} \right\} \\
 \lambda_3 &= - \left(\frac{\partial W_1}{\partial P_r} \right)_0 = \frac{W_o}{2 P_{ro}} \left(\frac{2 - \frac{P_s}{P_{ro}}}{\frac{P_s}{P_{ro}} - 1} \right) \\
 \lambda_4 &= \left(\frac{\partial W_2}{\partial H} \right)_0 = \frac{3 W_o}{H_o} \\
 \lambda_5 &= \left(\frac{\partial W_2}{\partial P_r} \right)_0 = \frac{2 P_{ro} W_o}{P_{ro}^2 - P_{at}^2}
 \end{aligned} \right\} \quad (A2-4b)$$

Combining equations (A2-1) and (A2-2) we obtain:

$$\ddot{h} + \left(\frac{\lambda_3 + \lambda_5}{\lambda_2} \right) \dot{h} + \left(\frac{\lambda_e}{m} \frac{\lambda_1}{\lambda_2} \right) \dot{h} + \left(\frac{\lambda_e}{m} \frac{\lambda_4}{\lambda_2} \right) h = g(t) \quad (A2-5)$$

The characteristic equation is a cubic:

$$s^3 + \Lambda_2 s^2 + \Lambda_1 s + \Lambda_0 = 0 \quad (A2-6)$$

and stability conditions require that all coefficients Λ_i be positive, and that

$$\Lambda_1 \Lambda_2 > \Lambda_0 \quad (\text{A2-7})$$

The inequality (A2-7) reduces to:

$$\frac{\lambda_1}{\lambda_2} > \frac{\lambda_4}{\lambda_3 + \lambda_5} \quad (\text{A2-8})$$

from which the critical recess depth, indicated with broken lines in Figures 3 and 5, was calculated.

It is to be noted that the coefficients λ_i are analogous to the coefficients C_i and K_i in the more exact analysis, but that there is no one-to-one correspondence, except for λ_3 and λ_4 .

Next, consider the relative, axial motion of two thrust plates, one integral with a rotor, of mass m , the other with a support, of mass M , resting on isolators, or on an elastic foundation. We associate with the supporting structure the lumped elastic and damping constants, K and c . For the resulting, two-degrees-of-freedom system, shown diagrammatically in the appended Figure A2-1, the following set of equations may be written:

$$m \ddot{x}_2 - A_e p_r = f(t) \quad (\text{A2-9})$$

$$M \ddot{x}_1 + c \dot{x}_1 + K x_1 + A_e p_r = 0 \quad (\text{A2-10})$$

$$\lambda_1 \dot{h} + \lambda_2 p_r + \lambda_4 h + (\lambda_3 + \lambda_5) p_r = 0 \quad (\text{A2-11})$$

in which

$$h = x_2 - x_1 \quad (\text{A2-12})$$

Applying the Laplace transformation to equations (A2-9) through (A2-11), and assuming initial rest conditions, we obtain:

$$s^2 \bar{x}_2 - \frac{A_e}{m} \bar{p}_r = \frac{\bar{f}(s)}{m} \quad (\text{A2-13})$$

$$\left(s^2 + s \frac{c}{M} + \frac{K}{M}\right) \bar{x}_1 + \frac{\lambda_e}{m} \bar{p}_r = 0 \quad (A2-14)$$

$$\bar{x}_2 - \bar{x}_1 - \left(\frac{s\lambda_2 + \lambda_3 + \lambda_5}{s\lambda_1 + \lambda_4}\right) \bar{p}_r = 0 \quad (A2-15)$$

The characteristic determinant, corresponding to the set of equations (A2-13) through (A2-15) is:

0	s^2	$-b$
$s^2 + Cs + \frac{K}{M}$	0	B
-1	1	$\frac{s\lambda_2 + \lambda_3 + \lambda_5}{s\lambda_1 + \lambda_4}$

$$= 0 \quad (A2-16)$$

in which

$$C = \frac{c}{M}; \quad B = \frac{\lambda_e}{M};$$

$$C = \frac{c}{M}; \quad b = \frac{\lambda_e}{m};$$

The characteristic equation is a quintic:

$$\Lambda_5 s^5 + \Lambda_4 s^4 + \Lambda_3 s^3 + \Lambda_2 s^2 + \Lambda_1 s + \Lambda_0 = 0 \quad (A2-17)$$

in which the coefficients, Λ_i , are as follows:

$$\left. \begin{aligned} \Lambda_5 &= \lambda_2 \\ \Lambda_4 &= C\lambda_2 + (\lambda_3 + \lambda_5) \\ \Lambda_3 &= \Omega^2 \lambda_2 + C(\lambda_3 + \lambda_5) + (B + b)\lambda_1 \\ \Lambda_2 &= \Omega^2 (\lambda_3 + \lambda_5) + Cb\lambda_1 + (B + b)\lambda_4 \\ \Lambda_1 &= b(\Omega^2 \lambda_1 + C\lambda_4) \\ \Lambda_0 &= b\Omega^2 \lambda_4 \end{aligned} \right\} \quad (A2-18)$$

Without loss of generality, one may assume that $\Lambda_3 > 0$. The necessary and sufficient conditions that all roots of the quintic have negative real parts and the system be stable can be stated as follows [59]:

$$\Delta_1 = \Lambda_4 > 0 \quad (\text{A2-19})$$

$$\Delta_2 = \begin{vmatrix} \Lambda_4 & \Lambda_5 \\ \Lambda_2 & \Lambda_3 \end{vmatrix} = (\Lambda_4 \Lambda_3 - \Lambda_5 \Lambda_2) > 0 \quad (\text{A2-20})$$

$$\Delta_3 = \begin{vmatrix} \Lambda_4 & \Lambda_5 & 0 \\ \Lambda_2 & \Lambda_3 & \Lambda_4 \\ \Lambda_0 & \Lambda_1 & \Lambda_2 \end{vmatrix} = \Lambda_4 (\Lambda_5 \Lambda_0 - \Lambda_4 \Lambda_1) + \Lambda_2 \Lambda_2 > 0 \quad (\text{A2-21})$$

$$\Delta_4 = \begin{vmatrix} \Lambda_4 & \Lambda_5 & 0 & 0 \\ \Lambda_2 & \Lambda_3 & \Lambda_4 & \Lambda_5 \\ \Lambda_0 & \Lambda_1 & \Lambda_2 & \Lambda_3 \\ 0 & 0 & \Lambda_0 & \Lambda_1 \end{vmatrix} = - [(\Lambda_5 \Lambda_0 - \Lambda_4 \Lambda_1)^2 + (\Lambda_3 \Lambda_0 - \Lambda_2 \Lambda_1) \Delta_2] > 0 \quad (\text{A2-22})$$

$$\Delta_5 = \Lambda_0 \Lambda_4 > 0 \quad (\text{A2-23})$$

Since Λ_5 , Λ_4 , and Λ_0 are generally positive, it is sufficient to examine the signs of Δ_2 , Δ_3 and Δ_4 .

Two points in the latter part of this analysis are of particular interest:

- a. If the damping coefficient, c , is zero, the stability conditions of this system are identical with those given in the inequality (A2-8) for the case of a rigidly supported bearing.
- b. Since $\Lambda_5 = \Lambda_2$ is the only coefficient containing the recess depth, δ , as a parameter, the determinants Δ_3 and Δ_4 yield a quadratic and a cubic in δ . Consequently, unlike in the case of the undamped, rigidly supported bearing, more than one value of δ_c may correspond to the same value of the pressure parameter, $P_s = P_{ro}/P_{ro}$.

In the foregoing analysis, it was assumed that the external damping for the rotor, of mass m , was negligible. This, indeed, would be the case if gas bearings were employed as a means of lateral support, but no difficulty, other than an algebraic one, is involved in adding a damping term, $-c_2 \dot{x}_2$, to the left hand side of equation (A2-9).

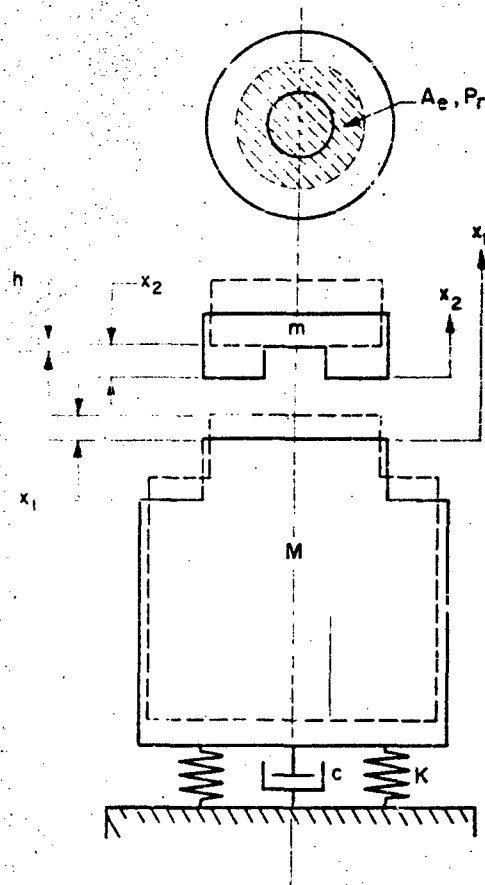


FIG. A2-1. SCHEMATIC DIAGRAM OF BEARING AND FLEXIBLE SUPPORT

APPENDIX 3

RECTANGULAR GEOMETRY - TABULATION OF CALCULATED RESULTS

$2X = 1 \text{ in}$ $P_{at} = 14.7 \text{ psia}$ $P_s = 88.2 \text{ psia}$ $m = 1.65 \times 10^{-3} \text{ lb-sec}^2/\text{in. unit length.}$ $T_o = 530^\circ \text{ F abs}$ $\mu = 2.65 \times 10^{-9} \text{ lb-sec/in}^2$ $\gamma = c_p/c_v = 1.4$	
I.	$2X_r = 0.2 \text{ in; } a_N = 7.54 \times 10^{-4} \text{ in}^2$
II.	$2X_r = 0.1 \text{ in; } a_N = 7.54 \times 10^{-4} \text{ in}^2$
III.	$2X_r = 0.1 \text{ in; } a_N = 6.86 \times 10^{-3} \text{ in}^2$

Note: δ'_c refers to results of the simplified analysis.

P_{ro}	$P_s - P_{ro}/P_{ro}$	α_c	δ_c	δ'_c
psia	-	$\frac{\text{rad}}{\text{sec}} \times 10^{-3}$	$\text{in} \times 10^3$	$\text{in} \times 10^3$
I				
72.5	0.217	4.93	1.90	2.21
75.0	0.176	4.82	2.65	2.93
80.0	0.103	4.35	5.75	5.64
83.2	0.060	3.75	11.8	9.70
85.0	0.0376	3.19	22.6	15.0
II				
72.5	0.217	4.72	3.57	4.10
75.0	0.176	4.61	5.17	5.63
80.0	0.103	4.16	12.0	11.0
83.2	0.060	3.58	26.2	19.1
85.0	0.0376	3.02	54.1	29.7
III				
72.5	0.217	3.26	7.45	8.55
75.0	0.176	3.19	10.8	11.8
80.0	0.103	2.89	24.8	27.0
83.2	0.060	2.51	52.5	39.8
85.0	0.0376	2.16	101.0	62.0

APPENDIX 4.

CIRCULAR GEOMETRY - DETERMINATION OF CRITICAL
RECESS DEPTHS. TABULATION OF CALCULATED AND
EXPERIMENTAL RESULTS.

When explicit expression of the coefficients C_{ij} in equation (16b), are substituted into the characteristic determinant (31b) and the complex variable, s , is taken as equal to $i\omega$, the latter can be written as:

$$\| \Delta \| = \begin{vmatrix} F_{11} & F_{12} \\ F_{21} & F_{22} \end{vmatrix} = \begin{vmatrix} F_{11} + G_{11} & F_{12} + G_{12} \\ F_{21} + G_{21} & F_{22} + G_{22} \end{vmatrix} = 0 \quad (A4-1)$$

in which

$$F_{11} = i \left[\frac{2H_o^2}{P_{ro} H_r^2} - \frac{m P_{ro} H_o^2}{144 \pi \mu^2 R_r^6} (\alpha H_o)^3 \right]$$

$$F_{12} = F_{21} = i a$$

$$F_{22} = -i \left(\frac{a}{y H_o} \delta + \frac{a}{y} \right) - \frac{\beta}{2} \left(\frac{2 - \frac{P_s}{P_{ro}}}{\frac{P_s}{P_{ro}} - 1} \right)$$

$$G_{11} = - \left\{ 2 \frac{\partial Q}{\partial \xi} (5, 1) + 2 \left(\frac{P_{at}}{P_{ro}} \right)^2 \left(\frac{R}{R_r} \right) \frac{\partial Q}{\partial \xi} (1, 5) \right.$$

$$\left. - 2 \left[1 + \left(\frac{P_{at}}{P_{ro}} \right)^2 \right] \left(\frac{R}{R_r} \right)^3 \frac{\partial Q}{\partial \xi} (1, 1) + \left[1 - \left(\frac{P_{at}}{P_{ro}} \right)^2 \right] \right\}$$

$$G_{12} = - \left\{ 2 \frac{\partial Q}{\partial \xi} (5, 1) + 2 \left(\frac{R}{R_r} \right)^3 \frac{\partial Q}{\partial \xi} (1, 1) + 1 \right\}$$

(A4-2)

$$C_{21} = \left\{ 2 \frac{\partial \eta}{\partial \xi} (5, 1) - 2 \left(\frac{P_{at}}{P_{ro}} \right)^2 \left(\frac{R}{R_r} \right)^{1/2} \frac{\partial \eta}{\partial \xi} (1, 1) + (1 + \beta) \right\} \quad \left. \begin{array}{l} \text{(A4-2)} \\ \text{Cont} \end{array} \right\}$$

$$C_{22} = \left\{ 2 \frac{\partial \eta}{\partial \xi} (5, 1) + 1 \right\}$$

and

$$\left. \begin{aligned} \frac{\partial \eta}{\partial \xi} (5, 1) &= \left[\frac{(\phi_I \phi_{II} + \psi_I \psi_{II}) + i(\phi_{II} \psi_I - \phi_I \psi_{II})}{\phi_{II}^2 + \psi_{II}^2} \right]_{\xi=5} \\ \frac{\partial \eta}{\partial \xi} (1, 5) &= \left[\frac{(\phi_{II} \phi_{II}' + \psi_{II} \psi_{II}') + i(\phi_{II} \psi_{II}' - \phi_{II}' \psi_{II})}{\phi_{II}^2 + \psi_{II}^2} \right]_{\xi=5} \\ \frac{\partial \eta}{\partial \xi} (1, 1) &= \left[\frac{\phi_{II} - i \psi_{II}}{\phi_{II}^2 + \psi_{II}^2} \right]_{\xi=5} \end{aligned} \right\} \quad \text{(A4-3)}$$

In the foregoing expressions:

$$\left. \begin{aligned} \alpha &= \frac{12 \mu R_r^2 \omega}{P_{ro} H_o^2} \\ \beta &= \frac{1 - \left(\frac{P_{at}}{P_{ro}} \right)^2}{\log_e \frac{R}{R_r}} \\ \delta &= \int_{R_r}^R P_o(r) r dr \quad (\text{Appendix 1.}) \end{aligned} \right\} \quad \text{(A4-4)}$$

and $\phi(\xi)$, $\psi(\xi)$ are the variables in equation (405), solutions of which, for discrete values of α and for $\beta = 0.596481$, are tabulated in Appendix 7.

Let the bearing geometry and the parameters P_{at} , P_{ro} , T_o , γ and μ be specified. The gap width, H_o , can then be expressed in terms of P_s , the supply pressure, by equating the steady-state mass-flow rates through the nozzle and through the slot, e.g.:

$$W_o = \frac{\pi \beta P_{ro}^2}{12 \mu^2 T_o} H_o^3 = 2 \left(\frac{\pi d_N^2}{4} \right) \left[\frac{\gamma}{RT_o} \left(\frac{2}{\gamma+1} \right)^{\frac{\gamma+1}{\gamma-1}} P_{ro}^2 \left(\frac{P_s}{P_{ro}} - 1 \right) \right]^{\frac{1}{2}} \quad (A4-5)$$

Given α , the unknown parameters which appear explicitly in the characteristic determinant are P_s and δ , which must be selected in such a manner as to reduce simultaneously to zero the real and imaginary parts of the characteristic equation. (e.g., $\delta_1 = \delta_2 = \delta_c$ in equation 43b.)

This reduction was accomplished by trial and error, as shown in the following sample calculation.

Sample Calculation

Given:

$$m = 6.477 \times 10^{-2} \text{ lb-sec}^2/\text{in}$$

$$R_r = 0.5 \text{ in}$$

$$R = 2.5 \text{ in}$$

$$P_{at} = 14.7 \text{ psia}$$

$$P_{ro} = 73.5 \text{ psia}$$

$$T_o = 530^\circ \text{ Fabs.}$$

$$E = 2.47 \times 10^5 \text{ in}^2/\text{sec}^2\text{-}^\circ\text{F}$$

$$\gamma = 1.4$$

$$\mu = 2.65 \times 10^{-9} \text{ lb-sec/in}^2$$

Let

$$\alpha = 0.050$$

and assume

$$P_s = 79.6 \text{ psia}$$

Then

$$P = 0.5965$$

$$V = 0.1124 \times 10^3$$

and from Appendix 7 have:

$$\psi_I(5) = 0.3733$$

$$\psi_I(5) = 0.4772$$

$$\psi_{II}(5) = 0.3528 \times 10^1; \quad \psi'_{II}(5) = 0.6841$$

$$\psi_{II}(5) = 0.9151; \quad \psi'_{II}(5) = 0.8906$$

From equation (A4-3) have:

$$2 \frac{\partial \psi}{\partial \xi}(5, 1) = 0.2640 + i 0.2020$$

$$2 \frac{\partial \psi}{\partial \xi}(1, 5) = 0.4860 + i 0.3788$$

$$2 \frac{\partial \psi}{\partial \xi}(1, 1) = 0.5312 - i 0.1378$$

Equation (A4-5) yields:

$$W_o = 0.2069 \times 10^{-4} \left(\frac{P_s}{P_{ro}} - 1 \right)^{1/2} = 0.6019 \times 10^{-5}$$

so that

$$H_o^3 = 0.4096 \times 10^{-3} W_o = 0.2465 \times 10^{-8}$$

$$H_o^2 = 0.1825 \times 10^{-5}$$

$$H_o = 0.1351 \times 10^{-2}$$

and

$$(a H_o)^3 = 0.3082 \times 10^{-12}$$

The elements of the determinant (A4-1) then become:

$$\begin{aligned}
 & \left. \begin{aligned} F_{11} &= i 0.5577 \\ G_{11} &= -0.8620 \times 10^{-1} - i 0.5983 \\ T_{11} &= -0.8620 \times 10^{-1} - i 0.4060 \times 10^{-1} \end{aligned} \right\} \\
 & \left. \begin{aligned} F_{22} &= -0.3295 \times 10^{-1} - i 0.3571 \times 10^{-1} - i 0.2544 \times 10^2 \delta \\ G_{22} &= -0.1254 \times 10^1 - i 0.2020 \\ T_{22} &= -0.4359 \times 10^1 - i 0.2377 - i 0.2644 \times 10^2 \delta \end{aligned} \right\} \\
 & \left. \begin{aligned} F_{12} &= i 0.5000 \times 10^{-1} \\ G_{12} &= 0.7600 \times 10^{-1} + i 0.5101 \\ T_{12} &= 0.7600 \times 10^{-1} + i 0.5601 \end{aligned} \right\} \\
 & \left. \begin{aligned} F_{21} &= i 0.5000 \times 10^{-1} \\ G_{21} &= 0.1812 \times 10^1 + i 0.2143 \\ T_{21} &= 0.1812 \times 10^1 + i 0.2643 \end{aligned} \right\}
 \end{aligned}$$

For $\alpha = 0.050$ and $P_s = 79.6$, the characteristic determinant (A4-1) reduces to:

$$\begin{aligned}
 \Delta &= T_{11} T_{22} - T_{12} T_{21} \\
 &= a(\delta - g_1) + ib(\delta - g_2) \\
 &= -1.073(\delta - 0.3668) + i 2.279(\delta - 0.3639)
 \end{aligned}$$

THE FRANKLIN INSTITUTE • *Laboratories for Research and Development*

I-A2049-12

Results of similar calculations for other values of P_N are as follows:

P_N	g_1	g_2
81.0	0.2550	0.3724
80.0	0.3274	0.3675
79.8	0.3455	0.3655
79.6	0.3668	0.3630

A plot of g_1 and g_2 vs. P_N , for $a = 0.050$, is shown in the appended Figure A4-1.

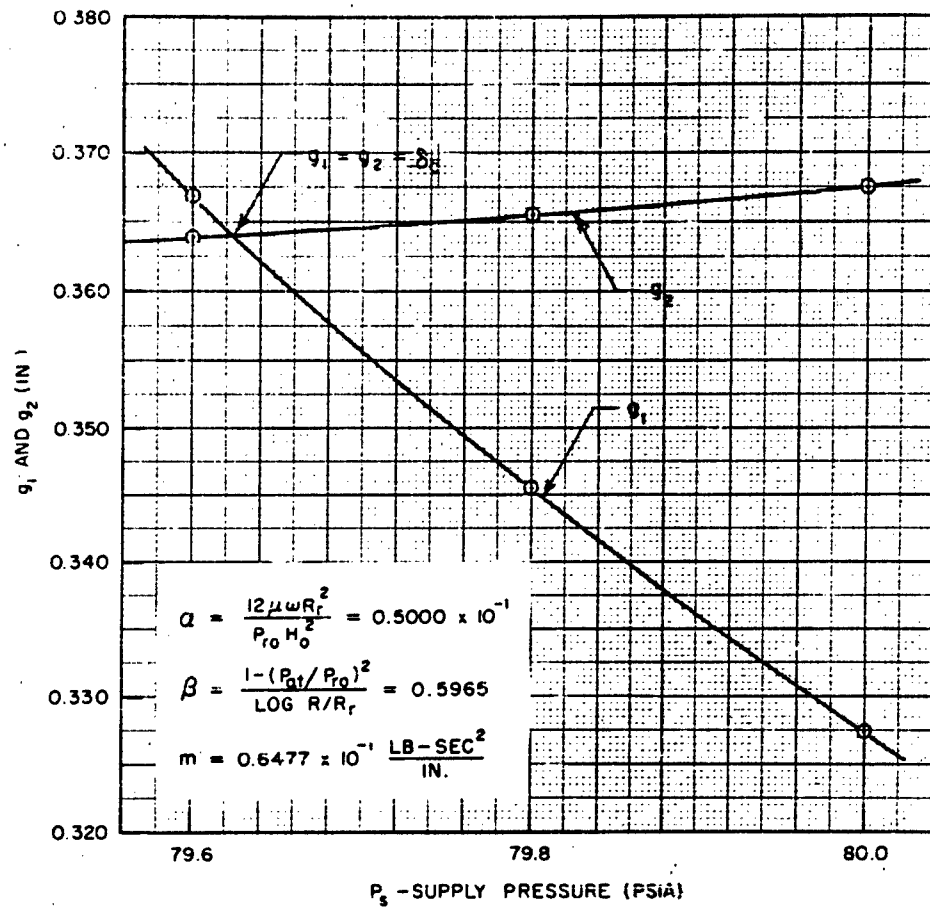


FIG. A4-1. DETERMINATION OF THE CRITICAL RECESS DEPTH FOR $\alpha = 0.050$

TABULATION OF CALCULATED RESULTS

PRESENT ANALYSIS

P_s	$P_s - P_{ro}/P_{ro}$	δ_c	ω_c
psia	-	in $\times 10^3$	$\frac{\text{rad}}{\text{sec}} \times 10^{-3}$
I. $m = 3.592 \times 10^{-2} \text{ lb-sec}^2/\text{in}$			
82.9	0.127	143	1.55
83.0	0.129	110	1.72
83.1	0.131	95.9	1.81
83.2	0.132	90.0	1.85
83.3	0.133	83.5	1.90
83.4	0.135	78.1	1.94
84.2	0.146	49.0	2.24
II. $m = 6.477 \times 10^{-2} \text{ lb-sec}^2/\text{in}$			
79.1	0.0803	2650	0.334
79.6	0.0830	364	0.845
80.3	0.0925	117	1.22
80.6	0.0966	116	1.33
81.0	0.102	90.1	1.44
82.2	0.118	54.6	1.67
82.8	0.127	45.4	1.75
83.1	0.131	41.6	1.79
83.6	0.137	36.6	1.84
84.2	0.146	31.4	1.89
85.2	0.159	25.4	1.97
87.1	0.185	18.1	2.09
89.6	0.219	12.3	2.19
91.8	0.249	9.09	2.27
93.8	0.276	6.96	2.32
III. $m = 11.68 \times 10^{-2} \text{ lb-sec}^2/\text{in}$			
78.1	0.0626	273	0.769
81.4	0.108	50.8	1.29
82.4	0.121	39.9	1.36
88.4	0.203	13.8	1.62
91.0	0.238	9.60	1.68

$$2R = 5 \text{ in}$$

$$2R_r = 1 \text{ in}$$

$$d_N = 0.055 \text{ in } (a_N = 0.237 \times 10^{-6} \text{ in}^2)$$

$$P_{a2} = 14.7 \text{ psia}$$

$$P_{ro} = 73.5 \text{ psia}$$

$$T_o = 530^\circ \text{ F abs.}$$

$$\mu = 2.65 \times 10^{-9} \text{ lb-sec/in}^2$$

$$\gamma = \frac{c_p}{c_v} = 1.4$$

SIMPLIFIED ANALYSIS

P_s	$P_s - P_{ro}/P_{ro}$	δ_c	ω_c
psia	-	in $\times 10^3$	$\frac{\text{rad}}{\text{sec}} \times 10^{-3}$
75.0	0.0204	158	1.05
80.0	0.0884	42.0	1.76
85.0	0.157	23.3	2.07
90.0	0.225	15.2	2.25
95.0	0.293	10.5	2.37

TABULATION OF EXPERIMENTAL RESULTS

 $2L = 5$ in $2R_p = 1$ inTwelve 0.0167 in diam. nozzles (Total throat area = 0.263×10^{-2} in²)I = 172 lb (Theoretical load at $P_{ro} = 5 P_{at} = 73.5$ psia)I. $m = 6.477 \times 10^{-2}$ lb-sec² in; $P_{at} = 14.74$ psia; $T_o = 537^\circ$ F abs.II. $m = 11.66 \times 10^{-2}$ lb-sec² in; $P_{at} = 14.63$ psia; $T_o = 536^\circ$ F abs.

I

P_c	δ_c	ω_c
psia	in $\times 10^3$	rad/sec
96.45	7.1	2242
95.45	7.7	2227
91.45	8.3	2214
93.45	9.4	2185
92.45	10.7	2153
91.45	13.0	2126
90.50	16.8	2076
89.50	23.5	1987
88.50	32.7	1884
87.50	46.0	1802
86.50	59.0	1727
86.05	69.0	1689
85.75	89.5	1610
85.75	122	1487
86.05	146	1424
86.50	170	1380
87.50	200	1330
89.50	244	1307
91.45	274	1277
93.45	293	1232
95.45	302	1334
97.40	308	1346

II

P_s	δ_c	ω_c
psia	in $\times 10^3$	rad/sec
96.45	6.1	1713
95.45	6.9	1706
94.45	7.5	1699
93.45	8.3	1684
92.45	9.2	1676
91.45	10.6	1647
90.50	12.5	1621
89.50	14.7	1590
88.50	17.7	1552
87.50	22.2	1515
86.50	29.3	1471
85.55	38.2	1421
84.55	49.1	1362
83.55	62.5	1313
82.60	84.5	1239
82.10	107	1179
81.60	147	1094
81.60	206	1055
82.10	290	929
82.60	335	910
83.55	405	873
84.55	451	864
85.55	487	857
87.50	545	866
89.50	590	873
91.45	620	903
93.45	635	908
95.45	640	937
97.40	630	970

APPENDIX 5

THE PERIODIC CHARGING AND DISCHARGING
OF A VARIABLE-VOLUME RECESS

The purpose of this appendix is to investigate, at least quantitatively, the adequacy of the assumption that the process of alternate charging and discharging of the variable-volume recess could be represented by the isentropic pressure-density relation $P/\rho^\gamma = \text{constant}$ to a reasonable degree of approximation.

In the course of experimentation, small amplitude auto-oscillations and sine waves have been viewed simultaneously and compared on the display of the cathode ray oscilloscope. Observed differences in wave form were slight. We shall consider, therefore, the case of prescribed, sinusoidal motion of one bearing surface and, making a series of simplifying assumptions, similar to those in Appendix 2, utilize the energy equation, instead of resorting to an a priori assumption of the pressure-density relation in the recess region.

In what follows, pertinent equations will be developed and linearized. Resulting perturbation amplitudes of pressure and density, as well as phase angles, will be related to those obtained when $P/\rho^\gamma = \text{constant}$. Numerical examples will be given for parameter values corresponding to representative points on the double valued, experimental stability locus I, Figure 55.

It will be assumed that perfect mixing of the entering gas occurs, but that fluid velocities in the region V_r are negligible and properties uniform throughout at any instant of time. Adiabaticity and equality of temperatures T_u and T_r of initially steady flow will also be assumed (e.g., $T_u = T_{r0} = T_0$). The flow rates and their perturbations will be expressed identically as in Appendix 2, implying the quasi-steady flow and lumped parameter approach to the problem. The fluid will be treated as a perfect gas with constant specific heats, e.g.:

$$\frac{P}{\rho} = \gamma T; \quad h = c_p - c_v; \quad \frac{c_p}{c_v} = \gamma$$

so that

$$\left. \begin{aligned} \underline{u} - c_v T &= \frac{1}{\gamma - 1} \frac{P}{\rho} \\ \underline{h} &= c_p T = \frac{\gamma}{\gamma - 1} \frac{P}{\rho} \end{aligned} \right\}$$

where \underline{u} is the internal energy and \underline{h} the enthalpy.

The continuity and energy equations for the system shown in Figure A5-1 are as follows:

$$W_1 - W_2 = \frac{dM_r}{dt} = \frac{d}{dt} (\rho_r V_r) \quad (A5-1)$$

$$W_1 h_s - W_2 h_r = \frac{d}{dt} (\rho_r V_r u_r) + P_r \frac{dV_r}{dt} \quad (A5-2)$$

which can be written as:

$$W_1 - W_2 = \rho_r \frac{dV_r}{dt} + V_r \frac{d\rho_r}{dt} \quad (A5-3)$$

$$W_1 \frac{P_s}{\rho_s} - W_2 \frac{P_r}{\rho_r} = P_r \frac{dV_r}{dt} + \frac{1}{\gamma} V_r \frac{dP_r}{dt} \quad (A5-4)$$

The following dimensionless perturbation quantities are now introduced:

$$\left. \begin{aligned} W_1 &= W_0 + w_1 = W_0 (1 + \bar{w}_1) \\ W_2 &= W_0 + w_2 = W_0 (1 + \bar{w}_2) \\ P_r &= P_{ro} + p = P_{ro} (1 + \bar{p}) \\ \rho_r &= \rho_{ro} + \sigma = \rho_{ro} (1 + \bar{\sigma}) \\ H &= H_0 + h = H_0 (1 + \bar{h}) \\ V_r &= A_s (\delta + H_0) + A_r h = V_{ro} + A_r h = V_{ro} (1 + \beta \bar{h}); \quad \beta = \frac{H_0}{\delta + H_0} \\ t &= \frac{1}{\omega} \bar{t} \end{aligned} \right\} \quad (A5-5)$$

Let also h be prescribed as:

$$\left. \begin{aligned} h &= h_0 \sin \omega t = H_0 \epsilon \sin \omega t; \quad \epsilon = \frac{h_0}{H_0} \ll 1 \\ \text{so that} \\ \bar{h} &= \epsilon \sin \bar{t} \end{aligned} \right\} \quad (A5-6)$$

Also, as in Appendix 2, we take:

$$\left. \begin{aligned} \lambda_3 &= - \left(\frac{\partial W_1}{\partial P_r} \right)_0 = \frac{W_0}{P_{ro}} \bar{\lambda}_3 ; \bar{\lambda}_3 = \frac{1}{2} \left(\frac{2 - \frac{P_s}{P_{ro}}}{\frac{P_s}{P_{ro}} - 1} \right) \\ \lambda_5 &= - \left(\frac{\partial W_2}{\partial P_r} \right)_0 = \frac{W_0}{P_{ro}} \bar{\lambda}_5 ; \bar{\lambda}_5 = \frac{2}{1 - \left(\frac{P_{at}}{P_{ro}} \right)^2} \\ \lambda_4 &= - \left(\frac{\partial W_2}{\partial H} \right)_0 = \frac{W_0}{H_0} \bar{\lambda}_4 ; \bar{\lambda}_4 = 3 \\ \lambda_3 + \lambda_5 &= \frac{W_0}{P_{ro}} (\bar{\lambda}_3 + \bar{\lambda}_5) = \frac{W_0}{P_{ro}} \bar{\lambda} \end{aligned} \right\} \quad (A5-7)$$

so that with:

$$\bar{w}_1 - \bar{w}_2 = - \bar{\lambda} \bar{p} - \bar{\lambda}_4 \bar{h} \quad (A5-8)$$

equations (A5-3) and (A5-4) yield:

$$\ddot{\bar{\sigma}} + Q \bar{\sigma} - \frac{1}{\gamma} \dot{\bar{p}} - Q p = 0 \quad (A5-9)$$

$$\ddot{\bar{\sigma}} + Q \bar{\lambda} \bar{p} = - Q \bar{\lambda}_4 \epsilon \sin \bar{t} - \beta \epsilon \cos \bar{t} \quad (A5-10)$$

in which

$$\left. \begin{aligned} Q &= \frac{W_0}{\rho_{ro} V_{ro} \omega} \\ \beta &= \frac{H_0}{\delta + H_0} \end{aligned} \right\} \quad (A5-11)$$

and $(\cdot) = \frac{d}{dt} = \frac{1}{\omega} \frac{d}{d\bar{t}}$ denotes differentiation with respect to dimensionless time, \bar{t} .

In operational form, equations (A5-9) and (A5-10) are:

$$(1+Q)\bar{\sigma} - \left(\frac{1}{\gamma} D + Q\right)\bar{p} = 0 \quad (A5-12)$$

$$D\bar{\sigma} + Q\bar{\Lambda}\bar{p} = -\epsilon(\beta D + Q\bar{\Lambda}_4)\sin\bar{t} \quad (A5-13)$$

where

$$D = \frac{d}{d\bar{t}}$$

On the other hand, an assumed relation

$$\frac{P_r}{P_{ro}} = \left(\frac{\rho_r}{\rho_{ro}}\right)^\gamma \quad (A5-14)$$

yields

$$\frac{\bar{p}}{\bar{\sigma}} = \gamma \quad (A5-15)$$

so that equation (A5-3), with the aid of equations (A5-8) and (A5-15), reduces to:

$$\frac{1}{\gamma} \bar{p} + Q\bar{\Lambda}\bar{p} = -Q\bar{\Lambda}_4\epsilon\sin\bar{t} - \beta\epsilon\cos\bar{t} \quad (A5-16)$$

or:

$$\left(\frac{1}{\gamma} D + Q\bar{\Lambda}\right)\bar{p} = -\epsilon(\beta D + Q\bar{\Lambda}_4)\sin\bar{t} \quad (A5-17)$$

Operation on equations (A5-12) and (A5-13) with (D) and (D+Q), followed by subtraction, and operation with (QA) and (1/γ D + Q), followed by addition, yields the following set of equations:

$$\begin{aligned} \bar{p} &= \mathcal{D} \frac{-\epsilon[\beta D^2 + Q(\beta + \bar{\Lambda}_4)D + Q^2\bar{\Lambda}_4]\epsilon i\bar{t}}{\left[\frac{1}{\gamma} D^2 + Q(1 + \bar{\Lambda})D + Q^2\bar{\Lambda}\right]} \\ &= \mathcal{D} \frac{-\epsilon[(Q^2\bar{\Lambda}_4 - \beta) + iQ(\beta + \bar{\Lambda}_4)]}{\left(Q^2\bar{\Lambda} - \frac{1}{\gamma}\right) + iQ(1 + \bar{\Lambda})} (\cos\bar{t} + i\sin\bar{t}) \end{aligned} \quad (A5-18)$$

$$\begin{aligned} &= \frac{-\epsilon \left[\frac{1}{\gamma} P^0 + Q \left(\beta + \frac{1}{\gamma} \bar{\lambda}_4 \right) P + Q^2 \bar{\lambda}_4 \right] e^{i\bar{t}}}{\left[\frac{1}{\gamma} P^0 + Q Q^0 + \bar{\lambda}_4 P + Q^2 \bar{\lambda}_4 \right]} \\ &= \frac{-\epsilon \left[\left(Q^2 \bar{\lambda}_4 + \frac{1}{\gamma} \right) + i Q \left(\beta + \frac{1}{\gamma} \bar{\lambda}_4 \right) \right]}{\left(Q^2 \bar{\lambda}_4 + \frac{1}{\gamma} \right) + i Q (1 + \bar{\lambda}_4)} (\cos \bar{t} + i \sin \bar{t}) \quad (A5-19) \end{aligned}$$

On the other hand, from equation (A5-17) we obtain:

$$\bar{P}_1 = \frac{-\epsilon (Q P + Q \bar{\lambda}_4) e^{i\bar{t}}}{\left(\frac{1}{\gamma} P + Q \bar{\lambda}_4 \right)} = \frac{-\epsilon (Q \bar{\lambda}_4 + i \beta)}{Q \bar{\lambda}_4 + i \frac{1}{\gamma}} (\cos \bar{t} + i \sin \bar{t}) \quad (A5-20)$$

In the foregoing equations, the subscript 1 denotes the isentropic relation assumed in obtaining equation (A5-17), and i refers to the imaginary part of a complex quantity.

The steady-state pressure and density responses to a sinusoidal displacement input:

$$\bar{x} = \epsilon \sin \bar{t}$$

are as follows:

$$\begin{aligned} \bar{P} &= \frac{\epsilon Q \left[(Q^2 \bar{\lambda}_4 + \beta)(1 + \bar{\lambda}_4) + (\beta + \bar{\lambda}_4) \left(Q^2 \bar{\lambda}_4 + \frac{1}{\gamma} \right) \right]}{\left(Q^2 \bar{\lambda}_4 + \frac{1}{\gamma} \right)^2 + Q^2 (1 + \bar{\lambda}_4)^2} \cos \bar{t} \\ &\quad - \frac{\epsilon \left[(Q^2 \bar{\lambda}_4 + \beta) \left(Q^2 \bar{\lambda}_4 + \frac{1}{\gamma} \right) + Q^2 (\beta + \bar{\lambda}_4)(1 + \bar{\lambda}_4) \right]}{\left(Q^2 \bar{\lambda}_4 + \frac{1}{\gamma} \right)^2 + Q^2 (1 + \bar{\lambda}_4)^2} \sin \bar{t} \quad (A5-21) \end{aligned}$$

$$\frac{\epsilon \left[\left(Q^2 \bar{\lambda}_4 - \frac{1}{\gamma} \beta \right) (1 + \bar{\lambda}) - \left(\beta + \frac{1}{\gamma} \bar{\lambda}_4 \right) \left(Q^2 \bar{\lambda} - \frac{1}{\gamma} \right) \right]}{\left(Q^2 \bar{\lambda} - \frac{1}{\gamma} \right)^2 + Q^2 (1 + \bar{\lambda})^2} \cos \bar{t}$$

$$+ \frac{\epsilon \left[\left(Q^2 \bar{\lambda}_4 - \frac{1}{\gamma} \right) \left(Q^2 \bar{\lambda} - \frac{1}{\gamma} \right) + Q^2 \left(\beta + \frac{1}{\gamma} \bar{\lambda}_4 \right) (1 + \bar{\lambda}) \right]}{\left(Q^2 \bar{\lambda} - \frac{1}{\gamma} \right)^2 + Q^2 (1 + \bar{\lambda})^2} \sin \bar{t} \quad (\text{A5-22})$$

$$1_1 = \frac{\epsilon \left(\frac{1}{\gamma} \bar{\lambda}_4 - \bar{\lambda} \right)}{Q^2 \bar{\lambda}^2 + \frac{1}{\gamma^2}} \cos \bar{t} - \frac{\epsilon \left(Q^2 \bar{\lambda} \bar{\lambda}_4 - \frac{1}{\gamma} \beta \right)}{Q^2 \bar{\lambda}^2 + \frac{1}{\gamma^2}} \sin \bar{t} \quad (\text{A5-23})$$

and, on the basis of assumption [A5-14], from equation [A5-15]

$$\bar{u}_1 = \frac{1}{\gamma} \bar{v}_1 \quad (\text{A5-24})$$

The expressions for \bar{p} and $\bar{\sigma}$ contain the parameters ϵ , γ , $\bar{\lambda}_4$, $\bar{\lambda}$, β and Q , of which ϵ , γ and $\bar{\lambda}_4$ are constants and $\bar{\lambda}$ is fixed for any given set of pressure ratios P_a/P_{ro} and P_{at}/P_{ro} . We note, once again, the form of the parameters β and Q :

$$\beta = \frac{H_o}{\delta + H_o}$$

and

$$Q = \frac{W_o}{\rho_{ro} V_{ro} \omega}$$

Prior to solving equations (A5-21) through (A5-24) for a set of numerical values, it is of interest to consider the asymptotic behavior of \bar{p} and $\bar{\sigma}$ for limiting values of the "charge" parameter Q . We shall consider the cases when:

- (a) Q is a very large number
and (b) Q is a very small number
while β remains finite.

Case (a), Q is very large

Equations (A5-1) and (A5-22) reduce to:

$$\bar{p} = -\epsilon \frac{\bar{\lambda}_4}{\bar{\lambda}} \sin \bar{t} \quad (\text{A5-25})$$

$$\bar{\sigma} = -\epsilon \frac{\bar{\lambda}_4}{\bar{\lambda}} \sin \bar{t} \quad (\text{A5-26})$$

so that

$$\frac{\bar{p}}{\bar{\sigma}} = 1 \quad \text{or} \quad \frac{p}{\sigma} = \frac{P_{ro}}{\rho_{ro}} = \frac{a_o^2}{\gamma} \quad (\text{A5-27})$$

We note that equation (A5-23) also reduces to:

$$\bar{p}_i = -\epsilon \frac{\bar{\lambda}_4}{\bar{\lambda}} \sin \bar{t} \quad (\text{A5-28})$$

but since the assumption $(P_r/P_{ro}) = (\rho_r/\rho_{ro})^\gamma$ prescribes the \bar{p}_i and $\bar{\sigma}_i$ relation, we have:

$$\frac{\bar{p}_i}{\bar{\sigma}_i} = \gamma \quad \text{or} \quad \frac{p_i}{\sigma_i} = \frac{\gamma P_{ro}}{\rho_{ro}} = a_o^2 \quad (\text{A5-29})$$

In case (a), the following conclusions can be drawn:

1. The pressure-density relation is nearly isothermal.
2. The pressure and density are in phase and both are 180° out of phase with the displacement $\bar{h} = \epsilon \sin \bar{t}$. (e.g., increasing with decreasing gap width.) The coefficient

$$-\epsilon \frac{\bar{\lambda}_4}{\bar{\lambda}} = -\epsilon \frac{\bar{\lambda}_4}{\bar{\lambda}_3 + \bar{\lambda}_5}$$

is a measure of the "static stiffness". The physical significance of the foregoing is that, if the motion is very slow (quasi-static), or if the mass flow rate is relatively large and the mass content of the recess region is relatively small, the changes occur nearly isothermally.

Case (b): ϵ is very small.

Equations (A5-21) and (A5-22) reduce to:

$$\bar{p} = -\epsilon\gamma\beta\sin\bar{t} \quad (\text{A5-30})$$

$$\bar{a} = -\epsilon\beta\sin\bar{t} \quad (\text{A5-31})$$

so that:

$$\frac{\bar{p}}{\bar{a}} = \gamma \quad \text{or} \quad \frac{p}{\sigma} = \frac{\gamma P_{ro}}{\rho_{ro}} = a_o^2 \quad (\text{A5-32})$$

Equation (A5-23) also reduces to:

$$\bar{p}_i = -\epsilon\gamma\beta\sin\bar{t} \quad (\text{A5-33})$$

so that identically as in equation (A5-32):

$$\frac{\bar{p}_i}{\bar{\sigma}_i} = \gamma \quad \text{or} \quad \frac{p_i}{\sigma_i} = \frac{\gamma P_{ro}}{\rho_{ro}} = a_o^2 \quad (\text{A5-34})$$

which was the assumed relation.

In case (b), the following conclusions can be drawn:

1. The pressure-density relation is nearly isentropic.
2. The pressure and density are in phase and both are 180° out of phase with the displacement $\bar{h} = \epsilon \sin \bar{t}$ (e.g., increasing with decreasing gap width.) The coefficient

$$-\epsilon\gamma\beta = -\gamma\epsilon \frac{H_o}{\delta + H_o} = -\gamma \frac{v_o}{V_o}$$

is indicative of the "dynamic stiffness", such as would be the case of gas in a closed cylinder and piston system undergoing isentropic compression or expansion. The physical significance of the foregoing is that, if the motion is very fast, or if the mass flow rate is relatively small and the recess mass content is relatively large, the changes occur nearly isentropically.

To correlate the analysis with experimental results, the numerical examples were selected to correspond approximately to two points of the experimental stability locus I, Figure 55, for which the data are as follows:

		1	2
P_s	psia	91.5	
P_{ro}	psia	75.9	
P_{at}	psia	14.7	
T_o	$^{\circ}$ F abs.	537	
ρ_{ro}	lb-sec ² /in ⁴	0.5722×10^{-6}	
W_o	lb-sec/in	10×10^{-6}	
H_o	in	1.64×10^{-3}	
A_r	in ²	0.7854	
$\bar{\lambda}_3$	—	1.933	
$\bar{\lambda}_5$	—	2.078	
$\bar{\lambda}_1$	—	4.011	
$\bar{\lambda}_4$	—	3.000	
γ	—	1.4 (1/ γ = 0.7143)	
ϵ	—	10^{-2}	
δ	in	13×10^{-3}	275×10^{-3}
ω	rad/sec	2125	1280
V_s	in ²	11.50×10^{-3}	217.3×10^{-3}
Q	—	0.7153	6.224×10^{-2}
β	—	0.1120	5.928×10^{-3}

(A5-35)

Example 1

$$\bar{p} = \epsilon \bar{p}_m \sin(\bar{t} - \phi) = \epsilon(-0.6792 \sin \bar{t} + 0.1624 \cos \bar{t})$$

$$\tan \phi = \frac{0.1624}{-0.6792} = -0.2391$$

$$\phi = 180^\circ - 13.45^\circ = 166.6^\circ$$

$$\bar{p}_m = 0.6985$$

(A5-35)

$$\bar{\sigma} = \epsilon \bar{\sigma}_m \sin(\bar{t} - \psi) = \epsilon(-0.5291 \sin \bar{t} + 0.2232 \cos \bar{t})$$

$$\tan \psi = \frac{0.2232}{-0.5291} = -0.4218$$

$$\psi = 180^\circ - 22.87^\circ = 157.1^\circ$$

$$\bar{\sigma}_m = 0.5713$$

(A5-37)

$$\phi - \psi = 9.5^\circ$$

(A5-38)

$$\bar{p}_i = \epsilon \bar{p}_{mi} \sin(\bar{t} - \phi_i) = \epsilon(-0.7135 \sin \bar{t} + 0.1386 \cos \bar{t})$$

$$\tan \phi_i = \frac{0.1386}{-0.7135} = -0.1943$$

$$\phi_i = 180^\circ - 11^\circ = 169^\circ$$

$$\bar{p}_{mi} = 0.7269$$

$$\bar{\sigma}_{mi} = \frac{1}{y} \bar{p}_{mi} = 0.5192$$

(A5-39)

$$\phi_i - \phi = 2.4^\circ$$

(A5-40)

$$\phi_i - \psi = 11.9^\circ$$

(A5-41)

Example 2.

$$\bar{p} = \epsilon \bar{p}_m \sin(\bar{t} - \phi) = \epsilon(-0.0911 \sin \bar{t} + 0.2248 \cos \bar{t})$$

$$\tan \phi = \frac{0.2248}{-0.0911} = -2.468$$

$$\phi = 180^\circ - 67.93^\circ = 112.1^\circ$$

$$\bar{p}_m = 0.2445$$

(A5-42)

$$\bar{\sigma} = \epsilon \bar{\sigma}_m \sin(\bar{t} - \psi) = \epsilon(-0.0611 \sin \bar{t} + 0.1625 \cos \bar{t})$$

$$\tan \psi = \frac{0.1625}{-0.0611} = -2.660$$

$$\psi = 180^\circ - 69.4^\circ = 110.6^\circ$$

$$\bar{\sigma}_m = 0.1765$$

(A5-43)

$$\phi - \psi = 1.5^\circ$$

(A5-44)

$$\bar{p}_i = \epsilon \bar{p}_{mi} \sin(\bar{t} - \phi_i) = \epsilon(-0.0923 \sin \bar{t} + 0.2322 \cos \bar{t})$$

$$\tan \phi_i = \frac{0.2322}{-0.0923} = -2.516$$

$$\phi_i = 180^\circ - 68.32^\circ = 111.7^\circ$$

$$\bar{p}_{mi} = 0.2499$$

$$\bar{\sigma}_{mi} = \frac{1}{\gamma} \bar{p}_{mi} = 0.1785$$

(A5-45)

$$\phi_i - \phi = -0.4^\circ$$

(A5-46)

$$\phi_i - \psi = 1.1^\circ$$

(A5-47)

Comparison of results of examples 1 and 2 shows that pressure-density phase angles are relatively small, approximately 5.5° and 1.5° respectively. When the assumed relation is $P_r/P_m = (\rho_r/\rho_m)^{1/\gamma}$, this is equivalent to prescribing that the density and pressure be in phase. In example 1, the angle between pressures is approximately 2.4° and that between densities 11.9° . In example 2, the corresponding angles are very small; 0.1° and 1.1° respectively.

Since all angles are relatively small, so that all densities and pressures are "almost in phase", a comparison of amplitudes is of interest as a criterion of validity of the isentropic assumption.

From example 1 we have:

$$\frac{\bar{P}_{mi}}{\bar{P}_m} = 1.04 \quad \text{and} \quad \frac{\bar{\sigma}_{mi}}{\bar{\sigma}_m} = 0.904 \quad (\text{A5-48})$$

also:

$$\frac{\bar{P}_m}{\bar{\sigma}_m} = 1.22, \text{ as compared with } \frac{\bar{P}_{mi}}{\bar{\sigma}_{mi}} = \gamma = 1.40 \quad (\text{A5-49})$$

In example 2 the ratios are:

$$\frac{\bar{P}_{mi}}{\bar{P}_m} = 1.02 \quad \text{and} \quad \frac{\bar{\sigma}_{mi}}{\bar{\sigma}_m} = 1.01 \quad (\text{A5-50})$$

also:

$$\frac{\bar{P}_m}{\bar{\sigma}_m} = 1.37, \text{ as compared with } \frac{\bar{P}_{mi}}{\bar{\sigma}_{mi}} = \gamma = 1.40 \quad (\text{A5-51})$$

In the foregoing examples, all parameters were identical, with the exception of the frequencies and the recess volumes. The ratio of the former was of the order 2; that of the latter of the order 1/20. Significantly, as might have been anticipated from physical considerations, the pressure and density amplitudes of example 2 were barely 1/3 of those in example 1.

For a sufficiently large volume, pressure and density changes in the recess, associated with small but finite motion, could become negligible. A very different condition, of course, would prevail in the bearing gap, due to the combined squeezing and trapping of the fluid between the narrowly spaced boundaries.

Results of calculations of examples 1 and 2 are illustrated in Figure A5-2.

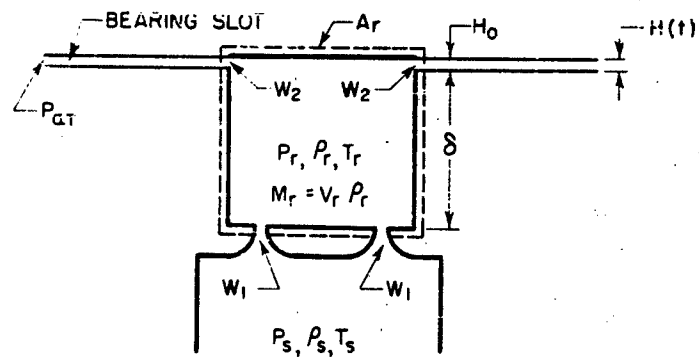
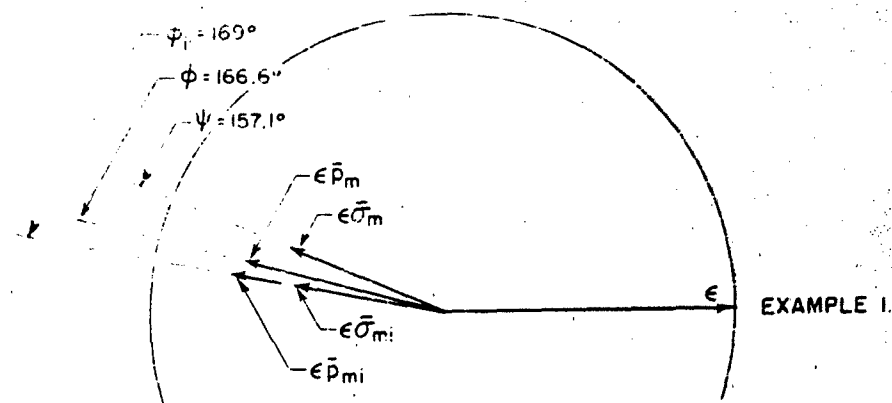
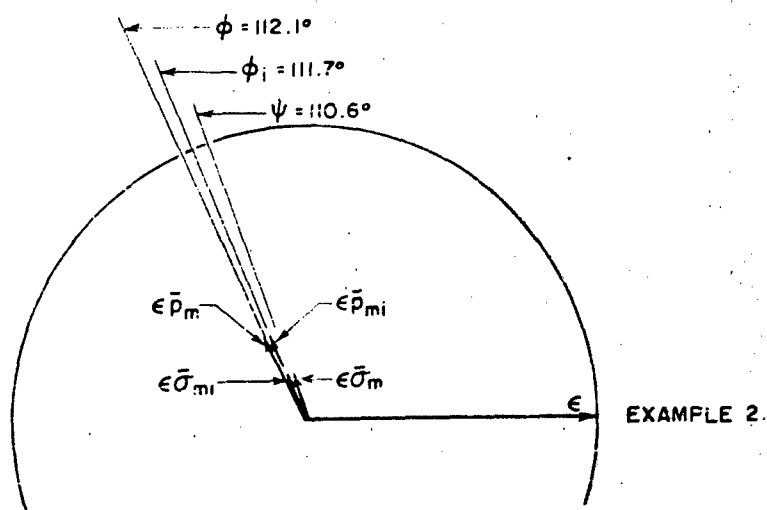


FIG. A5-1. SCHEMATIC DIAGRAM OF VARIABLE-
VOLUME BEARING RECESS



EXAMPLE 1.



EXAMPLE 2.

FIG. A5-2. AMPLITUDES AND PHASE RELATIONS OF PRESSURE AND DENSITY
IN VARIABLE VOLUME RECESS

APPENDIX 6

DERIVATION OF THE DYNAMIC LUBRICATION EQUATION

The purpose of this appendix is to show that the differential equation (4) of the main text provides an adequate description of fluid-dynamical phenomena in the bearing slot, provided orders of magnitude of characteristic parameters fulfill certain requirements. The development follows closely the method of Elrod [45] who employed a small-parameter technique in the derivation of equations for gas lubrication.

It will be assumed that the fluid obeys the perfect gas law and that the specific heats, viscosity and thermal conductivity are constant. Continuity and constancy of temperature of the boundaries will also be assumed. In the range of pressures and temperatures considered, the foregoing assumptions are reasonable for gas flow in a narrow slot between metallic members.

The momentum, continuity and energy equations, stated in cylindrical coordinates, for axially symmetric, laminar motion, and the equation of state are [65]:

$$\rho \left(\frac{\partial u}{\partial t} + u \frac{\partial u}{\partial r} + w \frac{\partial u}{\partial z} \right) = - \frac{\partial P}{\partial r} + \frac{\mu}{3} \frac{\partial}{\partial r} \left(\frac{\partial u}{\partial r} + \frac{u}{r} + \frac{\partial w}{\partial z} \right) + \mu \left(\frac{\partial^2 u}{\partial r^2} + \frac{1}{r} \frac{\partial u}{\partial r} - \frac{u}{r^2} + \frac{\partial^2 u}{\partial z^2} \right) \quad (\text{A6-1})$$

$$\rho \left(\frac{\partial w}{\partial t} + u \frac{\partial w}{\partial r} + w \frac{\partial w}{\partial z} \right) = - \frac{\partial P}{\partial z} + \frac{\mu}{3} \frac{\partial}{\partial r} \left(\frac{\partial u}{\partial r} + \frac{u}{r} + \frac{\partial w}{\partial z} \right) + \mu \left(\frac{\partial^2 w}{\partial z^2} + \frac{1}{r} \frac{\partial w}{\partial r} + \frac{\partial^2 w}{\partial z^2} \right) \quad (\text{A6-2})$$

$$\frac{\partial \rho}{\partial t} + \frac{1}{r} \frac{\partial}{\partial r} (r \rho u) + \frac{\partial}{\partial z} (\rho w) = 0 \quad (\text{A6-3})$$

$$c_p \rho \left(\frac{\partial T}{\partial t} + u \frac{\partial T}{\partial r} + w \frac{\partial T}{\partial z} \right) - \left(\frac{\partial P}{\partial t} + u \frac{\partial P}{\partial r} + w \frac{\partial P}{\partial z} \right) = \frac{k}{r} \frac{\partial}{\partial r} \left(r \frac{\partial T}{\partial r} \right) + k \frac{\partial^2 T}{\partial z^2} + \mu \left[2 \left(\frac{\partial u}{\partial r} \right)^2 + 2 \left(\frac{\partial w}{\partial z} \right)^2 + \left(\frac{\partial u}{\partial z} + \frac{\partial w}{\partial r} \right)^2 - \frac{2}{3} \left(\frac{\partial u}{\partial r} + \frac{\partial w}{\partial z} \right)^2 \right] \quad (\text{A6-4})$$

$$\frac{P}{\rho} = R T \quad (\text{A6-5})$$

in which $\alpha, k = c_p - c_v, \gamma = \frac{c_p}{c_v}$ are constant.

The boundary conditions are:

$$\left. \begin{array}{ll} \text{At } z = 0; & u = w = 0 \\ & T = T^* \\ \\ \text{At } z = H(t); & u = 0 \\ & w = \frac{dH}{dt} \\ & T = T^* \end{array} \right\} \quad (\text{A6-6})$$

Denoting reference quantities with (*) and dimensionless quantities with ($\bar{}$), the following set of variables is formed:

$$\left. \begin{array}{l} \rho = \rho^* \bar{\rho} \\ T = T^* \bar{T} \\ P = \rho^* \left(\frac{\nu^*}{H^*} \right)^2 \bar{P} \\ H = H^* f(t), \text{ where } f(t) \text{ is 0, (1)} \\ r = L \bar{r}, \text{ where } L = R - R_r \\ z = H^* \bar{z} \\ t = \frac{L^2}{\nu^*} \bar{t} \\ u = \frac{\nu^*}{L} \bar{u} \\ w = \frac{H^*}{L} \frac{\nu^*}{L} \bar{w} = \epsilon \frac{\nu^*}{L} \bar{w}, \text{ where } \epsilon = \frac{H^*}{L} \end{array} \right\} \quad (\text{A6-7})$$

also:

(A6-7)
Cont

$$\frac{\bar{P}}{\bar{T}} = \frac{\nu^* \left(\frac{H^*}{T^*} \right)^2}{T^*} \frac{\bar{P}}{\bar{T}} = \frac{\nu^* \left(\frac{H^*}{T^*} \right)^2}{T^*} \frac{P^*}{T^*} \frac{\bar{P}}{\bar{T}}$$

$$\bar{P} = \frac{\nu^*}{P^*} = \frac{1}{P^*} \frac{\bar{P}}{\bar{T}}$$

In the foregoing $\epsilon = \frac{H^*}{H - R_0} = \frac{H^*}{L}$ is the small parameter used in developing the dynamic lubrication equations.

In transforming the equations of fluid motion into their dimensionless equivalents, the following relations between derivatives hold:

$$\left. \begin{aligned} \frac{\partial \bar{t}}{\partial t} &= \frac{1}{L^2} & \frac{\partial \bar{t}}{\partial r} &= 0 & \frac{\partial \bar{t}}{\partial z} &= 0 \\ \frac{\partial \bar{r}}{\partial r} &= \frac{1}{L} & \frac{\partial \bar{r}}{\partial z} &= 0 & \frac{\partial \bar{r}}{\partial t} &= 0 \\ \frac{\partial \bar{z}}{\partial z} &= \frac{1}{f H^*} & \frac{\partial \bar{z}}{\partial t} &= -\frac{\nu^*}{L^2} \bar{z} \frac{f}{f} & \frac{\partial \bar{z}}{\partial r} &= 0 \end{aligned} \right\}$$

(A6-8)

so that:

$$\begin{aligned} \frac{\partial}{\partial r} &= \frac{1}{L} \frac{\partial}{\partial \bar{r}} & \frac{\partial^2}{\partial r^2} &= \frac{1}{L^2} \frac{\partial^2}{\partial \bar{r}^2} \\ \frac{\partial}{\partial z} &= \frac{1}{f H^*} \frac{\partial}{\partial \bar{z}} & \frac{\partial^2}{\partial z^2} &= \frac{1}{f^2 H^{*2}} \frac{\partial^2}{\partial \bar{z}^2} \\ \frac{\partial}{\partial t} &= \frac{\nu^*}{L^2} \left(\frac{\partial}{\partial \bar{t}} - \bar{z} \frac{\partial}{\partial \bar{z}} \right) \end{aligned}$$

in which $(\cdot) = \frac{d}{d\bar{t}} = \frac{\nu^*}{L^2} \frac{d}{dt}$

The dimensionless form of equations (A6-1) through (A6-5) then is:

$$\left[\frac{\partial \bar{u}}{\partial \bar{t}} + \left(\frac{1}{f} \bar{w} - \frac{f}{f} \bar{z} \right) \frac{\partial \bar{u}}{\partial \bar{z}} + \bar{u} \frac{\partial \bar{u}}{\partial \bar{r}} \right] = - \frac{1}{\epsilon^2} \frac{\partial \bar{P}}{\partial \bar{r}} - \frac{1}{3} \frac{\partial}{\partial \bar{r}} \left(\frac{\partial \bar{u}}{\partial \bar{r}} + \frac{\bar{u}}{f} + \frac{1}{f} \frac{\partial \bar{w}}{\partial \bar{z}} \right) \\ \left(\frac{\partial^2 \bar{u}}{\partial \bar{r}^2} + \frac{1}{f} \frac{\partial \bar{u}}{\partial \bar{r}} - \frac{\bar{u}}{f^2} + \frac{1}{\epsilon^2} \frac{1}{f^2} \frac{\partial^2 \bar{u}}{\partial \bar{z}^2} \right) \quad (\text{A6-9})$$

$$\left[\frac{\partial \bar{w}}{\partial \bar{t}} + \left(\frac{1}{f} \bar{w} - \frac{f}{f} \bar{z} \right) \frac{\partial \bar{w}}{\partial \bar{z}} + \bar{w} \frac{\partial \bar{w}}{\partial \bar{r}} \right] = - \frac{1}{\epsilon^2} \frac{1}{f} \frac{\partial \bar{P}}{\partial \bar{z}} \\ + \frac{1}{3} \frac{1}{f} \frac{\partial}{\partial \bar{z}} \left(\frac{\partial \bar{u}}{\partial \bar{r}} + \frac{\bar{u}}{f} + \frac{1}{f} \frac{\partial \bar{w}}{\partial \bar{z}} \right) + \left(\frac{\partial^2 \bar{w}}{\partial \bar{r}^2} + \frac{1}{f} \frac{\partial \bar{w}}{\partial \bar{r}} + \frac{1}{\epsilon^2} \frac{1}{f} \frac{\partial^2 \bar{w}}{\partial \bar{z}^2} \right) \quad (\text{A6-10})$$

$$\frac{\partial \bar{\rho}}{\partial \bar{t}} - \frac{f}{f} \bar{z} \frac{\partial \bar{P}}{\partial \bar{z}} + \frac{1}{f} \frac{\partial}{\partial \bar{r}} (\bar{r} \bar{\rho} \bar{u}) + \frac{1}{f} \frac{\partial}{\partial \bar{z}} (\bar{\rho} \bar{w}) = 0 \quad (\text{A6-11})$$

$$\frac{c_p T^* L^2}{k L^2} \bar{\rho} \left[\frac{\partial \bar{T}}{\partial \bar{t}} + \left(\frac{1}{f} \bar{w} - \frac{f}{f} \bar{z} \right) \frac{\partial \bar{T}}{\partial \bar{z}} + \bar{u} \frac{\partial \bar{T}}{\partial \bar{r}} \right] - \frac{1}{\epsilon^2} \left[\frac{\partial \bar{P}}{\partial \bar{t}} + \left(\frac{1}{f} \bar{w} - \frac{f}{f} \bar{z} \right) \frac{\partial \bar{P}}{\partial \bar{z}} + \bar{u} \frac{\partial \bar{P}}{\partial \bar{r}} \right] \\ = \frac{k}{\mu c_p} \frac{c_p T^* L^2}{L^2} \left[\frac{1}{f} \frac{\partial}{\partial \bar{r}} \left(\bar{r} \frac{\partial \bar{T}}{\partial \bar{r}} \right) + \frac{1}{\epsilon^2} \frac{1}{f^2} \frac{\partial^2 \bar{T}}{\partial \bar{z}^2} \right] \\ + \left[2 \left(\frac{\partial \bar{u}}{\partial \bar{r}} \right)^2 + 2 \frac{1}{f^2} \left(\frac{\partial \bar{w}}{\partial \bar{z}} \right)^2 + \left(\frac{1}{\epsilon} \frac{1}{f} \frac{\partial \bar{u}}{\partial \bar{z}} + \epsilon \frac{\partial \bar{w}}{\partial \bar{r}} \right)^2 - \frac{2}{3} \left(\frac{\partial \bar{u}}{\partial \bar{r}} + \frac{1}{f} \frac{\partial \bar{w}}{\partial \bar{z}} \right)^2 \right] \quad (\text{A6-12})$$

$$\frac{\bar{P}}{\rho} = \bar{P}^* \bar{T} \quad (\text{A6-13})$$

The boundary conditions are:

$$\left. \begin{array}{lll} \text{At } \bar{z} = 0 & ; & \bar{u} = \bar{w} = 0, \quad \bar{T} = 1 \\ \text{At } \bar{z} = 1 & ; & \bar{u} = 0, \quad \bar{T} = 1 \\ & & \bar{w} = f \end{array} \right\} \quad (\text{A6-14})$$

Consider now solutions of equations (A6-9) through (A6-12) which can be expanded in terms of the small parameter ϵ as follows:

$$\left. \begin{aligned} \bar{U} &= \bar{U}_0 + \epsilon^2 \bar{U}_1 + \epsilon^4 \bar{U}_2 + \dots \\ \bar{W} &= \bar{W}_0 + \epsilon^2 \bar{W}_1 + \epsilon^4 \bar{W}_2 + \dots \\ \bar{V} &= \bar{V}_0 + \epsilon^2 \bar{V}_1 + \epsilon^4 \bar{V}_2 + \dots \\ \bar{T} &= \bar{T}_0 + \epsilon^2 \bar{T}_1 + \epsilon^4 \bar{T}_2 + \dots \end{aligned} \right\} \quad (\text{A6-15})^\dagger$$

so that:

$$\bar{v} = \frac{1}{\bar{P}^*} \frac{\bar{P}}{\bar{T}} = \frac{1}{\bar{P}^*} \frac{\bar{\pi}_0 + \epsilon^2 \bar{\pi}_1 + \dots}{\bar{\theta}_0 + \epsilon^2 \bar{\theta}_1 + \dots} = \frac{1}{\bar{P}^*} \left[\frac{\bar{\pi}_0}{\bar{\theta}_0} + \epsilon^2 \left(\frac{\bar{\pi}_1}{\bar{\theta}_0} - \frac{\bar{\pi}_0 \bar{\theta}_1}{\bar{\theta}_0^2} \right) + \dots \right]$$

The functions appearing in equation (A6-15) depend in general on \bar{t} , \bar{r} and \bar{z} and are independent of f . The zeroth order functions are made to assume the boundary values (A6-14), so that approximating functions of higher order vanish at the boundaries. e.g.:

$$\left. \begin{aligned} \text{At } \bar{z} = 0 : \quad & \bar{U}_0 = \bar{U}_1 = \bar{U}_2 \dots = 0 \\ & \bar{W}_0 = \bar{W}_1 = \bar{W}_2 \dots = 0 \\ & \bar{\theta}_0 = 1 ; \quad \bar{\theta}_2 = \bar{\theta}_3 = 0 \\ \\ \text{At } \bar{z} = 1 : \quad & \bar{U}_0 = \bar{U}_1 = \bar{U}_2 \dots = 0 \\ & \bar{W}_0 = \bar{f} ; \quad \bar{W}_1 = \bar{W}_2 \dots = 0 \\ & \bar{\theta}_0 = 1 ; \quad \bar{\theta}_2 = \bar{\theta}_3 \dots = 0 \end{aligned} \right\} \quad (\text{A6-16})$$

Substituting the series (A6-15) in equations (A6-9) through (A6-12), the zeroth equations are:

$$0 = - \frac{\partial \bar{\pi}_0}{\partial \bar{r}} + \frac{1}{f} \frac{\partial^2 \bar{U}_0}{\partial \bar{z}^2} \quad (\text{A6-17})$$

[†] Powers of ϵ differing by two are taken since exponents of ϵ in the differential equations differ by two.

$$0 = - \frac{1}{f} \frac{\partial \pi_o}{\partial \bar{z}} \quad (\text{A6-18})$$

and, noting from equation (A6-18) that $\pi_o = \pi_o(\bar{r}, \bar{t})$ only, the continuity equation (A6-11) yields:

$$0 = \frac{\partial}{\partial \bar{t}} \left(\frac{\bar{\pi}_o}{\bar{\theta}_o} \right) + \frac{1}{\bar{r}} \frac{\partial}{\partial \bar{r}} \left(\bar{r} \frac{\bar{\pi}_o}{\bar{\theta}_o} \bar{U}_o \right) + \frac{\bar{\pi}_o}{\bar{\theta}_o^2} \left(\frac{\partial \bar{U}_o}{\partial \bar{z}} - \frac{1}{\bar{r}} \bar{W}_o \right) \frac{\partial \bar{\theta}_o}{\partial \bar{z}} + \frac{1}{\bar{r}} \frac{\bar{\pi}_o}{\bar{\theta}_o} \frac{\partial \bar{W}_o}{\partial \bar{z}} \quad (\text{A6-19})$$

and the energy equation (A6-12):

$$\begin{aligned} - \frac{k}{c_p \mu} \frac{c_p T^* L^2}{\nu^{*2}} \frac{1}{f^2} \frac{\partial^2 \bar{\theta}_o}{\partial \bar{z}^2} &= \frac{1}{f^2} \left(\frac{\partial \bar{U}_o}{\partial \bar{z}} \right)^2 + \bar{U}_o \frac{\partial \pi_o}{\partial \bar{r}} + \frac{\partial \pi_o}{\partial \bar{t}} \\ &= \frac{1}{f^2} \left(\frac{\partial \bar{U}_o}{\partial \bar{z}} \right)^2 + \frac{1}{f^2} \bar{U}_o \frac{\partial^2 \bar{U}_o}{\partial \bar{z}^2} + \frac{\partial \pi_o}{\partial \bar{t}} \quad (\text{A6-20}) \end{aligned}$$

where in the penultimate step, use was made of equation (A6-17).

Integration of equation (A6-20) with respect to \bar{z} gives:

$$- \left(\frac{k}{c_p \mu} \frac{c_p T^* L^2}{\nu^{*2}} \right) \bar{\theta}_o = \frac{\bar{U}_o^2}{2} + \frac{f^2 \bar{z}^2}{2} \frac{\partial \pi_o}{\partial \bar{t}} + \bar{z} F(\bar{r}, \bar{t}) + G(\bar{r}, \bar{t}) \quad (\text{A6-21})$$

and, applying the boundary conditions (A6-16):

$$F = \frac{f^2}{2} \frac{\partial \pi_o}{\partial \bar{t}} \quad ; \quad G = - \frac{k}{c_p \mu} \frac{c_p T^* L^2}{\nu^{*2}} \quad (\text{A6-22})$$

so that equation (A6-21) becomes:

$$\bar{\theta}_o = 1 + \frac{1}{2} \left(\frac{c_p \mu}{k} \frac{\nu^{*2}}{c_p T^* L^2} \right) \left[\bar{z}(1 - \bar{z}) f^2 \frac{\partial \pi_o}{\partial \bar{t}} - \bar{U}_o^2 \right] \quad (\text{A6-23})$$

Letting

$$U^* = \frac{U}{U^*}$$

be the reference velocity, corresponding to the steady-flow condition when $f = 1$, equation (A6-23) can be written in the following form:

$$\bar{u} = 1 + \frac{\gamma-1}{2} N_p M^2 \left[\bar{z}(1-\bar{z}) \left(\frac{f}{U^*} \right)^2 \frac{\partial \bar{\pi}_0}{\partial \bar{t}} - \left(\frac{\bar{U}_0}{U^*} \right)^2 \right] \quad (\text{A6-24})$$

in which

$$N_p = \frac{c_p \mu}{k} \quad ; \quad M = \frac{U^*}{\sqrt{\gamma k T^*}} \quad (\text{A6-25})$$

Since, generally, $\frac{\gamma-1}{2} N_p M^2 \ll 1$, one may assume that to the first degree of approximation

$$\bar{U} \approx \bar{U}_0 \approx 1 \quad (\text{A6-26})$$

which is equivalent to the assumption made in equation (2) of the main text, e.g., $P/\rho = \text{constant}$. Equation (A6-10) then reduces to:

$$\frac{\partial \bar{\pi}_0}{\partial \bar{t}} + \frac{1}{\bar{r}} \frac{\partial}{\partial \bar{r}} (\bar{r} \bar{\pi}_0 \bar{U}_0) + \frac{1}{f} \bar{\pi}_0 \frac{\partial \bar{U}_0}{\partial \bar{z}} = 0 \quad (\text{A6-27})$$

Integration of equation (A6-17) with respect to \bar{z} yields:

$$\bar{U}_0 = \frac{f^2 \bar{z}^2}{2} \frac{\partial \bar{\pi}_0}{\partial \bar{r}} + \bar{z} A(\bar{r}, \bar{t}) + B(\bar{r}, \bar{t}) \quad (\text{A6-28})$$

and application of boundary conditions (A6-16) gives:

$$A = -\frac{f^2}{2} \frac{\partial \bar{\pi}_0}{\partial \bar{r}} \quad ; \quad B = 0 \quad (\text{A6-29})$$

so that:

$$\bar{\Gamma}_0 = \frac{1}{2} (\bar{z}^2 - \bar{z}) f^2 \frac{\partial \bar{\pi}_0}{\partial \bar{r}} \quad (\text{A6-30})$$

Substitution of equation (A6-30) in equation (A6-27) gives:

$$\frac{\partial \bar{\pi}_0}{\partial \bar{t}} + \frac{1}{2} (\bar{z}^2 - \bar{z}) f^2 \frac{1}{\bar{r}} \frac{\partial}{\partial \bar{r}} \left(\bar{r} \bar{\pi}_0 \frac{\partial \bar{\pi}_0}{\partial \bar{r}} \right) - \frac{1}{f} \bar{\pi}_0 \frac{\partial \bar{\pi}_0}{\partial \bar{z}} = 0 \quad (\text{A6-31})$$

and integration between the limits $\bar{z} = 0$ and $\bar{z} = 1$ yields:

$$\frac{1}{\bar{r}} \frac{\partial}{\partial \bar{r}} \left(\bar{r} \bar{\pi}_0 \frac{\partial \bar{\pi}_0}{\partial \bar{r}} \right) = \frac{12}{f^3} \frac{\partial}{\partial \bar{t}} (f \bar{\pi}_0) \quad (\text{A6-32})$$

which is the dimensionless equivalent of equation (4) of the main text, when it is assumed that $\bar{\pi}_0$ is a good approximation of \bar{P} .

The error involved in neglecting higher order terms of the expansions could be estimated only if zeroth solutions were available; through substitution in the initial equations, for example. It is self-evident that the degree to which zeroth terms of ϵ -expansions approximate the actual functions depends on magnitudes of other coefficients which appear in the dimensionless equations of fluid motion. Of particular importance is the magnitude of f which characterizes the effect of boundary motion.

It was tacitly assumed in taking Taylor's equation [1] as the starting point of the analysis, and subsequently implied in the linearization thereof, that f was arbitrarily small. In doing so one was encouraged by the fact that equation (4) of the main text is exact in the limiting case, whenever:

$$L \rightarrow \infty, \quad \text{with} \quad \dot{f} = \frac{L^2}{\nu^*} \frac{df}{dt} \text{ finite}$$

or

$$H^* \rightarrow 0, \quad \text{with} \quad \frac{P^*}{\rho^*} \left(\frac{H^*}{\nu^*} \right)^2 \text{ finite.}$$

APPENDIX 7

TABULATION OF COMPUTER SOLUTIONS

This appendix contains a tabulation of computer solutions of the set of simultaneous equations (40b) subject to the boundary condition (41b). The solutions are for a fixed value of $B = 0.596481$ and for discrete values of the parameter α . The range of the independent variable is $1 \leq \xi \leq 5$ and the interval size is $\Delta \xi = 0.1$. The numerical method employed was that of Chipinger and Dimsdale and is contained in "Numerical Analysis", Kaiser S. Kunz, McGraw-Hill Book Co., 1957 pp 206-208.

The following code is to be used in reading the tables. The first digit is zero if the number is positive and is a minus sign if the number is negative. The second and third digits stand for $50 \cdot n$, where n is the exponent in 10^n . The remaining digits represent a decimal, which must be multiplied by 10^n in order to read the required number.

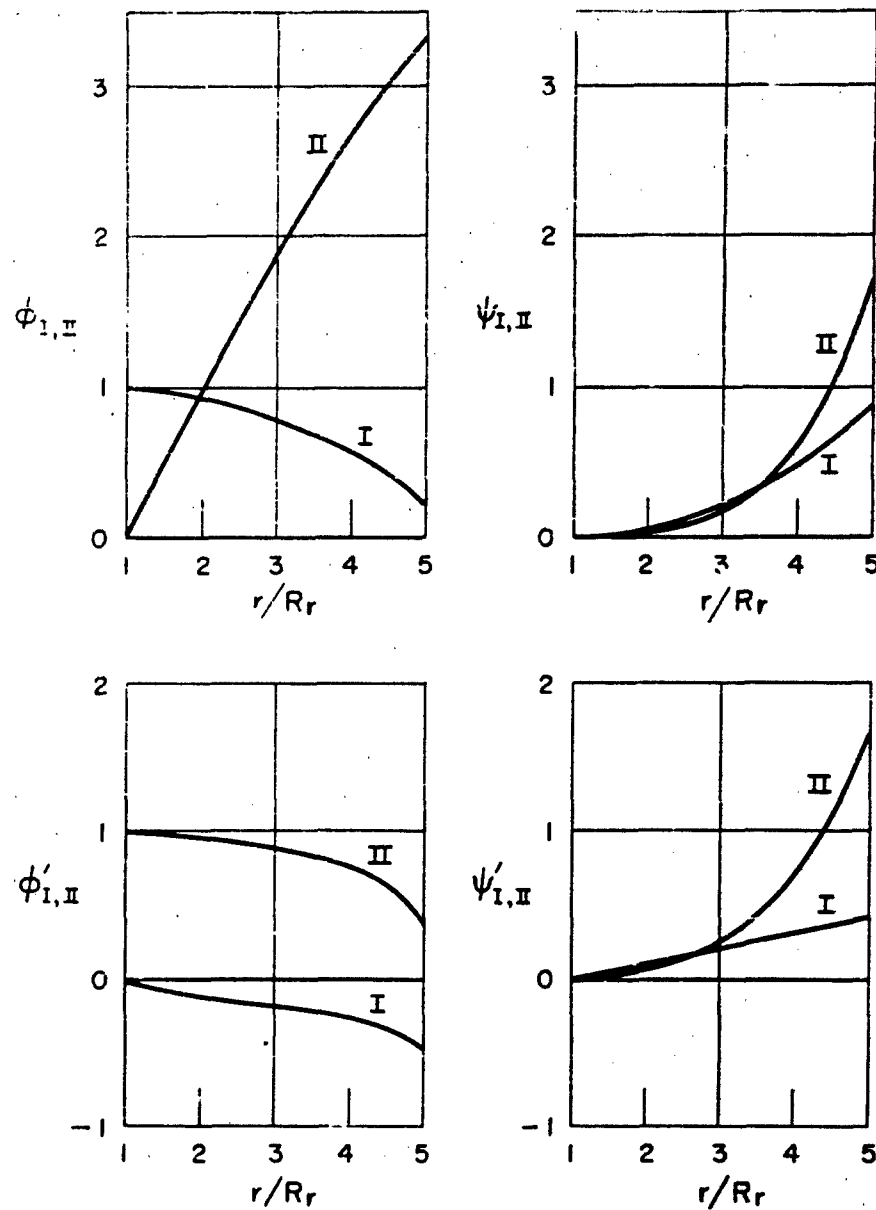


FIG. A7-1. PLOT OF COMPUTER SOLUTIONS OF EQUATIONS 40b FOR $\alpha = 0.093$

I-A2049-12

105

1-A2049-12

106

I-A2049-12

ξ	α	ϕ_1	ψ_1	$\phi_1^{\#}$	$\psi_1^{\#}$	$\psi_1^{\#}$	$\psi_1^{\#}$	$\psi_1^{\#}$
051100000000	049200000000	051100000000	000000000000	049200000000	000000000000	000000000000	000000000000	049199999999
051110000000		050999999150	049227438888	0492000007152	0491100978249	048202809750	049205190215	
051120000000		05099995501772	049416113767	049172880674	048740742043	04811722873	049211000780	
051130000000		0509999008895	049375797725	049166880304	0487023827440	048633078070	049214351552	
051140000000		0509999142050	049710099337	049175946730	0481145671386	048339247296	049210748942	
051150000000		050976444720	049827805710	049109493825	0482044451388	049115712130	049221492758	
051160000000		049097458480	049929121084	049045858390	048377401286	049128106625	049224464745	
051170000000		049097300440	050101774381	0498294887501	049114011940	049150781246	049227360609	
051180000000		049047390130	0501009472188	049114011940	048479035193	049173012020	049229773161	
051190000000		0490498210818	050116077028	049085013945	048204234080	049156740703	049232213222	
051200000000		0490294040119	050122421190	049580337999	049107361449	049220009746	049234407041	
051210000000		049011517265	051128116814	049529227365	0491100931091	049243618306	049235774947	
051220000000		0490081004818	050133052373	049446344016	049119602158	049267441187	049238436294	
051230000000		0490084372525	050137908679	049423370022	049118029252	049291488459	049240790957	
051240000000		049070306712	051141940104	049346224291	049214400256	049315617853	049242703501	
051250000000		0490486503180	0501450208341	049329275034	04924173667	049339901545	049244431048	
051260000000		0490241945758	050148853587	049310074626	049232300380	049360312522	049246433144	
051270000000		0490206009745	050151819171	049239072367	049310071367	049340242273	049248493928	
051280000000		049011600187	050154436094	04920403675	049041100340	049412187537	049251285302	
051290000000		0490203720495	050157035700	04920994560	0494028007004	049839215730	049251872709	
051300000000		0490780219417	050159043583	049231989133	049404800912	049464443814	049253338131	
051310000000		0490744100340	050161482807	049216176092	049404870602	049480816117	049255126949	
051320000000		0490747427858	050163773410	04928793665	049545032188	049515471005	049256900046	
051330000000		0490731309415	050165734584	049100226352	049508000785	049541277905	049258001819	
051340000000		0490714744713	050167483555	049179743159	049644025347	049567244817	049260033274	
051350000000		049097400280	050169334204	0491707181528	049172365215	049593447600	049263096504	
051360000000		0490802000418	050171003470	049131188334	049772050364	0496195279814	049265435004	
051370000000		0490443603775	050172001824	049146800284	0498984247615	049646504060	049267783633	
051380000000		049046362330	050174145470	04915188793	0499002378399	049673484547	049270005480	
051390000000		0490208048758	050175443501	04916126768	049979555588	04970071810	049273059677	
051400000000		049041124480	050177112160	04914513781	050104349397	049728021415	049277735856	
051410000000		049049349635	050178459810	049146375156	050111181397	049756246050	049281838616	
051420000000		049047552708	050180004127	049146478663	049119440997	049794061434	0492860110262	
051430000000		049045741830	050181453302	049146025454	050127450544	049813546585	049292442131	
051440000000		0490439241144	050182730095	049149108609	049119544393	0498433087155	049298799399	
051450000000		0490470884170	050184443502	049146263967	050114021175	0498773374085	049307830839	
051460000000		0490402300351	050186022502	049141576008	0501193113961	0499004541048	0493172095022	
051470000000		049048364810	050187483962	049171789988	0501162910077	049936927450	049330041559	
051480000000		0490464769503	050188171318	049185028904	0501171857599	049970700637	0493347408674	
051490000000		049046477421	050191441040	049442671218	050118191340	050100649770	049371259092	
051500000000		0490462947477	050193815526	049234800181	050102001477	050104543373	0494007002775	
051510000000		04904007034898	050196156701	049234800487	049723488778	0501020000333	0494155777725	

T-A2049-12

[illegible]

f-A2049-12

[illegible]

I-A2049-12

[illegible]

I-A2049-12

111

THE FRANKLIN INSTITUTE • Laboratories for Research and Development

I-A2049-12

[illegible]

I-A2049 12

113

I-A2049-12

114

T-A2049-12

[illegible]

THE FRANKLIN INSTITUTE • Laboratories for Research and Development

I-A2049-12

[illegible]

ϵ	α	ϕ_1	ϕ_1'	ϕ_1''	ψ_1	ψ_1'	ψ_1''
051100000000	049800000000	041100000000	000000000000	000000000000	000000000000	000000000000	040399999712
041110000000	040099999999	040227348230	040206182942	047302719055	048608119435	040016713578	
041120000000	040099999999	040415159237	040172021671	048122190312	049173217041	040050223425	
041130000000	040099999999	040575934470	040146720079	048277144497	049176911593	040043053957	
041140000000	040099999999	040711198071	040149842386	04840404528	04925173190	040054144352	
041150000000	040099999999	040824451470	040150071204	048415334440	049317006227	040064160202	
041160000000	040099999999	040930475045	040152947593	049111512161	049384597963	040073326784	
041170000000	040099999999	041010944500	040154049369	049144064096	049452300072	040081755620	
041180000000	040099999999	041074608125	040154608125	049204707246	049520918576	040089471760	
041190000000	040099999999	041146070917	040154942528	049249271116	049590218695	040096450779	
041200000000	040099999999	04123710752	040154942528	049249271116	049590218695	040096450779	
041210000000	040099999999	04124056101	040154942528	049249271116	049590218695	040096450779	
041220000000	040099999999	04134301737	040154942528	049249271116	049590218695	040096450779	
041230000000	040099999999	04139131590	040154942528	049249271116	049590218695	040096450779	
041240000000	040099999999	04143417137	040154942528	049249271116	049590218695	040096450779	
041250000000	040099999999	04147421741	040154942528	049249271116	049590218695	040096450779	
041260000000	040099999999	04151401127	040154942528	049249271116	049590218695	040096450779	
041270000000	040099999999	04155400040	040154942528	049249271116	049590218695	040096450779	
041280000000	040099999999	04159380609	040154942528	049249271116	049590218695	040096450779	
041290000000	040099999999	04162463016	040154942528	049249271116	049590218695	040096450779	
041300000000	040099999999	04166441128	040154942528	049249271116	049590218695	040096450779	
041310000000	040099999999	0417042369	040154942528	049249271116	049590218695	040096450779	
041320000000	040099999999	04174407405	040154942528	049249271116	049590218695	040096450779	
041330000000	040099999999	0417839108	040154942528	049249271116	049590218695	040096450779	
041340000000	040099999999	0418237480	040154942528	049249271116	049590218695	040096450779	
041350000000	040099999999	0418635859	040154942528	049249271116	049590218695	040096450779	
041360000000	040099999999	0419034239	040154942528	049249271116	049590218695	040096450779	
041370000000	040099999999	0419432619	040154942528	049249271116	049590218695	040096450779	
041380000000	040099999999	0419831000	040154942528	049249271116	049590218695	040096450779	
041390000000	040099999999	0420229381	040154942528	049249271116	049590218695	040096450779	
041400000000	040099999999	0420627762	040154942528	049249271116	049590218695	040096450779	
041410000000	040099999999	0421026143	040154942528	049249271116	049590218695	040096450779	
041420000000	040099999999	0421424524	040154942528	049249271116	049590218695	040096450779	
041430000000	040099999999	0421822905	040154942528	049249271116	049590218695	040096450779	
041440000000	040099999999	0422221286	040154942528	049249271116	049590218695	040096450779	
041450000000	040099999999	0422619667	040154942528	049249271116	049590218695	040096450779	
041460000000	040099999999	0423018048	040154942528	049249271116	049590218695	040096450779	
041470000000	040099999999	0423416429	040154942528	049249271116	049590218695	040096450779	
041480000000	040099999999	0423814810	040154942528	049249271116	049590218695	040096450779	
041490000000	040099999999	0424213191	040154942528	049249271116	049590218695	040096450779	
041500000000	040099999999	0424611572	040154942528	049249271116	049590218695	040096450779	
041510000000	040099999999	0425009953	040154942528	049249271116	049590218695	040096450779	
041520000000	040099999999	0425408334	040154942528	049249271116	049590218695	040096450779	
041530000000	040099999999	0425806715	040154942528	049249271116	049590218695	040096450779	
041540000000	040099999999	0426205096	040154942528	049249271116	049590218695	040096450779	
041550000000	040099999999	0426603477	040154942528	049249271116	049590218695	040096450779	
041560000000	040099999999	0427001858	040154942528	049249271116	049590218695	040096450779	
041570000000	040099999999	0427399239	040154942528	049249271116	049590218695	040096450779	
041580000000	040099999999	0427797620	040154942528	049249271116	049590218695	040096450779	
041590000000	040099999999	0428195991	040154942528	049249271116	049590218695	040096450779	
041600000000	040099999999	0428594372	040154942528	049249271116	049590218695	040096450779	
041610000000	040099999999	0428992753	040154942528	049249271116	049590218695	040096450779	
041620000000	040099999999	0429391134	040154942528	049249271116	049590218695	040096450779	
041630000000	040099999999	0429789515	040154942528	049249271116	049590218695	040096450779	
041640000000	040099999999	0430187896	040154942528	049249271116	049590218695	040096450779	
041650000000	040099999999	0430586277	040154942528	049249271116	049590218695	040096450779	
041660000000	040099999999	0430984658	040154942528	049249271116	049590218695	040096450779	
041670000000	040099999999	0431383039	040154942528	049249271116	049590218695	040096450779	
041680000000	040099999999	0431781420	040154942528	049249271116	049590218695	040096450779	
041690000000	040099999999	0432179801	040154942528	049249271116	049590218695	040096450779	
041700000000	040099999999	0432578182	040154942528	049249271116	049590218695	040096450779	
041710000000	040099999999	0432976563	040154942528	049249271116	049590218695	040096450779	
041720000000	040099999999	0433374944	040154942528	049249271116	049590218695	040096450779	
041730000000	040099999999	0433773325	040154942528	049249271116	049590218695	040096450779	
041740000000	040099999999	0434171706	040154942528	049249271116	049590218695	040096450779	
041750000000	040099999999	0434570087	040154942528	049249271116	049590218695	040096450779	
041760000000	040099999999	0434968468	040154942528	049249271116	049590218695	040096450779	
041770000000	040099999999	0435366849	040154942528	049249271116	049590218695	040096450779	
041780000000	040099999999	0435765230	040154942528	049249271116	049590218695	040096450779	
041790000000	040099999999	0436163611	040154942528	049249271116	049590218695	040096450779	
041800000000	040099999999	0436561992	040154942528	049249271116	049590218695	040096450779	
041810000000	040099999999	0436960373	040154942528	049249271116	049590218695	040096450779	
041820000000	040099999999	0437358754	040154942528	049249271116	049590218695	040096450779	
041830000000	040099999999	0437757135	040154942528	049249271116	049590218695	040096450779	
041840000000	040099999999	0438155516	040154942528	049249271116	049590218695	040096450779	
041850000000	040099999999	0438553897	040154942528	049249271116	049590218695	040096450779	
041860000000	040099999999	0438952278	040154942528	049249271116	049590218695	040096450779	
041870000000	040099999999	0439350659	040154942528	049249271116	049590218695	040096450779	
041880000000	040099999999	0439749040	040154942528	049249271116	049590218695	040096450779	
041890000000	040099999999	0440147421	040154942528	049249271116	049590218695	040096450779	
041900000000	040099999999	0440545802	040154942528	049249271116	049590218695	040096450779	
041910000000	040099999999	0440944183	040154942528	049249271116	049590218695	040096450779	
041920000000	040099999999	0441342564	040154942528	049249271116	049590218695	040096450779	
041930000000	040099999999	0441740945	040154942528	049249271116	049590218695	040096450779	
041940000000	040099999999	0442139326	040154942528	049249271116	049590218695	040096450779	
041950000000	040099999999	0442537707	040154942528	049249271116	049590218695	040096450779	
041960000000	040099999999	0442936088	040154942528	049249271116	049590218695	040096450779	
041970000000	040099999999	0443334469	040154942528	049249271116	049590218695	040096450779	
041980000000	040099999999	0443732850	040154942528	049249271116	049590218695	040096450779	
041990000000	040099999999	0444131231	040154942528	049249271116	049590218695	040096450779	
042000000000	040099999999	0444529612	040154942528	049249271116	049590218695	040096450779	

I-A2049-12

118

THE FRANKLIN INSTITUTE • Laboratories for Research and Development

I-A2049-12

[illegible]

THE FRANKLIN INSTITUTE • Laboratories for Research and Development

I-A2049-12

[illegible]

THE FRANKLIN INSTITUTE • Laboratories for Research and Development

--I-A2049-12

[illegible]

THE FRANKLIN INSTITUTE • Laboratories for Research and Development

I-A2049-12

[illegible]

THE FRANKLIN INSTITUTE • Laboratories for Research and Development

I-A2049-12

ξ	α	ϕ	ϕ'	ϕ''	ψ	ψ'	ψ''
051107000000	046750000000	051100000000	040000000000	040200000000	000000000000	000000000000	049747335640
051110000000		050900000000	040220000000	040230000000	000737033900	046740534400	049770000000
051120000000		050700000000	040400000000	040410000000	000737033900	046740534400	049770000000
051130000000		050500000000	040500000000	040510000000	000737033900	046740534400	049770000000
051140000000		050300000000	040600000000	040610000000	000737033900	046740534400	049770000000
051150000000		050100000000	040700000000	040710000000	000737033900	046740534400	049770000000
051160000000		049900000000	040800000000	040810000000	000737033900	046740534400	049770000000
051170000000		049700000000	040900000000	040910000000	000737033900	046740534400	049770000000
051180000000		049500000000	041000000000	041010000000	000737033900	046740534400	049770000000
051190000000		049300000000	041100000000	041110000000	000737033900	046740534400	049770000000
051200000000		049100000000	041200000000	041210000000	000737033900	046740534400	049770000000
051210000000		048900000000	041300000000	041310000000	000737033900	046740534400	049770000000
051220000000		048700000000	041400000000	041410000000	000737033900	046740534400	049770000000
051230000000		048500000000	041500000000	041510000000	000737033900	046740534400	049770000000
051240000000		048300000000	041600000000	041610000000	000737033900	046740534400	049770000000
051250000000		048100000000	041700000000	041710000000	000737033900	046740534400	049770000000
051260000000		047900000000	041800000000	041810000000	000737033900	046740534400	049770000000
051270000000		047700000000	041900000000	041910000000	000737033900	046740534400	049770000000
051280000000		047500000000	042000000000	042010000000	000737033900	046740534400	049770000000
051290000000		047300000000	042100000000	042110000000	000737033900	046740534400	049770000000
051300000000		047100000000	042200000000	042210000000	000737033900	046740534400	049770000000
051310000000		046900000000	042300000000	042310000000	000737033900	046740534400	049770000000
051320000000		046700000000	042400000000	042410000000	000737033900	046740534400	049770000000
051330000000		046500000000	042500000000	042510000000	000737033900	046740534400	049770000000
051340000000		046300000000	042600000000	042610000000	000737033900	046740534400	049770000000
051350000000		046100000000	042700000000	042710000000	000737033900	046740534400	049770000000
051360000000		045900000000	042800000000	042810000000	000737033900	046740534400	049770000000
051370000000		045700000000	042900000000	042910000000	000737033900	046740534400	049770000000
051380000000		045500000000	043000000000	043010000000	000737033900	046740534400	049770000000
051390000000		045300000000	043100000000	043110000000	000737033900	046740534400	049770000000
051400000000		045100000000	043200000000	043210000000	000737033900	046740534400	049770000000
051410000000		044900000000	043300000000	043310000000	000737033900	046740534400	049770000000
051420000000		044700000000	043400000000	043410000000	000737033900	046740534400	049770000000
051430000000		044500000000	043500000000	043510000000	000737033900	046740534400	049770000000
051440000000		044300000000	043600000000	043610000000	000737033900	046740534400	049770000000
051450000000		044100000000	043700000000	043710000000	000737033900	046740534400	049770000000
051460000000		043900000000	043800000000	043810000000	000737033900	046740534400	049770000000
051470000000		043700000000	043900000000	043910000000	000737033900	046740534400	049770000000
051480000000		043500000000	044000000000	044010000000	000737033900	046740534400	049770000000
051490000000		043300000000	044100000000	044110000000	000737033900	046740534400	049770000000
051500000000		043100000000	044200000000	044210000000	000737033900	046740534400	049770000000
051510000000		042900000000	044300000000	044310000000	000737033900	046740534400	049770000000
051520000000		042700000000	044400000000	044410000000	000737033900	046740534400	049770000000
051530000000		042500000000	044500000000	044510000000	000737033900	046740534400	049770000000
051540000000		042300000000	044600000000	044610000000	000737033900	046740534400	049770000000
051550000000		042100000000	044700000000	044710000000	000737033900	046740534400	049770000000
051560000000		041900000000	044800000000	044810000000	000737033900	046740534400	049770000000
051570000000		041700000000	044900000000	044910000000	000737033900	046740534400	049770000000
051580000000		041500000000	045000000000	045010000000	000737033900	046740534400	049770000000
051590000000		041300000000	045100000000	045110000000	000737033900	046740534400	049770000000
051600000000		041100000000	045200000000	045210000000	000737033900	046740534400	049770000000
051610000000		040900000000	045300000000	045310000000	000737033900	046740534400	049770000000
051620000000		040700000000	045400000000	045410000000	000737033900	046740534400	049770000000
051630000000		040500000000	045500000000	045510000000	000737033900	046740534400	049770000000
051640000000		040300000000	045600000000	045610000000	000737033900	046740534400	049770000000
051650000000		040100000000	045700000000	045710000000	000737033900	046740534400	049770000000
051660000000		039900000000	045800000000	045810000000	000737033900	046740534400	049770000000
051670000000		039700000000	045900000000	045910000000	000737033900	046740534400	049770000000
051680000000		039500000000	046000000000	046010000000	000737033900	046740534400	049770000000
051690000000		039300000000	046100000000	046110000000	000737033900	046740534400	049770000000
051700000000		039100000000	046200000000	046210000000	000737033900	046740534400	049770000000
051710000000		038900000000	046300000000	046310000000	000737033900	046740534400	049770000000
051720000000		038700000000	046400000000	046410000000	000737033900	046740534400	049770000000
051730000000		038500000000	046500000000	046510000000	000737033900	046740534400	049770000000
051740000000		038300000000	046600000000	046610000000	000737033900	046740534400	049770000000
051750000000		038100000000	046700000000	046710000000	000737033900	046740534400	049770000000
051760000000		037900000000	046800000000	046810000000	000737033900	046740534400	049770000000
051770000000		037700000000	046900000000	046910000000	000737033900	046740534400	049770000000
051780000000		037500000000	047000000000	047010000000	000737033900	046740534400	049770000000
051790000000		037300000000	047100000000	047110000000	000737033900	046740534400	049770000000
051800000000		037100000000	047200000000	047210000000	000737033900	046740534400	049770000000
051810000000		036900000000	047300000000	047310000000	000737033900	046740534400	049770000000
051820000000		036700000000	047400000000	047410000000	000737033900	046740534400	049770000000
051830000000		036500000000	047500000000	047510000000	000737033900	046740534400	049770000000
051840000000		036300000000	047600000000	047610000000	000737033900	046740534400	049770000000
051850000000		036100000000	047700000000	047710000000	000737033900	046740534400	049770000000
051860000000		035900000000	047800000000	047810000000	000737033900	046740534400	049770000000
051870000000		035700000000	047900000000	047910000000	000737033900	046740534400	049770000000
051880000000		035500000000	048000000000	048010000000	000737033900	046740534400	049770000000
051890000000		035300000000	048100000000	048110000000	000737033900	046740534400	049770000000
051900000000		035100000000	048200000000	048210000000	000737033900	046740534400	049770000000
051910000000		034900000000	048300000000	048310000000	000737033900	046740534400	049770000000
051920000000		034700000000	048400000000	048410000000	000737033900	046740534400	049770000000
051930000000		034500000000	048500000000	048510000000	000737033900	046740534400	049770000000
051940000000		034300000000	048600000000	048610000000	000737033900	046740534400	049770000000
051950000000		034100000000	048700000000	048710000000	000737033900	046740534400	049770000000
051960000000		033900000000	048800000000	048810000000	000737033900	046740534400	049770000000
051970000000		033700000000	048900000000	048910000000	000737033900	046740534400	049770000000
051980000000		033500000000	049000000000	049010000000	000737033900	046740534400	049770000000
051990000000		033300000000	049100000000	049110000000	000737033900	046740534400	049770000000
052000000000		033100000000	049200000000	049210000000	000737033900	046740534400	049770000000
052010000000		032900000000	049300000000	049310000000	000737033900	046740534400	049770000000
052020000000		032700000000	049400000000	049410000000	000737033900	046740534400	049770000000
052030000000		032500000000	049500000000	049510000000	000737033900	046740534400	049770000000
052040000000		032300000000	049600000000	049610000000	000737033900	046740534400	049770000000
052050000000		032100000000	049700000000	049710000000	000737033900	046740534400	049770000000
052060000000		031900000000	049800000000	049810000000	000737033900		

THE FRANKLIN INSTITUTE • Laboratories for Research and Development

I-A2049-12

[illegible]

I-A2049-12

[illegible]

I-A2049 12

126

THE FRANKLIN INSTITUTE • Laboratories for Research and Development

I-A2049-12

[illegible]

I-A2049-12

[illegible]

I-A2049-12

[illegible]

I-A2049-12

Σ	α	φ _{II}	φ _{III}	φ _{IV}	ψ _{II}	ψ _{III}	ψ _{IV}
051100000000	049000000000	000000000000	051100000000	000000000000	000000000000	000000000000	000000000000
051110000000		049099000000	050999000000	049200500000	046100533000	047400770000	049015750000
051120000000		050100000000	050999000000	049300000000	047120000000	048100720000	04901000757000
051130000000		050200000000	050999000000	049400000000	047000000000	048000000000	049000000000
051140000000		050300000000	050999000000	049500000000	046900000000	047900000000	048900000000
051150000000		050400000000	050999000000	049600000000	046800000000	047800000000	048800000000
051160000000		050500000000	050999000000	049700000000	046700000000	047700000000	048700000000
051170000000		050600000000	050999000000	049800000000	046600000000	047600000000	048600000000
051180000000		050700000000	050999000000	049900000000	046500000000	047500000000	048500000000
051190000000		050800000000	050999000000	050000000000	046400000000	047400000000	048400000000
051200000000		050900000000	050999000000	050100000000	046300000000	047300000000	048300000000
051210000000		051000000000	050999000000	050200000000	046200000000	047200000000	048200000000
051220000000		051100000000	050999000000	050300000000	046100000000	047100000000	048100000000
051230000000		051200000000	050999000000	050400000000	046000000000	047000000000	048000000000
051240000000		051300000000	050999000000	050500000000	045900000000	046900000000	047900000000
051250000000		051400000000	050999000000	050600000000	045800000000	046800000000	047800000000
051260000000		051500000000	050999000000	050700000000	045700000000	046700000000	047700000000
051270000000		051600000000	050999000000	050800000000	045600000000	046600000000	047600000000
051280000000		051700000000	050999000000	050900000000	045500000000	046500000000	047500000000
051290000000		051800000000	050999000000	051000000000	045400000000	046400000000	047400000000
051300000000		051900000000	050999000000	051100000000	045300000000	046300000000	047300000000
051310000000		052000000000	050999000000	051200000000	045200000000	046200000000	047200000000
051320000000		052100000000	050999000000	051300000000	045100000000	046100000000	047100000000
051330000000		052200000000	050999000000	051400000000	045000000000	046000000000	047000000000
051340000000		052300000000	050999000000	051500000000	044900000000	045900000000	046900000000
051350000000		052400000000	050999000000	051600000000	044800000000	045800000000	046800000000
051360000000		052500000000	050999000000	051700000000	044700000000	045700000000	046700000000
051370000000		052600000000	050999000000	051800000000	044600000000	045600000000	046600000000
051380000000		052700000000	050999000000	051900000000	044500000000	045500000000	046500000000
051390000000		052800000000	050999000000	052000000000	044400000000	045400000000	046400000000
051400000000		052900000000	050999000000	052100000000	044300000000	045300000000	046300000000

THE FRANKLIN INSTITUTE • Laboratories for Research and Development

I-A2049-12

[illegible]

THE FRANKLIN INSTITUTE • Laboratories for Research and Development

I-A2049-12

[illegible]

THE FRANKLIN INSTITUTE • Laboratories for Research and Development

T 42049-12

ξ	α	ϕ_1	ϕ_1'	ϕ_1''	ψ_1	ψ_1'	ψ_1''
05110000000	00991000000	05110000000	00000000000	-00250000000	00000000000	00000000000	04990000000
05111000000	05009881000	-00277556373	-00206413905	04777777777	04899777777	04993498185	
05112000000	06099558110	-04981625293	-00173022495	04818552212	04918487916	04995644511	
05113000000	09099060213	-04957506305	-00146955960	04849033494	04928348252	04975296707	
05114000000	09088413777	-04771018186	-00124294073	04877284767	04938167070	04999211314	
05115000000	09087443777	-04879067390	-00109729751	04911847166	04948128089	05010073094	
05116000000	09087660347	-04993244201	-00096334180	04917171492	04958324824	05010211819	
05117000000	09085710700	-00102316484	-00080444523	04927510137	04968001565	05010339349	
05118000000	09084717000	-00110401475	-00076572979	04930895477	04978004383	05010447439	
05119000000	09083574083	-00117886074	-00069356305	04933324234	04988165911	05010567253	
05120000000	09082364430	-00124119421	-00063527070	04948042640	04998174604	05010649813	
05121000000	09081091491	-00130430484	-00058873154	04958352445	05008174314	05010765927	
05122000000	09079758224	-00136127093	-00052371188	04970970234	05018164630	05010856169	
05123000000	09078369949	-0014107810	-00045288710	04980686363	05028454074	05010941064	
05124000000	09076992867	-00146454451	-00039062749	04997491994	05038435063	05011020962	
05125000000	09075543079	-00151632342	-00032626461	05011234064	05048416094	05011106064	
05126000000	09074094884	-00156449470	-00026446628	05028417324	05058417746	05011146947	
05127000000	09072304706	-00161421246	-00020497478	05048455436	05068418462	05011233247	
05128000000	09070667018	-00166364002	-00014972095	05068438097	05078419267	05011295303	
05129000000	09068989944	-00171784016	-00009107301	05088431019	05088431019	05011353114	
05130000000	09067239684	-00176499040	-00003301147	05108437101	05098437101	05011409966	
05131000000	09065480122	-00182008040	-00002557531	05128437101	05108437101	05011454649	
05132000000	09063735958	-00187737112	-00001835484	05148437101	05118437101	05011497402	
05133000000	09062169400	-00193785716	-00001170032	05168437101	05128437101	05011535632	
05134000000	09060472144	-00199805073	-00000613503	05188437101	05138437101	05011564691	
05135000000	09058764406	-00205725471	-00000174060	05208437101	05148437101	05011591059	
05136000000	09057057444	-00211780884	-00000074999	05228437101	05158437101	05011617780	
05137000000	09055338444	-00217801794	-00000027753	05248437101	05168437101	05011645726	
05138000000	09053627714	-00223873044	-00000004026	05268437101	05178437101	05011673340	
05139000000	09051916431	-00229841840	-00000001999	05288437101	05188437101	05011699181	
05140000000	09050205707	-00235811245	-00000000157	05308437101	05198437101	05011725045	
05141000000	09048494922	-00241780247	-00000000000	05328437101	05208437101	05011750907	
05142000000	09046784144	-00247748747	-00000000000	05348437101	05218437101	05011776767	
05143000000	09045073366	-00253717247	-00000000000	05368437101	05228437101	05011802627	
05144000000	09043362588	-00259685747	-00000000000	05388437101	05238437101	05011828487	
05145000000	09041651810	-00265654247	-00000000000	05408437101	05248437101	05011854347	
05146000000	09039941032	-00271622747	-00000000000	05428437101	05258437101	05011880207	
05147000000	09038230254	-00277591247	-00000000000	05448437101	05268437101	05011906067	
05148000000	09036519476	-00283560747	-00000000000	05468437101	05278437101	05011931927	
05149000000	09034808698	-00289530247	-00000000000	05488437101	05288437101	05011957787	
05150000000	09033097920	-00295500747	-00000000000	05508437101	05298437101	05011983647	
05151000000	09031387142	-00301470247	-00000000000	05528437101	05308437101	05012009507	
05152000000	09029676364	-00307440747	-00000000000	05548437101	05318437101	05012035367	
05153000000	09027965586	-00313410247	-00000000000	05568437101	05328437101	05012061227	
05154000000	09026254808	-00319380747	-00000000000	05588437101	05338437101	05012087087	
05155000000	09024544030	-00325350247	-00000000000	05608437101	05348437101	05012112947	
05156000000	09022833252	-00331320747	-00000000000	05628437101	05358437101	05012138807	
05157000000	09021122474	-00337290247	-00000000000	05648437101	05368437101	05012164667	
05158000000	09019411696	-00343260747	-00000000000	05668437101	05378437101	05012190527	
05159000000	09017700918	-00349230247	-00000000000	05688437101	05388437101	05012216387	
05160000000	09015990140	-00355200747	-00000000000	05708437101	05398437101	05012242247	
05161000000	09014279362	-00361170247	-00000000000	05728437101	05408437101	05012268107	
05162000000	09012568584	-00367140747	-00000000000	05748437101	05418437101	05012293967	
05163000000	09010857806	-00373110247	-00000000000	05768437101	05428437101	05012319827	
05164000000	09009147028	-00379080747	-00000000000	05788437101	05438437101	05012345687	
05165000000	09007436250	-00385050247	-00000000000	05808437101	05448437101	05012371547	
05166000000	09005725472	-00391020747	-00000000000	05828437101	05458437101	05012397407	
05167000000	09004014694	-00396990247	-00000000000	05848437101	05468437101	05012423267	
05168000000	09002303916	-00402960747	-00000000000	05868437101	05478437101	05012449127	
05169000000	09000593138	-00408930247	-00000000000	05888437101	05488437101	05012474987	
05170000000	08998882360	-00414900747	-00000000000	05908437101	05498437101	05012500847	
05171000000	08997171582	-00420870247	-00000000000	05928437101	05508437101	05012526707	
05172000000	08995460804	-00426840747	-00000000000	05948437101	05518437101	05012552567	
05173000000	08993750026	-00432810247	-00000000000	05968437101	05528437101	05012578427	
05174000000	08992039248	-00438780747	-00000000000	05988437101	05538437101	05012604287	
05175000000	08990328470	-00444750247	-00000000000	06008437101	05548437101	05012630147	
05176000000	08988617692	-00450720747	-00000000000	06028437101	05558437101	05012656007	
05177000000	08986906914	-00456690247	-00000000000	06048437101	05568437101	05012681867	
05178000000	08985196136	-00462660747	-00000000000	06068437101	05578437101	05012707727	
05179000000	08983485358	-00468630247	-00000000000	06088437101	05588437101	05012733587	
05180000000	08981774580	-00474600747	-00000000000	06108437101	05598437101	05012759447	
05181000000	08980063802	-00480570247	-00000000000	06128437101	05608437101	05012785307	
05182000000	08978353024	-00486540747	-00000000000	06148437101	05618437101	05012811167	
05183000000	08976642246	-00492510247	-00000000000	06168437101	05628437101	05012837027	
05184000000	08974931468	-00498480747	-00000000000	06188437101	05638437101	05012862887	
05185000000	08973220690	-00504450247	-00000000000	06208437101	05648437101	05012888747	
05186000000	08971509912	-00510420747	-00000000000	06228437101	05658437101	05012914607	
05187000000	08969799134	-00516390247	-00000000000	06248437101	05668437101	05012940467	
05188000000	08968088356	-00522360747	-00000000000	06268437101	05678437101	05012966327	
05189000000	08966377578	-00528330247	-00000000000	06288437101	05688437101	05012992187	
05190000000	08964666800	-00534300747	-00000000000	06308437101	05698437101	05013018047	
05191000000	08962956022	-00540270247	-00000000000	06328437101	05708437101	05013043907	

I-A2049-12

[illegible]

I-A2049-12

α	φ ₁	φ ₂	φ ₃	ψ ₁	ψ ₂	ψ ₃
051100000000	049420000000	051100000000	000000000000	000000000000	000000000000	000000000000
051110000000	050998031000	04927756000	000000000000	000000000000	000000000000	000000000000
051120000000	050995501150	0490416227076	000173020000	000173047000	000173047000	000173047000
051130000000	0509950002000	049075772000	000140900000	000140900000	000140900000	000140900000
051140000000	050984110000	049071100000	000126311700	000126311700	000126311700	000126311700
051150000000	050974000000	049070710000	000100757000	000100757000	000100757000	000100757000
051160000000	050963000000	049063000000	000083747000	000083747000	000083747000	000083747000
051170000000	050952012000	049052012000	000070000000	000070000000	000070000000	000070000000
051180000000	050941000000	049041000000	000060000000	000060000000	000060000000	000060000000
051190000000	050930000000	049030000000	000050000000	000050000000	000050000000	000050000000
051200000000	050919000000	049019000000	000040000000	000040000000	000040000000	000040000000
051210000000	050908000000	049008000000	000030000000	000030000000	000030000000	000030000000
051220000000	050897000000	049000000000	000020000000	000020000000	000020000000	000020000000
051230000000	050886000000	049000000000	000010000000	000010000000	000010000000	000010000000
051240000000	050875000000	049000000000	000000000000	000000000000	000000000000	000000000000
051250000000	050864000000	049000000000	000000000000	000000000000	000000000000	000000000000
051260000000	050853000000	049000000000	000000000000	000000000000	000000000000	000000000000
051270000000	050842000000	049000000000	000000000000	000000000000	000000000000	000000000000
051280000000	050831000000	049000000000	000000000000	000000000000	000000000000	000000000000
051290000000	050820000000	049000000000	000000000000	000000000000	000000000000	000000000000
051300000000	050809000000	049000000000	000000000000	000000000000	000000000000	000000000000
051310000000	050798000000	049000000000	000000000000	000000000000	000000000000	000000000000
051320000000	050787000000	049000000000	000000000000	000000000000	000000000000	000000000000
051330000000	050776000000	049000000000	000000000000	000000000000	000000000000	000000000000
051340000000	050765000000	049000000000	000000000000	000000000000	000000000000	000000000000
051350000000	050754000000	049000000000	000000000000	000000000000	000000000000	000000000000
051360000000	050743000000	049000000000	000000000000	000000000000	000000000000	000000000000
051370000000	050732000000	049000000000	000000000000	000000000000	000000000000	000000000000
051380000000	050721000000	049000000000	000000000000	000000000000	000000000000	000000000000
051390000000	050710000000	049000000000	000000000000	000000000000	000000000000	000000000000

T-A2049-12

ξ	α	φ _{II}	φ _{III}	φ _{IV}	ψ _I	ψ _{II}	ψ _{III}	ψ _{IV}
051100000000	449270000000	000730000000	051130000000	000000000000	000000000000	000000000000	000000000000	000000000000
051110000000		049099000047	050900012100	03700503089	008113540530	007404000127	049090013620	
051120000000		050100720470	050000000002	009340067111	009126213429	008101001070	049190011500	
051130000000		050200101617	049202115045	009047004705	007917205201	008040730163	049020011580	
051140000000		049300120737	050007031190	049500073710	008103079500	000700000000	049000000000	
051150000000		050000000000	050000000000	049503933700	008000000000	000000000000	049500000000	
051160000000		050000000000	050000000000	049500000000	008000000000	000000000000	049500000000	
051170000000		050000000000	050000000000	049500000000	008000000000	000000000000	049500000000	
051180000000		050000000000	050000000000	049500000000	008000000000	000000000000	049500000000	
051190000000		050000000000	050000000000	049500000000	008000000000	000000000000	049500000000	
051200000000		050000000000	050000000000	049500000000	008000000000	000000000000	049500000000	
051210000000		050000000000	050000000000	049500000000	008000000000	000000000000	049500000000	
051220000000		050000000000	050000000000	049500000000	008000000000	000000000000	049500000000	
051230000000		050000000000	050000000000	049500000000	008000000000	000000000000	049500000000	
051240000000		050000000000	050000000000	049500000000	008000000000	000000000000	049500000000	
051250000000		050000000000	050000000000	049500000000	008000000000	000000000000	049500000000	
051260000000		050000000000	050000000000	049500000000	008000000000	000000000000	049500000000	
051270000000		050000000000	050000000000	049500000000	008000000000	000000000000	049500000000	
051280000000		050000000000	050000000000	049500000000	008000000000	000000000000	049500000000	
051290000000		050000000000	050000000000	049500000000	008000000000	000000000000	049500000000	
051300000000		050000000000	050000000000	049500000000	008000000000	000000000000	049500000000	
051310000000		050000000000	050000000000	049500000000	008000000000	000000000000	049500000000	
051320000000		050000000000	050000000000	049500000000	008000000000	000000000000	049500000000	
051330000000		050000000000	050000000000	049500000000	008000000000	000000000000	049500000000	
051340000000		050000000000	050000000000	049500000000	008000000000	000000000000	049500000000	
051350000000		050000000000	050000000000	049500000000	008000000000	000000000000	049500000000	
051360000000		050000000000	050000000000	049500000000	008000000000	000000000000	049500000000	
051370000000		050000000000	050000000000	049500000000	008000000000	000000000000	049500000000	
051380000000		050000000000	050000000000	049500000000	008000000000	000000000000	049500000000	
051390000000		050000000000	050000000000	049500000000	008000000000	000000000000	049500000000	
051400000000		050000000000	050000000000	049500000000	008000000000	000000000000	049500000000	
051410000000		050000000000	050000000000	049500000000	008000000000	000000000000	049500000000	
051420000000		050000000000	050000000000	049500000000	008000000000	000000000000	049500000000	
051430000000		050000000000	050000000000	049500000000	008000000000	000000000000	049500000000	
051440000000		050000000000	050000000000	049500000000	008000000000	000000000000	049500000000	
051450000000		050000000000	050000000000	049500000000	008000000000	000000000000	049500000000	
051460000000		050000000000	050000000000	049500000000	008000000000	000000000000	049500000000	
051470000000		050000000000	050000000000	049500000000	008000000000	000000000000	049500000000	
051480000000		050000000000	050000000000	049500000000	008000000000	000000000000	049500000000	
051490000000		050000000000	050000000000	049500000000	008000000000	000000000000	049500000000	
051500000000		050000000000	050000000000	049500000000	008000000000	000000000000	049500000000	
051510000000		050000000000	050000000000	049500000000	008000000000	000000000000	049500000000	
051520000000		050000000000	050000000000	049500000000	008000000000	000000000000	049500000000	
051530000000		050000000000	050000000000	049500000000	008000000000	000000000000	049500000000	
051540000000		050000000000	050000000000	049500000000	008000000000	000000000000	049500000000	
051550000000		050000000000	050000000000	049500000000	008000000000	000000000000	049500000000	
051560000000		050000000000	050000000000	049500000000	008000000000	000000000000	049500000000	
051570000000		050000000000	050000000000	049500000000	008000000000	000000000000	049500000000	
051580000000		050000000000	050000000000	049500000000	008000000000	000000000000	049500000000	
051590000000		050000000000	050000000000	049500000000	008000000000	000000000000	049500000000	
051600000000		050000000000	050000000000	049500000000	008000000000	000000000000	049500000000	
051610000000		050000000000	050000000000	049500000000	008000000000	000000000000	049500000000	
051620000000		050000000000	050000000000	049500000000	008000000000	000000000000	049500000000	
051630000000		050000000000	050000000000	049500000000	008000000000	000000000000	049500000000	
051640000000		050000000000	050000000000	049500000000	008000000000	000000000000	049500000000	
051650000000		050000000000	050000000000	049500000000	008000000000	000000000000	049500000000	
051660000000		050000000000	050000000000	049500000000	008000000000	000000000000	049500000000	
051670000000		050000000000	050000000000	049500000000	008000000000	000000000000	049500000000	
051680000000		050000000000	050000000000	049500000000	008000000000	000000000000	049500000000	
051690000000		050000000000	050000000000	049500000000	008000000000	000000000000	049500000000	
051700000000		050000000000	050000000000	049500000000	008000000000	000000000000	049500000000	
051710000000		050000000000	050000000000	049500000000	008000000000	000000000000	049500000000	
051720000000		050000000000	050000000000	049500000000	008000000000	000000000000	049500000000	
051730000000		050000000000	050000000000	049500000000	008000000000	000000000000	049500000000	
051740000000		050000000000	050000000000	049500000000	008000000000	000000000000	049500000000	
051750000000		050000000000	050000000000	049500000000	008000000000	000000000000	049500000000	
051760000000		050000000000	050000000000	049500000000	008000000000	000000000000	049500000000	
051770000000		050000000000	050000000000	049500000000	008000000000	000000000000	049500000000	
051780000000		050000000000	050000000000	049500000000	008000000000	000000000000	049500000000	
051790000000		050000000000	050000000000	049500000000	008000000000	000000000000	049500000000	
051800000000		050000000000	050000000000	049500000000	008000000000	000000000000	049500000000	
051810000000		050000000000	050000000000	049500000000	008000000000	000000000000	049500000000	
051820000000		050000000000	050000000000	049500000000	008000000000	000000000000	049500000000	
051830000000		050000000000	050000000000	049500000000	008000000000	000000000000	049500000000	
051840000000		050000000000	050000000000	049500000000	008000000000	000000000000	049500000000	
051850000000		050000000000	050000000000	049500000000	008000000000	000000000000	049500000000	
051860000000		050000000000	050000000000	049500000000	008000000000	000000000000	049500000000	
051870000000		050000000000	050000000000	049500000000	008000000000	000000000000	049500000000	
051880000000		050000000000	050000000000	049500000000	008000000000	000000000000	049500000000	
051890000000		050000000000	050000000000	049500000000	008000000000	000000000000	049500000000	
051900000000		050000000000	050000000000	049500000000	008000000000	000000000000	049500000000	
051910000000		050000000000	050000000000	049500000000	008000000000	000000000000	049500000000	
051920000000		050000000000	050000000000	049500000000	008000000000	000000000000	049500000000	
051930000000		050000000000	050000000000	049500000000	008000000000	000000000000	049500000000	
051940000000		050000000000	050000000000	049500000000	008000000000	000000000000	049500000000	
051950000000		050000000000	050000000000	049500000000	008000000000	000000000000	049500000000	
051960000000		050000000000	050000000000	049500000000	008000000000	000000000000	049500000000	
051970000000		050000000000	050000000000	049500000000	008000000000	000000000000	049500000000	
051980000000		050000000000	050000000000	049500000000	008000000000	000000000000	049500000000	
051990000000		050000000000	050000000000	049500000000	008000000000	000000000000	049500000000	
052000000000		050000000000	050000000000	049500000000	008000000000	000000000000	049500000000	

I-A2049-12

137

THE FRANKLIN INSTITUTE • Laboratories for Research and Development

I-A2049-12

α	Φ_{II}	Φ_{III}	Φ_{IV}	Ψ_I	Ψ_{II}	Ψ_{III}	Ψ_{IV}
051100000000	049930000000	050000000000	051100000000	000000000000	000000000000	000000000000	000000000000
051110000000	049940000000	050010000000	051110000000	000010000000	000010000000	000010000000	000010000000
051120000000	049950000000	050020000000	051120000000	000020000000	000020000000	000020000000	000020000000
051130000000	049960000000	050030000000	051130000000	000030000000	000030000000	000030000000	000030000000
051140000000	049970000000	050040000000	051140000000	000040000000	000040000000	000040000000	000040000000
051150000000	049980000000	050050000000	051150000000	000050000000	000050000000	000050000000	000050000000
051160000000	049990000000	050060000000	051160000000	000060000000	000060000000	000060000000	000060000000
051170000000	050000000000	050070000000	051170000000	000070000000	000070000000	000070000000	000070000000
051180000000	050010000000	050080000000	051180000000	000080000000	000080000000	000080000000	000080000000
051190000000	050020000000	050090000000	051190000000	000090000000	000090000000	000090000000	000090000000
051200000000	050030000000	050100000000	051200000000	000100000000	000100000000	000100000000	000100000000
051210000000	050040000000	050110000000	051210000000	000110000000	000110000000	000110000000	000110000000
051220000000	050050000000	050120000000	051220000000	000120000000	000120000000	000120000000	000120000000
051230000000	050060000000	050130000000	051230000000	000130000000	000130000000	000130000000	000130000000
051240000000	050070000000	050140000000	051240000000	000140000000	000140000000	000140000000	000140000000
051250000000	050080000000	050150000000	051250000000	000150000000	000150000000	000150000000	000150000000
051260000000	050090000000	050160000000	051260000000	000160000000	000160000000	000160000000	000160000000
051270000000	050100000000	050170000000	051270000000	000170000000	000170000000	000170000000	000170000000
051280000000	050110000000	050180000000	051280000000	000180000000	000180000000	000180000000	000180000000
051290000000	050120000000	050190000000	051290000000	000190000000	000190000000	000190000000	000190000000
051300000000	050130000000	050200000000	051300000000	000200000000	000200000000	000200000000	000200000000
051310000000	050140000000	050210000000	051310000000	000210000000	000210000000	000210000000	000210000000
051320000000	050150000000	050220000000	051320000000	000220000000	000220000000	000220000000	000220000000
051330000000	050160000000	050230000000	051330000000	000230000000	000230000000	000230000000	000230000000
051340000000	050170000000	050240000000	051340000000	000240000000	000240000000	000240000000	000240000000
051350000000	050180000000	050250000000	051350000000	000250000000	000250000000	000250000000	000250000000
051360000000	050190000000	050260000000	051360000000	000260000000	000260000000	000260000000	000260000000
051370000000	050200000000	050270000000	051370000000	000270000000	000270000000	000270000000	000270000000
051380000000	050210000000	050280000000	051380000000	000280000000	000280000000	000280000000	000280000000
051390000000	050220000000	050290000000	051390000000	000290000000	000290000000	000290000000	000290000000
051400000000	050230000000	050300000000	051400000000	000300000000	000300000000	000300000000	000300000000
051410000000	050240000000	050310000000	051410000000	000310000000	000310000000	000310000000	000310000000
051420000000	050250000000	050320000000	051420000000	000320000000	000320000000	000320000000	000320000000
051430000000	050260000000	050330000000	051430000000	000330000000	000330000000	000330000000	000330000000
051440000000	050270000000	050340000000	051440000000	000340000000	000340000000	000340000000	000340000000
051450000000	050280000000	050350000000	051450000000	000350000000	000350000000	000350000000	000350000000
051460000000	050290000000	050360000000	051460000000	000360000000	000360000000	000360000000	000360000000
051470000000	050300000000	050370000000	051470000000	000370000000	000370000000	000370000000	000370000000
051480000000	050310000000	050380000000	051480000000	000380000000	000380000000	000380000000	000380000000
051490000000	050320000000	050390000000	051490000000	000390000000	000390000000	000390000000	000390000000
051500000000	050330000000	050400000000	051500000000	000400000000	000400000000	000400000000	000400000000
051510000000	050340000000	050410000000	051510000000	000410000000	000410000000	000410000000	000410000000
051520000000	050350000000	050420000000	051520000000	000420000000	000420000000	000420000000	000420000000
051530000000	050360000000	050430000000	051530000000	000430000000	000430000000	000430000000	000430000000
051540000000	050370000000	050440000000	051540000000	000440000000	000440000000	000440000000	000440000000
051550000000	050380000000	050450000000	051550000000	000450000000	000450000000	000450000000	000450000000
051560000000	050390000000	050460000000	051560000000	000460000000	000460000000	000460000000	000460000000
051570000000	050400000000	050470000000	051570000000	000470000000	000470000000	000470000000	000470000000
051580000000	050410000000	050480000000	051580000000	000480000000	000480000000	000480000000	000480000000
051590000000	050420000000	050490000000	051590000000	000490000000	000490000000	000490000000	000490000000
051600000000	050430000000	050500000000	051600000000	000500000000	000500000000	000500000000	000500000000

7

1-52549-10

[illegible]

THE FRANKLIN INSTITUTE • Laboratories for Research and Development

I-A2049-12

[illegible]

- *Laboratories for Research and Development*

I-A2049-12

[illegible]

I-A2049-12

143

THE FRANKLIN INSTITUTE • Laboratories for Research and Development

T-A2049-12

[illegible]

I-A2049-12

145

THE FRANKLIN INSTITUTE • *Laboratories for Research and Development*

1-A2049-12

[illegible]

I-A2049-12

147

THE FRANKLIN INSTITUTE • *Laboratories for Research and Development*

I-A2049-12

[illegible]

I-A2049-12

[illegible]

I-A2049-12

[illegible]

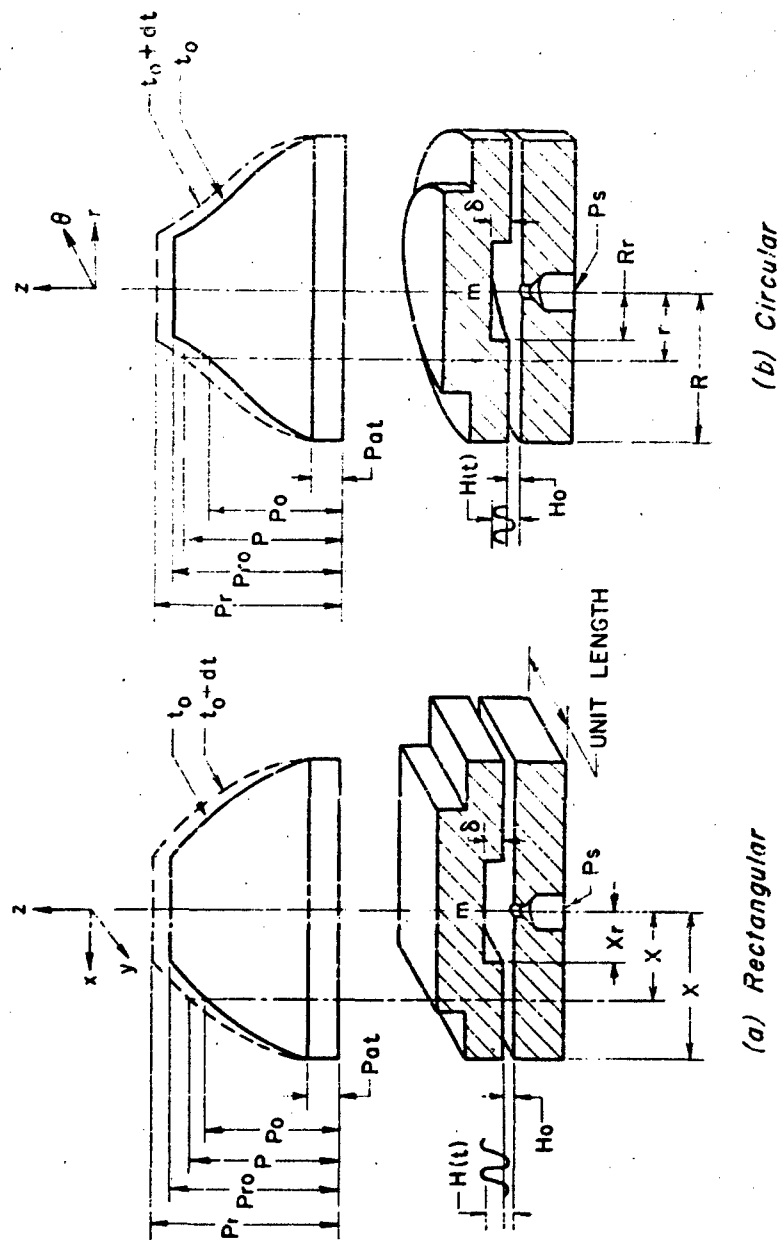


FIG. 1. SCHEMATIC DIAGRAM OF BEARING GEOMETRIES

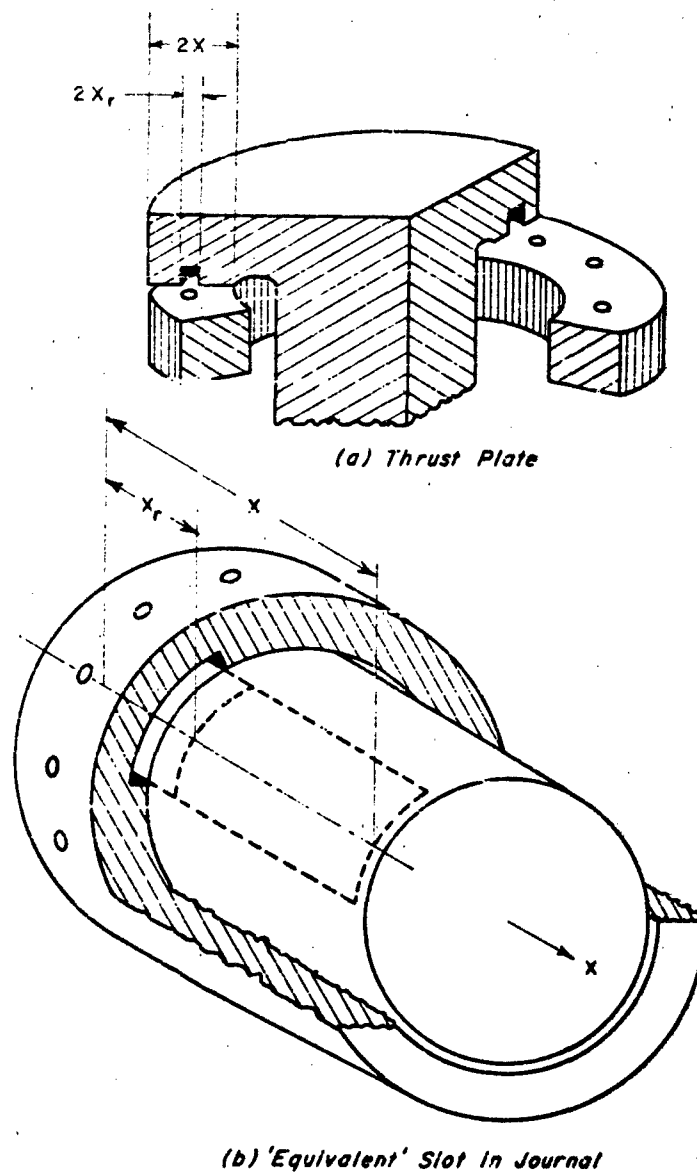


FIG. 2 APPROXIMATIONS TO RECTANGULAR GEOMETRY

BEARING WIDTH $2Y = 1$ IN.
 CONSTANT SUPPLY PRESSURE $P_s = 88.2$ PSIA
 CONSTANT AMBIENT PRESSURE $P_a = 14.7$ PSIA
 MASS PER UNIT LENGTH OF BEARING $m = 1.65 \times 10^{-3} \frac{\text{LB-SEC}^2}{\text{IN.}}$

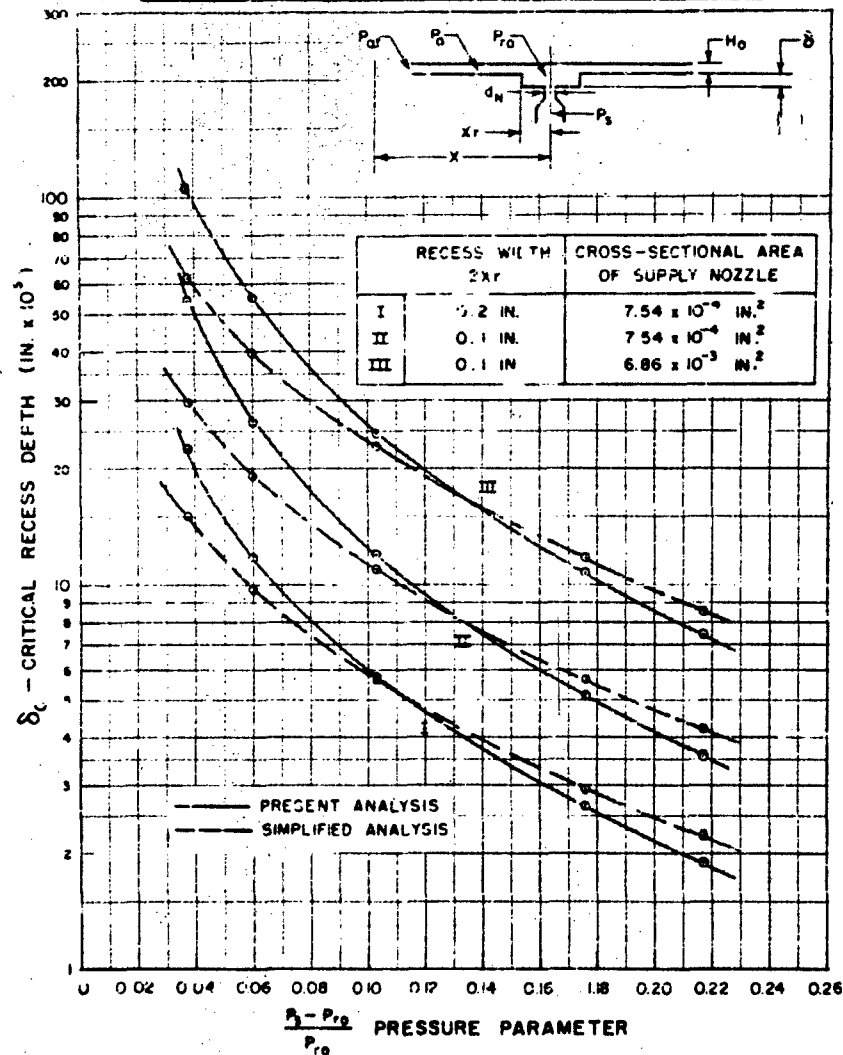


FIG. 3 CRITICAL RECESS DEPTH vs. PRESSURE PARAMETER (CALCULATED)
 (Rectangular Geometry)

RECESS DIAMETER $2R_r = 1$ IN
 BEARING DIAMETER $2R = 5$ IN
 CONSTANT RECESS PRESSURE $P_{r0} = 73.5$ PSIA
 CONSTANT AMBIENT PRESSURE $P_{a1} = 14.7$ PSIA
 SUPPLY NOZZLE CROSS-SECTIONAL AREA $= 0.237 \times 10^{-2}$ IN²
 BEARING MASS $m = 6.477 \times 10^{-2}$ LB-SEC²/IN

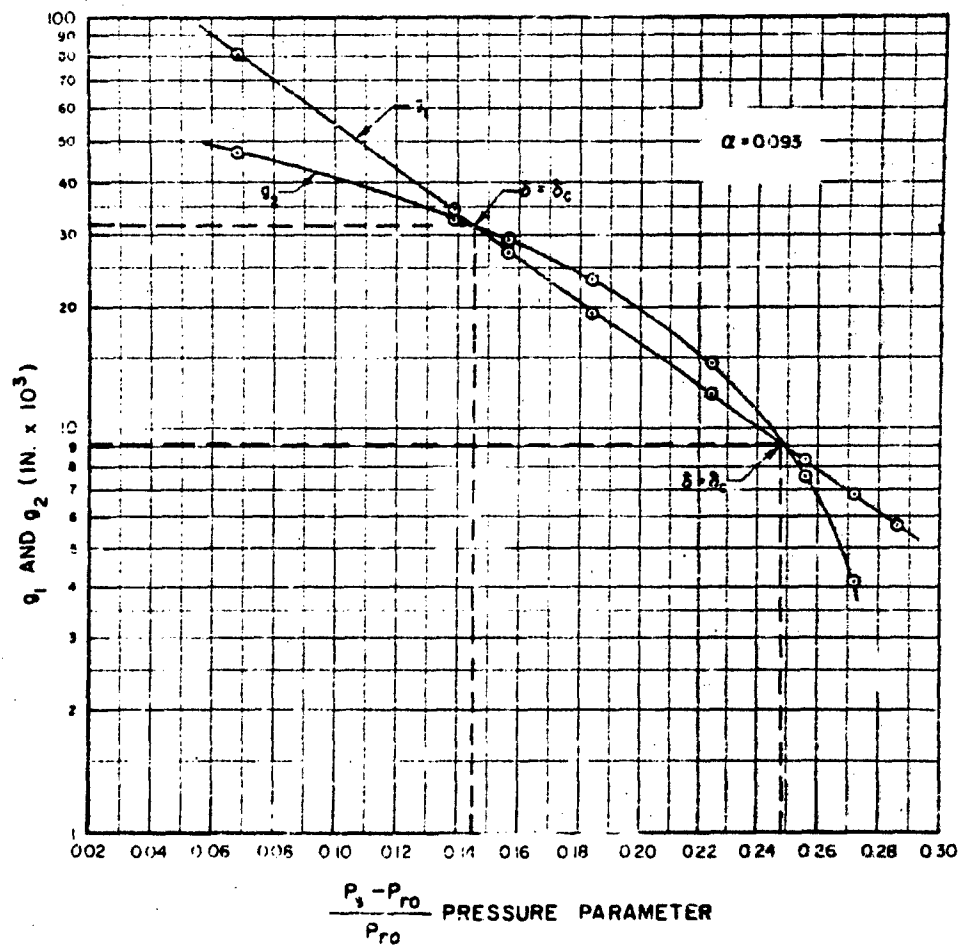


FIG 4 DETERMINATION OF CRITICAL RECESS DEPTH (EQUATION 43b)
 (Circular Geometry)

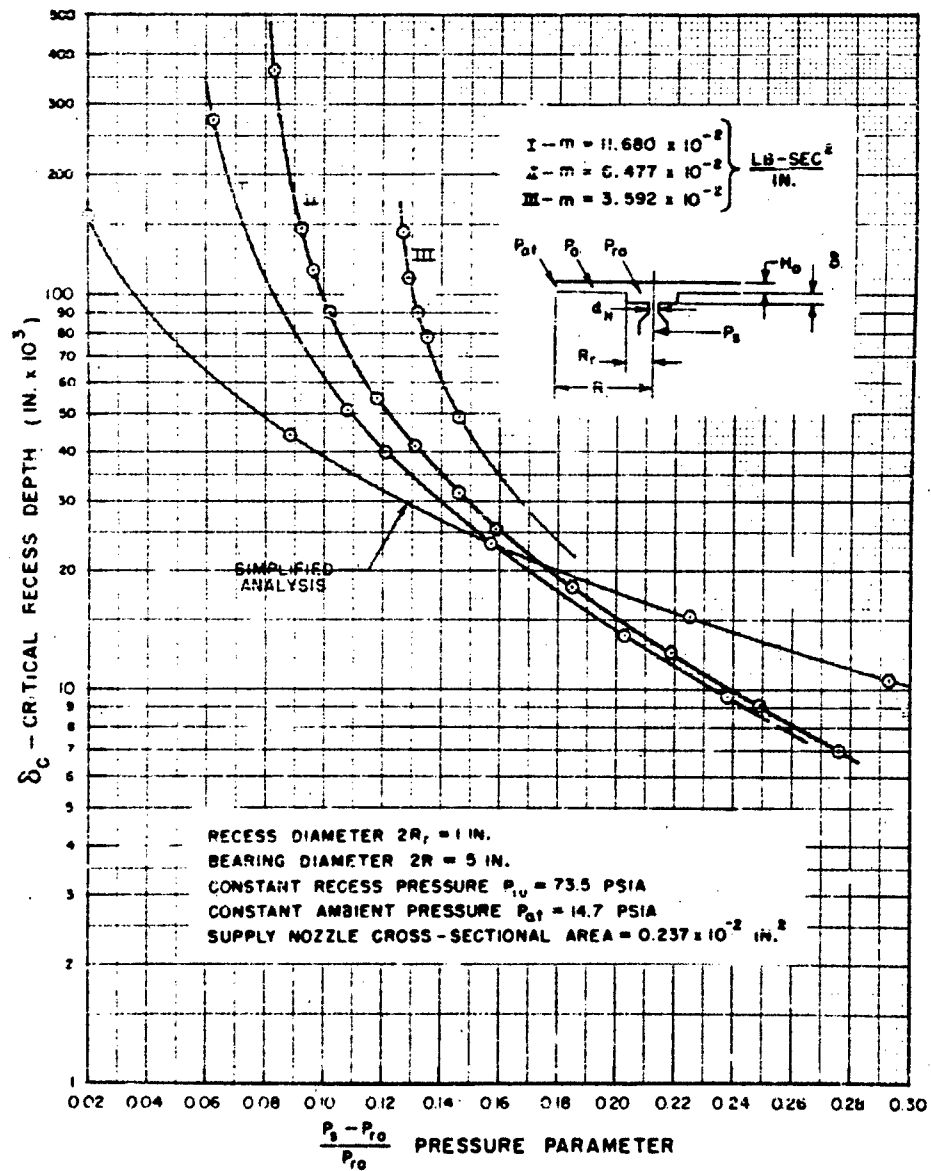
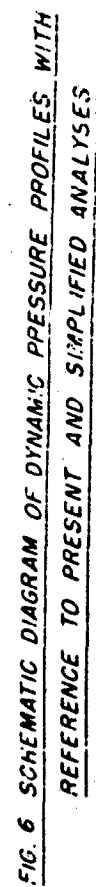
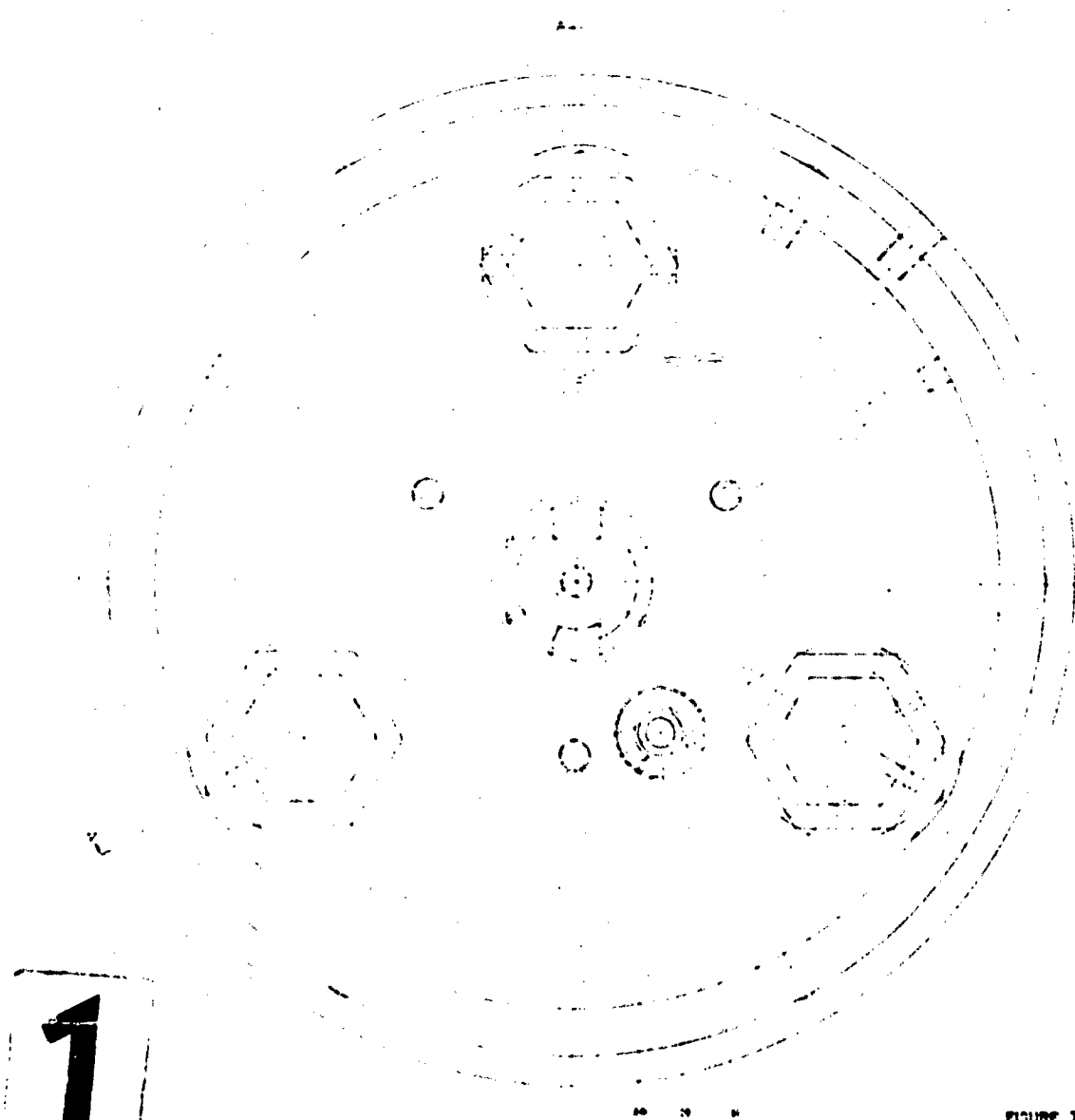


FIG 5 CRITICAL RECESS DEPTH VS. PRESSURE PARAMETER (CALCULATED)
(Circular Geometry)



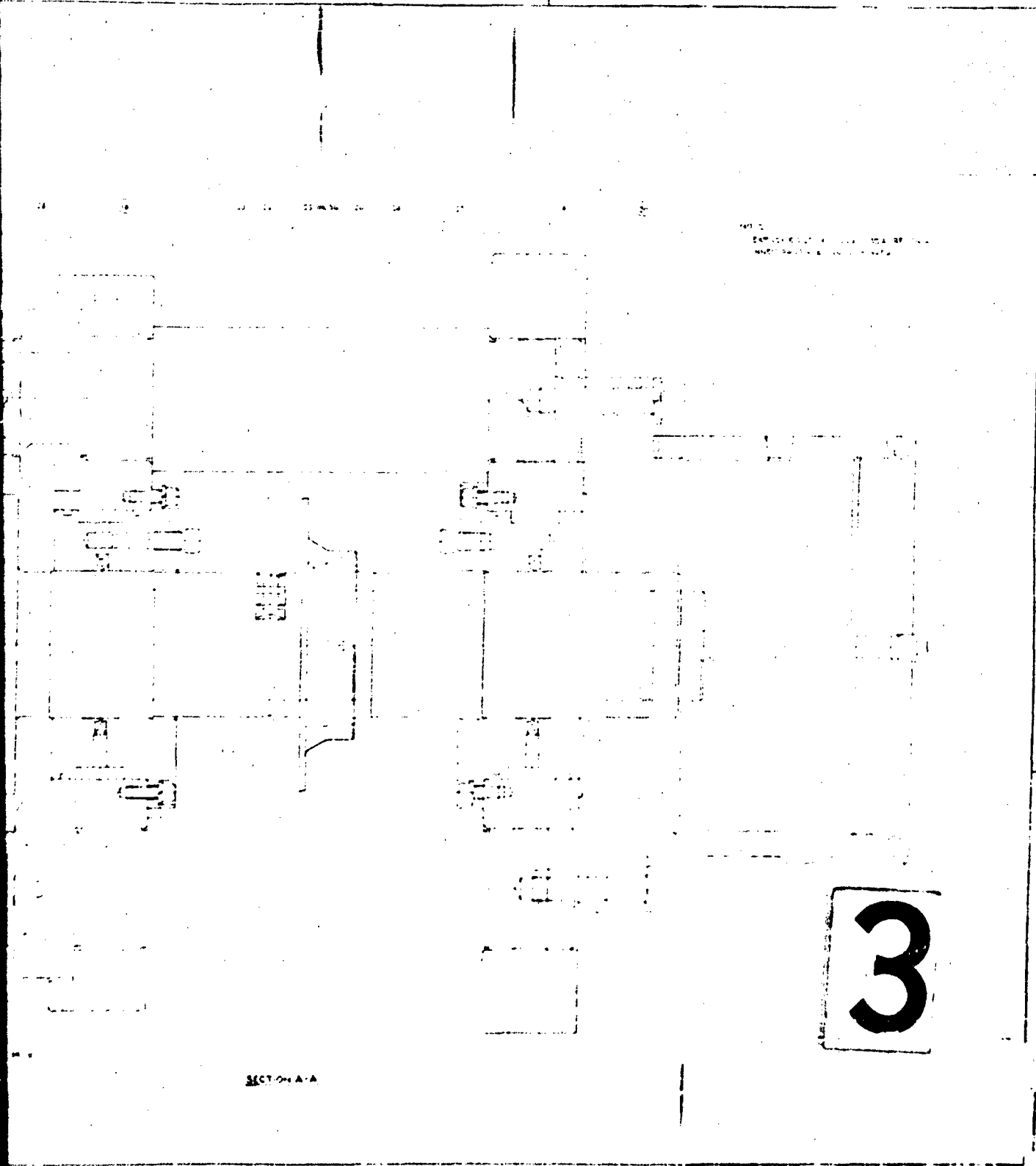
NO.	DESCRIPTION	DWG. NO.
1	UPPER THRUST PLATE	22040-B-01
2	UPPER TO LOW SCREW	22040-B-02
3	UPPER TO LOW NUT	22040-B-03
4	LOW SCREW	22040-B-04
5	LOW SCREW NUT	22040-B-05
6	LOW SCREW NUT	22040-B-06
7	LOW SCREW NUT	22040-B-07
8	LOW SCREW NUT	22040-B-08
9	LOW SCREW NUT	22040-B-09
10	LOW SCREW NUT	22040-B-10
11	LOW SCREW NUT	22040-B-11
12	LOW SCREW NUT	22040-B-12
13	LOW SCREW NUT	22040-B-13
14	LOW SCREW NUT	22040-B-14
15	LOW SCREW NUT	22040-B-15
16	LOW SCREW NUT	22040-B-16
17	LOW SCREW NUT	22040-B-17
18	LOW SCREW NUT	22040-B-18
19	LOW SCREW NUT	22040-B-19
20	LOW SCREW NUT	22040-B-20



1

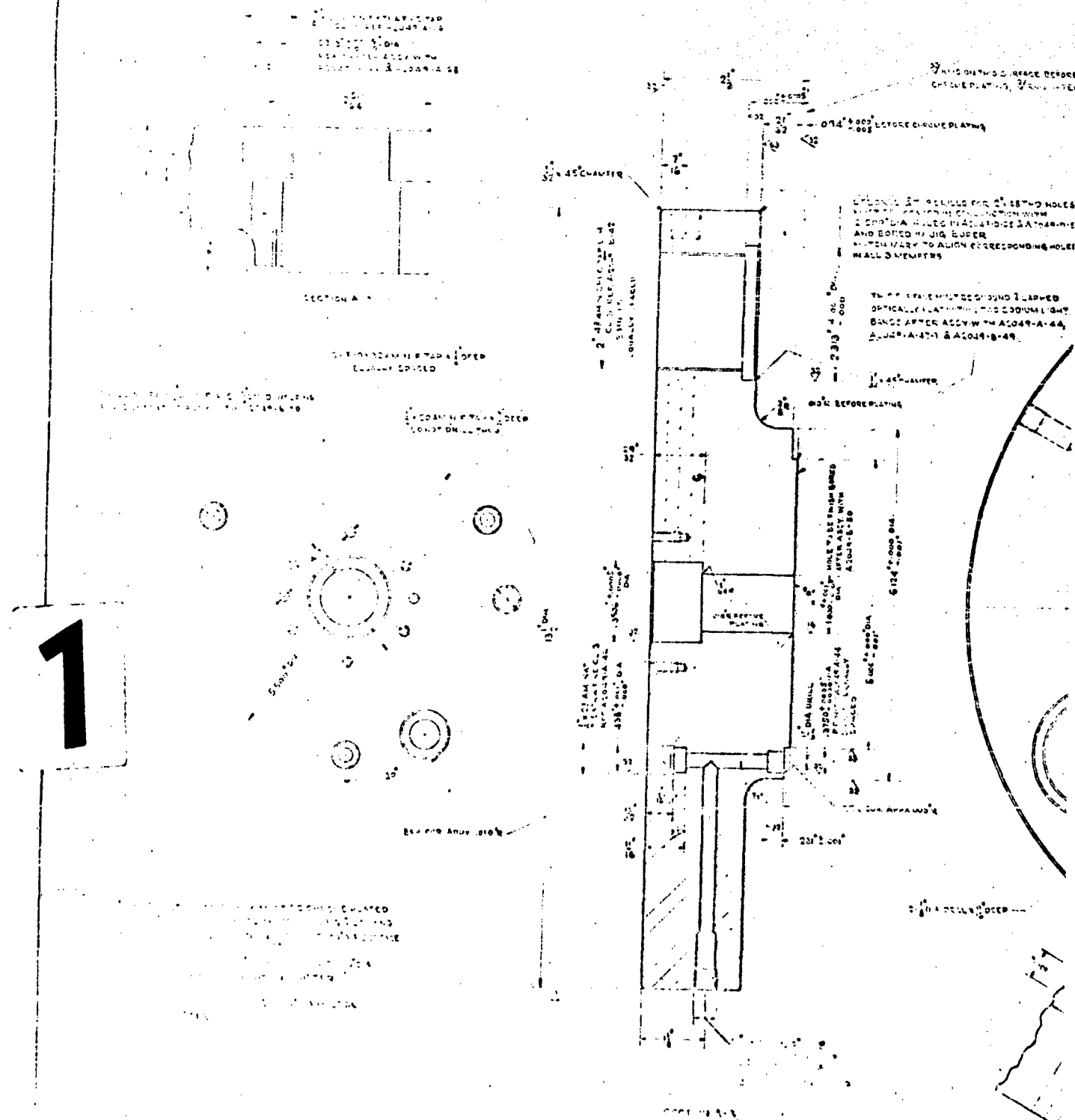
FIGURE 7

NO.	DESCRIPTION	DWG. NO.
1	UPPER THRUST PLATE	22040-B-01
2	UPPER TO LOW SCREW	22040-B-02
3	UPPER TO LOW NUT	22040-B-03
4	LOW SCREW	22040-B-04
5	LOW SCREW NUT	22040-B-05
6	LOW SCREW NUT	22040-B-06
7	LOW SCREW NUT	22040-B-07
8	LOW SCREW NUT	22040-B-08
9	LOW SCREW NUT	22040-B-09
10	LOW SCREW NUT	22040-B-10
11	LOW SCREW NUT	22040-B-11
12	LOW SCREW NUT	22040-B-12
13	LOW SCREW NUT	22040-B-13
14	LOW SCREW NUT	22040-B-14
15	LOW SCREW NUT	22040-B-15
16	LOW SCREW NUT	22040-B-16
17	LOW SCREW NUT	22040-B-17
18	LOW SCREW NUT	22040-B-18
19	LOW SCREW NUT	22040-B-19
20	LOW SCREW NUT	22040-B-20



3

SECTION A-A



2

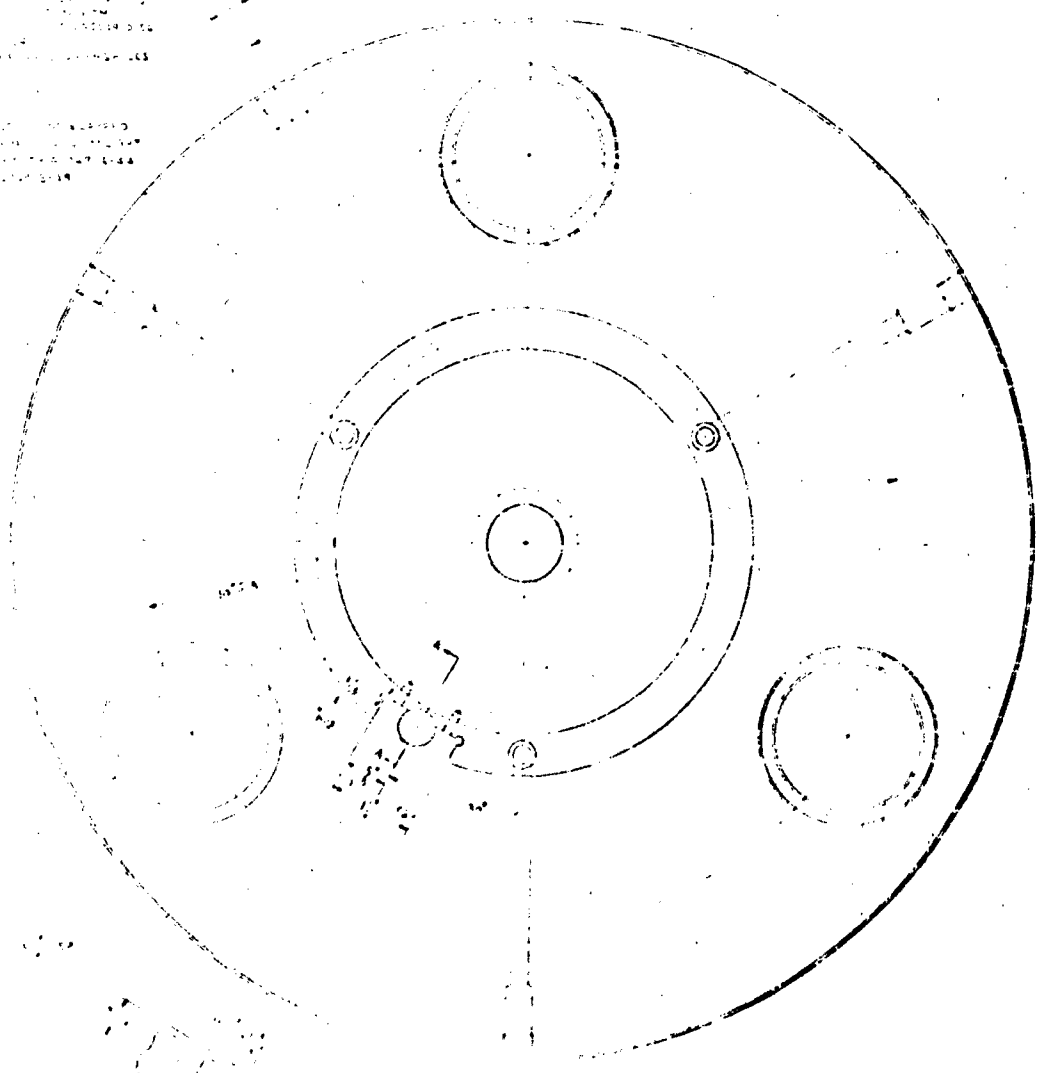
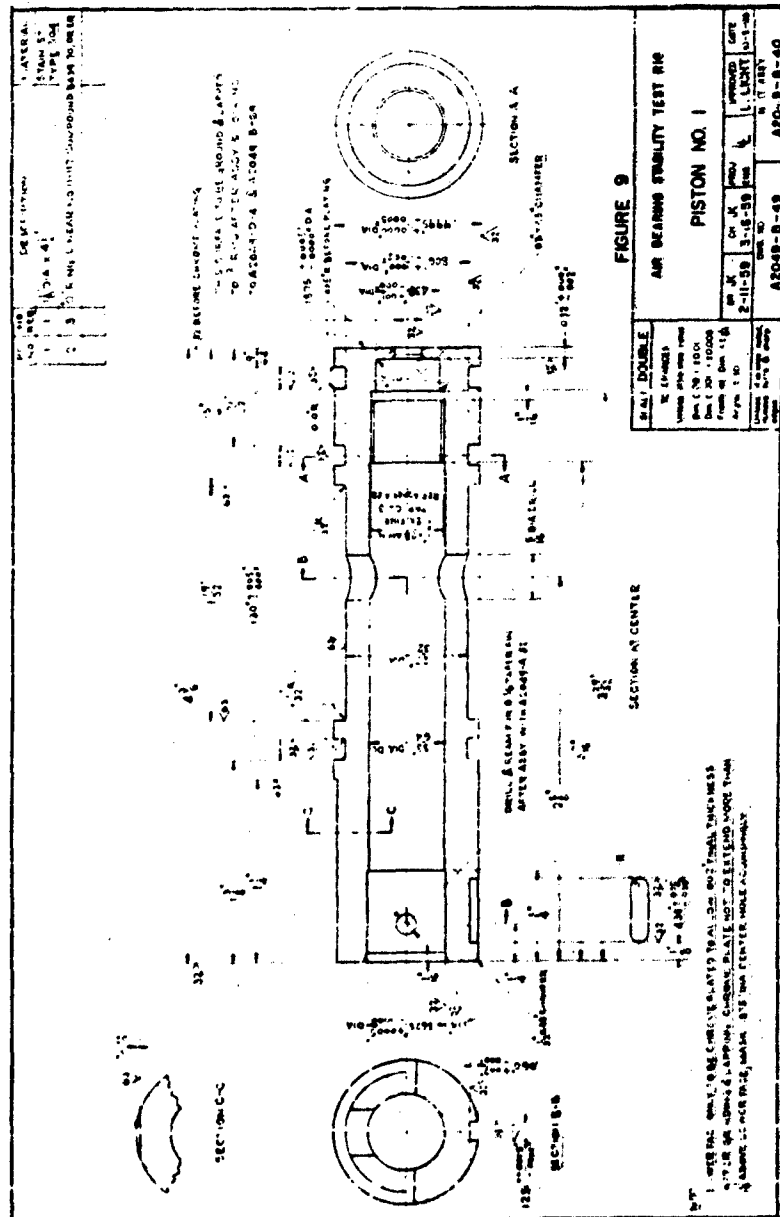
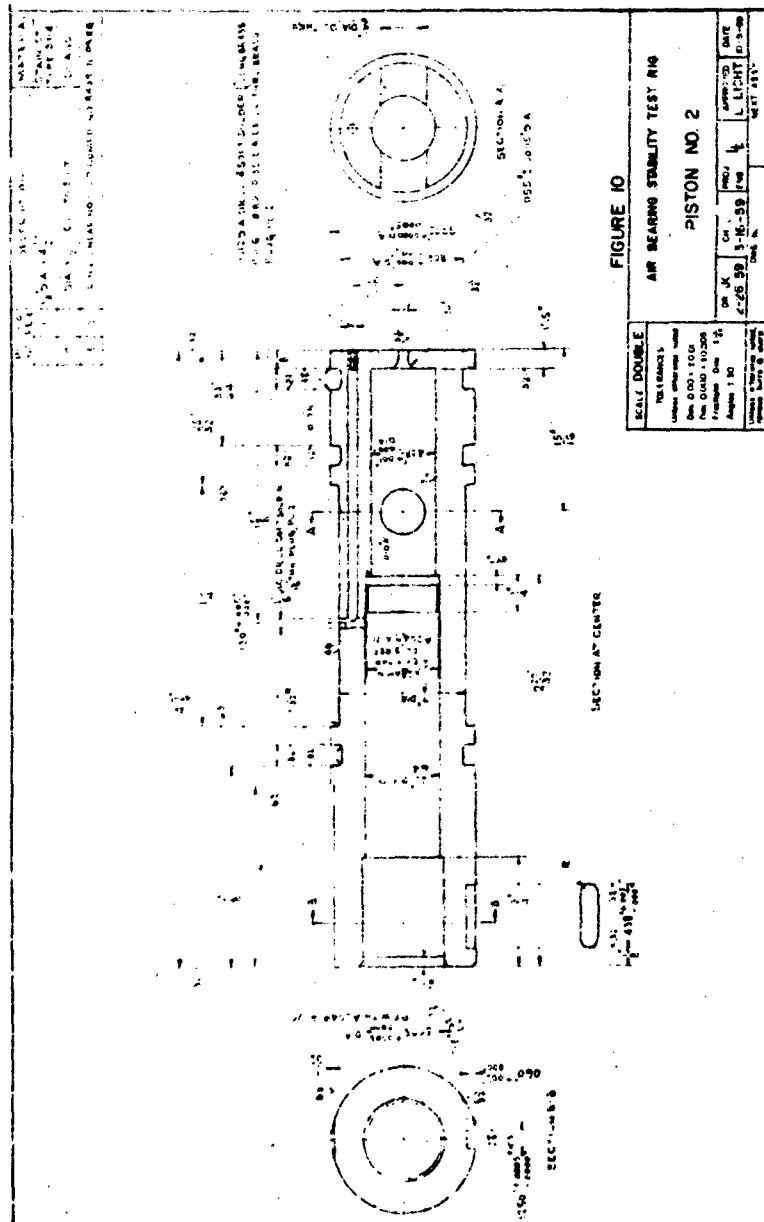
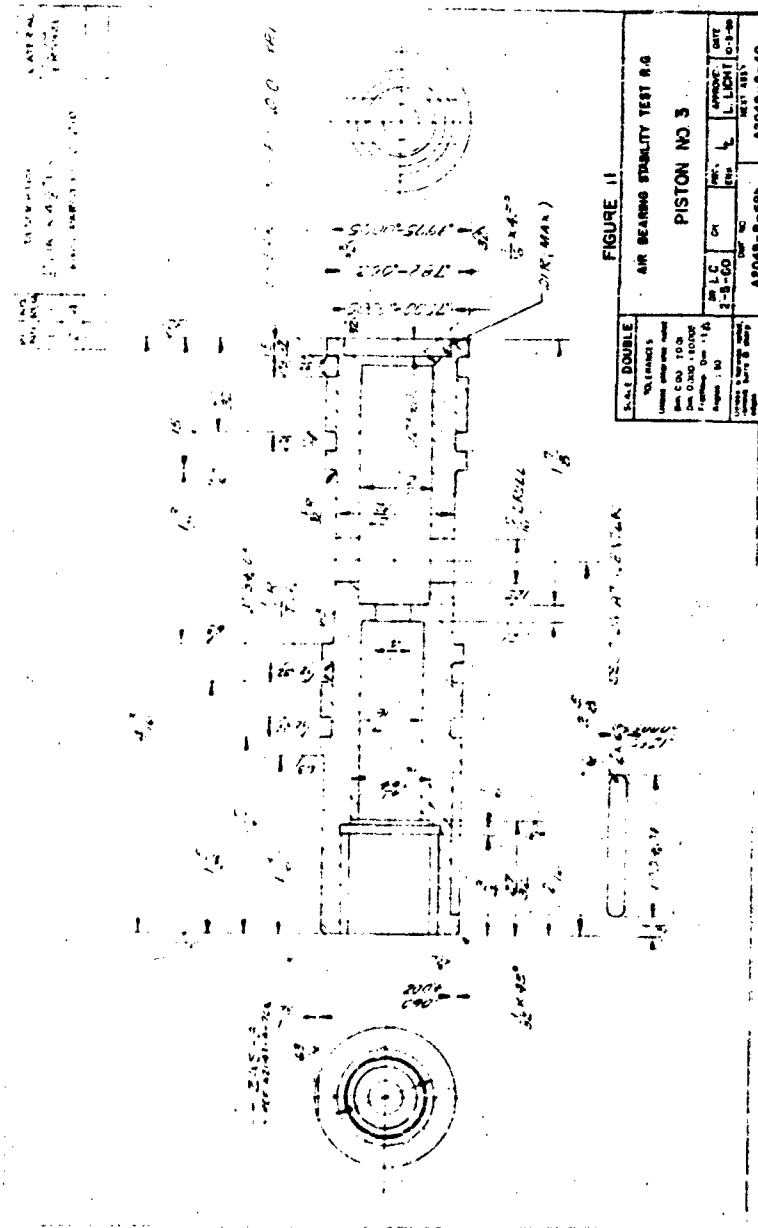


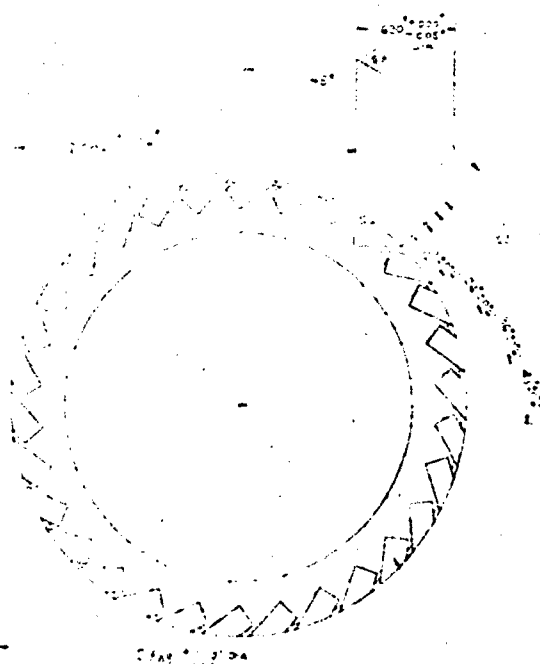
FIGURE 2	
VIEW	SECTION
FRONT	SECTION
TOP	SECTION
LEFT SIDE	SECTION
RIGHT SIDE	SECTION



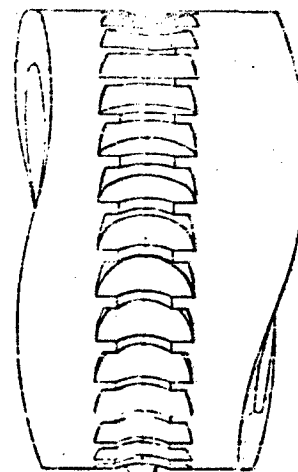








SECTION A-A
THIS SIDE



THESE EIGHTS EQUALLY
SPACED SHOWN AS TOLERANCE
APPLYING TO THE PATTERN
INDICATED.

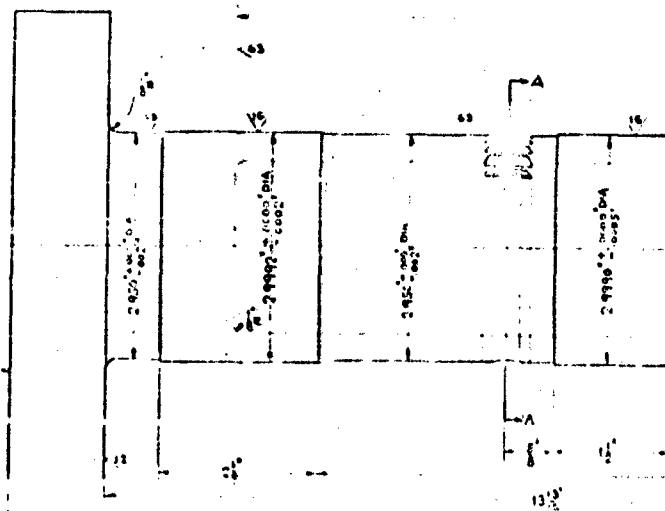


1

SECTION A-A
THIS SIDE

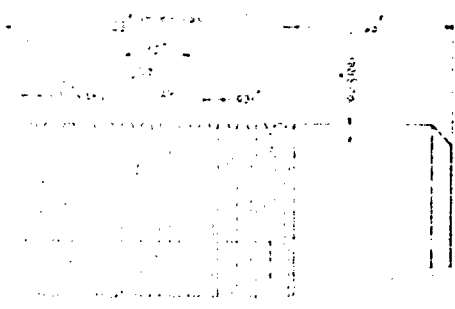
THESE EIGHTS EQUALLY
SPACED SHOWN AS TOLERANCE
APPLYING TO THE PATTERN
INDICATED.

THESE EIGHTS EQUALLY
SPACED SHOWN AS TOLERANCE
APPLYING TO THE PATTERN
INDICATED.



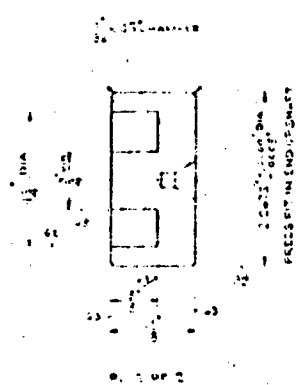
OFFICE OF THE
 SECRETARY OF THE ARMY
 WASHINGTON, D. C.

MAPS
 100-100000
 100-100000

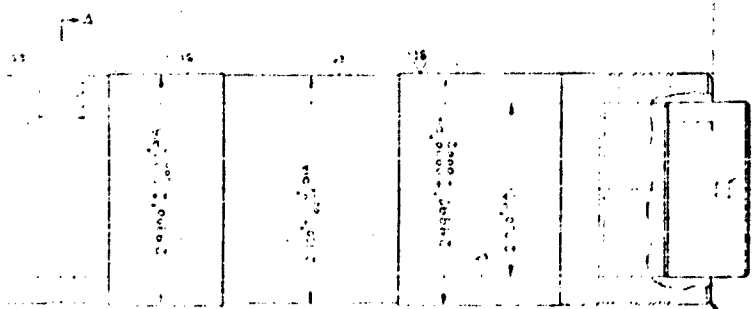


OFFICE OF THE SECRETARY OF THE ARMY
 WASHINGTON, D. C.

100-100000
 100-100000



2

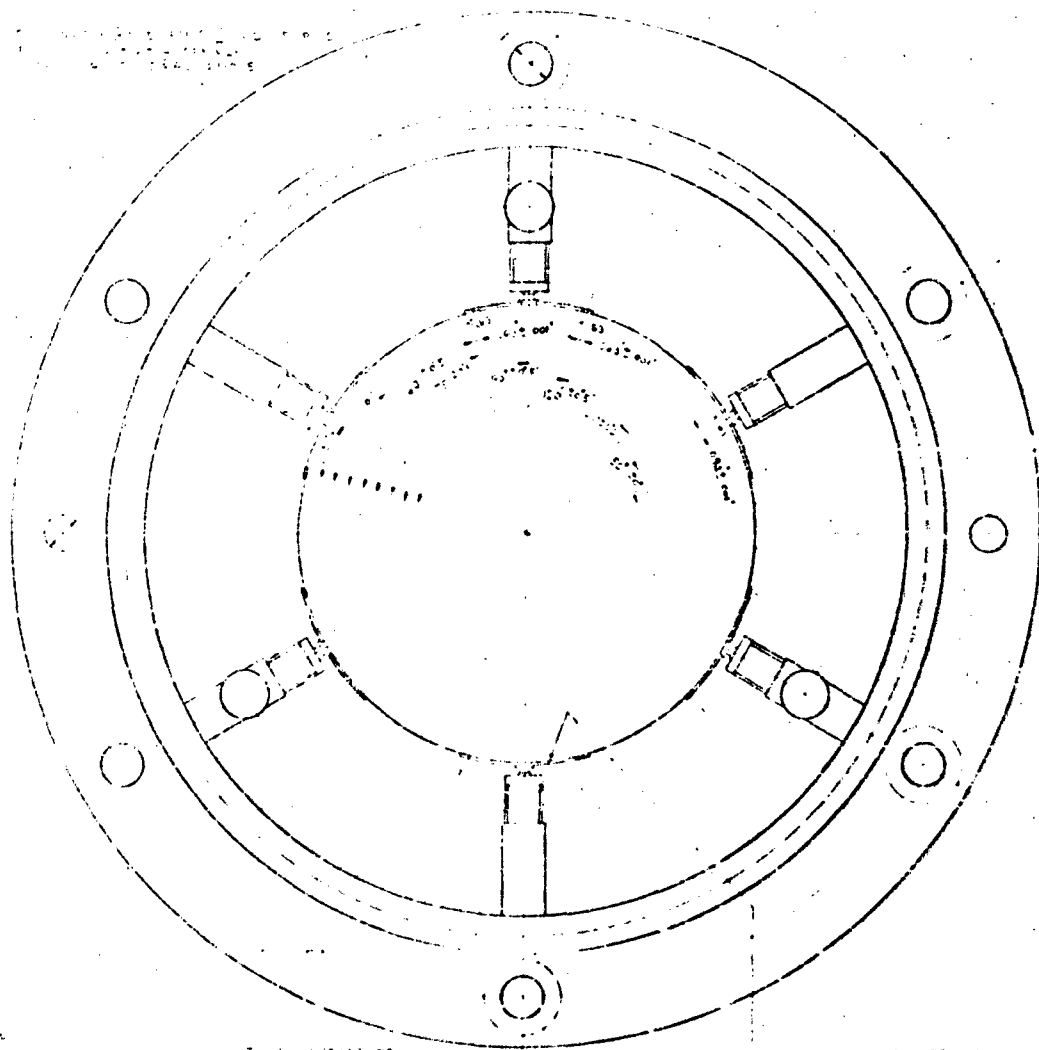


100-100000
 100-100000

OFFICE OF THE SECRETARY OF THE ARMY
 WASHINGTON, D. C.

1

5/16" CELLS THUS EQUALLY SPACED
5/16" CELLS EQUALLY SPACED



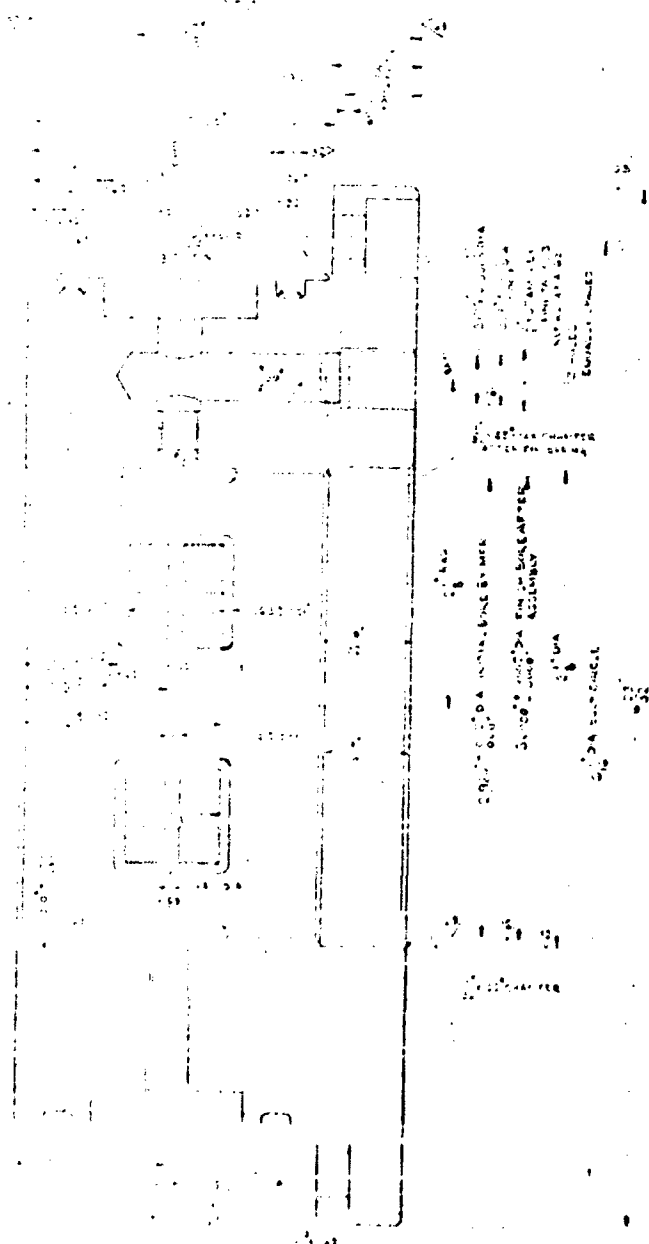
5.5000 inches
5.234 inches
5.014 inches

100
93.9
83.8
73.7
63.6
53.5
43.4
33.3
23.2
13.1

5/16" CELLS THUS EQUALLY SPACED
5/16" CELLS THUS EQUALLY SPACED

5/16" CELLS THUS EQUALLY SPACED
5/16" CELLS THUS EQUALLY SPACED

NO.		DESCRIPTION	UNIT
1	1	POSSIBLE NEW YORK AREA	STAN ST
2	2	CONSTRUCTION MATERIALS	STAN ST
3	3	LOCK WHEEL	STAN ST
4	4	LOCK WHEEL	STAN ST
5	5	LOCK WHEEL	STAN ST



NO.		DESCRIPTION	UNIT
1	1	POSSIBLE NEW YORK AREA	STAN ST
2	2	CONSTRUCTION MATERIALS	STAN ST
3	3	LOCK WHEEL	STAN ST
4	4	LOCK WHEEL	STAN ST
5	5	LOCK WHEEL	STAN ST

NOMINAL BEARING DIMENSIONS
 BEARING DIAM = 3 IN
 BEARING LENGTH = 2 IN
 DIAM CLEARANCE = 0.0014 IN
 SIX, EQUALLY SPACED
 PRESSURE PADS AND
 0.016 IN DIAMETER SUPPLY
 ORIFICE RESTRICTORS

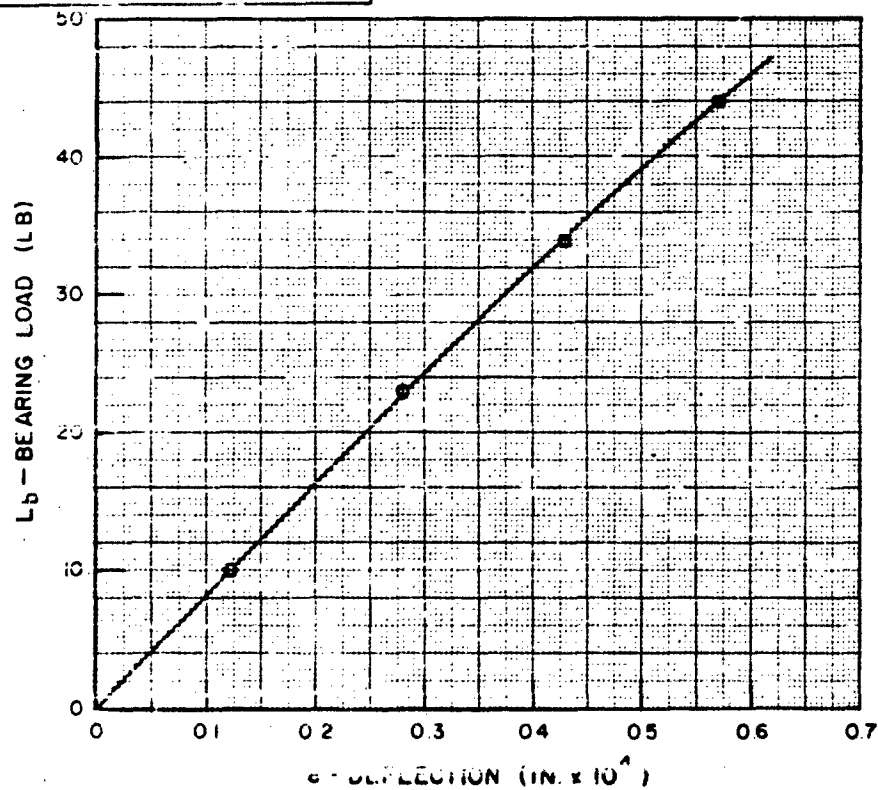
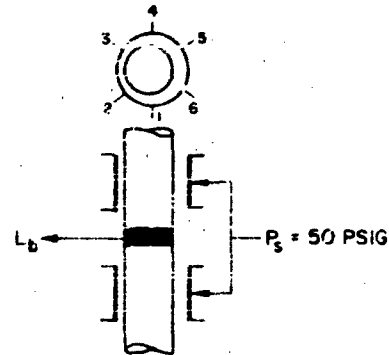


FIG 16 LOAD-DEFLECTION CHARACTERISTIC OF GUIDE BEARINGS

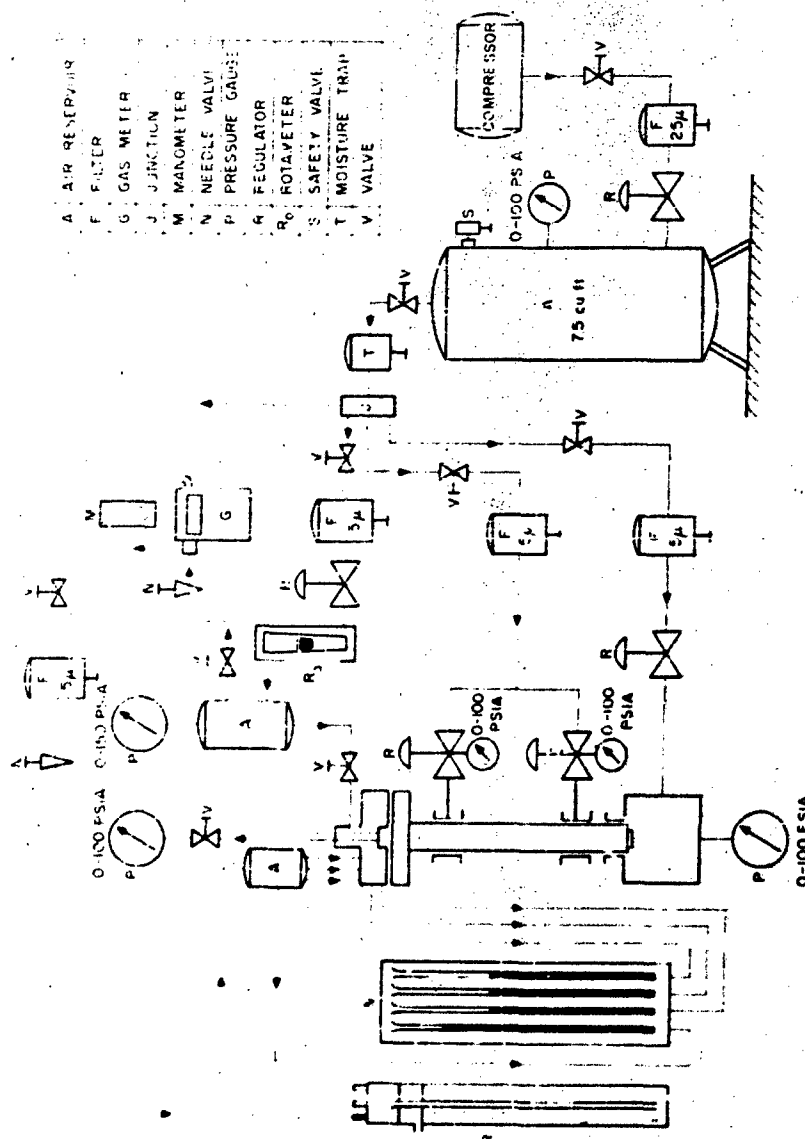


FIG. 17. SCHEMATIC DIAGRAM OF AIR SUPPLY SYSTEM.

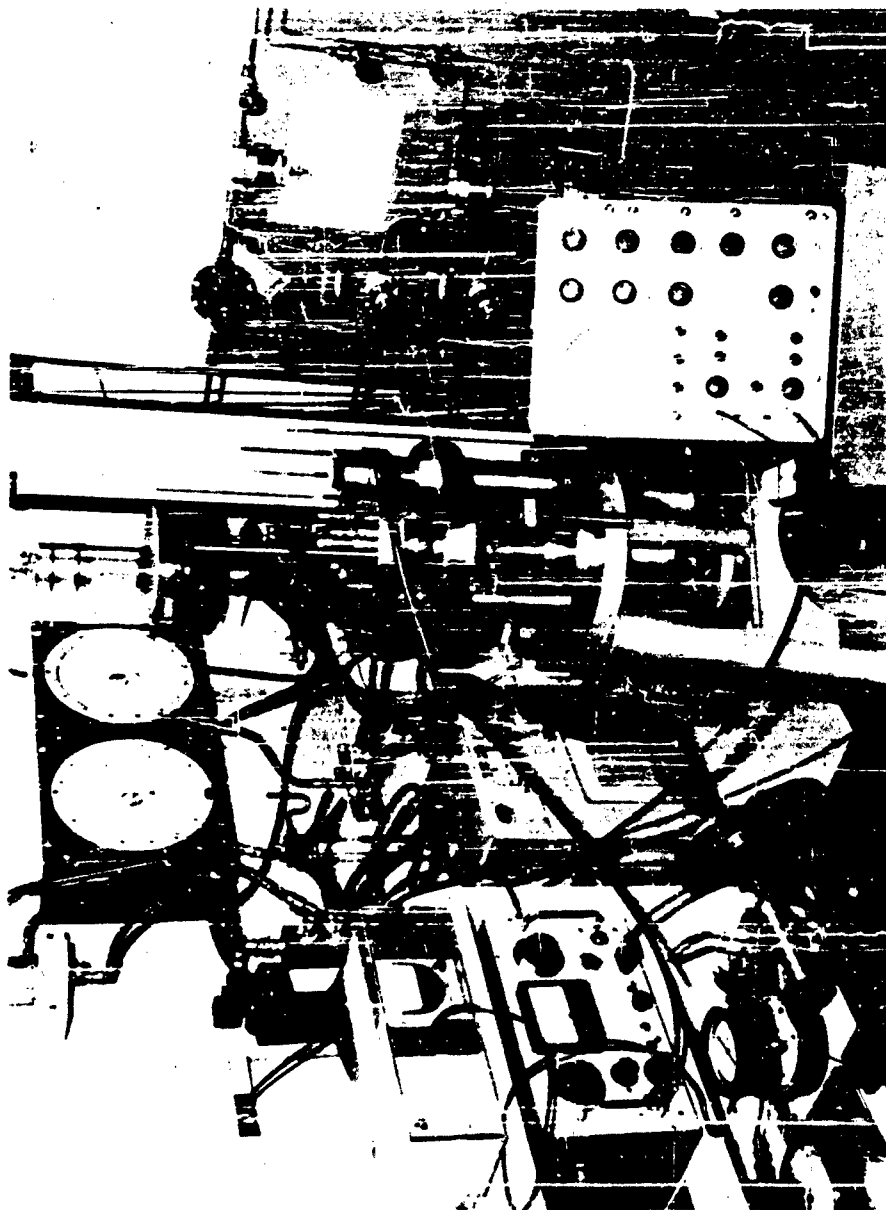


FIG. 18. VIEW OF TEST APPARATUS, INSTRUMENTS AND AIR SUPPLY SYSTEM

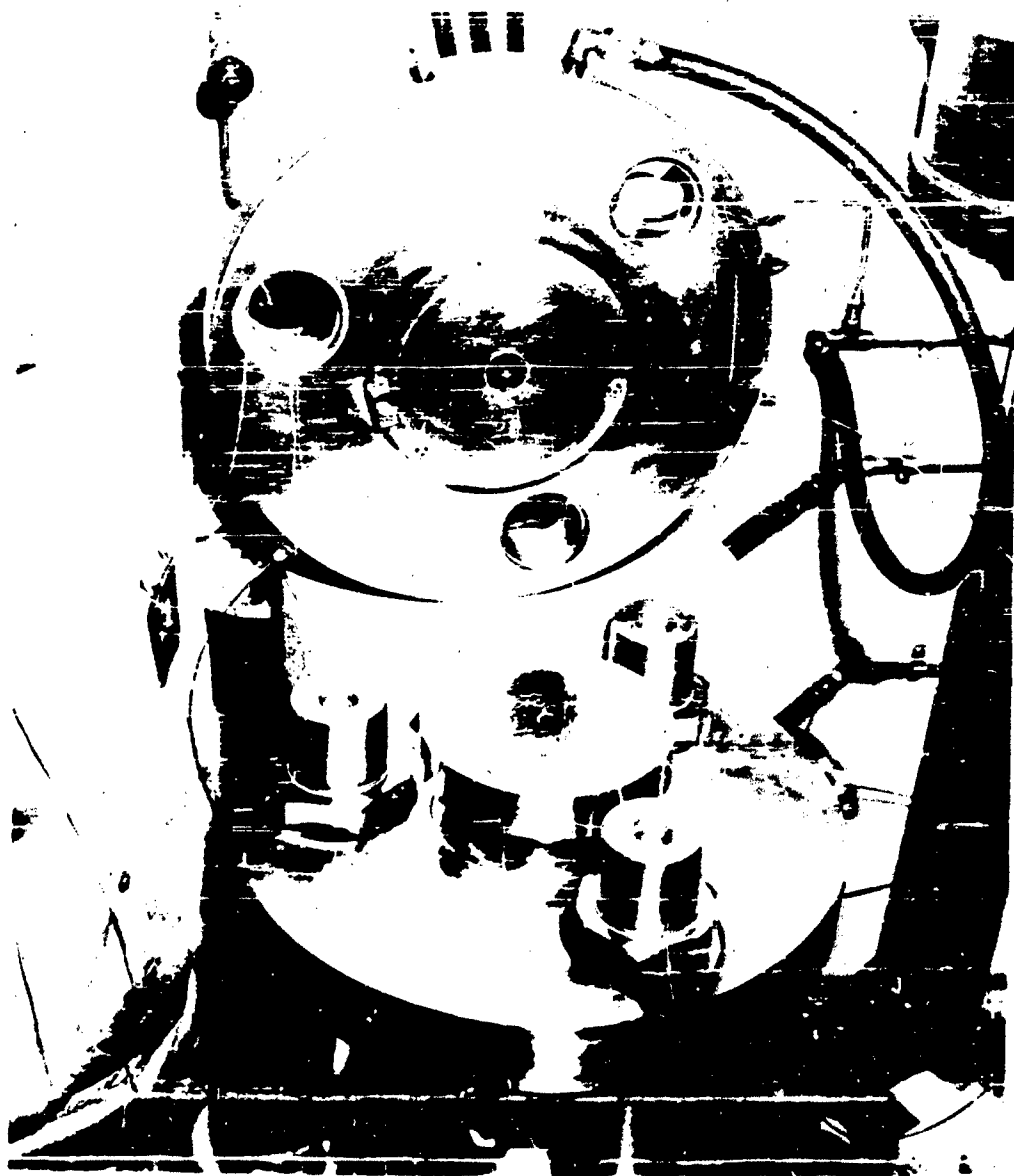


FIG 19. VIEW OF BEARING THRUST PLATES (1)

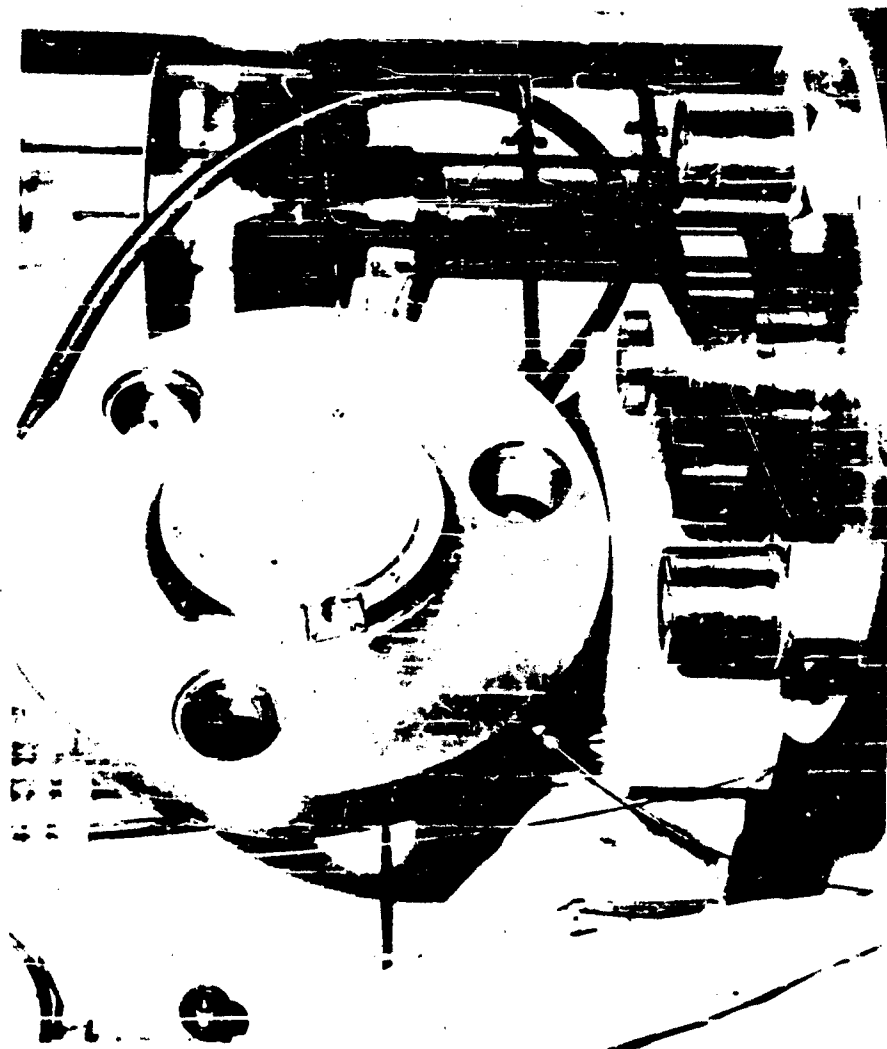


FIG. 20. VIEW OF BEARING THRUST PLATES (2)

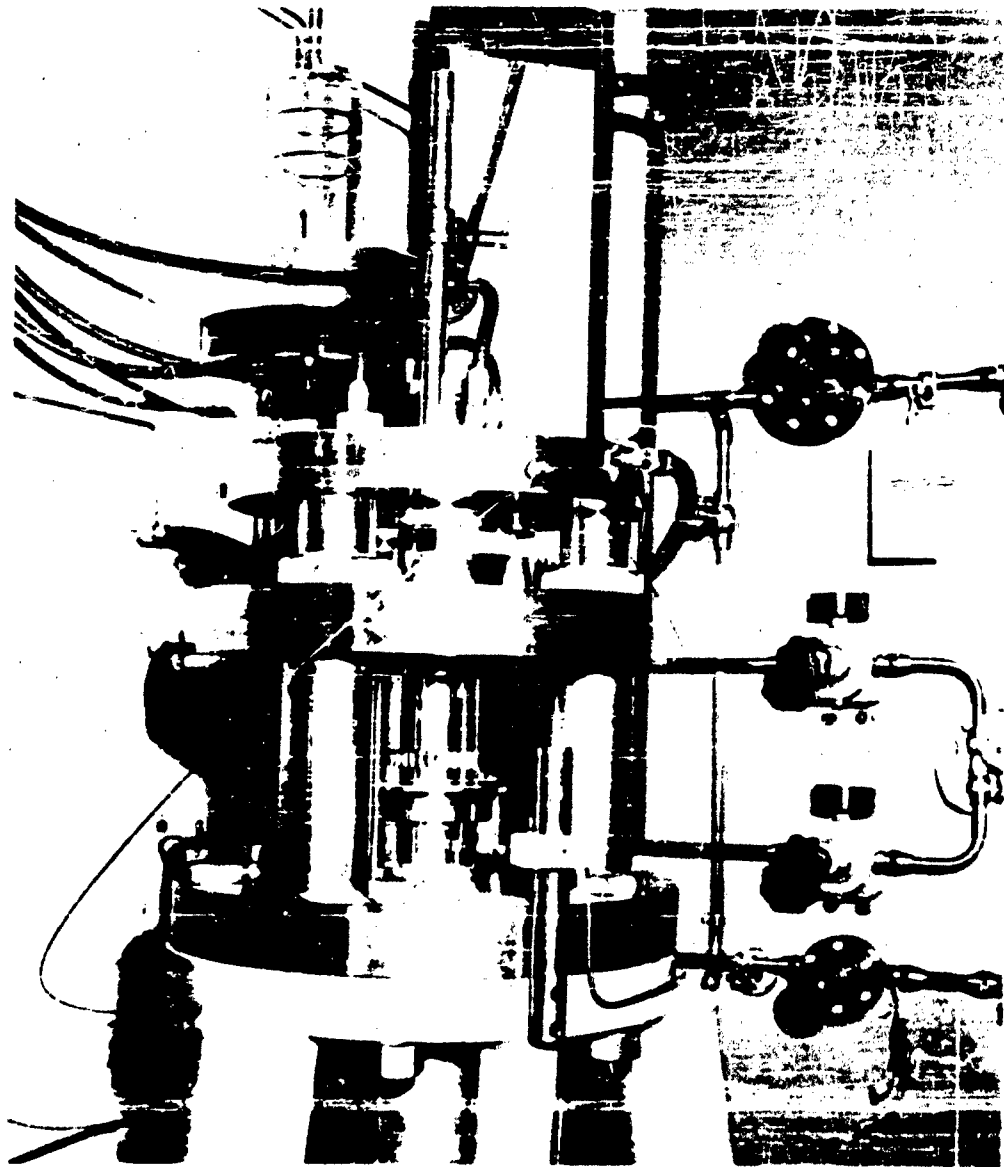


FIG 21. CLOSE VIEW OF TEST BEARING ASSEMBLY

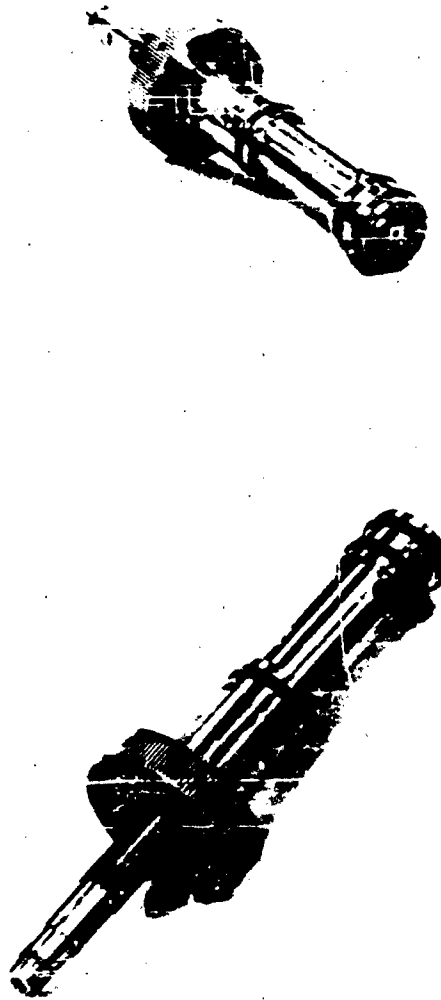


FIG. 22. MODIFIED PISTON NO. 2 - SECONDARY RECESS

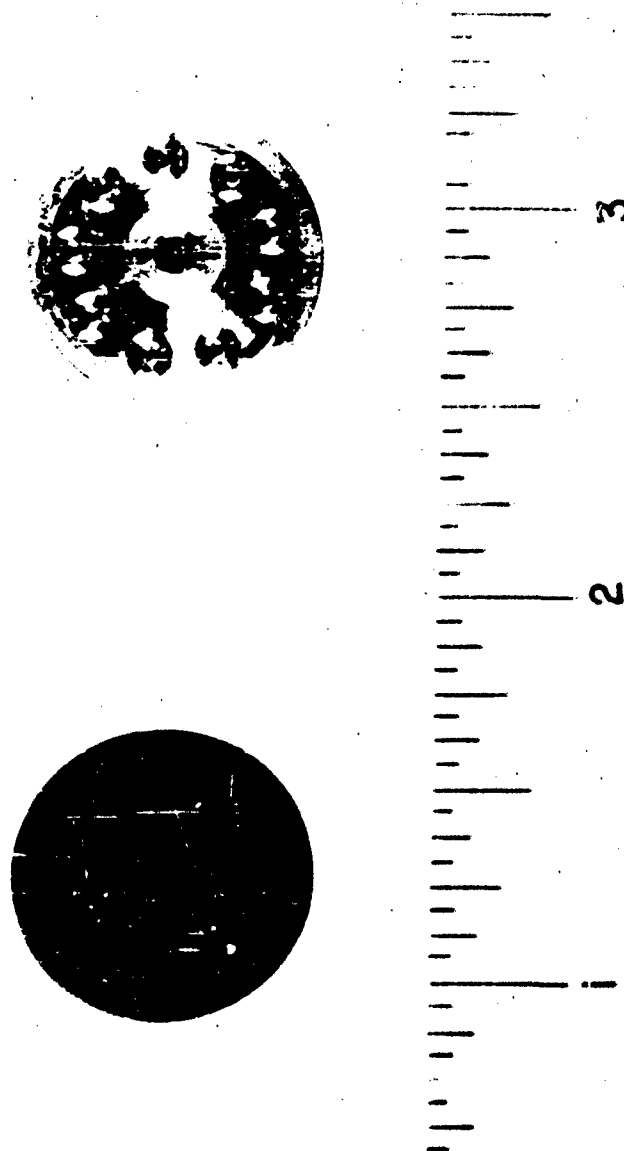


FIG. 23. NOZZLE PLATES FOR PISTON NO. 3

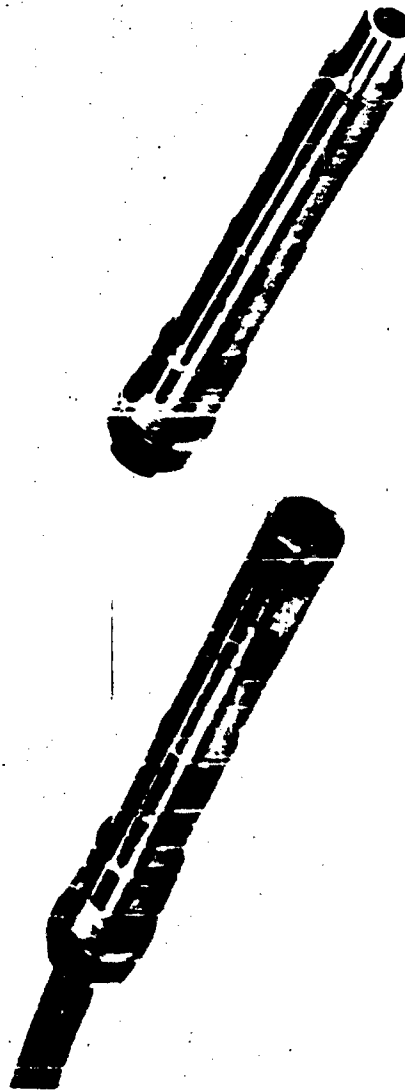


FIG. 24. PRIMARY CAPACITANCE PROBES AND PROBE HOLDERS

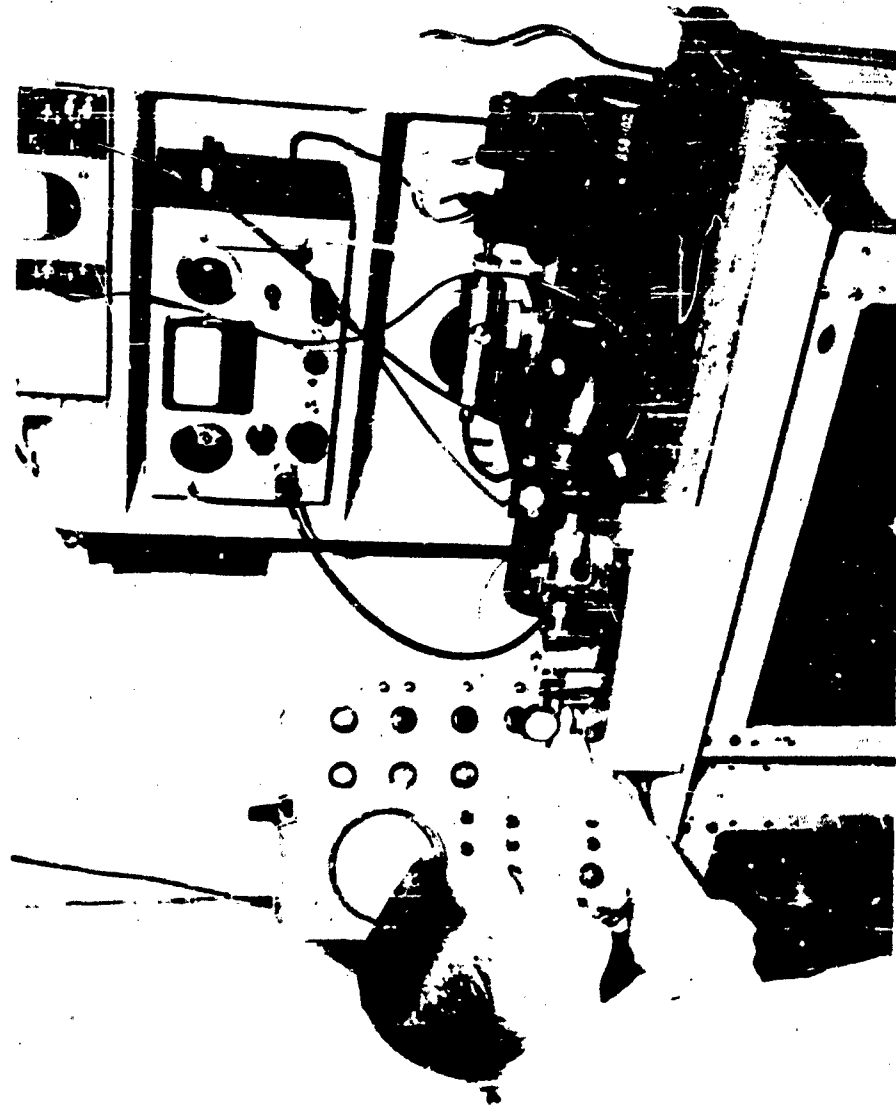


FIG. 25. CALIBRATION FIXTURES AND AUXILIARY PROBE

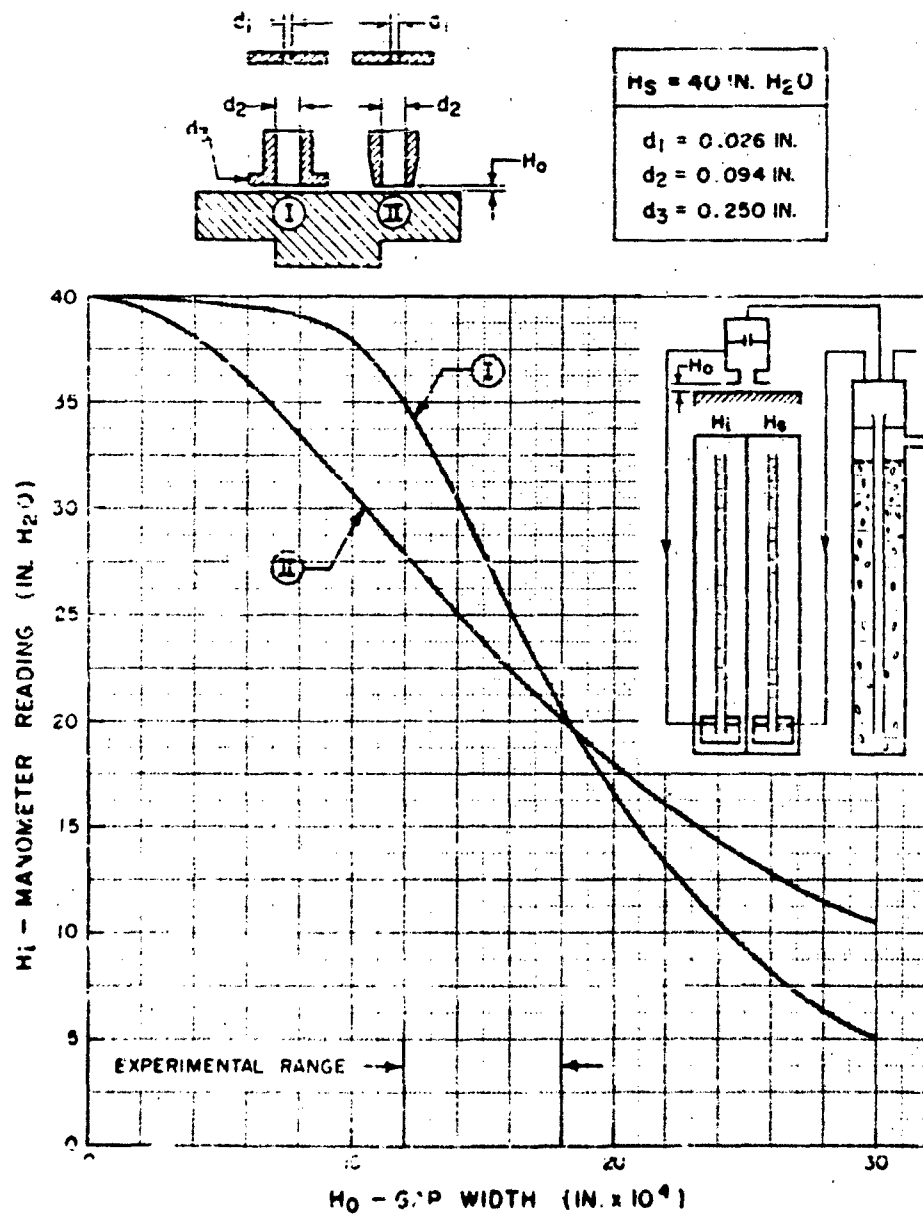


FIG 26 CALCULATED (APPROXIMATE) AIR GAUGE CHARACTERISTICS

SUPPLY ORIFICE DIAM.	$d_1 = 0.026"$
SUPPLY ORIFICE LENGTH	$l_1 = 0.060"$
PROBE INSIDE DIAM.	$d_2 = 0.094"$
PROBE OUTSIDE DIAM.	$d_3 = 0.250"$
PROBE LENGTH	$l_2 = 0.385"$
SUPPLY HEAD	$H_s = 39.2$ IN. H_2O
BAROMETRIC PRESSURE	$P_{at} = 14.72$ PSIA
ROOM TEMPERATURE	$T_0 = 74^\circ-76^\circ F$

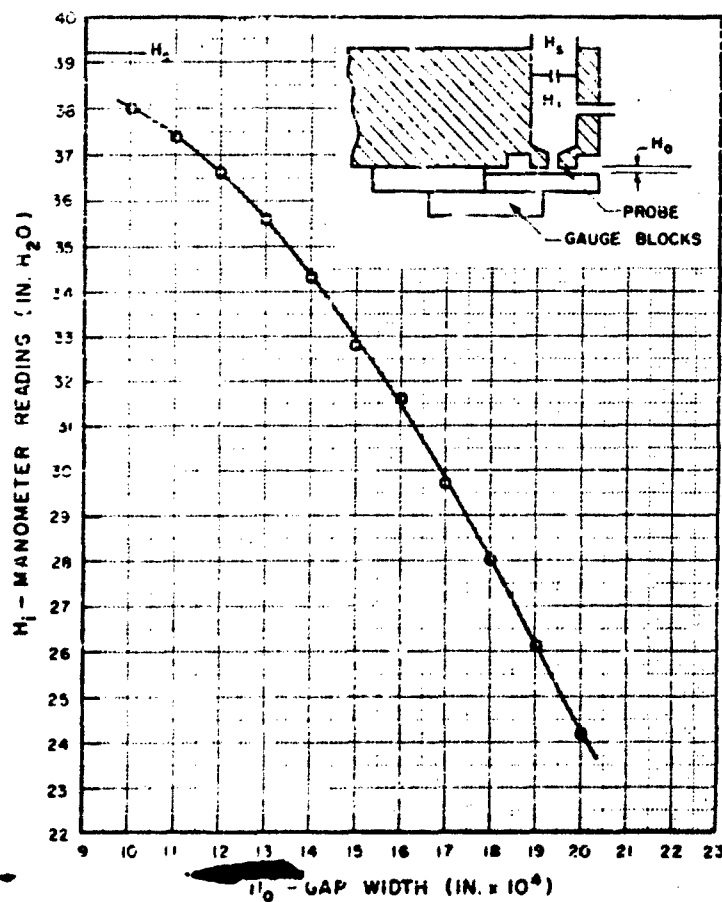


FIG. 21 CALIBRATION CURVE
(Air Gauge No 1)

SUPPLY ORIFICE DIAM	$d_1 = 0.036"$
SUPPLY ORIFICE LENGTH	$l_1 = 0.050"$
PROBE INSIDE DIAM	$d_2 = 0.094"$
PROBE OUTSIDE DIAM	$d_3 = 0.250"$
PROBE LENGTH	$l_2 = 0.385"$
SUPPLY HEAD	$H_s = 39.2$ IN H_2O
BAROMETRIC PRESSURE	$P_{at} = 14.72$ PSIA
ROOM TEMPERATURE	$T_0 = 74^\circ - 76^\circ F$

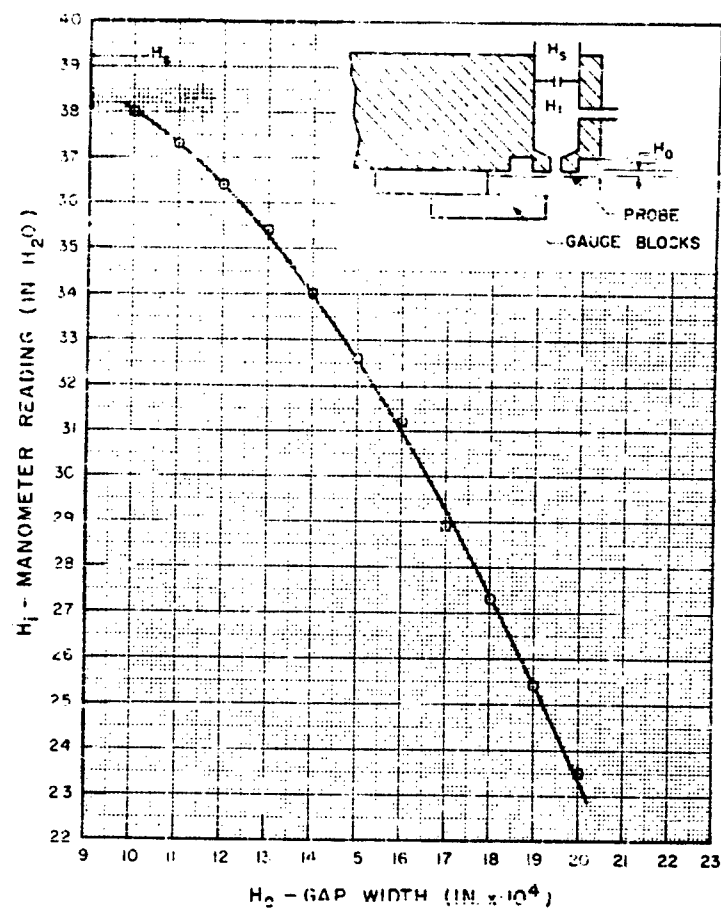


FIG. 26. CALIBRATION CURVE
(Air Gauge No. 2.)

SUPPLY ORIFICE DIAM.	$d_1 = 0.026"$
SUPPLY ORIFICE LENGTH	$l_1 = 0.000"$
PROBE INSIDE DIAM.	$d_2 = 0.094"$
PROBE OUTSIDE DIAM.	$d_3 = 0.250"$
PROBE LENGTH	$l_2 = 0.485"$
SUPPLY LIQ.	$H_s = 39.2 \text{ IN. } H_2O$
BAROMETRIC PRESSURE	$P_b = 14.72 \text{ PSIA}$
ROOM TEMPERATURE	$T_0 = 74^\circ - 76^\circ F$

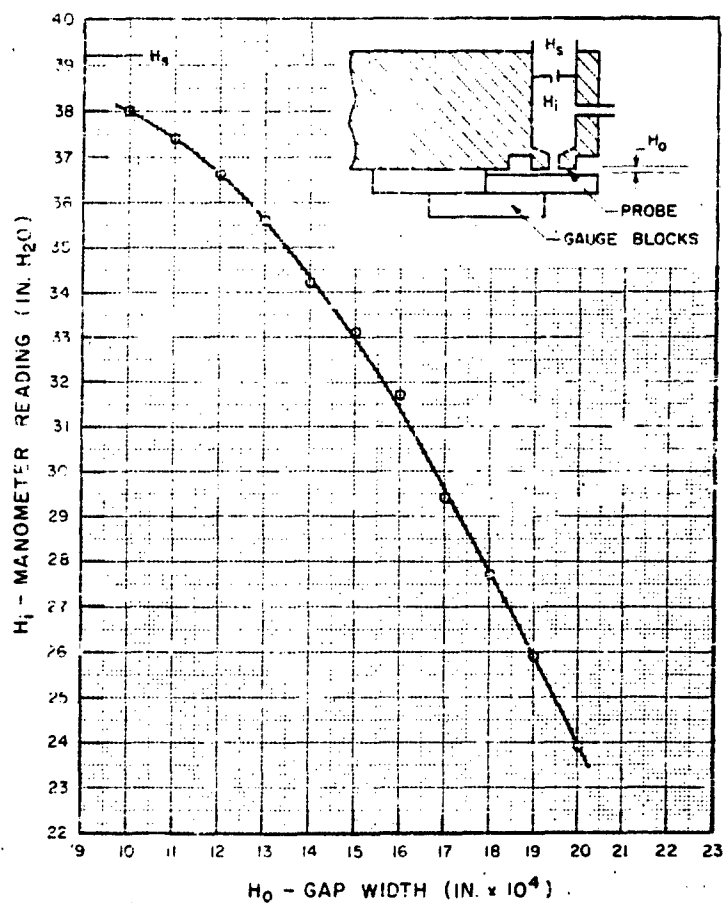


FIG. 20. CALIBRATION CURVE
(Air Gauge No. 3)

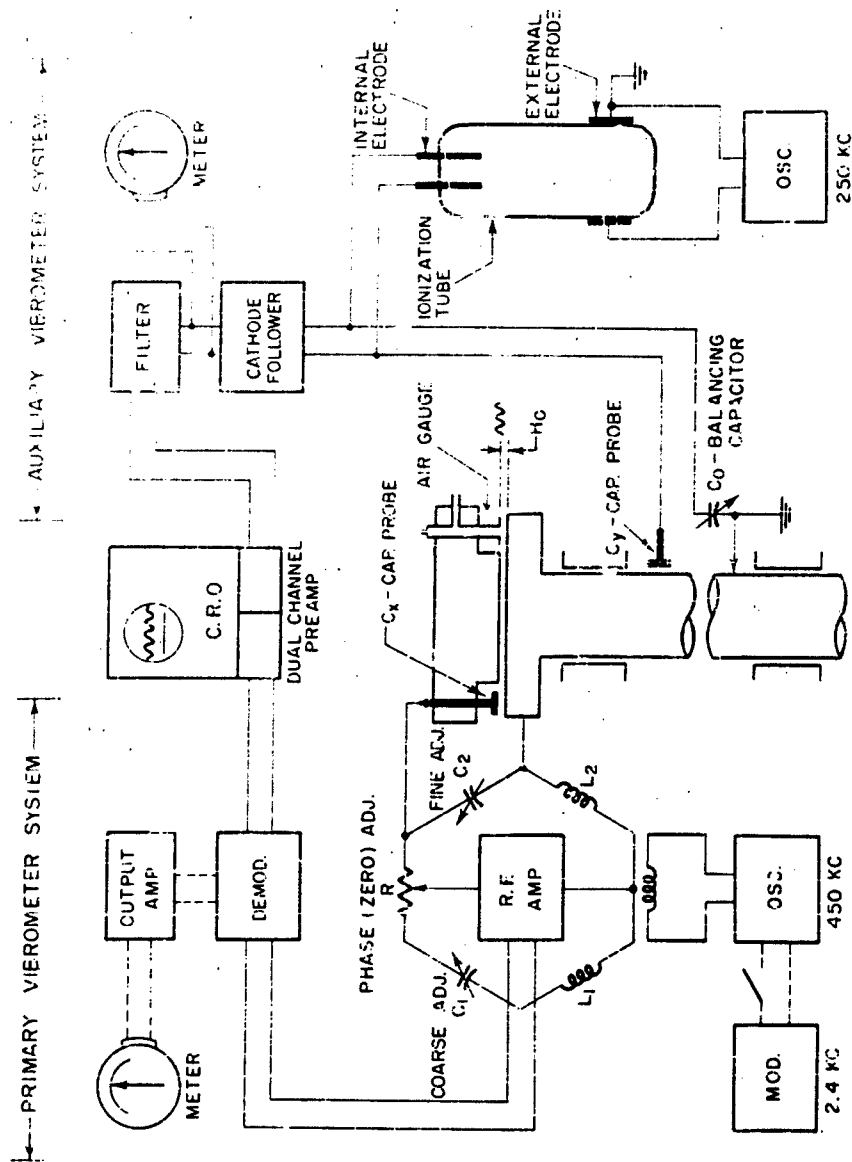


FIG. 30. SCHEMATIC DIAGRAM OF INSTRUMENTS FOR VIBRATION
DETECTION AND MEASUREMENT

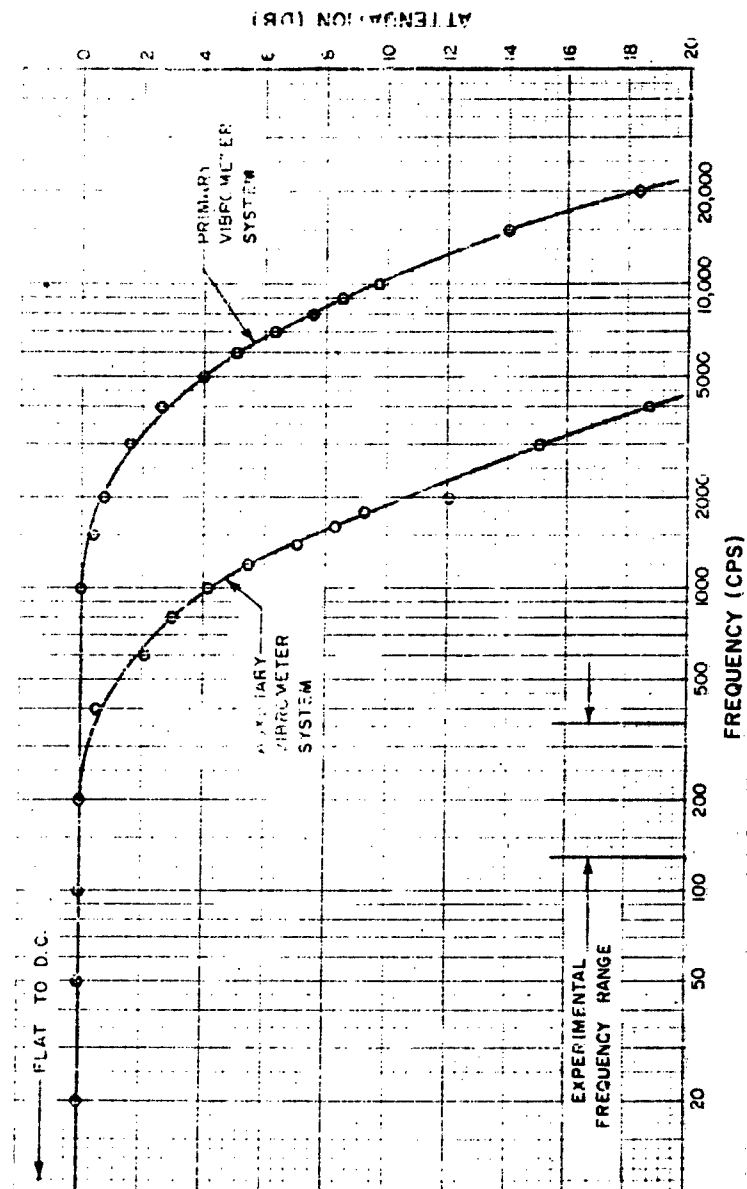


FIG. 31. FREQUENCY RESPONSE OF VIBRATION INSTRUMENTS

PROBE DIMENSION: 0.25 IN. DIAM
 INITIAL (NULL) OFFSET: 4.35×10^{-3} IN.
 SENSITIVITY: 1.05 V / 10^{-5} IN. AT NULL POINT

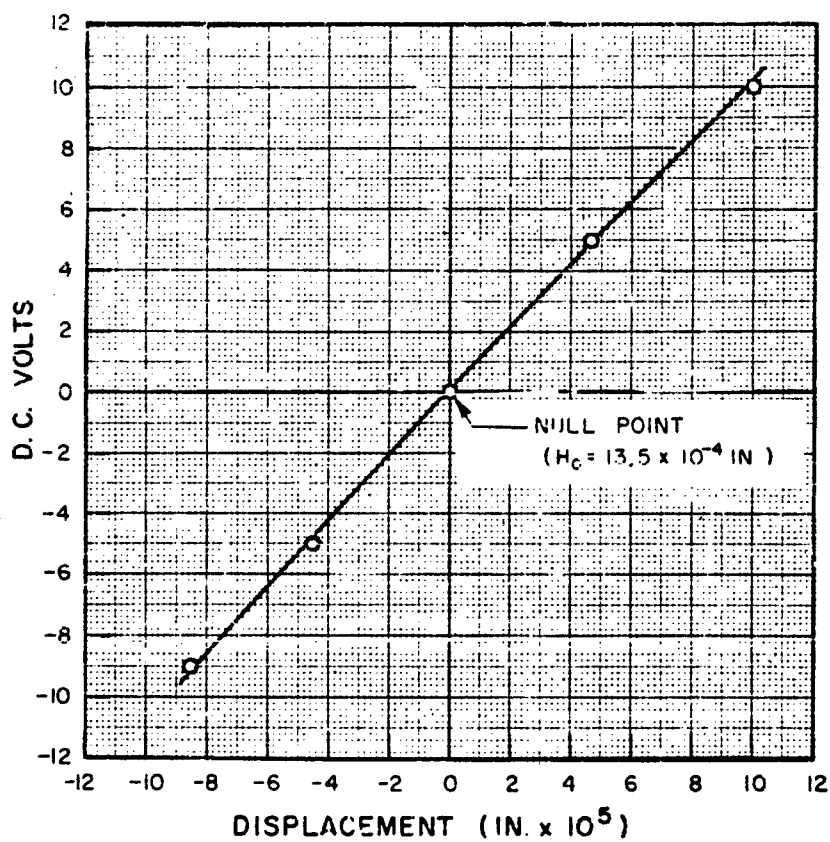


FIG. 32. CALIBRATION CURVE 1.
 (Primary Capacitance Probe)

PROBE DIMENSION: 0.25 IN. DIAM
 INITIAL (NULL) OFFSET: 4.50×10^{-3} IN.
 SENSITIVITY: 0.95V / 10^{-5} IN. AT NULL POINT

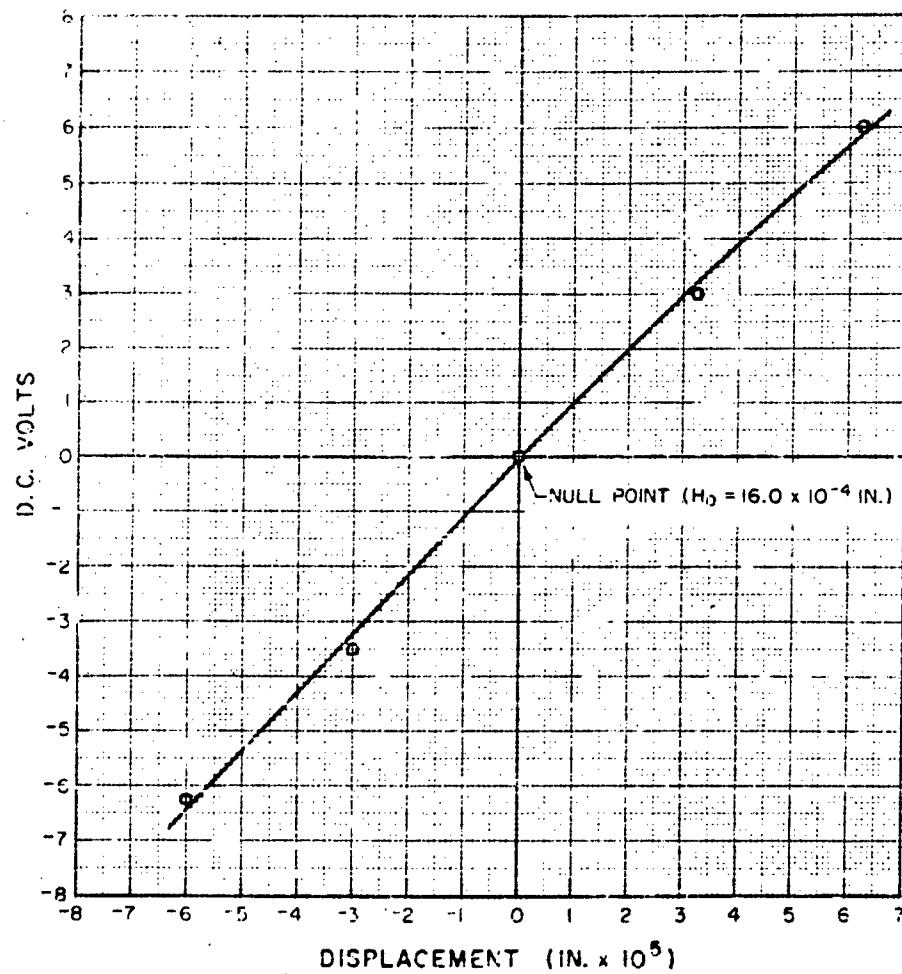


FIG. 33. CALIBRATION CURVE 2
 (Primary Capacitance Probe)

PROBE DIMENSION: 0.25 IN DIAM
 INITIAL (NULL) OFFSET: 4.80×10^{-3} IN.
 SENSITIVITY: $0.95 \text{ V}/10^{-5} \text{ IN.}$ AT NULL POINT

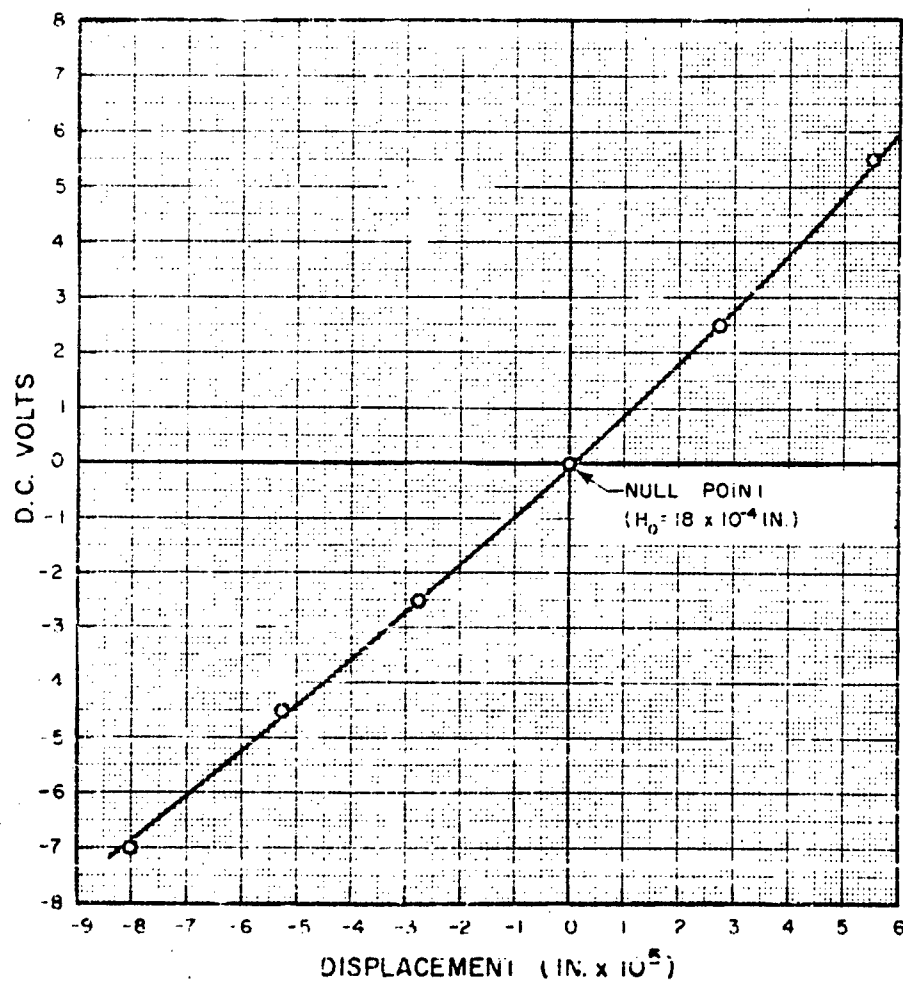


FIG. 34. CALIBRATION CURVE 3
 (Primary Capacitance Probe)

PROBE DIMENSION: $\frac{1}{4} \times \frac{7}{8}$
 INITIAL (NULL) OFFSET: 1.3×10^{-3} IN.
 SENSITIVITY: $0.02\text{V}/10^{-5}$ IN. AT NULL POINT

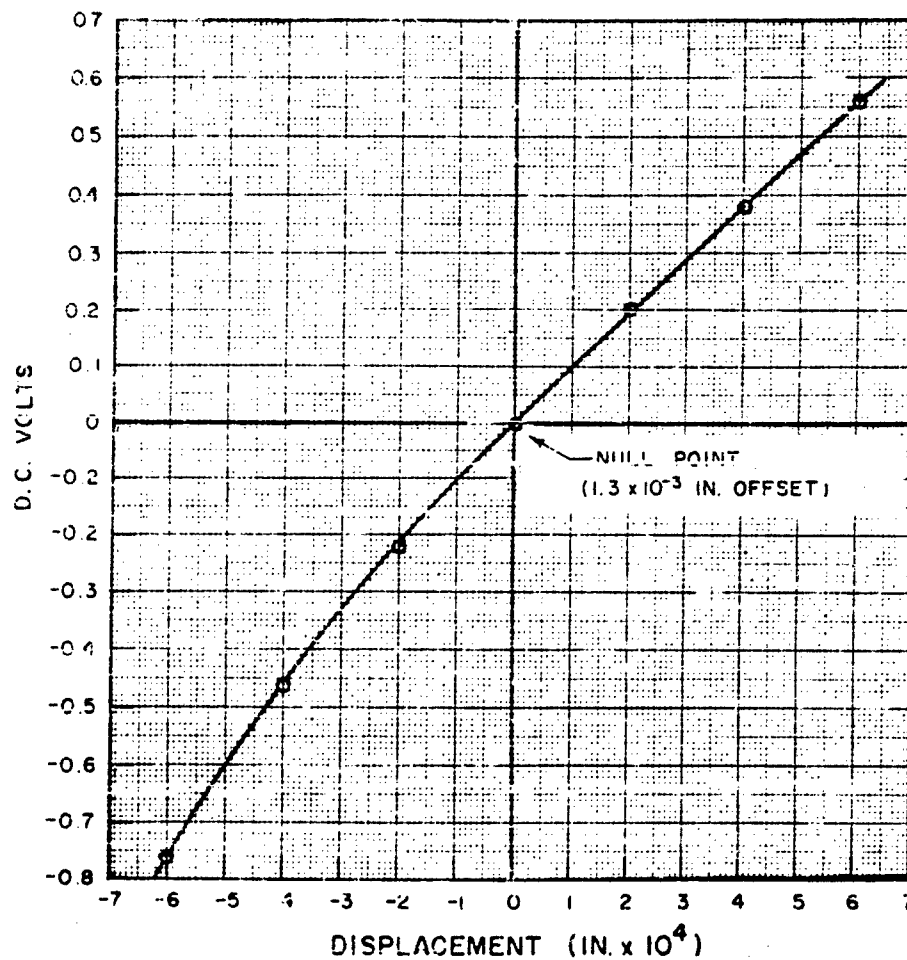
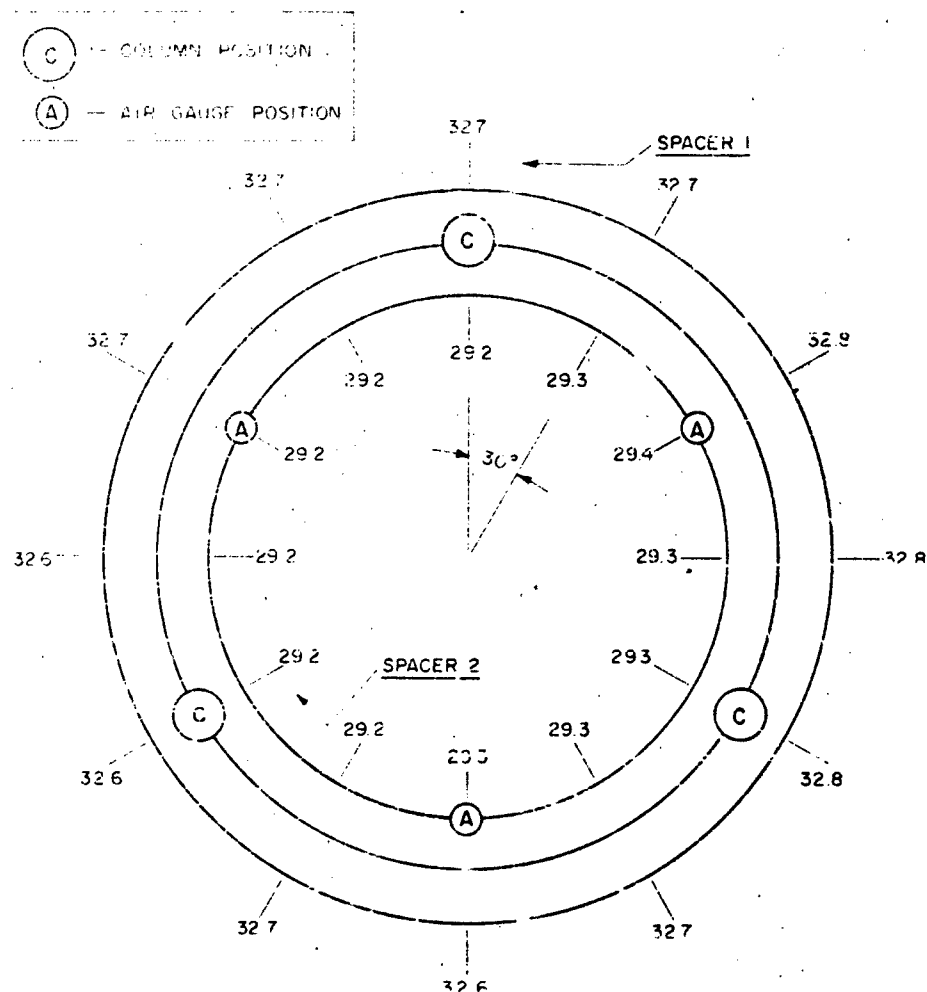


FIG. 35. CALIBRATION CURVE
 (Auxiliary Capacitance Probe)



NUMBERS REFER TO MANOMETER READINGS IN INCHES H₂O (SEE FIG 27)

FIG. 36 RESULTS OF THRUST PLATE ALIGNMENT TEST

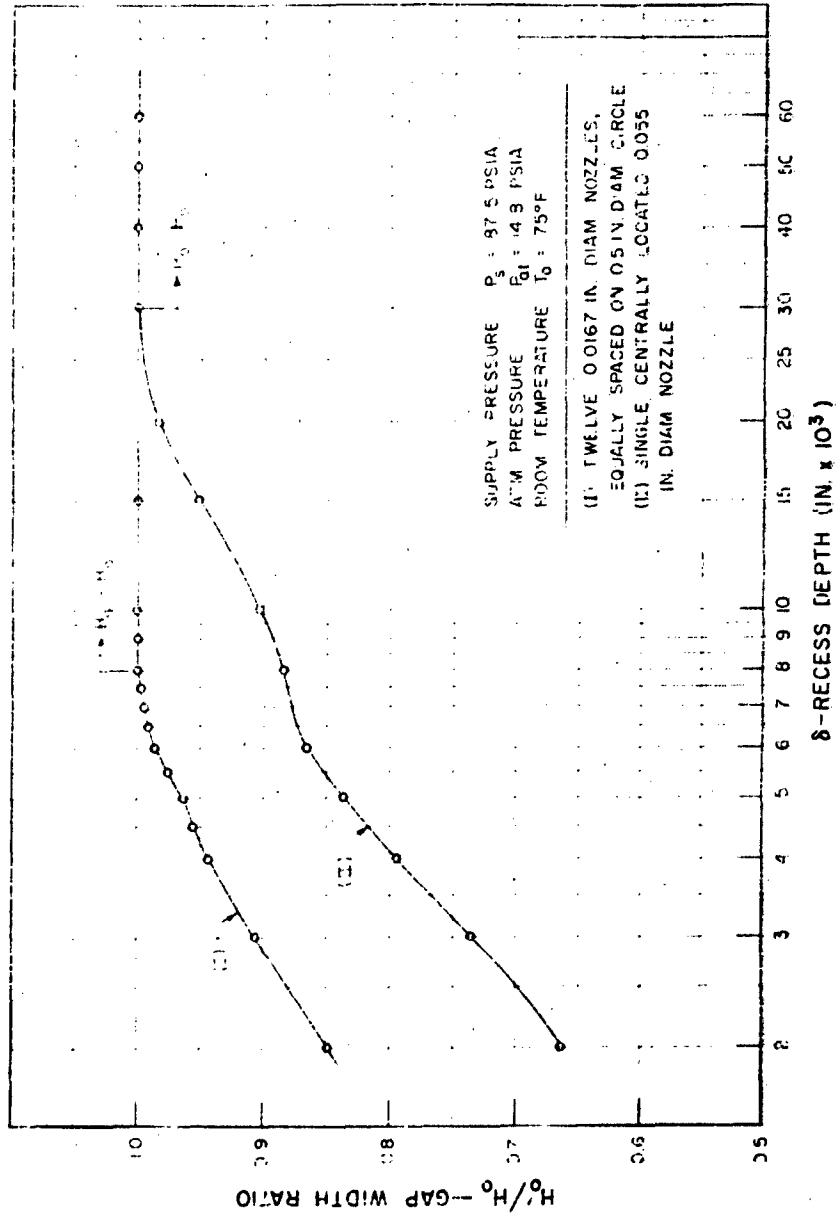


FIG. 37. EFFECT OF DECREASE IN RECESS DEPTH ON BEARING GAP WIDTH

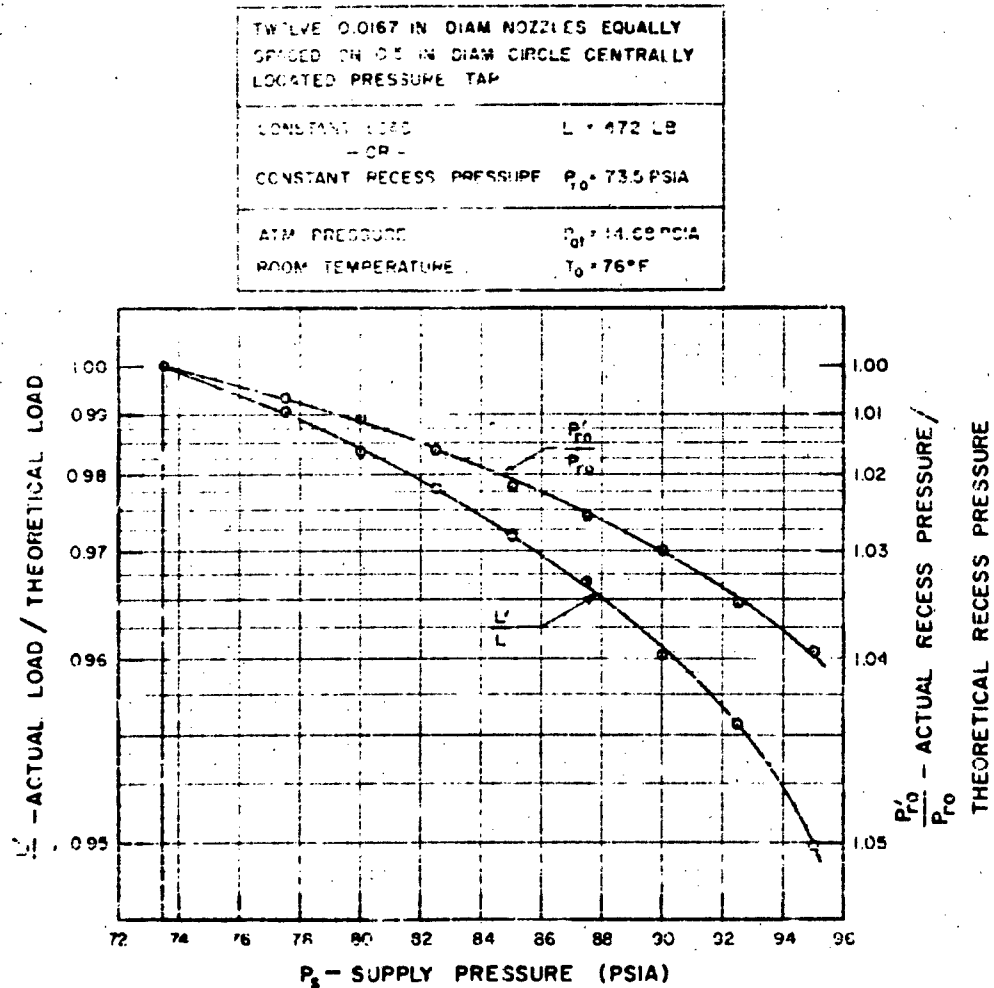


FIG. 38. VARIATION OF LOAD CAPACITY AND/OR RECESS PRESSURE WITH SUPPLY PRESSURE

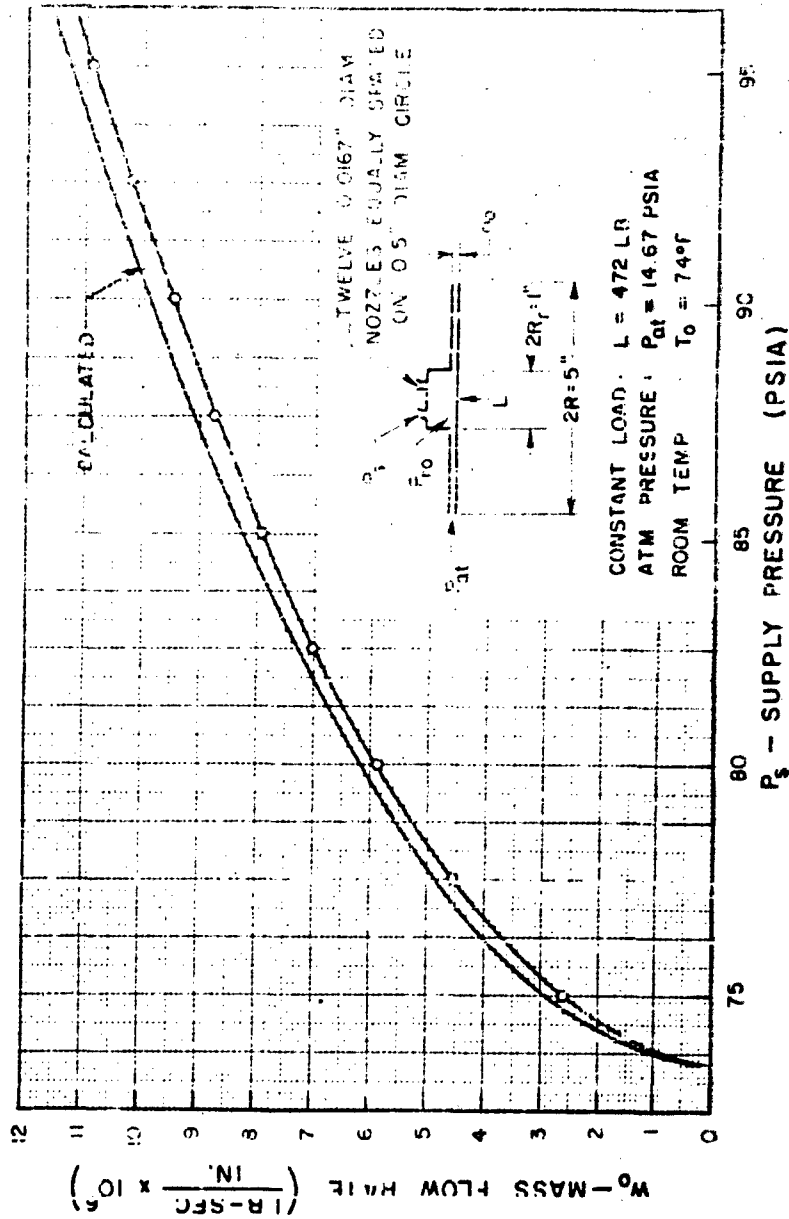


FIG. 39 BEARING MASS FLOW RATE VS. SUPPLY PRESSURE
(CONSTANT LOAD = 472 LB)

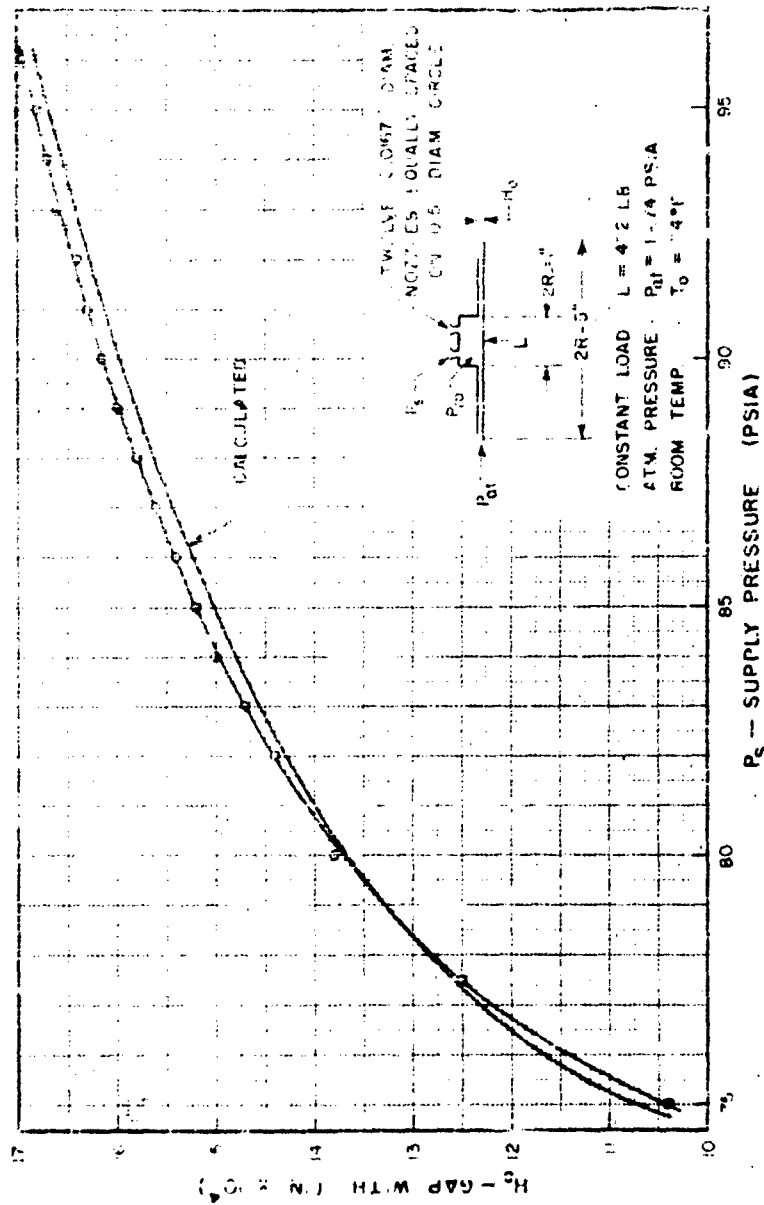


FIG. 40. GEARING GAP WIDTH vs SUPPLY PRESSURE
 (CONSTANT LOAD = 47.2 LB)

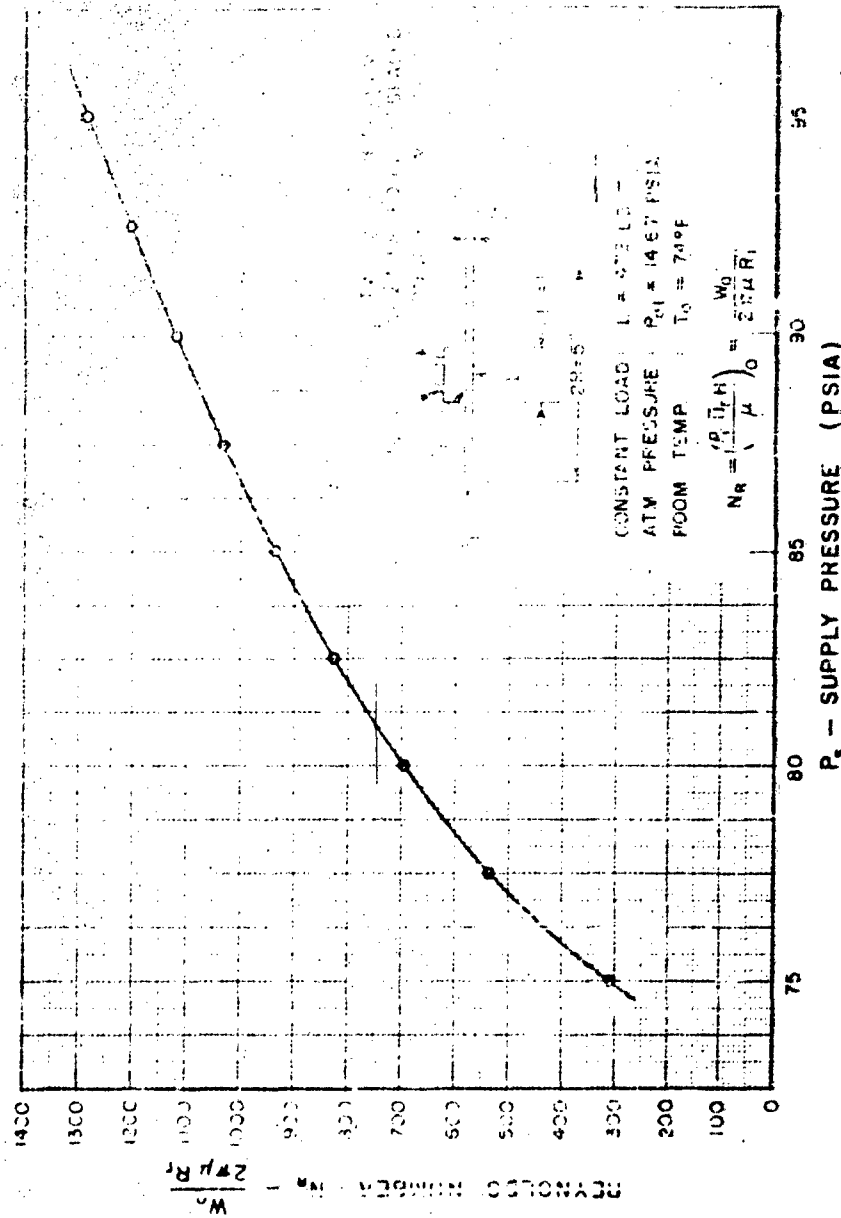


FIG. 41. BEARING REYNOLDS NUMBER VS. SUPPLY PRESSURE
 (CONSTANT LOAD = 472 LB)

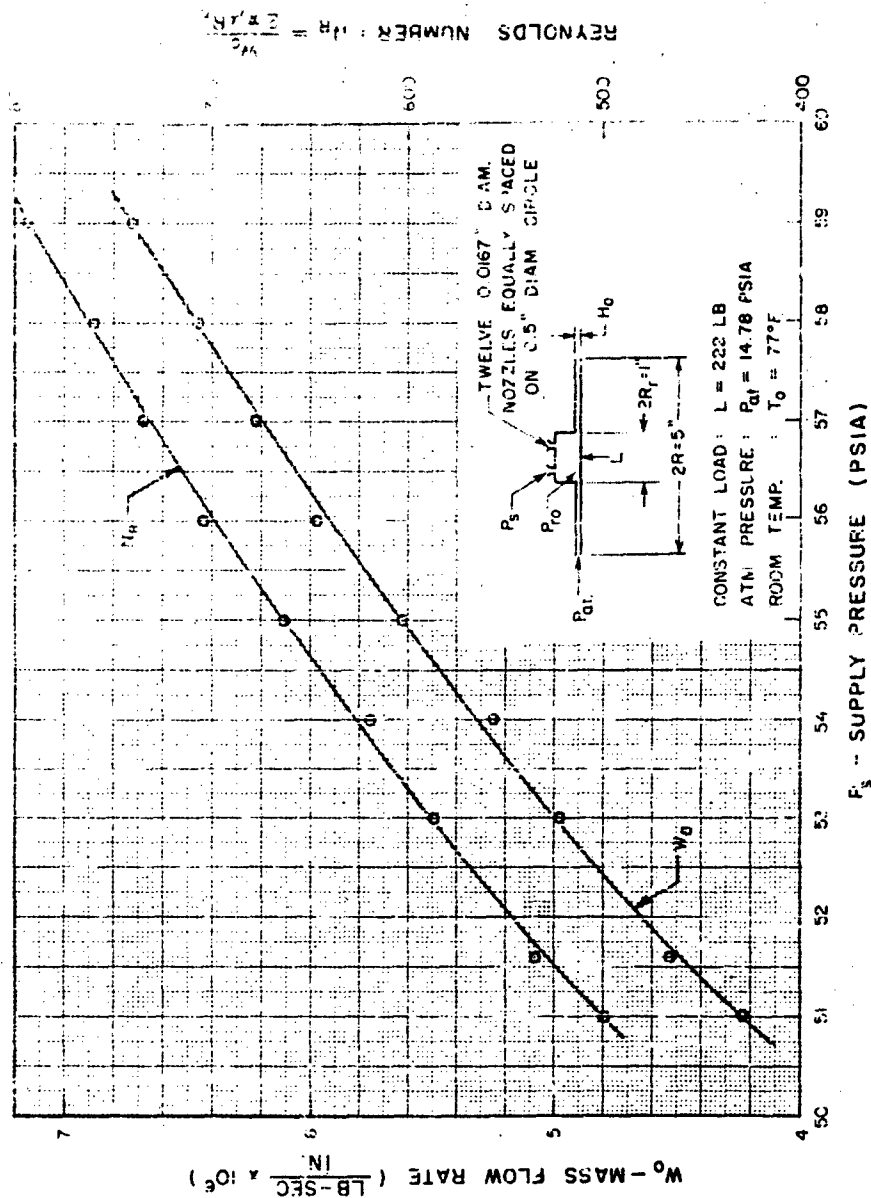


FIG. 42 BEARING MASS FLOW RATE AND REYNOLDS NUMBER VS. SUPPLY PRESSURE (CONSTANT LOAD = 2.22 LB)

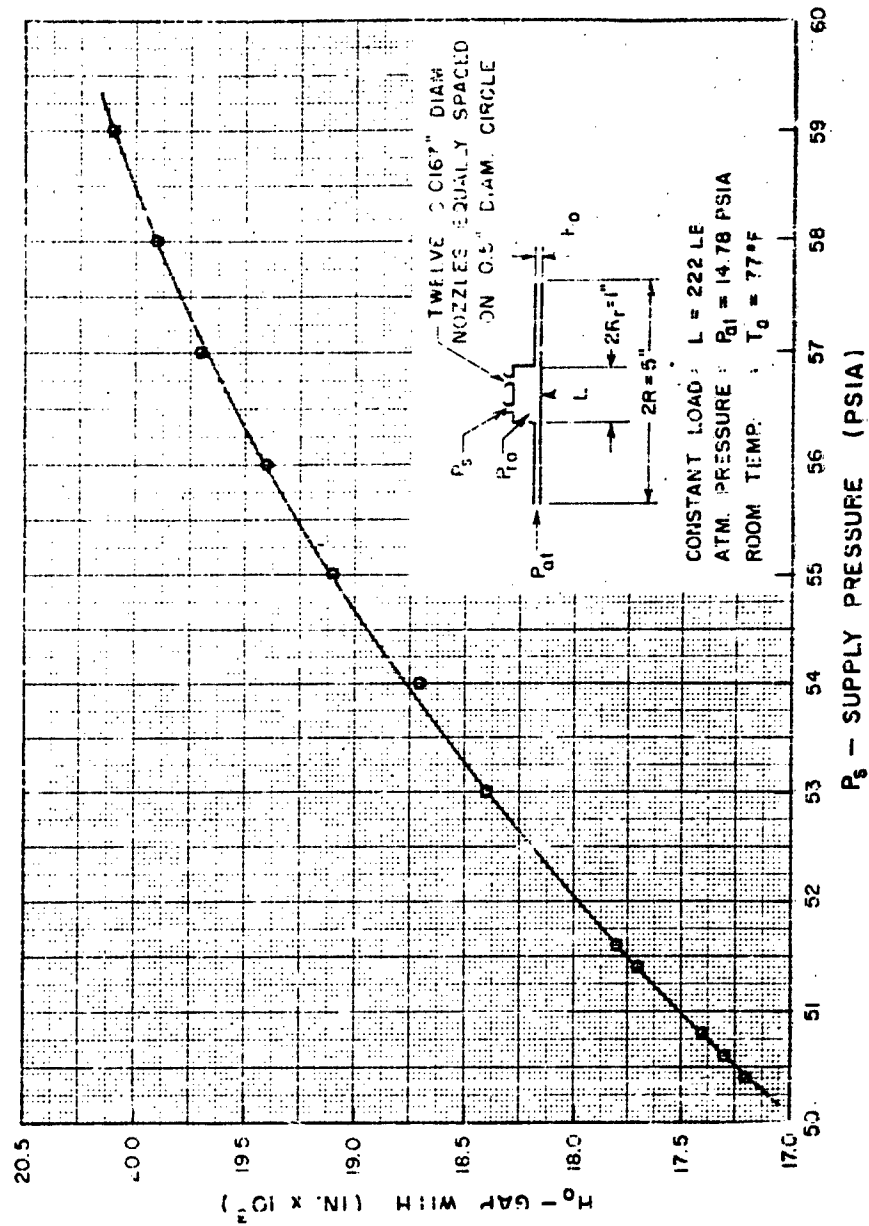


FIG. 43. BEARING GAP WIDTH vs. SUPPLY PRESSURE
(CONSTANT LOAD = 222 LB)

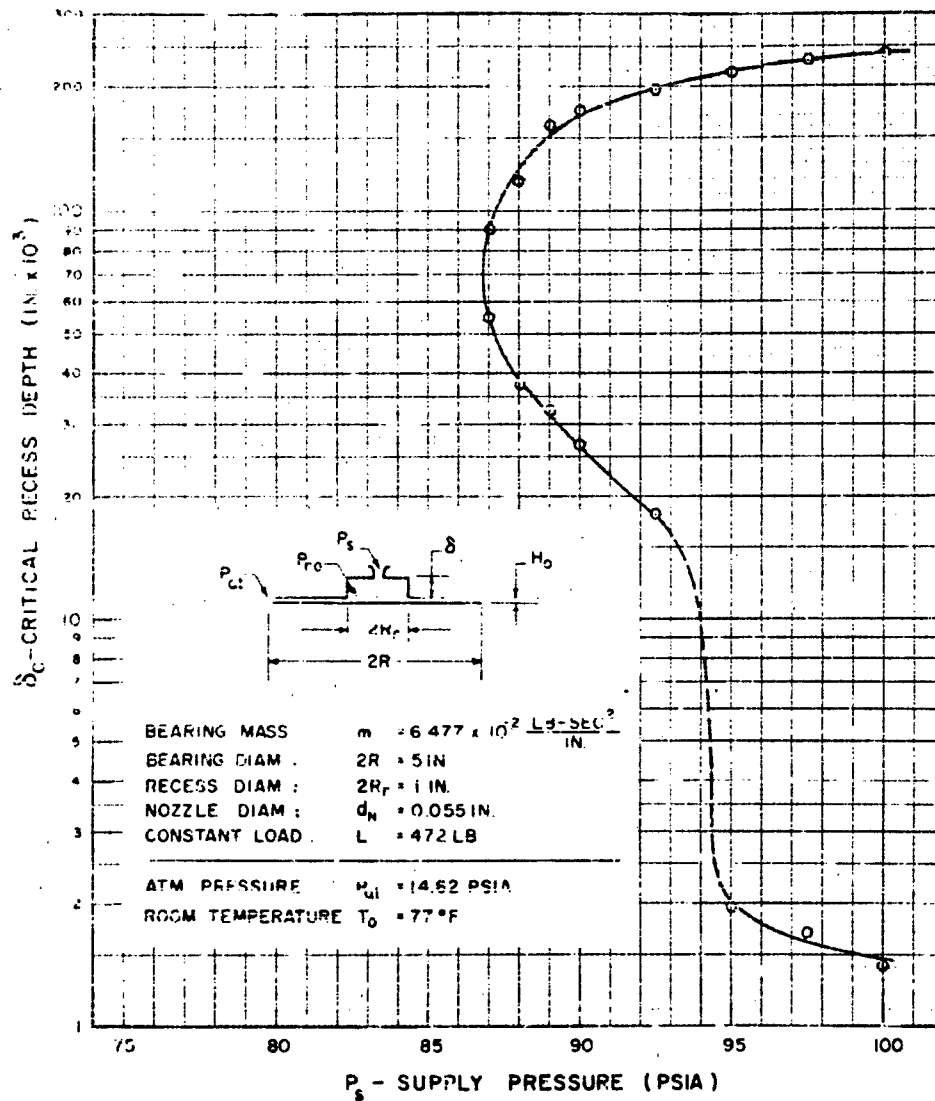


FIG 44 CRITICAL RECESS DEPTH vs. SUPPLY PRESSURE
(Effect of Decrease in Recess Depth for Single Nozzle Supply)

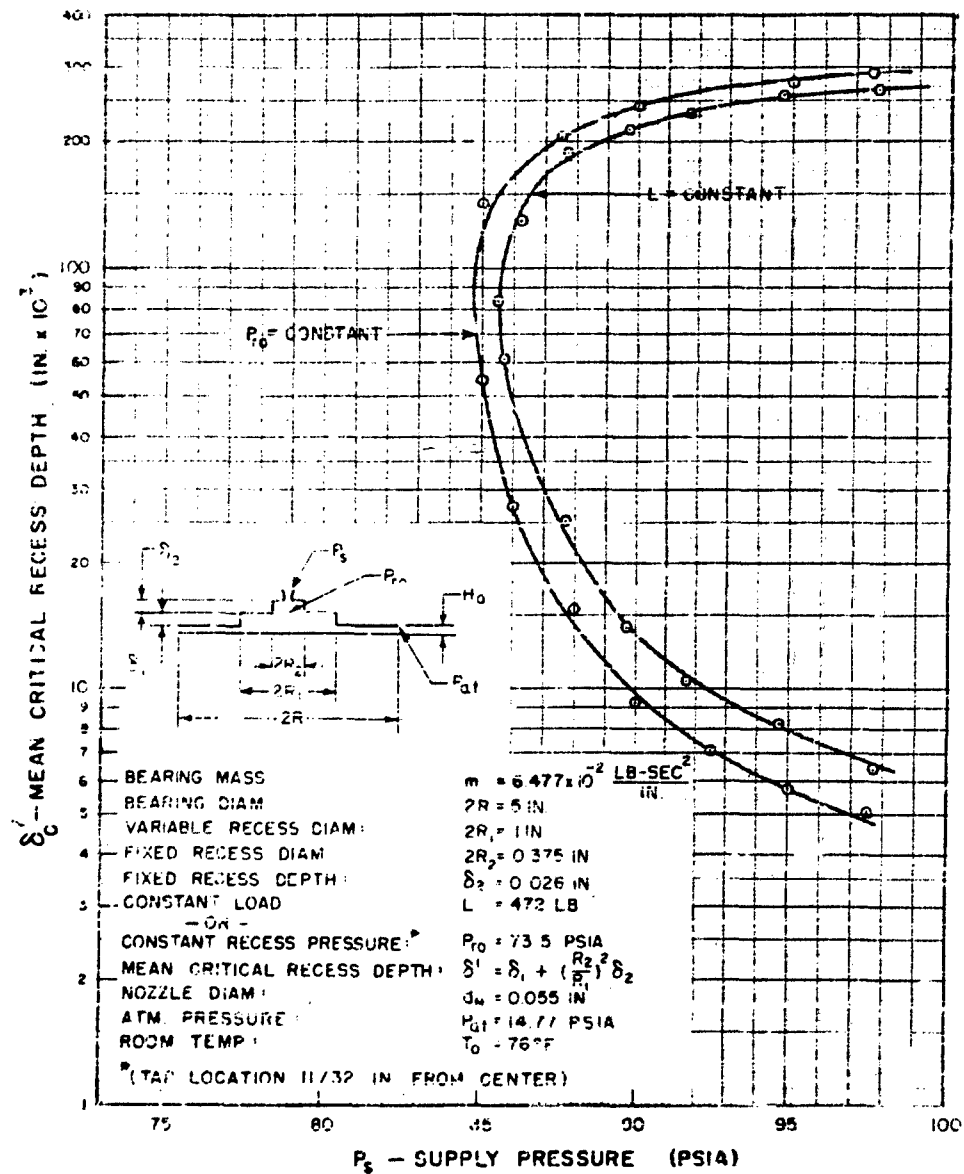


FIG. 45. MEAN CRITICAL RECESS DEPTH vs. SUPPLY PRESSURE

(Results of Constant Load and Constant Recess Pressure Tests)

Modified Piston No. 2 and Single Nozzle Supply

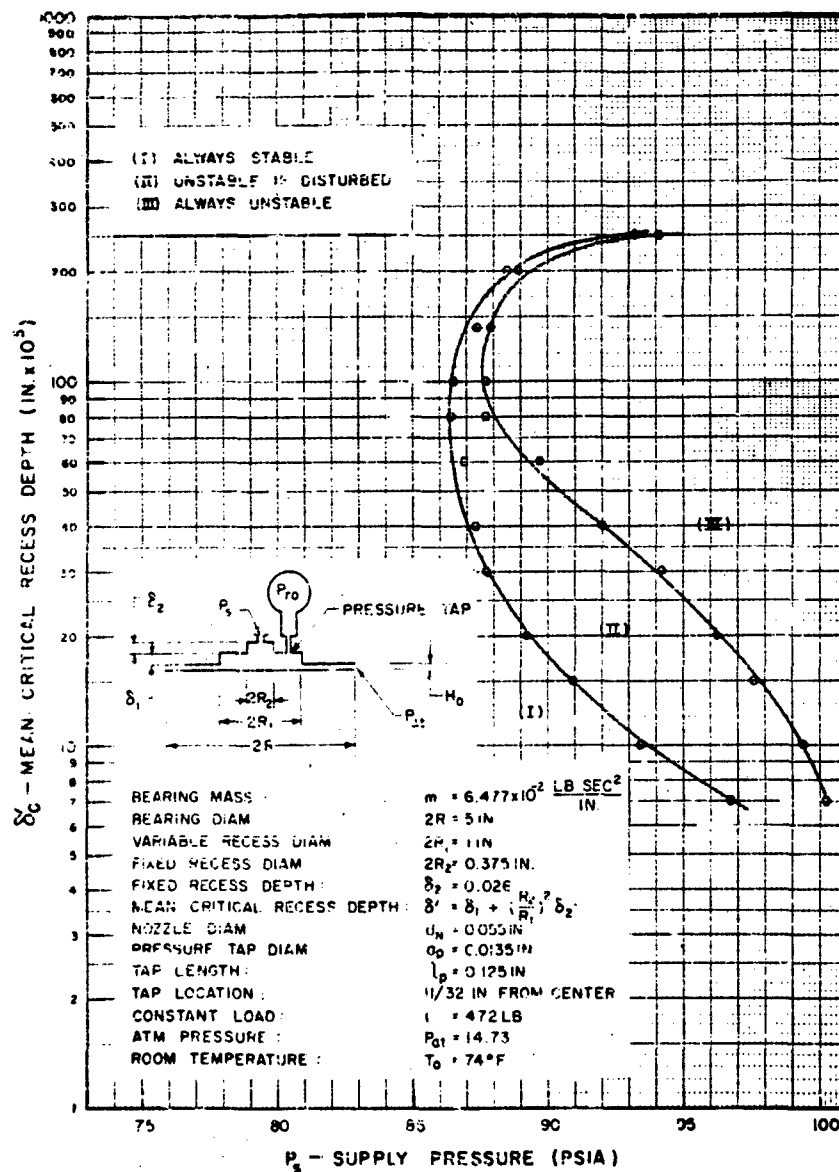


FIG 46. MEAN CRITICAL RECESS DEPTH vs. SUPPLY PRESSURE
(Hysteresis Effect)

Modified Piston No.2, Single Nozzle Supply and Open Pressure Tap

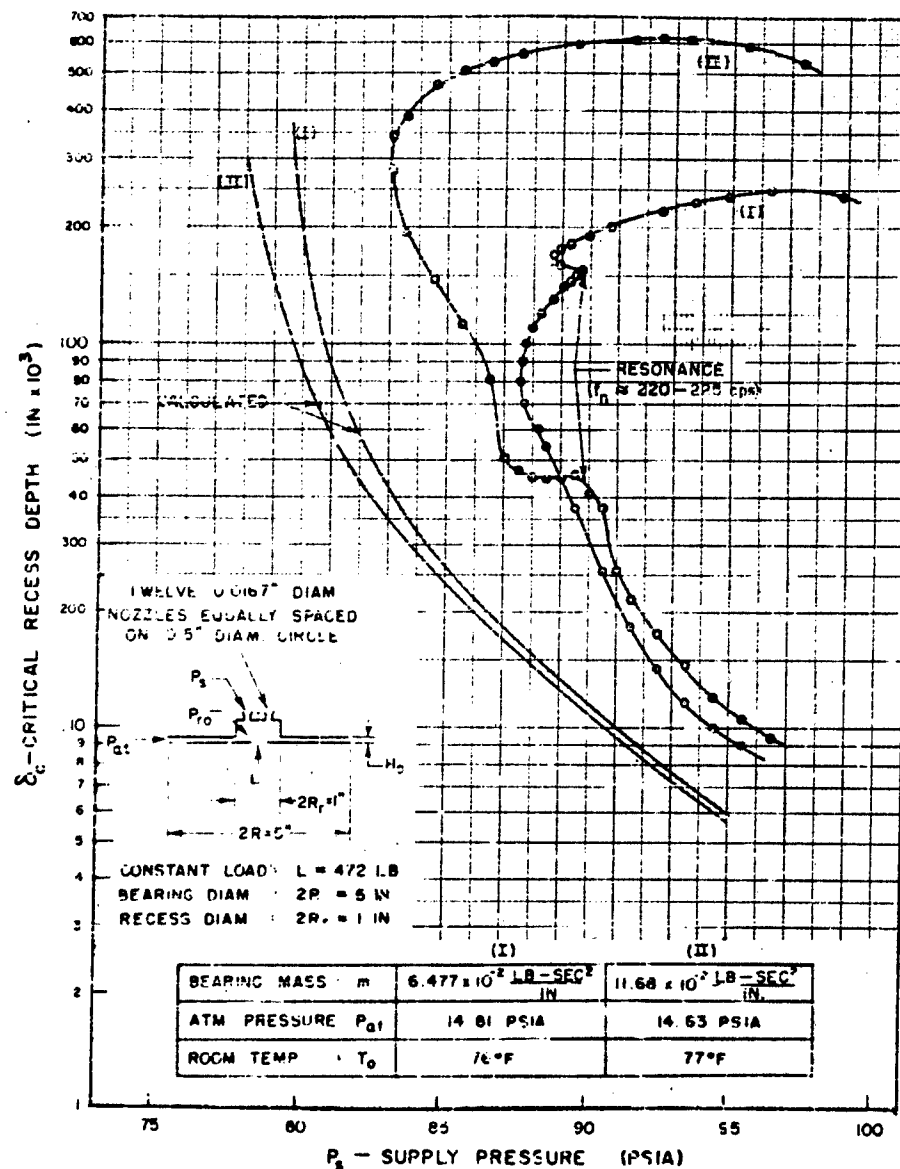


FIG. 47. CRITICAL RECESS DEPTH vs SUPPLY PRESSURE

(Effect of Resonance with Non-isolated Test Stand)

Twelve Nozzle Supply and Piston No 3

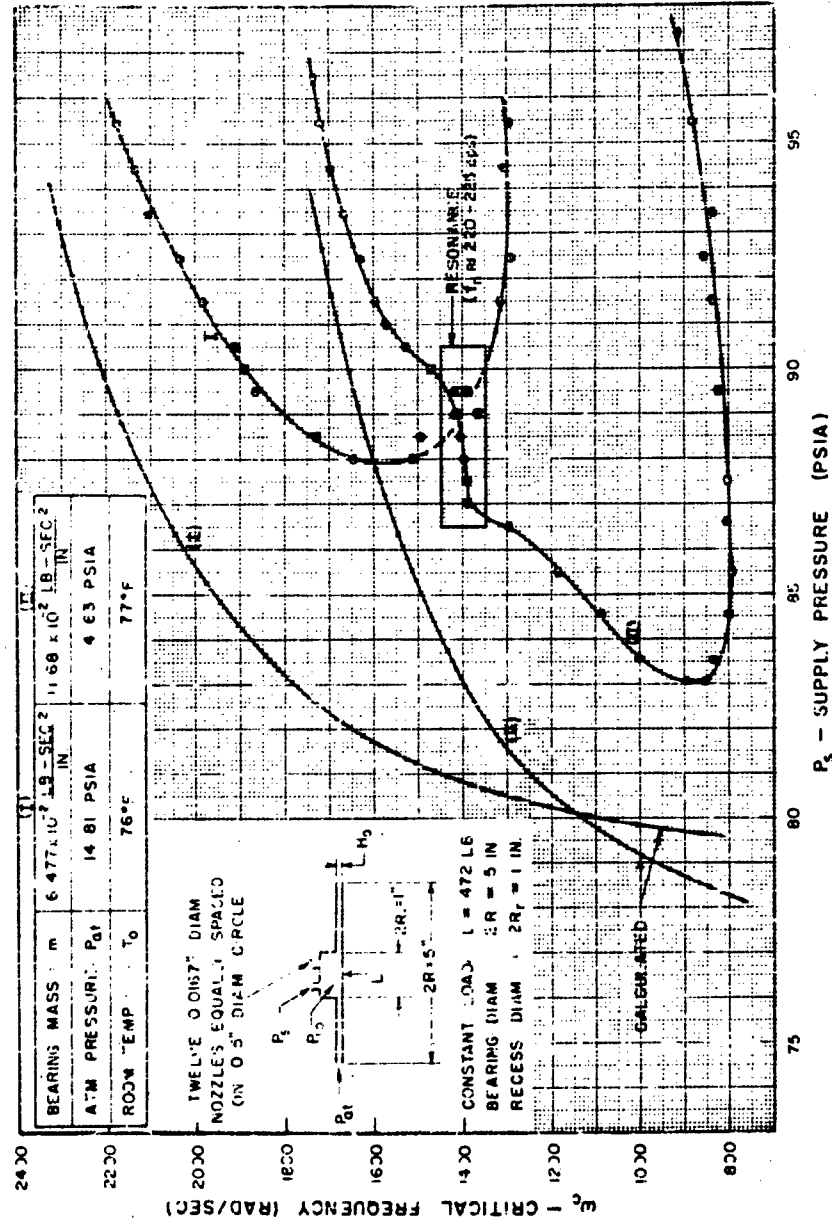


FIG. 48. CRITICAL FREQUENCY vs. SUPPLY PRESSURE
(Effect of Resonance with Non-Isolated Test Stand)
Twelve Nozzles Supply and Piston No. 3

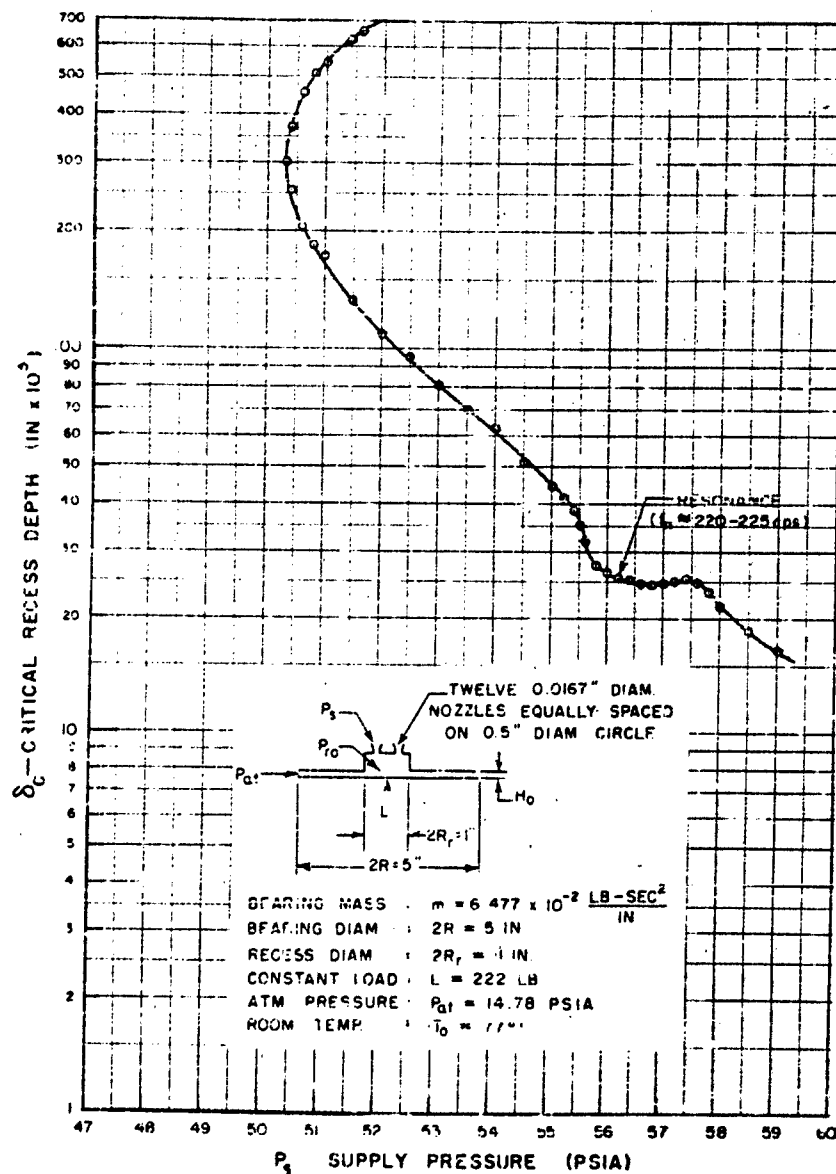
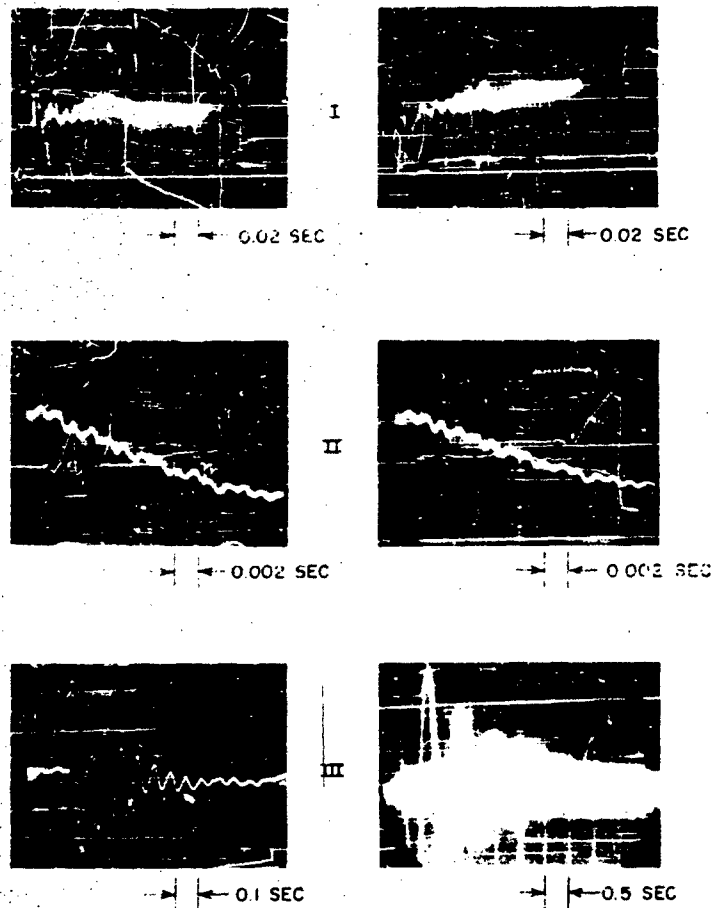


FIG 40 CRITICAL RECESS DEPTH VS. SUPPLY PRESSURE
 (Effect of Resonance With Non-Isolated Test Stand)
 Reduced, 222 lb Load, Twelve Nozzle Supply
 and Piston No. 3



- I TEST RIG AND BASE MOUNTED DIRECTLY ON FLOOR (220-225 CPS)
 II UPPER THRUST PLATE SECURED TO COLUMNS (730 CPS)
 III TEST RIG AND BASE MOUNTED ON ISOLATORS (15 CPS)

FIG. 50. DETERMINATION OF NATURAL FREQUENCIES OF TEST STAND AND UPPER THRUST PLATE

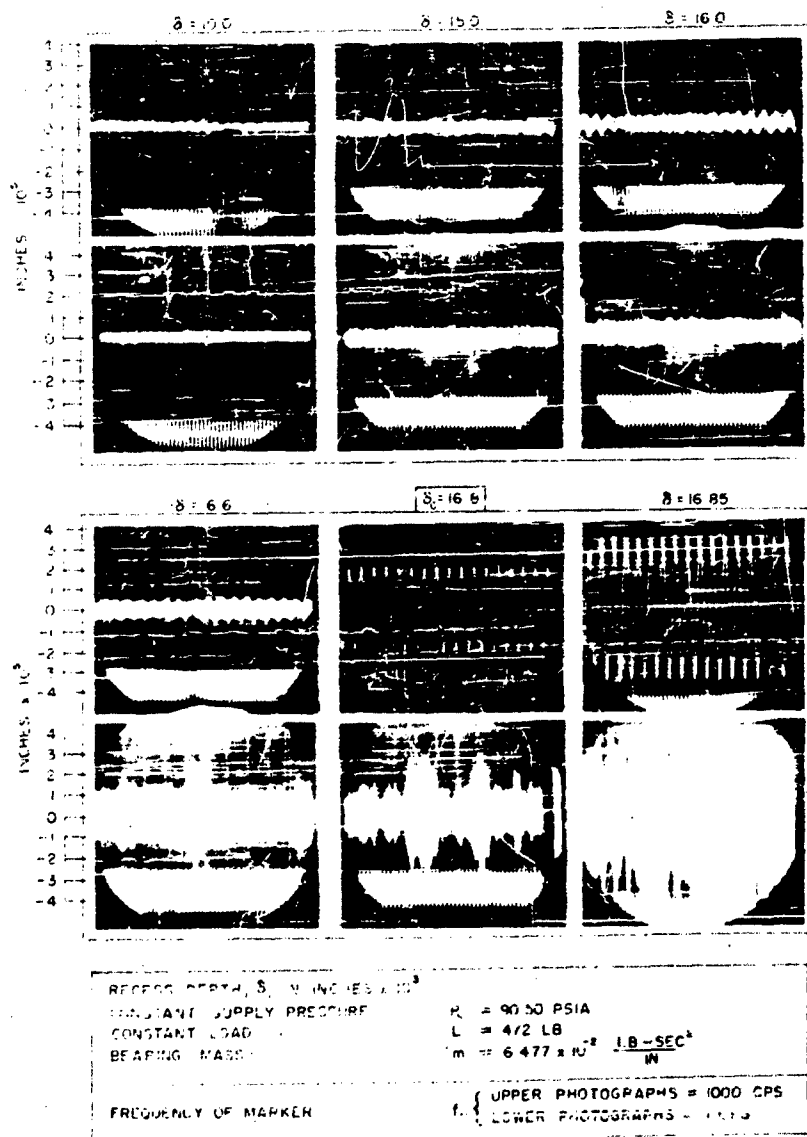


FIG. 51 AMPLITUDE GROWTH OF AUTO-OSCILLATIONS IN APPROACHING STABILITY BOUNDARY ($P_s = 90.50$ PSIA)

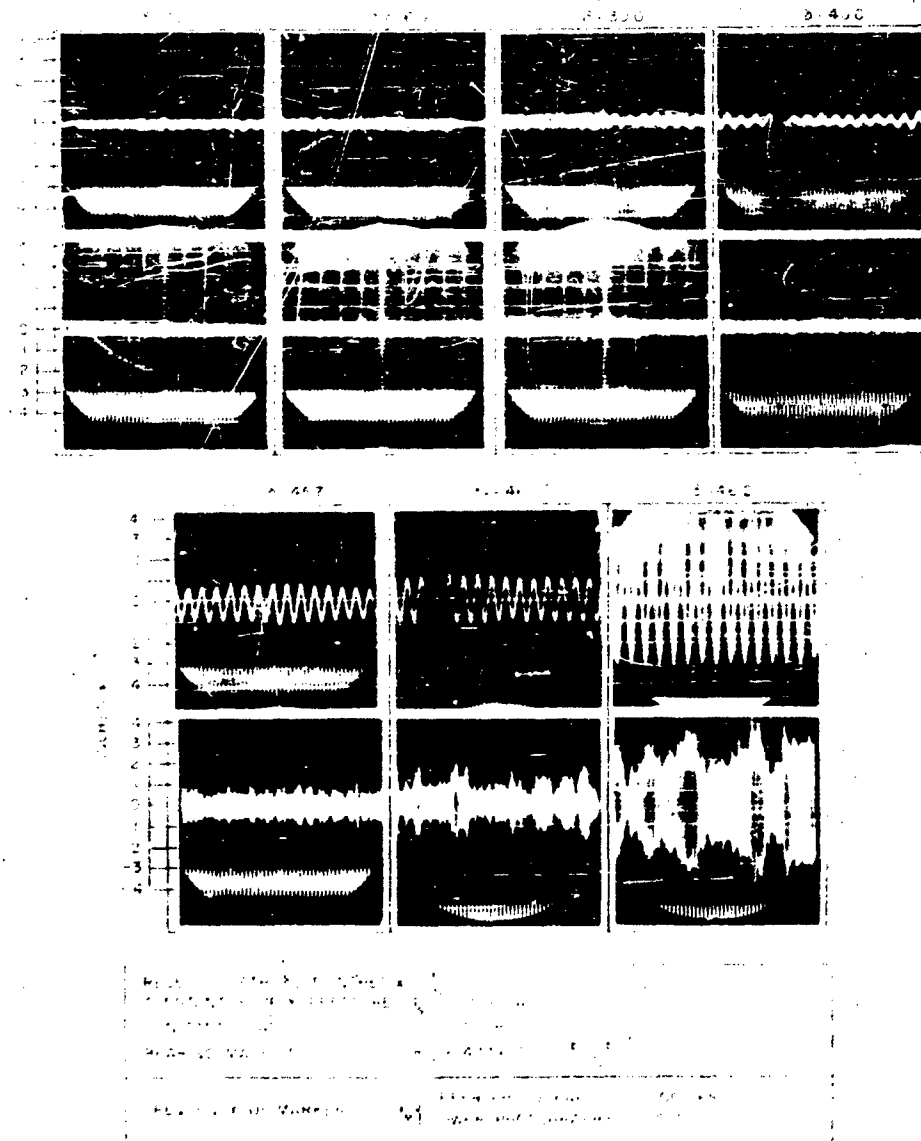


FIG. 52. AMPLITUDE GROWTH OF AUTO-OSCILLATIONS IN APPROACHING STABILITY BOUNDARY ($P_s = 87.50$ PSIA)

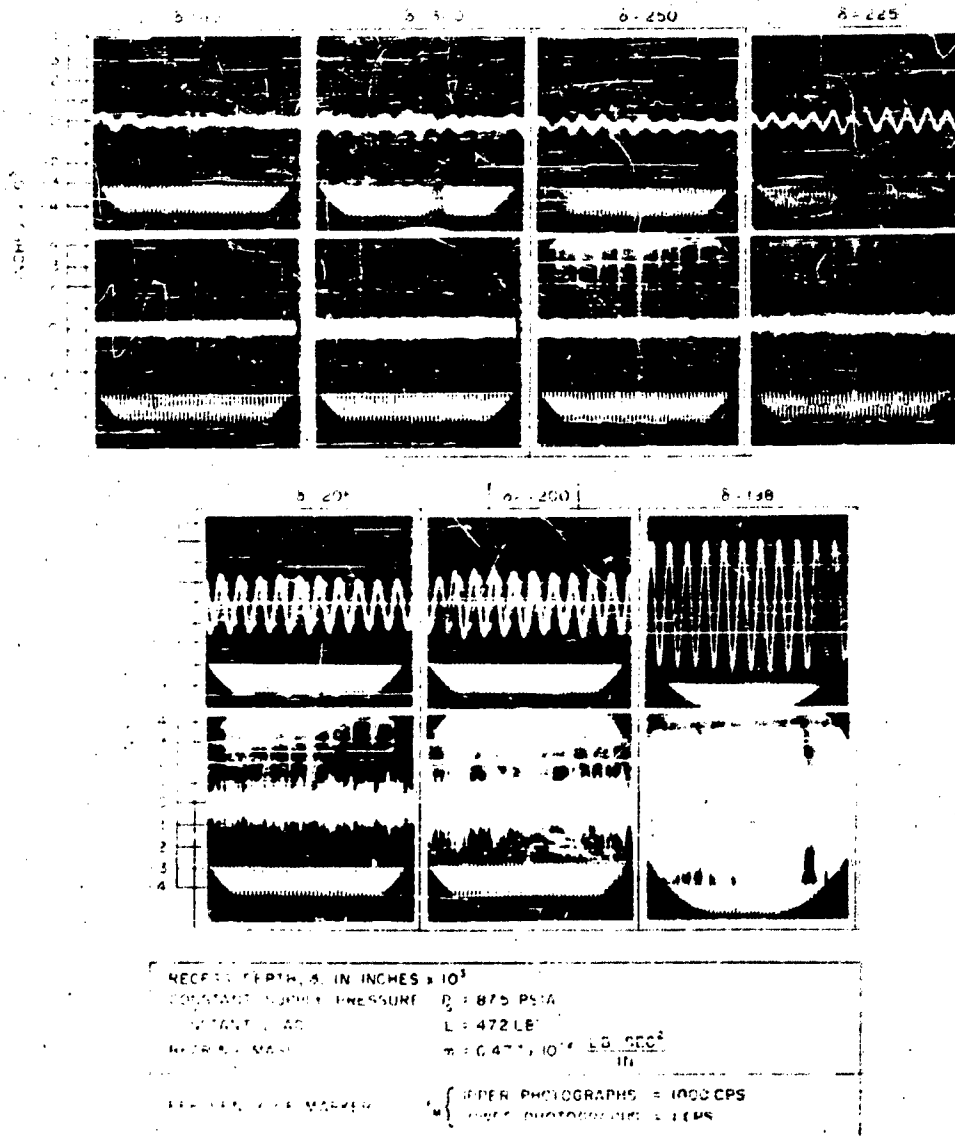


FIG. 53. AMPLITUDE GROWTH OF AUTO OSCILLATIONS IN APPROACHING STABILITY BOUNDARY ($P_s = 87.50 \text{ PSIA}$)

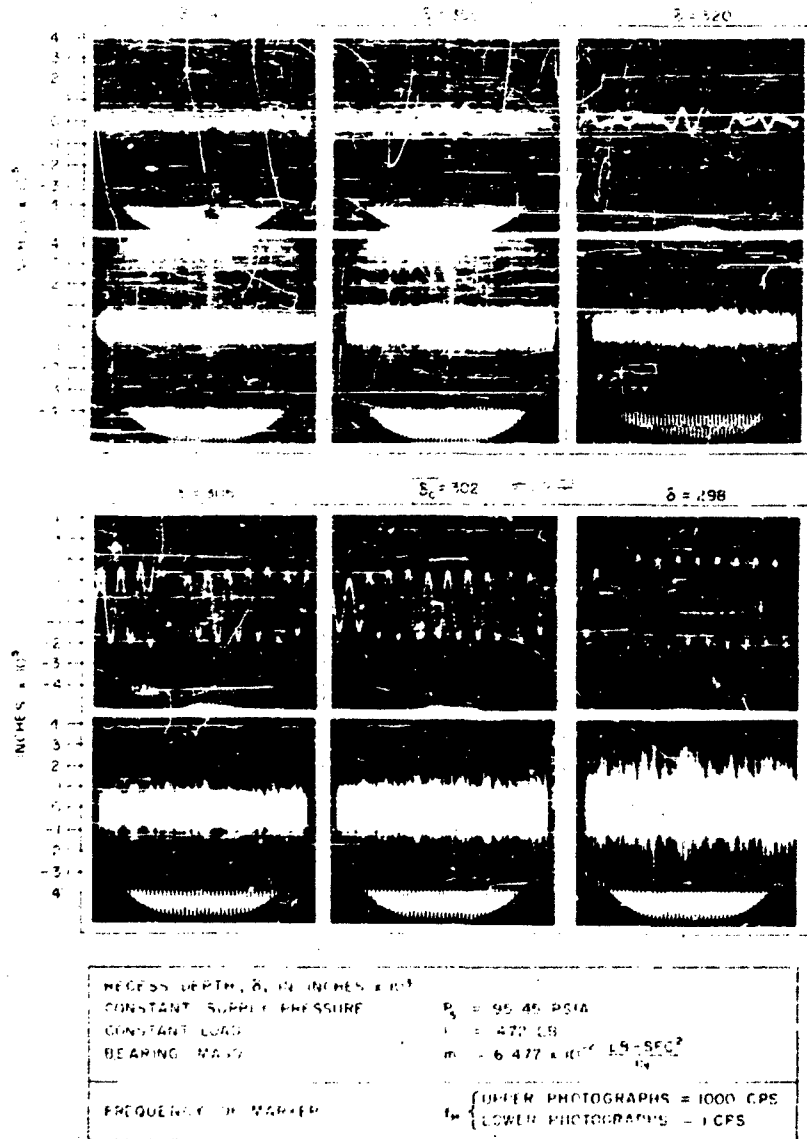


FIG 54 AMPLITUDE GROWTH OF AUTO-OSCILLATIONS IN APPROACHING STABILITY BOUNDARY ($P_s = 95.45$ PSIA)

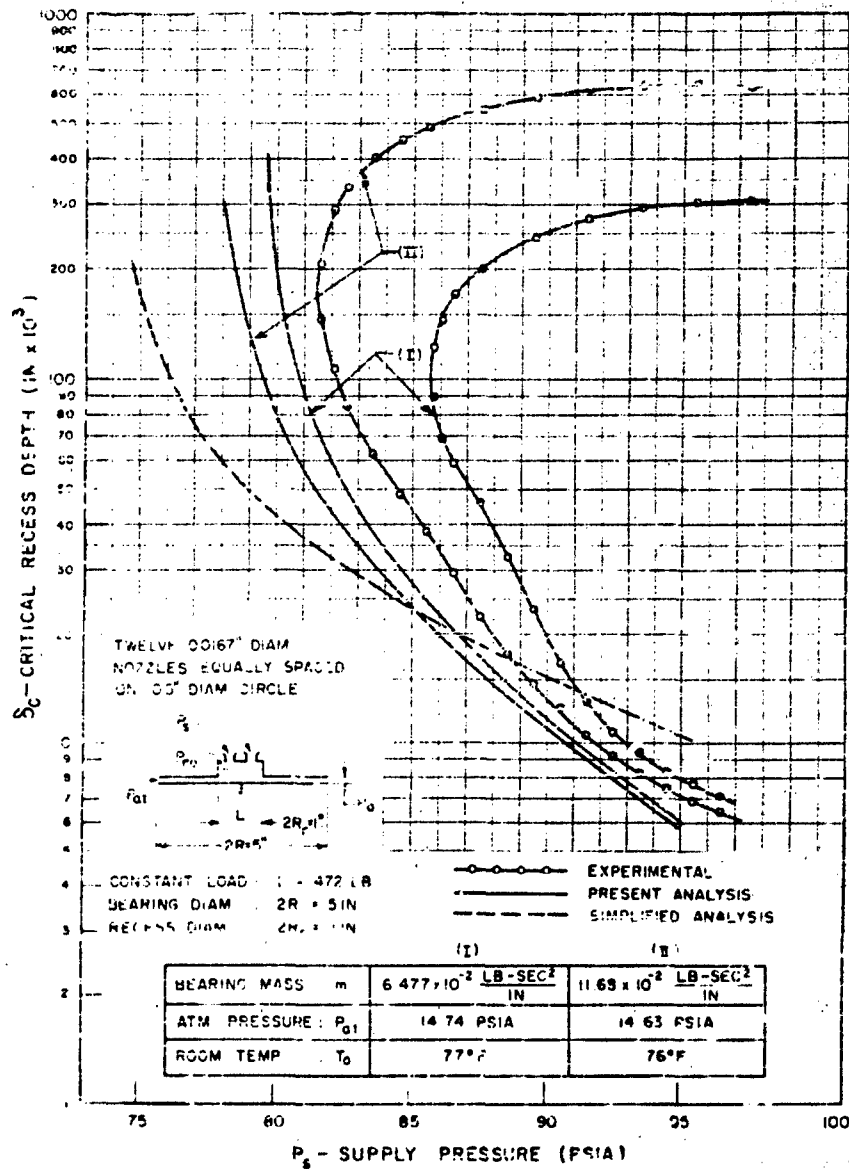


FIG. 55 CRITICAL RECESS DEPTH vs. SUPPLY PRESSURE

(Concluding Results)

Twelve Nozzle Supply and Piston No. 3

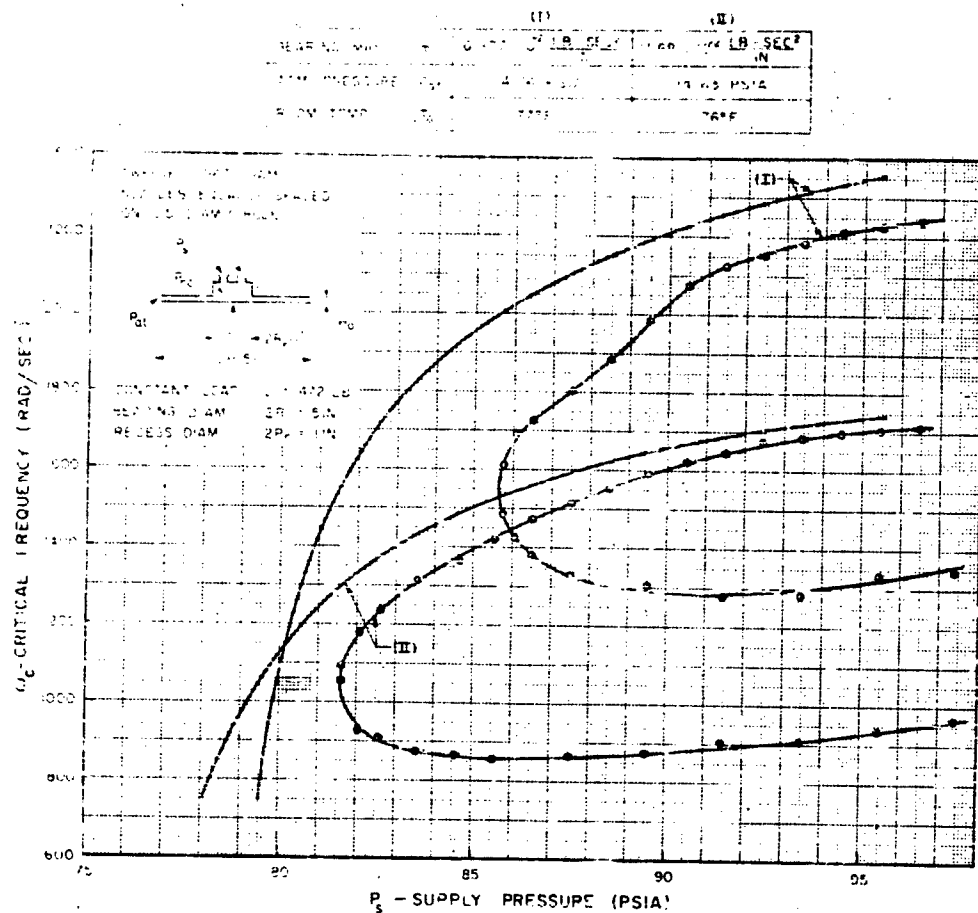


FIG. 56. CRITICAL FREQUENCY vs. SUPPLY PRESSURE

(Concluding Results)

Twelve Nozzle Supply and Piston No. 3

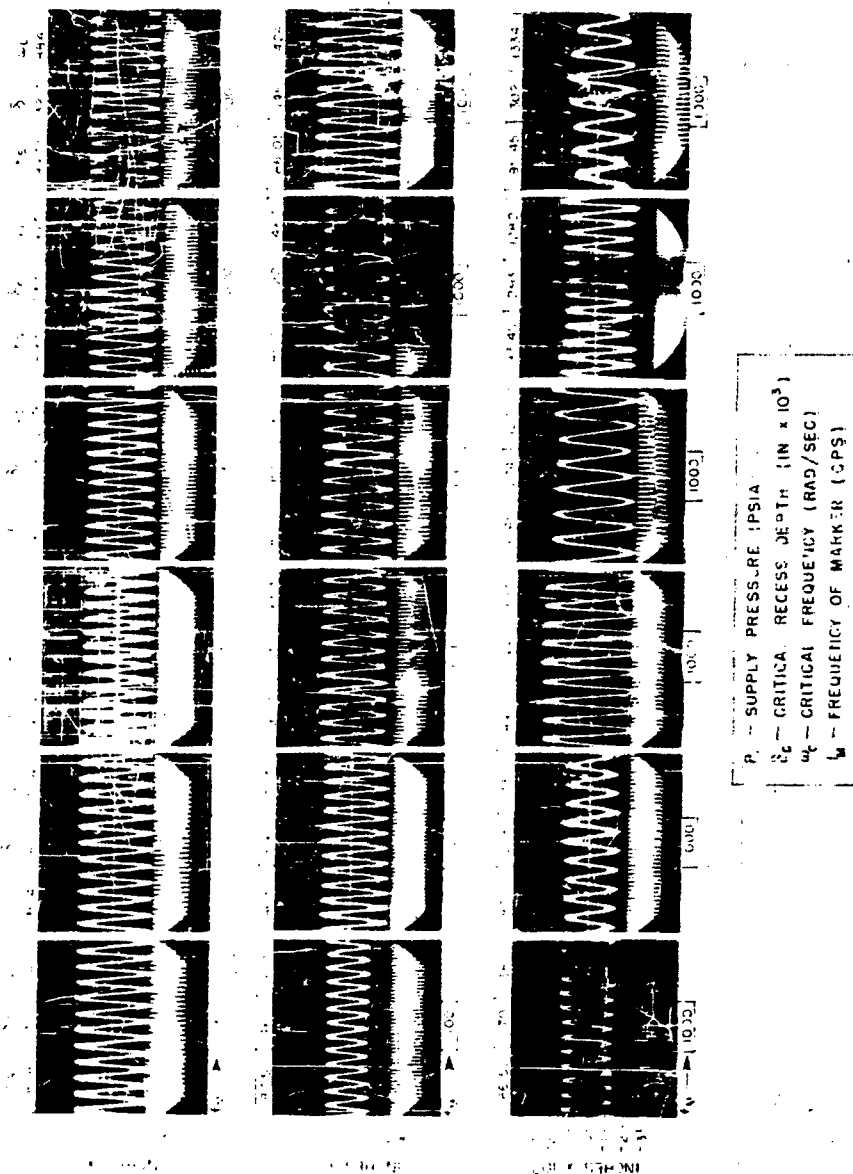


FIG. 57. DETERMINATION OF CRITICAL FREQUENCIES (READING)

$$MASC = 6.477 \times 10^{-2} \frac{\text{LB-SEC}^2}{\text{IN}}$$

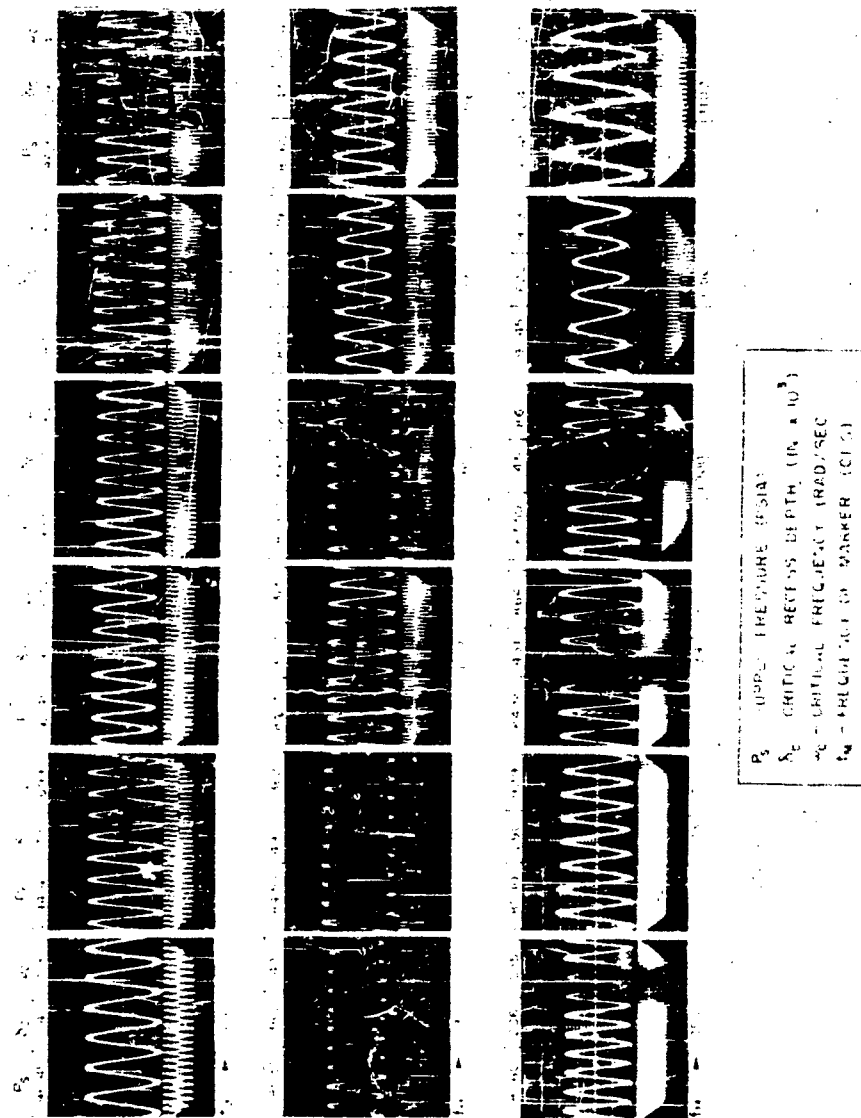


FIG. 58 DETERMINATION OF CRITICAL FREQUENCIES (BEARING)

$$MASS = 11.68 \times 10^2 \frac{LB-SEC^2}{IN.}$$

I-A-20.

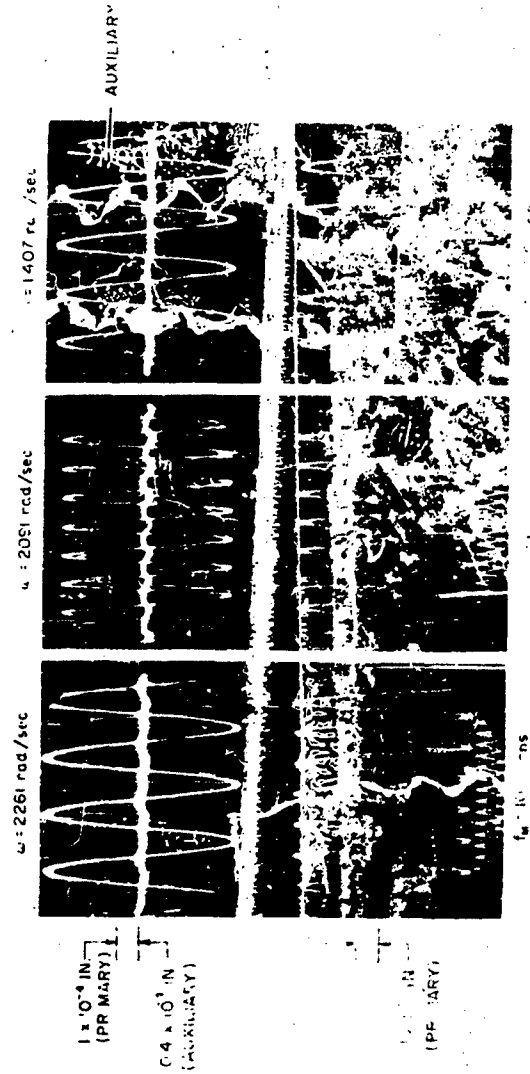
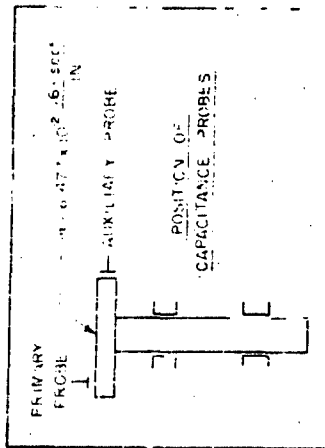


FIG. 59. COMPARISON OF AMPLITUDES OF AXIAL AND PITCHING VIBRATIONS